PN-AAV-388
IAN-45991

NOTES ON SOLAR ENERGY

from the
Training in Alternative Energy
Technologies Program
at the
University of Florida

A report to the Office of Energy
Bureau for Science and Technology
U.S. Agency for International Development
Washington, D.C.

December 1984

Martin Bush, Ph.D.
Associate in Engineering
Department of Mechanical Engineering
University of Florida
Gainesville, Florida 32611

Preface

The Training in Alternative Energy Technologies (TAET) program at the University of Florida, ran for nearly five years--from late 1979 until June 1984. The training program was sponsored by the Office of Energy of the US Agency for International Development (USAID). The purpose of the TAET program was to train technical personnel from the developing countries in the theory and application of the renewable energy technologies: solar energy, hydropower, biomass energy, wind power, and geothermal energy. A total of 286 participants from 54 developing countries attended the nine training session that were organized by the University.

The TAET curriculum was designed to meet the following specific objectives:

1. To acquaint the participants with the alternative energy technologies.

2. To provide the participants with sufficient knowledge to assess the natural renewable energy resources of the participant's country and to determine the best possible technological options to utilize these resources so that the participant can provide input in establishing realistic national alternative energy programs for the participant's country.

3. To provide technically trained people with the knowledge to select among technological options and to identify their most appropriate applications.

The training program consisted of lectures, seminars, demonstrations, laboratory work, and field trips--activities designed to explain the theory, illustrate the practice, demonstrate the operation and maintenance of the alternative energy systems, and to provide detailed training for the program participants.

As part of that effort, a number of technical notebooks and laboratory manuals were written by the program faculty at the University of Florida. All of the written material and other documentation was collected, and reorganized at the end of the training program in June 1984. This manual makes available most of the material on solar energy that was presented to the TAET participants during the course of the training program.

Table of Contents

Basic Principles

Solar Constant

The solar constant is the intensity of solar radiation incident on a surface normal to the sun's rays, outside the earth's atmosphere, at the mean distance of the earth from the sun. Because of the slightly elliptical orbit of the earth, the solar constant is, in fact, not quite constant; but it is generally given as 1353 W/m^2. The small variation in its value can be approximated by the relationship

$$G_{on} = G_{sc} [1 + 0.033 \cos 360n/365] \qquad (1)$$

where G_{on} = extraterrestrial radiation on a normal surface, W/m^2
G_{sc} = solar constanct (1353 W/m^2)
n = the day of the year

Solar Angles

The axis about which the earth rotates is tilted at an angle of 23.45° to the plane of the elliptic. This tilted axis results in a continual variation in the angle between the earth-sun line and the earth's equatorial plane; this angle is called the solar declination, Δ. The angle changes with the day of the year according to the approximate relationship

$$\Delta = 23.45 \sin [360 \times (284 + n)/365] \qquad (2)$$

There is also a very small change from year to year, but this variation may be neglected.

The position of the sun with respect to a point on the surface of the earth can be defined in terms of a number of angles. The coordinate system and the nomenclature used here is shown below

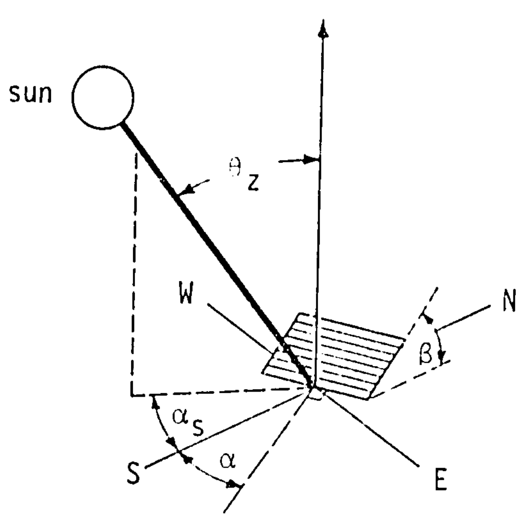

Figure 1. Zenith angle, slope, surface azimuth angle, and solar azimuth angle for a tilted surface.

In the discussion that now follows, the nomenclature listed below also will be used.

L = latitude (north positive)

β = slope of a plane surface with respect to the horizontal

α = surface azimuth; the angle subtended by the projection of the normal to a plane surface onto the horizontal, and the local meridian. Deviations east of south are taken as negative, west of south as positive; a southern projection has an azimuth angle of zero.

α_S = azimuth angle of the sun; the angle subtended by the projection of the sun's beam onto the horizontal plane and the local meridian; the same sign convention applies as for surface azimuth.

Ω = hour angle; the angular displacement of the sun from the local meridian, morning negative, afternoon positive.

θ = angle of incidence; the angle between the beam radiation on a surface and the normal to that surface.

θ_Z = zenith angle; the angle between the vertical (directly overhead) and the sun's beam radiation.

Angle of Incidence

The angle of incidence of the sun's radiation on a plane surface is the angle subtended by the sun's beam and the normal to the surface. The angle of incidence, θ, can be expressed in terms of the other solar angles as

$$\begin{aligned}\cos\theta = {} & \sin\Delta \sin L \cos\beta - \sin\Delta \cos L \sin\beta \cos\alpha \\ & + \cos\Delta \cos L \cos\beta \cos\Omega \\ & + \cos\Delta \sin L \sin\beta \cos\alpha \cos\Omega \\ & + \cos\Delta \sin\beta \sin\alpha \sin\Omega \end{aligned} \tag{3}$$

This equation simplifies considerably for some common situations; for instance, if the surface faces south, then $\alpha = 0$ and the last term drops out.

If the surface is horizontal, then $\beta = 0$, and the equation reduces to

$$\cos\theta = \sin\Delta \sin L + \cos\Delta \cos L \cos\Omega \tag{4}$$

In this equation θ is now equal to the zenith angle θ_Z. From equation 4 can also be found the sunrise and sunset angles--the angles when the zenith angle of the sun is 90°. With $\theta = \theta_Z = 90°$, equation 4 reduces to

$$\cos\Omega = -\tan\Delta \tan L \tag{5}$$

which has two solutions of different sign. The negative angle is sunrise, the positive angle is sunset.

Since the hour angle is equal to 15° per hour each side of solar noon, it follows that the length of the day can be found from

$$h = \frac{2\Omega_{SS}}{15} = \frac{2}{15}(-\tan\Delta \tan L) \tag{6}$$

where Ω_{SS} is the sunset hour angle found from Equation 5.

Extraterrestrial Radiation

Estimates of daily and average levels of insolation at the surface of the earth usually rely on correlations with extraterrestrial radiation. The extraterrestrial radiation on a surface normal to the sun's ray is given by Equation 1 and is close to the solar constant, G_{sc}, of 1353 W/m^2.

The extraterrestrial insolation on a horizontal surface, G_o, is given by

$$G_o = G_{sc}\,[1 + 0.033 \cos 360n/365] \cos \theta_z \qquad W/m^2 \qquad (7)$$

where the zenith angle, θ_z, is found from Equation 4. This equation can be integrated over the period from sunrise to sunset (specified by the hour angles Ω_{sr} and Ω_{ss} found from Equation 5) to give the total daily radiation on a horizontal surface outside the earth's atmosphere. This figure, H_o, is given by

$$H_o = \frac{24}{\pi} \times 3600 G_{sc}\,[1 + 0.033 \cos(360\, n/365)]$$

$$\times\,[\cos L \cos \Delta \sin \Omega_{ss} + \frac{2\pi\Omega_{ss}}{360} \cdot \sin L \sin \Delta] \qquad J/m^2 \qquad (8)$$

The daily insolation, H_o, can be used to represent the mean daily insolation, $\bar{H}_o$, for a particular month. In this case, H_o is found from Equation 8 for a particular day in the month--the day that will give a value for insolation closest to the mean of the daily values over the month. This day is not always the middle of the month. The days to use for estimating monthly mean daily extraterrestrial radiation are given below

Table 1 Day number for monthly means [1]

Month	date	day number (n)
January	17	17
February	16	47
March	16	75
April	15	105
May	15	135
June	11	162
July	17	198
August	16	228
September	15	258
October	15	288
November	14	318
December	10	334

Example 1

What is the mean daily radiation on a horizontal surface outside the earth's atmosphere, during the month of June, at a latitude of 30° South

Solution

From Table 1 the day number to use is 162; so from Equation 2, the declination is given by

$$\Delta = 23.45 \sin [360 \times (284 + 162)/365] = 23.086°$$

The sunset angle, Ω_{ss}, is found from Equation 5

$$\cos \Omega_{ss} = -\tan (23.086) \tan (-30) = 0.2461$$

so $\Omega_{ss} = 75.75°$

Then from Equation 8 we have

$$\overline{H}_0 = \frac{24 \times 3600}{\pi} \times 1353 [1 + 0.033 \cos(360 \times 162/365)]$$

$$\times [\cos(-30) \cos(23.086) \sin(75.75) + \frac{2\pi \times 75.75}{360} \cdot \sin(-30) \sin(23.086)]$$

$$\underline{\overline{H}_0 = 18.50 \text{ MJ/m}^2}$$

Table 2, overleaf, gives monthly mean daily values of extraterrestrial radiation for north and south latitudes calculated using the procedure indicated above.

Table 2 Monthly Average Daily Extraterrestrial Radiation, $\overline{H}_o$, MJ/m^2, for $G_{sc} = 1353\ W/m^2$

Latitude	Average Daily Extraterrestrial Radiation											
	Jan.	Feb.	Mar.	Apr.	May	June	July	Aug.	Sept.	Oct.	Nov.	Dec.
60	3.5	8.2	16.7	27.3	36.3	40.6	38.4	30.6	20.3	10.7	4.5	2.3
55	6.1	11.2	19.6	29.3	37.2	40.8	39.0	32.2	22.9	13.6	7.2	4.8
50	9.1	14.2	22.3	31.2	38.1	41.1	39.6	33.7	25.3	16.6	10.2	7.6
45	12.1	17.2	24.8	32.9	38.8	41.3	40.0	35.0	27.5	19.4	13.2	10.5
40	15.1	20.1	27.2	34.3	39.3	41.3	40.2	36.1	29.5	22.1	16.2	13.6
35	18.1	22.8	29.3	35.5	39.5	41.1	40.2	36.9	31.3	24.7	19.1	16.7
30	21.1	25.5	31.2	36.4	39.6	40.7	40.0	37.5	32.9	27.1	22.0	19.7
25	23.9	27.9	32.9	37.1	39.4	40.0	39.6	37.8	34.2	29.3	24.8	22.6
20	26.7	30.2	34.4	37.5	38.9	39.1	38.9	37.8	35.3	31.3	27.4	25.5
15	29.3	32.3	35.5	37.6	38.1	38.0	37.9	37.6	36.1	33.1	29.8	28.2
10	31.7	34.1	36.4	37.5	37.1	36.6	36.7	37.1	36.6	34.6	32.1	30.8
5	33.9	35.7	37.1	37.1	35.9	35.0	35.3	36.3	36.8	35.9	34.1	33.1
0	35.9	37.0	37.4	36.4	34.4	33.2	33.6	35.3	36.8	36.9	36.0	35.3
-5	37.6	38.1	37.5	35.4	32.7	31.1	31.7	34.1	36.5	37.7	37.5	37.3
-10	39.1	38.9	37.3	34.2	30.7	28.9	29.6	32.6	35.9	38.1	38.9	39.0
-15	40.4	39.4	36.8	32.7	28.6	26.5	27.4	30.8	35.0	38.3	39.9	40.4
-20	41.4	39.6	36.0	31.0	26.3	23.9	24.9	28.8	33.9	38.2	40.7	41.7
-25	42.1	39.6	35.0	29.0	23.8	21.3	22.3	26.7	32.5	37.8	41.3	42.6
-30	42.5	39.3	33.7	26.9	21.2	18.5	19.7	24.3	30.9	37.2	41.5	43.3
-35	42.7	38.7	32.1	24.5	18.4	15.7	16.9	21.8	29.0	36.3	41.5	43.8
-40	42.7	37.8	30.3	22.0	15.6	12.8	14.0	19.2	27.0	35.1	41.3	44.0
-45	42.4	36.7	28.3	19.4	12.8	9.9	11.2	16.5	24.7	33.7	40.8	44.0
-50	41.9	35.3	26.1	16.6	9.9	7.1	8.3	13.6	22.2	32.0	40.1	43.8
-55	41.3	33.8	23.6	13.7	7.1	4.5	5.6	10.8	19.6	30.2	39.2	43.5
-60	40.6	32.1	21.0	10.8	4.4	2.1	3.1	7.9	16.8	28.1	38.3	43.2

Terrestrial Radiation

The monthly mean daily extraterrestrial insolation levels, $\overline{H}_0$, can be related to terrestrial levels, $\overline{H}$, by the use of a monthly average clearness index, $\overline{K}_T$, where $\overline{K}_T$ is simply the ratio of the two monthly mean daily values:

$$\overline{K}_T = \overline{H}/\overline{H}_0 \quad (9)$$

Values for the monthly average clearness index, $\overline{K}_T$, are available from many locations around the world. Table 3 which follows gives values of $\overline{K}_T$ for many countries and locations throughout the world.

The monthly average clearness index can also be reasonably well correlated with the fraction of insolation which is diffuse. If $\overline{H}_d$ is the mean monthly daily diffuse radiation, the ratio $\overline{H}_d/\overline{H}$, i.e. the ratio of diffuse to total radiation on a horizontal plane on the earth's surface, can be found from $\overline{K}_T$ as follows:

$$\frac{\overline{H}_d}{\overline{H}} = 0.775 + 0.00653\ (\Omega_{ss} - 90)$$

$$- [0.505 + 0.00455\ (\Omega_{ss} - 90)] \cos\ (115\ \overline{K}_T - 103) \quad (10)$$

TABLE 3

Values of monthly $\overline{K}_T$ x 1000

STATION	LAT	LONG	ELEV	JAN	FEB	MAR	APR	MAY	JUN	JUL	AUG	SEP	OCT	NOV	DEC
							ADEN								
ADEN	12 50'N	45 01'E	4	573	607	627	656	634	592	562	597	618	663	668	632
							ALGERIA								
ADRAR	27 52'N	0 17'W	258	716	708	730	706	699	723	721	716	686	665	666	658
AIN SEFRA	32 45'N	0 36'W	1072	693	694	690	700	687	703	704	701	702	672	672	672
AOULEF	26 58'N	1 05'E	290	700	681	697	693	689	673	691	682	694	671	653	622
BENI ABBES	30 08'N	2 11'W	498	702	690	668	690	666	656	666	664	661	629	610	639
BISKRA	34 51'N	5 44'E	124	602	619	611	590	593	609	631	638	599	584	566	574
CHOTTECH CHERQUI	34 00'N	1 00'E	-	505	577	672	622	612	638	634	663	586	719	651	566
COLOMB-BECHAR	31 36'N	2 13'W	-	669	677	680	672	676	654	664	666	644	644	633	625
DJANET	24 33'N	9 29'E	-	677	801	719	698	670	700	717	703	659	663	620	675
DJELFA	34 41'N	3 15'E	160	553	581	567	554	603	609	620	627	624	566	564	545
EL GOLEA	30 35'N	2 53'E	397	690	696	699	680	687	686	707	709	689	663	636	670
EL OUED	33 22'N	6 53'E	70	766	790	664	806	787	674	725	676	798	722	716	786
FORT FLATTERS	28 06'N	6 49'E	381	680	693	678	673	678	671	710	705	687	680	668	640
FORT DE POLIGNAC	26 30'N	8 29'E	566	674	690	694	680	668	684	703	704	692	680	663	633
GERRYVILLE	33 41'N	1 01'E	1305	558	603	587	586	613	620	621	625	630	588	548	550
GHARDAIA	32 29'N	3 40'E	527	698	700	697	697	697	694	705	711	672	679	659	678
LAGHOUAT	33 48'N	2 53'E	767	589	594	582	584	603	601	621	613	501	565	558	561
OUALLEN	24 36'N	1 14'E	347	703	808	715	697	681	681	687	681	681	685	694	630
OUARGLA	31 57'N	5 20'E	138	676	683	683	673	655	633	705	689	659	648	639	632
TAMANRASSET	22 42'N	5 30'E	1376	716	717	723	709	691	658	687	654	611	643	654	678
TIMIMOUN	29 15'N	0 14'E	284	704	710	715	699	698	699	708	696	694	664	597	643
TOUGGOURT	33 07'N	6 04'E	69	655	698	665	607	676	652	704	702	690	644	617	631
							ANGOLA								
DUNDO	7 04'S	20 08'E	745	470	472	482	538	584	578	520	476	490	509	490	471
LUANDA	8 49'S	13 13'E	42	536	558	527	525	556	542	420	416	462	477	512	558
LUSO	11 08'S	19 09'E	1328	465	539	509	641	690	729	741	760	606	550	532	507
MALANGE	9 33'S	16 22'E	1151	489	543	515	509	614	664	610	549	514	514	488	506
MOCAMEDES	15 02'S	12 02'E	44	578	586	591	584	590	459	449	450	471	516	589	576
							ANTARCTICA								
AMUNDSEN-SCOTT	90 00'S		2800	*	*	*	-	-	-	-	-	*	*	*	*
BASE ROI BAUDOUIN	70 26'S	24 19'E	37	*	651	532	438	*	-	*	571	619	627	669	*
BYRD STATION	79 59'S	120 01'W	1515	-	-	-	*	*	*	*	*	535	541	*	*
CHARCOT	69 22'S	139 01'E	2401	*	381	-	-	-	-	*	613	754	785	845	*
ELLSWORTH STATION	77 44'S	41 07'W	43	*	*	578	-	-	-	-	-	617	646	*	*
HALLETT STATION	72 18'S	170 19'E	5	*	449	384	383	*	*	*	-	675	680	*	*
HALLEY BAY	75 31'S	26 36'W	30	*	528	550	543	*	*	*	*	582	669	*	*
LITTLE AMERICA V	75 31'S	26 36'W	30	*	466	487	230	*	*	*	*	514	590	*	*
MAWSON	67 37'S	62 53'E	8	643	584	534	614	769	*	882	*	746	697	684	*
MIRNY	66 33'S	93 01'E	37	729	768	679	595	571	*	*	596	694	773	820	712
NORWAY STATION	70 30'S	2 32'W	58	*	614	564	513	*	*	*	581	622	673	718	*
PIONERSKAJA	69 44'S	95 30'E	2700	-	900	830	518	978	-	-	584	622	775	848	*
SCOTT BASE	77 15'S	166 48'E	16	*	*	488	429	-	-	-	*	572	719	*	*
WILKES STATION	66 16'S	110 34'W	12	-	-	476	366	333	985	412	507	529	576	545	576

The data listed in this table are values of $\overline{K}_T$, the ratio of the monthly mean daily extraterrestrial radiation on a horizontal surface to the terrestrial value. The numbers should be divided by 1000 to obtain the correct value. Where the • is shown, data is Percent Possible Sunshine. The data is from Macomber .

STATION	LAT	LONG	ELEV	JAN	FEB	MAR	APR	MAY	JUN	JUL	AUG	SEP	OCT	NOV	DEC
ARCTIC OCEAN (CON'T)															
ICE ISLAND T-3	83 00'N	102 30'W	8	*	*	*	*	*	*	*	*	602	*	*	*
NP-6	82 18'N	123 08'E	0	*	*	642	*	*	*	*	*	451	*	*	*
NP-7	85 40'N	24 30'W	0	*	*	*	*	*	*	*	*	490	*	*	*
ARGENTINA															
ANDALGALA	27 36'S	66 20'W	1081	575	562	571	587	494	450	564	616	645	678	616	548
ARGENTINE IS.	65 15'S	64 16'W	10	466	459	358	413	431	*	704	570	540	590	518	558
BARILOCHE	41 09'S	71 01'W	826	591	507	569	413	382	362	365	486	534	545	576	621
BUENOS AIRES OBS.	34 35'S	58 29'W	25	623	599	'562	543	522	482	505	540	558	568	575	614
CASTELAR	34 36'S	58 40'W	16	600	552	554	530	473	413	513	558	571	594	584	578
CIPOLLETTI	38 57'S	67 59'W	265	666	659	630	552	480	423	488	532	609	602	601	674
COLONIA SARMIENTO	45 35'S	69 04'W	272	543	564	522	528	518	432	495	567	527	551	528	502
COMODORO RIVADAVIA	45 47'S	67 30'W	61	-	650	-	478	-	-	329	438	537	501	632	604
CONCORDIA	31 23'S	58 02'W	37	633	633	587	-	451	344	450	508	542	607	633	608
CORDOBA	31 19'S	64 13'W	484	-	-	-	-	509	429	381	469	652	516	545	548
CORRIENTES	27 28'S	58 49'W	52	590	581	570	549	535	527	524	550	565	566	590	573
ESQUEL	42 54'S	71 21'W	568	585	579	500	479	409	403	432	495	559	577	552	562
HUINCA RENANCO	34 50'S	64 22'W	182	613	625	610	556	470	508	527	528	561	590	612	611
LA QUIACA	22 06'S	65 36'W	3458	-	-	749	822	793	798	806	841	876	871	835	796
LABOULAYE	34 08'S	63 24'W	0	624	583	584	612	946	-	-	640	609	644	628	627
LAS LAJAS	38 32'S	70 23'W	713	674	676	639	586	497	448	522	549	626	636	618	691
LAS LOMITAS	24 42'S	60 35'W	130	-	-	-	-	449	360	455	466	457	469	482	537
LAURIE IS.	60 00'S	45 00'W	8	177	171	151	181	145	165	211	274	312	211	178	196
LORETO	27 21'S	55 30'W	163	575	546	587	509	458	431	448	443	463	525	585	556
MAR DEL PLATA	37 56'S	57 35'W	19	624	601	568	493	-	-	365	523	530	512	-	-
MAZARUCA	33 35'S	59 24'W	4	658	591	569	483	483	394	474	499	625	607	613	633
MENDOZA	32 53'S	68 52'W	827	702	693	318	545	518	539	544	564	657	690	686	646
NEUGUEN	38 57'S	68 09'W	270	599	539	479	444	411	315	289	545	616	490	520	546
ORCADAS	60 44'S	44 44'W	0	-	-	-	-	-	-	-	-	-	361	329	269
PASO DE LOS LIBRES	29 43'S	57 06'W	66	617	594	556	568	545	518	557	575	538	572	580	521
PATAGONES	40 48'S	62 59'W	34	584	587	571	556	519	514	473	552	553	544	567	579
PILAR	31 40'S	63 53'W	338	617	579	545	553	485	441	521	573	594	618	590	582
POSADAS	27 22'S	55 56'W	117	551	570	568	530	511	479	517	512	508	543	560	545
PUELCHES	38 08'S	65 66'W	160	-	731	-	-	447	383	328	456	513	614	647	683
PUERTO MADRYN	42 46'S	65 02'W	8	576	572	558	543	531	641	552	539	557	566	550	379
RAFAELE	31 15'S	61 30'W	130	431	440	390	333	356	266	427	361	280	398	430	432
RESISTENCIA	27 28'S	58 29'W	49	538	469	465	347	343	409	415	454	476	528	523	515
ROSARIO	32 56'S	60 42'W	222	594	589	573	536	509	500	495	524	561	559	570	536
SAN CARLOS DE BAR LO	41 09'S	71 18'W	825	594	615	573	502	441	339	410	473	544	576	604	553
SAN JUAN	31 36'S	68 33'W	630	541	529	543	517	556	684	642	552	636	611	559	499
SAN LUIZ	33 16'S	66 21'W	716	-	-	-	525	436	437	453	486	656	663	644	733
SAN MIGUEL	34 33'S	58 42'W	27	539	515	461	388	406	344	380	422	483	496	456	511
SANTA CRUZ	50 01'S	68 32'W	11	348	580	524	456	372	360	280	*	516	552	508	476
SANTIAGO DEL ESTERO	27 47'S	64 18'W	0	560	550	548	521	502	490	548	570	553	590	580	563
TRELEW	43 14'S	63 18'W	39	676	609	582	509	403	336	345	492	572	536	555	515
TRES CRUCES	23 05'S	65 44'W	4580	802	565	720	934	913	907	892	-	942	860	782	753
TUCUMA'N	26 50'S	65 12'W	421	365	571	524	473	431	419	543	054	567	552	550	510
ATLANTIC OCEAN NORTH															
A	62 00'N	33 00'W	6	256	408	266	327	414	240	347	433	-	154	335	-
I	59 00'N	19 00'W	6	355	201	420	326	371	340	401	399	433	270	356	261
J	52 30'N	20 00'W	6	351	-	419	-	187	481	446	401	359	342	258	292

STATION	LAT	LONG	ELEV	JAN	FEB	MAR	APR	MAY	JUN	JUL	AUG	SEP	OCT	NOV	DEC
							ATLANTIC OCEAN NORTH (CON'T)								
K	45 00'N	16 00'W	6	-	484	434	482	555	-	-	600	525	442	-	-
								AUSTRALIA							
ALICE SPRINGS	23 48'S	133 53'E	546	642	653	658	656	628	645	664	718	713	661	637	631
ASPENDALE	38 02'S	145 06'E	-	663	598	514	565	470	472	496	489	469	517	491	566
BOX HILL	37 48'S	145 08'E	100	549	541	538	458	423	423	444	471	493	507	508	542
BRISBANE	27 28'S	153 02'E	-	551	550	546	549	553	549	564	567	565	566	560	554
DARWIN	12 26'S	130 52'E	27	464	488	541	547	632	658	675	704	653	612	563	509
DRY CREEK S. A.	34 50'S	138 35'E	4	672	648	632	717	521	526	524	559	586	565	612	632
GUILDFORD	31 56'S	115 57'E	15	649	652	637	562	526	529	542	581	602	615	636	659
GARBUTT	19 15'S	146 46'E	4	511	518	557	596	584	626	644	664	689	660	644	623
MELBOURNE	37 49'S	144 58'E	35	625	592	423	519	529	528	531	507	520	523	479	510
MOUNT STROMLO	35 21'S	149 10'E	-	611	598	587	594	609	567	590	610	643	606	615	616
SYDNEY	33 52'S	151 12'E	42	428	537	527	529	522	542	559	573	554	551	540	535
WILLIAMTOWN	32 49'S	151 50'E	4	513	483	559	507	526	513	550	615	551	620	593	527
								AUSTRIA							
GMUNDEN	47 55'N	13 47'E	425	369	400	431	401	453	395	406	425	453	370	725	275
GRAFENHOF	47 19'N	13 10'E	766	412	584	474	481	450	369	414	413	585	489	374	351
GUMPENSTEIN	47 30'N	14 06'E	710	388	442	483	453	493	400	420	442	441	422	317	319
KLAGENFURT	46 38'N	14 19'E	448	446	505	563	452	510	434	488	485	481	439	226	271
KRIPPENSTEIN	47 32'N	13 41'E	2064	591	581	551	550	510	380	388	410	506	556	530	486
LUNZ-AM-SEE	47 50'N	15 00'E	615	284	391	464	384	444	399	368	395	388	402	270	241
MONICHKIRCHEN	47 32'N	16 02'E	978	498	418	464	415	469	378	415	449	446	495	395	454
NEUSIEDLAM SEE	47 57'N	16 51'E	116	365	284	449	452	559	431	470	508	400	394	231	281
OBERGURGL	46 52'N	11 02'N	1950	409	494	563	605	533	300	456	457	448	468	359	324
OBERSIEBEN-BRUHN	48 46'N	16 43'E	150	358	330	441	428	489	421	425	477	444	379	230	242
PERTISAU/ACHENSEE	47 26'N	11 42'E	933	475	377	516	425	430	354	345	370	424	434	339	303
RETZ	48 46'N	15 58'E	243	262	347	379	402	493	445	433	459	454	679	183	211
SALZBURG	47 48'N	13 00'E	437	395	431	446	420	452	387	396	274	434	423	260	311
SEMMERING	47 39'N	15 50'E	995	326	359	362	386	454	368	381	422	383	450	299	243
SONNBLICK	47 03'N	12 57'E	3106	594	660	621	586	561	461	421	433	561	587	537	520
STEYR	48 04'N	14 35'E	309	368	392	427	463	456	417	417	457	451	385	225	240
VIENNA	48 15'N	16 22'E	-	292	359	398	438	473	461	473	467	581	355	273	248
YBBS-PERSENBEUG	48 11'N	15 '3	228	374	383	435	482	490	408	414	448	443	377	244	227
								AZORES							
ANGRA	38 07'N	27 02'W	92	416	431	438	498	544	582	533	546	533	499	429	433
CORVO	39 40'N	31 07'W	28	442	431	469	514	536	525	563	582	559	483	415	403
PONTA DELGADA	37 45'N	25 40'W	36	488	497	514	507	554	520	570	610	616	586	479	488
								BELGIUM							
BRUSSEL-UCCLE	50 48'N	4 22'E	100	290	323	353	392	422	402	402	403	390	344	277	241
								BOLIVIA							
LA PAZ	16 31'S	68 93'W	3658	425	457	519	556	658	756	611	542	611	613	552	516

BRAZIL

STATION	LAT	LONG	ELEV	JAN	FEB	MAR	APR	MAY	JUN	JUL	AUG	SEP	OCT	NOV	DEC
ALEGRETE	29 47'S	55 47'W	-	607	616	594	569	546	519	536	559	552	573	600	608
ARACAJU	10 55'S	37 03'W	-	625	588	515	454	384	353	374	418	483	550	609	649
ARAXA	19 36'S	46 56'W	-	425	533	519	539	590	552	569	567	501	477	501	371
BAGE	31 20'S	54 06'W	-	586	576	552	553	548	521	516	541	521	543	580	586
BARBACENA	21 15'S	43 46'W	-	464	490	482	514	561	608	622	592	472	453	418	377
BARRA CORDA	5 30'S	45 16'W	-	404	400	393	414	441	526	550	509	496	491	465	473
BAURU	22 19'S	49 04'W	-	489	473	516	607	595	591	605	609	523	512	554	505
BELEM	1 28'S	48 29'W	-	518	459	456	495	576	652	682	682	672	673	652	642
BELO HORIZONTE	19 56'S	43 57'W	-	504	516	521	550	585	612	626	617	550	509	495	451
BLUMENAU	26 55'S	49 04'W	-	470	489	511	479	460	477	434	437	398	430	433	458
CABO FRIO	22 52'S	42 01'W	-	488	516	517	514	518	543	540	538	462	446	471	455
CAMPINAS	22 53'S	47 05'W	-	558	558	565	584	602	599	613	600	564	568	563	544
CAMPOS	21 45'S	41 20'W	-	480	515	479	493	523	529	545	528	444	422	441	437
CAMPOS DE JORDAO	22 52'S	43 22'W	-	438	442	470	473	518	543	558	569	487	457	440	405
CANANEIA	25 01'S	47 56'W	5	502	477	446	446	426	448	449	421	342	374	462	453
CATALAO	18 10'S	47 57'W	-	488	506	539	591	613	640	637	644	567	540	518	476
CAXIAS	4 52'S	43 22'W	-	504	506	500	515	543	584	615	624	608	589	559	543
CAXIAS	29 10'S	51 12'W	-	529	530	529	518	519	532	549	534	521	525	539	531
CORRENTES	9 06'S	36 21'W	-	540	492	472	446	396	444	394	428	574	577	626	568
CORUMBA	19 00'S	57 39'W	-	405	411	415	424	435	429	448	449	422	419	424	413
CRUZ ALTA	28 38'S	53 37'W	-	559	561	539	528	531	502	540	546	504	547	570	571
CUIABA	15 36'S	56 06'W	-	396	391	402	490	527	518	541	484	445	483	474	422
CURITIBA	25 26'S	49 16'W	-	504	506	502	504	511	519	536	530	500	506	510	509
DIAMANTINA	18 15'S	43 36'W	-	458	580	512	459	514	538	536	620	528	477	405	374
FLORINOPOLIS	27 36'S	48 34'W	-	513	523	545	521	537	502	502	488	466	472	485	509
FORTALEZA	3 46'S	38 31'W	-	565	520	500	489	525	577	582	607	618	624	608	606
GOIANIA	16 40'S	49 15'W	-	491	507	353	569	613	637	635	631	549	528	500	450
GOIAS	15 56'S	50 08'W	-	483	486	512	552	591	628	595	611	546	528	501	462
GRAJAU	5 49'S	46 09'W	-	387	366	402	439	492	560	609	569	530	474	482	456
GUANABARA OBS.	22 54'S	43 10'W	-	498	505	506	514	518	524	541	523	462	446	471	474
GUARAMIRANGA	4 16'S	39 01'W	-	468	426	389	405	442	449	490	479	482	498	491	483
IGUATU	6 22'S	39 18'W	-	550	523	534	545	581	587	604	623	612	609	595	577
ILHEUS	14 48'S	39 02'W	-	590	565	543	544	555	587	553	627	569	590	524	549
JUIZ DE FORA	21 46'S	43 21'W	-	430	452	444	466	474	511	492	498	419	411	411	387
JOAO PESSOA	7 06'S	34 52'W	-	589	586	568	561	562	554	558	579	591	596	601	593
LAGES	27 49'S	50 20'W	-	521	508	511	492	502	490	528	537	499	522	529	524
LAGUNA	28 29'S	48 47'W	-	521	508	554	560	613	601	554	520	525	497	546	541
LORENA	22 42'S	45 05'W	-	459	473	470	485	500	485	538	521	435	445	471	435
MACEIO	9 34'S	35 47'W	-	602	581	569	568	562	557	560	564	572	595	594	594
MANAUS	3 08'S	60 02'W	-	418	398	400	407	462	525	556	571	538	513	473	446
NATAL	5 46'S	35 12'W	-	588	580	556	553	562	566	570	593	610	621	621	605
NITEROI HORTO BOTANI	22 54'S	43 07'W	-	478	484	494	501	485	487	505	523	449	446	450	445
OLINDA	8 01'S	34 51'W	-	624	531	526	527	512	519	468	568	620	616	600	625
OURO PRETO	20 23'S	43 30'W	-	398	487	418	467	472	538	519	552	452	417	379	339
PALMAS	26 29'S	51 56'W	-	522	528	530	526	523	534	569	557	519	530	540	526
PARANAGUA	25 31'S	48 31'W	-	453	455	502	479	503	545	477	445	441	421	425	433
PASSO FUNDO	28 16'S	52 25'W	-	550	540	537	525	526	518	535	542	515	534	549	542
PESQUERIA	8 24'S	36 46'W	-	568	535	547	517	436	474	479	557	631	684	631	629
PERTOPOLIS	22 31'S	43 11'W	-	449	410	469	484	514	538	536	535	460	434	430	416
PIRACICABA	21 43'S	47 38'W	-	489	541	601	556	553	617	648	677	566	538	546	471
POCOS DE CALDAS	21 47'S	46 33'W	-	407	478	495	561	557	581	604	612	520	553	507	433
PORTO NACIONAL	10 42'S	48 25'W	-	510	482	493	539	615	645	645	652	577	528	492	490
RIO GRANDE	32 02'S	52 06'W	-	585	577	555	559	538	533	504	531	469	556	580	595
SALVADOR	12 56'S	38 31'W	-	616	582	586	569	521	579	553	618	603	616	575	583

BRAZIL (CON'T)

STATION	LAT	LONG	ELEV	JAN	FEB	MAR	APR	MAY	JUN	JUL	AUG	SEP	OCT	NOV	DEC
SAN PAULO	23 33'S	46 38'W	-	467	484	461	491	474	514	476	466	490	491	481	463
SANTA CRUZ	22 56'S	43 22'W	-	478	494	506	501	519	544	541	538	449	435	461	445
SANTA MARIA	29 41'S	53 49'W	-	548	552	531	522	506	495	513	505	497	526	549	559
SANTAREM	2 45'S	54 42'W	-	434	400	389	405	433	466	498	530	525	515	499	474
SANTOS	23 56'S	46 20'W	-	437	453	462	465	495	519	480	469	402	425	439	403
SAO LUIZ	2 32'S	44 18'W	-	468	434	411	428	457	517	536	530	513	503	511	520
SOURE	0 44'S	48 31'W	-	548	473	456	493	582	657	674	701	705	699	693	686
TEREZINA	5 05'S	42 49'W	-	522	515	511	542	587	619	583	655	621	599	588	560
TERE-ZOPOLIS	22 27'S	42 56'W	-	449	463	446	470	481	500	500	504	447	412	420	396
UAUPES	0 08'S	67 05'W	-	454	473	456	436	437	442	462	499	500	484	484	461
UBERABA	19 45'S	47 56'W	-	484	516	520	562	630	592	606	615	549	531	526	482
URUGUAIANA	29 45'S	57 05'W	-	587	595	569	553	546	519	557	558	552	538	580	502
VASSOURAS	22 24'S	43 40'W	-	459	484	481	484	513	537	535	488	460	445	451	446
VITORIA	20 19'S	40 19'W	-	503	526	510	512	525	423	528	546	489	454	453	460

BRITISH GUIANA

STATION	LAT	LONG	ELEV	JAN	FEB	MAR	APR	MAY	JUN	JUL	AUG	SEP	OCT	NOV	DEC
GEORGETOWN	7 45'N	58 04'W	-	495	512	498	504	470	469	513	536	555	538	521	480
MAZARUNI	5 58'N	59 37'W	-	433	421	427	416	453	442	451	437	419	427	437	455

BULGARIA

STATION	LAT	LONG	ELEV	JAN	FEB	MAR	APR	MAY	JUN	JUL	AUG	SEP	OCT	NOV	DEC
KARDJALI	41 39'N	25 22'E	231	379	446	393	382	-	436	418	463	447	390	270	206
POLIANOVGRAD	42 31'N	26 51'E	196	484	626	504	532	592	557	607	603	612	555	461	520
SOFIA OBS.	42 49'N	23 23'E	582	342	521	442	041	460	503	574	555	485	436	321	324
SOMMET STALIN	42 11'N	23 35'E	2925	335	524	550	491	409	344	439	490	481	495	490	450
TCHERNI-VRAH	42 34'N	23 17'E	2286	670	813	665	603	539	523	669	664	617	718	650	632
TCHIRPAN	42 12'N	25 20'E	170	425	626	539	484	598	569	642	647	601	575	474	396
VARNA	43 12'N	27 55'E	51	429	520	458	420	447	475	488	594	554	*	365	388

BUPMA

STATION	LAT	LONG	ELEV	JAN	FEB	MAR	APR	MAY	JUN	JUL	AUG	SEP	OCT	NOV	DEC
RANGOON	17 00'N	96 00'E	30	727	743	701	678	576	424	414	386	405	595	697	708

CANADA

STATION	LAT	LONG	ELEV	JAN	FEB	MAR	APR	MAY	JUN	JUL	AUG	SEP	OCT	NOV	DEC
AKLAVIK	68 14'N	135 00'W	9	*	612	719	697	622	*	482	432	386	381	441	*
CHURCHILL	58 45'N	94 04'W	35	697	704	731	676	587	543	541	499	427	383	435	515
DARTMOUTH	44 36'N	63 28'W	31	414	444	467	478	491	454	498	498	512	474	354	387
DEPARTURE BAY	49 13'N	123 57'W	-	359	370	418	429	560	320	640	597	457	438	360	-
EDMONTON	53 34'N	113 31'W	676	551	611	640	582	570	522	556	512	506	503	529	497
FORT SIMPSON	61 52'N	121 21'W	129	534	534	615	623	586	534	497	502	451	431	309	290
GOOSE BAY	53 19'N	60 25'W	44	424	548	591	534	492	437	443	412	406	371	375	441
GUELPH	43 33'N	80 16'W	320	475	475	531	473	495	529	570	530	512	461	367	384
KAPUSKASING	49 25'N	82 28'W	229	500	546	573	496	451	486	502	484	425	371	297	422
KNOB LAKE	54 48'N	66 49'W	512	414	518	658	602	451	438	381	418	366	336	364	429
LETHBRIDGE	49 38'N	112 48'W	920	553	609	632	564	572	587	638	631	585	560	526	483
MONCTON	46 07'N	64 41'W	76	374	455	499	491	477	454	488	485	463	441	347	381
MONTREAL	45 30'N	73 37'W	133	398	495	543	514	509	494	530	519	459	413	307	326
MOOSONEE	51 16'N	80 39'W	10	490	529	589	541	449	477	457	424	439	369	309	427
NANAIMO	49 00'N	123 00'W	-	363	359	434	570	594	526	680	590	460	444	389	292
NORMANDIN	48 51'N	72 32'W	137	504	842	648	473	504	470	475	470	445	387	378	456
OTTAWA	45 27'N	75 37'W	98	519	563	568	518	538	563	568	553	525	456	377	443
RESOLUTE BAY	74 43'N	94 59'W	64	*	*	*	766	*	*	*	413	397	443	*	*

STATION	LAT	LONG	ELEV	JAN	FEB	MAR	APR	MAY	JUN	JUL	AUG	SEP	OCT	NOV	DEC
						CANADA (CON'T)									
ST. JOHN'S WEST	47 31'N	52 47'W	114	324	400	425	420	436	434	458	406	428	372	270	324
SASKATOON	52 08'N	106 38'W	515	551	631	632	575	556	528	589	557	537	507	456	493
SUFFIELD	50 16'N	111 11'W	775	553	700	605	623	582	546	634	605	521	498	517	535
SUMMERLAND	49 34'N	119 39'W	454	367	405	501	577	539	536	586	582	521	419	[illegible]	320
TORONTO	43 40'N	79 24'W	116	399	430	478	470	515	524	546	506	496	441	349	350
VANCOUVER	49 33'N	123 30'W	-	349	300	347	460	515	488	570	482	398	372	355	298
WINNIPEG	49 54'N	97 14'W	240	615	659	679	592	562	532	595	574	507	482	454	504
						CANTON ISLAND									
CANTON ISLAND	2 46'S	171 43'W	9	674	690	698	699	694	706	699	715	729	730	685	670
						CAPE VERDI ISLANDS									
MINDELO	16 52'N	25 00'W	2	634	669	739	752	745	689	637	581	629	617	612	582
PRAIA	14 54'N	23 31'W	27	666	686	738	746	703	684	590	548	590	635	614	575
						CAROLINE ISLANDS									
TRUK	• 7 23'N	151 54'E	110	057	063	056	058	050	056	055	050	056	053	050	048
YAP	• 9 30'N	138 07'E	35	056	065	067	061	058	056	042	041	048	055	055	056
						CENTRAL AFRICA									
BANGUI	4 22'N	18 34'E	-	474	516	562	552	549	496	460	462	496	521	480	467
						CEYLON									
BATTICALOA	7 43'N	81 42'E	3	558	607	622	605	619	598	606	604	611	584	583	545
COLOMBO	6 54'N	79 52'E	7	589	625	620	595	565	556	576	573	589	558	589	589
						CHAD									
FORT LAMY	12 08'N	15 02'E	297	689	711	725	668	666	649	605	556	625	699	729	713
						CHILE									
ATACAMA DESERT	23 40'S	69 45'W	-	757	755	748	765	749	748	809	849	818	801	779	780
SANTIAGO	33 27'S	70 40'W	520	662	708	652	607	473	432	455	473	478	608	591	669
						CHINA									
AIGUN	50 15'N	127 29'E	131	529	595	547	487	485	506	482	500	479	476	505	506
CHANGCHUN	43 52'N	125 20'E	215	533	562	543	519	506	504	497	502	521	514	515	521
CHEFOO	37 34'N	121 31'E	27	510	526	532	553	531	516	496	498	522	531	501	498
CHINCHOW	41 08'N	121 07'E	52	558	559	548	531	513	504	496	494	530	537	515	551
CHINKIANG	32 10'N	119 40'E	12	362	411	397	442	433	398	446	478	444	495	506	477
DARIEN	38 54'N	121 14'E	97	550	557	566	569	525	540	498	463	539	553	528	524
HANKOW	30 35'N	114 17'E	36	487	448	457	484	507	502	478	520	476	467	505	454
HARBIN	44 50'N	126 38'E	145	559	580	536	511	497	504	498	505	499	507	507	510
HULUN	49 13'N	119 44'E	619	539	598	552	508	516	516	502	508	487	507	661	520
KHINGAN	48 50'N	121 40'E	984	526	589	565	519	493	496	491	506	484	478	576	556
KOSHAN	48 04'N	125 52'E	223	543	571	538	502	492	505	490	492	493	511	519	528
LUSKAING	47 20'N	123 56'E	147	560	582	476	511	501	505	458	501	503	522	501	548

STATION	LAT	LONG	ELEV	JAN	FEB	MAR	APR	MAY	JUN	JUL	AUG	SEP	OCT	NOV	DEC
							CHINA (CON'T)								
MANCHOULI	49 35'N	117 26'E	641	552	607	575	524	495	506	513	497	490	536	674	534
MUKDEN	41 47'N	123 24'E	43	544	548	538	509	514	504	496	508	521	564	527	501
NAIJUMATU	50 28'N	120 06'E	-	537	601	549	516	508	496	503	488	465	503	472	515
SHANGHAI	31 17'N	121 28'E	3	477	387	461	474	497	429	540	577	541	518	476	464
SUIFENHO	44 23'N	131 09'E	-	546	548	532	509	475	484	498	492	481	521	497	497
TAILEN	38 54'N	121 38'E	96	536	525	543	534	521	515	475	501	530	528	524	498
TIENTSIN	39 09'N	117 09'E	3	542	528	530	523	532	515	506	501	518	531	528	503
TSINAN	36 40'N	116 58'E	-	543	514	525	525	498	516	516	507	530	538	531	508
TSINGTAU	36 04'N	120 19'E	77	580	544	549	535	509	506	527	529	514	565	544	548
							COLOMBIA								
BOGOTA	4 38'N	74 05'W	2560	554	517	469	423	441	474	487	478	470	408	464	500
							CONGO								
ALBERTVILLE	5 53'S	29 11'E	790	486	527	522	527	672	642	644	588	612	537	471	531
BAMBESA	3 27'N	25 43'E	621	483	-	506	507	543	504	433	465	496	524	554	531
BOENDE	0 13'S	20 51'E	370	467	489	476	500	480	494	429	455	500	471	450	424
BUKAVU	2 31'S	28 51'E	1635	-	-	487	509	561	575	551	530	427	508	487	481
BUNIA-RUAMPARA	1 32'N	30 10'E	1225	516	549	544	575	554	520	479	515	524	507	525	550
COQUILHATVILLE	0 03'N	18 16'E	325	441	489	497	490	503	460	434	439	466	472	479	459
ELIZABETHVILLE-KARAV	11 39'S	27 25'E	1260	468	439	509	571	659	691	690	684	650	620	515	464
GANDAJIKA	6 45'S	23 57'E	780	481	467	513	624	586	568	542	502	501	505	513	517
KAMINA-BAKA	8 38'S	25 15'E	1085	459	415	524	615	721	684	701	597	557	512	508	477
KINDU	2 57'S	25 55'E	475	-	-	-	-	-	417	350	435	463	459	421	405
KIYAKA-PLATEAU	5 16'S	18 57'E	715	-	-	-	480	559	536	509	503	477	506	501	476
LEOPOLDVILLE	4 22'S	15 15'E	445	422	464	498	505	466	423	377	416	421	425	464	438
LULUABOURG	5 53'S	22 25'E	670	488	508	512	530	605	551	531	510	543	522	515	486
LWIRO	2 03'S	28 08'E	1680	515	502	528	528	497	492	520	496	536	514	538	536
RUBONA	2 29'S	29 46'E	1706	497	495	531	504	557	589	573	580	550	526	513	545
SIMAMA	9 37'S	27 01'E	852	-	-	-	575	662	666	640	606	551	451	461	450
STANLEYVILLE	0 31'N	25 11'E	415	459	496	507	513	509	468	424	419	481	486	491	461
YANGAMBI	0 49'N	24 29'E	500	478	508	510	511	530	499	438	433	464	462	489	442
							CONGO REPUBLIC								
BRAZZAVILLE	4 15'S	15 14'E	320	479	486	509	544	472	445	387	430	446	443	504	474
							CZECHOSLAVAKIA								
BRATISLAVA	48 10'N	17 06'E	289	378	393	429	481	551	498	509	563	489	426	258	232
DOKSANY	50 27'N	14 10'E	158	321	405	441	494	525	510	461	498	500	374	228	217
HURBANOVO	47 52'N	18 12'E	120	392	410	486	539	593	544	539	576	539	488	312	308
LOMNICKY STIT	49 12'N	20 13'E	2638	637	646	662	594	526	407	453	438	527	596	576	587
MILESOVKA	50 33'N	13 56'E	835	417	497	475	482	516	508	459	491	517	433	285	299
NOVY HRADEC KRALOVE	50 11'N	15 50'E	200	359	409	463	480	523	489	454	496	472	385	256	257
PODERSAM	50 13'N	13 24'E	320	254	351	397	390	450	409	428	441	402	309	233	230
PRAHA-KARLOV	50 04'N	14 26'E	254	271	336	398	424	468	455	420	455	446	329	215	200
SKALNATE PLESO	49 11'N	20 15'E	1783	564	609	546	496	444	352	376	397	427	501	491	477
							EQUADOR								
AMBATO	1 15'S	78 44'W	2621	395	362	286	419	344	306	309	337	279	374	408	419

STATION	LAT	LONG	ELEV	JAN	FEB	MAR	APR	MAY	JUN	JUL	AUG	SEP	OCT	NOV	DEC
							EQUADOR (CON'T)								
QUITO	0 17'S	78 32'W	2851	505	490	397	428	437	476	505	584	449	467	484	487
							EL SALVADOR								
SAN SALVADOR	13 34'N	89 13'W	698	696	692	653	609	582	499	589	664	519	621	688	727
							FALKLAND ISLANDS								
PORT STANLEY	51 42'S	57 52'W	-	455	431	468	431	421	384	401	453	504	515	491	459
							FINLAND								
HELSINGFORS	60 10'N	24 57'E	40	250	358	485	443	456	480	474	397	359	293	185	230
HELSINKI	60 12'N	24 55'E	60	305	432	561	536	500	519	518	484	432	337	219	174
JOKIONEN	60 49'N	23 28'E	104	279	387	530	493	475	501	487	441	415	266	190	221
LUONETJARVI	62 25'N	25 39'E	145	340	436	558	485	448	509	472	482	418	263	189	239
SODANKYLA	67 22'N	26 39'E	180	833	473	527	548	459	*	481	419	344	325	300	*
							FORMOSA								
KOSHUN	22 00'N	120 45'E	22	538	554	505	499	500	530	405	382	475	472	487	535
KWARENKO	23 58'N	121 37'E	176	475	394	342	397	472	601	571	587	550	558	490	485
SHINCHIKU	24 48'N	120 58'E	-	461	369	291	473	484	633	507	512	561	-	-	-
TAICHU	24 09'N	120 41'E	-	461	474	363	435	483	439	464	417	489	486	468	446
TAINAN	23 00'N	120 13'E	13	649	623	496	495	522	520	425	435	532	590	590	672
TAIPEI	25 02'N	121 31'E	23	327	323	331	352	405	410	421	453	410	472	488	416
TAITO	22 45'N	121 09'E	10	524	468	416	436	514	681	599	527	560	615	557	524
							FRANCE								
AGEN	44 10'N	0 40'E	-	372	426	496	508	485	504	560	550	494	459	377	302
ALENCON	48 25'N	0 05'E	-	341	414	452	477	482	475	501	493	434	427	352	295
ANGERS	47 30'N	0 35'W	-	364	426	478	538	491	495	531	526	473	459	370	369
ANGOULEME	45 40'N	0 10'E	-	438	448	511	541	509	525	561	543	505	477	402	371
AUXXERRE	47 15'N	3 35'E	-	358	422	493	523	501	505	541	525	487	456	366	318
BAGNERES-DE-BIGORRE	43 05'N	0 05'E	-	417	434	470	440	419	434	455	453	430	466	444	357
BAUGE	47 35'N	0 05'W	-	365	427	461	552	491	495	531	526	474	438	338	325
BERGERAC	44 50'N	0 30'E	-	384	411	503	511	475	504	539	517	484	446	388	353
BESANCON	47 20'N	6 02'E	-	360	397	512	498	501	525	552	537	503	479	367	320
BREST	48 35'N	4 30'W	-	345	389	472	465	471	455	470	494	435	429	355	348
CHATEAU-CHINON	47 09'N	0 13'E	-	396	394	492	497	479	495	531	500	471	476	397	316
CHATEAU ROUX	46 50'N	1 40'E	-	389	415	489	482	468	495	531	499	469	450	359	310
CLERMONT-FD	49 25'N	2 25'E	-	364	460	499	496	473	496	544	521	488	487	408	422
DIJON	47 20'N	5 02'E	-	360	423	529	524	512	535	562	549	518	479	367	320
LA MOTHE-ACHARD	46 44'N	0 17'W	-	425	440	505	547	533	505	562	535	483	470	390	396
LE MANS	48 00'N	0 10'E	-	375	380	483	541	492	495	532	503	462	444	380	334
LE PUY	45 05'N	3 50'E	-	389	463	522	512	497	545	591	553	530	490	422	398
LIMOGES	48 50'N	1 15'E	-	438	449	511	519	482	496	543	531	515	523	432	405
LILLE	50 04'N	3 03'E	-	380	413	432	473	463	466	461	450	414	426	308	333
LYON	45 45'N	4 50'E	-	366	399	529	541	531	545	592	567	520	458	341	331
LUXEMBOURG-VILLE	49 35'N	6 08'E	-	322	376	464	470	477	466	481	473	427	419	300	321
MARSEILLE	43 20'N	5 20'E	-	454	506	521	541	516	365	642	593	575	488	476	434
MONTELIMAR	44 33'N	4 47'E	-	413	575	550	573	540	605	664	609	599	524	442	386
MONTPELLIER	43 35'N	3 50'E	-	493	557	556	581	560	625	704	629	605	511	481	440

STATION	LAT	LONG	ELEV	JAN	FEB	MAR	APR	MAY	JUN	JUL	AUG	SEP	OCT	NOV	DEC
						FRANCE (CON'T)									
						==============									
MONTPELLIER	43 15'N	3 50'E	-	485	528	488	528	516	605	663	570	545	468	475	432
NANTES	47 15'N	1 35'W	-	398	422	440	497	501	495	531	501	441	434	366	363
NICE	43 42'N	7 18'E	-	545	559	539	558	567	637	671	663	567	530	489	494
NIMES	43 50'N	4 20'E	-	499	538	542	569	538	615	684	607	579	494	486	445
PARIS-ST. MAUR	48 49'N	2 30'E	50	328	367	452	449	472	486	476	461	454	387	306	313
PERPIGNAN	42 45'N	2 50'E	-	505	565	548	551	526	565	621	580	570	519	520	453
POITIERS	46 40'N	2 50'E	-	385	439	504	546	511	515	562	535	513	491	388	350
REIMS	49 20'N	4 02'E	-	362	401	461	495	483	465	491	472	441	416	333	315
ROUEN	49 30'N	1 05'E	-	320	375	444	483	473	466	481	460	426	395	336	319
ST. QUENTIN	49 50'N	3 20'E	-	327	380	429	471	451	445	461	437	413	399	304	327
ST. RAPHAEL	43 25'N	6 50'E	-	489	577	587	605	581	645	725	664	647	548	534	472
STRASBOURG	48 40'N	7 00'E	-	347	390	454	452	493	506	522	518	451	453	321	300
SUR SEINE	48 48'N	0 06'W	-	358	423	439	496	556	524	482	494	463	477	356	237
TARARE	45 55'N	4 25'E	-	370	402	480	490	477	515	561	532	507	460	375	334
TOULON	43 05'N	5 55'E	-	513	571	567	590	580	645	714	651	630	543	527	499
TOULOUSE	43 40'N	0 45'E	-	396	465	524	518	495	504	559	560	534	492	426	368
TOURS	47 20'N	0 45'E	-	360	423	476	537	480	485	531	501	472	457	334	320
VICHY	46 10'N	3 25'E	-	375	405	482	518	499	525	561	545	494	463	380	339
VILLEFRANCHE-DE-ROUE	44 20'N	3 25'E	-	375	404	498	508	485	504	560	538	510	461	379	343
						GERMANY									
						=======									
BOCHUM	51 29'N	7 13'E	118	205	258	317	378	356	362	341	357	335	288	217	187
BRAUNLAGE	51 43'N	10 37'E	-	262	359	416	435	399	408	372	396	358	368	250	260
BRAUNSCHWEIG-VOLKENR	52 18'N	10 27'E	97	385	378	420	434	459	455	447	422	473	396	246	247
COLLM OBS.	51 19'N	13 00'E	247	326	427	439	422	461	506	426	469	505	368	248	251
DRESDEN	51 07'N	13 41'E	271	306	328	398	435	441	441	432	442	430	392	270	265
FICHTELBERG	50 26'N	12 57'E	1214	307	573	479	460	422	433	421	413	534	436	318	268
FREIBURG	48 01'N	7 52'E	285	237	304	457	413	446	494	471	482	474	408	249	306
GOTHA	50 57'N	10 41'E	335	353	414	403	433	440	466	450	441	466	380	222	232
GRIEFSWALD	54 06'N	13 23'E	23	246	317	424	460	509	525	493	493	448	385	257	222
HAMBURG-FUHLSBUTTEL	53 38'N	10 00'E	14	317	355	405	449	462	439	425	423	434	367	263	250
HANNOVER-LANGENHAGEN	52 28'N	9 42'E	-	254	362	382	448	429	403	392	418	394	444	284	264
HEILIGENDAMM	54 09'N	11 51'E	21	280	300	363	475	566	535	487	456	519	415	218	240
HOEFCHEN	51 06'N	7 06'E	-	250	259	339	390	413	379	409	402	393	321	175	205
HOHENPEISSENBERG	47 48'N	11 01'E	1005	498	512	535	473	479	456	467	502	494	485	414	438
KARLSRUHE	49 01'N	8 25'E	130	301	418	440	456	551	524	549	447	473	462	251	267
KONIGSTEIN-TAUNUS	50 11'N	8 29'E	-	325	356	435	469	472	464	465	471	452	397	271	235
LEIPZIG	51 18'N	12 28'E	146	259	349	387	438	494	479	452	463	479	380	211	202
LINDENBERG	52 13'N	14 07'E	98	360	387	305	402	453	473	418	441	417	372	231	252
MUNCHEN-RIEM	48 08'N	11 42'E	528	474	491	488	476	500	471	482	490	460	459	264	357
OBERSTDORF	47 24'N	10 17'E	-	341	358	401	409	386	373	397	400	390	371	312	321
POTSDAM	52 23'N	13 04'E	105	326	341	421	443	461	478	464	451	455	366	269	269
QUICKBORN	33 44'N	9 53'E	14	116	220	289	372	392	417	365	389	326	204	102	089
SAARBRUCKEN	49 13'N	7 01'E	-	229	293	392	427	464	430	435	445	416	355	272	244
TRIER-PETRISBERG	49 45'N	6 40'E	276	-	-	510	502	-	419	450	420	385	361	242	276
TUBINGEN	48 31'N	9 03'E	-	249	324	388	360	380	372	387	380	345	363	298	233
WURZBURG-STEIN	49 48'N	9 54'E	263	420	391	442	450	438	432	477	472	539	401	212	250
WYK/FOHR	54 43'N	8 35'E	-	343	387	436	520	513	460	433	450	460	400	310	280
						GHANA									
						=====									
ACCRA	5 36'N	0 10'W	65	445	509	543	559	558	461	432	427	473	542	558	506
HO	6 00'N	0 00'	-	437	475	543	559	558	487	364	317	431	499	592	540

STATION	LAT	LONG	ELEV	JAN	FEB	MAR	APR	MAY	JUN	JUL	AUG	SEP	OCT	NOV	DEC
GHANA (CON'T)															
KUMASI	6 43'N	1 36'W	287	292	356	441	465	413	308	254	206	278	355	371	328
TAFO	6 00'N	0 00'	-	420	450	492	517	481	393	313	283	295	397	456	455
TAKORADI	4 53'N	1 46'W	4	437	509	552	551	499	402	432	376	362	474	541	481
TAMALE	9 25'N	0 53'W	183	600	582	570	580	565	552	505	463	499	569	623	602
GREECE															
ATHENS	37 58'N	23 43'E	107	466	543	496	551	548	563	591	564	532	477	432	453
GREENLAND															
THULE	76 00'N	70 00'W	-	*	*	664	711	*	*	*	*	-	-	*	*
GUINEA															
BOKE	● 10 56'N	14 19'W	69	067	074	078	075	060	047	030	020	039	054	059	062
CONAKRY	● 9 34'N	13 37'W	46	041	056	066	057	042	029	016	013	027	044	047	028
LABE	● 11 19'N	12 18'W	1025	079	079	075	067	055	044	036	025	041	052	061	070
HONG KONG															
HONG KONG	22 18'N	114 10'E	65	528	449	382	367	417	438	506	441	443	623	621	566
HUNGARY															
BEKESCSABA	46 41'N	21 05'E	88	401	369	487	471	537	501	531	524	538	495	337	311
BUDAPEST	47 26'N	19 11'E	140	382	293	492	526	580	495	566	578	563	515	292	280
DEBRECEN	47 30'N	21 38'E	113	384	357	524	500	610	568	590	595	597	544	381	328
KALOCSA	46 32'N	18 59'E	108	428	401	507	535	600	522	583	581	594	534	331	339
KECSKEMET	46 54'N	19 46'E	116	398	409	507	511	585	533	566	578	572	548	357	364
KEKESTETO	47 52'N	20 01'E	991	413	502	486	469	581	511	562	589	587	563	377	336
KESZTHELY	46 46'N	17 14'E	143	426	425	560	643	631	541	602	619	608	548	328	335
KISVARDA	48 14'N	22 07'E	114	312	348	527	548	494	492	489	456	460	480	321	204
MARTONVASAR	47 21'N	18 49'E	150	409	410	575	528	633	513	557	579	521	481	284	283
PECS	46 04'N	18 12'E	124	403	427	512	551	570	501	551	556	530	468	299	321
SIOFOK	46 54'N	18 03'E	112	425	432	542	571	617	533	620	594	581	524	321	293
SOPRON	47 41'N	16 35'E	234	343	340	469	486	543	456	492	549	490	486	268	285
SZEGED	46 15'N	20 06'E	83	354	389	479	466	535	497	541	531	529	487	324	320
TISZAORS	47 32'N	20 50'E	99	389	346	501	482	556	495	537	534	542	514	310	278
ICELAND															
KEFLAVIK	64 00'N	22 40'W	-	238	375	449	491	431	506	463	526	434	312	424	704
REYKJAVIK	64 08'N	21 54'W	56	371	410	405	439	470	375	440	414	360	297	260	343
INDIA															
ADARTAL	23 05'N	79 56'E	-	722	709	684	695	672	526	445	406	571	691	729	633
ADUTHURAI	11 01'N	79 32'E	-	658	692	724	667	670	634	577	594	648	553	626	649
AGRA	27 10'N	78 02'E	-	592	574	569	568	551	507	482	473	525	572	586	567
AHMEDABAD	23 02'N	72 38'E	-	738	738	721	740	715	642	488	439	642	731	744	668
AKOLA	20 45'N	77 00'E	-	751	740	720	714	729	606	460	484	599	698	743	723
ALLAHBAD	25 28'N	81 52'E	-	728	708	674	700	690	573	515	495	579	699	731	728
BABBUR	13 57'N	76 37'E	-	760	754	758	722	715	587	499	534	584	591	746	697

STATION	LAT	LONG	ELEV	JAN	FEB	MAR	APR	MAY	JUN	JUL	AUG	SEP	OCT	NOV	DEC
						INDIA (CON'T)									
BANGALORE	12 58'N	77 35'E	-	706	707	731	688	663	513	446	513	525	549	669	699
BARODA	22 15'N	73 15'E	-	742	743	716	728	737	633	479	439	639	630	748	724
BOMBAY	18 56'N	72 50'E	-	708	708	698	679	680	494	421	407	536	659	734	721
CALCUTTA	22 30'N	88 20'E	-	630	602	607	594	577	506	457	461	521	565	611	607
CALCUTTA/DUM DUM	22 39'N	88 27'E	10	*	613	604	579	579	483	450	475	463	508	635	630
CHINSURA	22 52'N	88 25'E	-	735	721	695	695	683	516	478	505	570	635	694	718
COIMBATORE	11 00'N	76 55'E	-	685	692	712	667	659	544	486	583	637	589	599	676
DELHI	28 40'N	77 15'E	-	693	686	671	663	666	628	522	552	555	702	714	714
DHARWAR	15 27'N	75 00'E	-	751	741	729	666	645	461	396	443	529	574	722	747
HAGARI	15 10'N	77 04'E	-	704	752	740	710	679	571	506	565	586	597	746	743
JAIPUR	26 55'N	75 50'E	-	736	726	723	715	710	590	471	484	645	727	738	718
JALGAON	21 03'N	75 34'E	-	755	730	722	726	729	595	460	495	588	714	732	738
JODHPUR	26 18'N	73 01'E	-	743	734	718	714	721	706	556	528	655	721	745	726
JULLUNDAR	31 25'N	75 35'E	-	666	692	652	706	697	674	550	577	668	718	726	710
KARJAT	18 55'N	73 18'E	-	739	735	722	723	723	526	410	407	547	646	734	736
KODAIKANAL	10 14'N	77 28'E	-	664	675	675	635	640	524	421	484	523	490	529	654
KOILPATTI	9 12'N	77 53'E	-	652	667	695	636	644	587	562	576	658	557	635	655
LABANDHE	21 20'N	81 45'E	-	744	704	674	659	664	530	448	418	554	663	705	709
LAHORE	31 35'N	74 18'E	-	669	694	694	707	697	664	571	632	694	736	748	691
MADRAS	13 05'N	80 15'E	-	708	721	719	700	663	569	513	524	583	586	643	687
MADRAS	13 11'N	80 11'E	16	661	704	706	637	627	540	481	508	608	485	478	530
NAGPUR	21 09'N	79 07'E	-	741	717	698	681	675	509	427	418	565	662	733	.706
NEW DELHI	28 35'N	77 12'E	210	676	752	738	688	687	624	416	531	582	697	730	684
NIPHAD	20 06'N	74 07'E	-	757	747	728	725	731	629	451	484	621	706	749	739
PATTAMBI	10 48'N	76 12'E	-	736	716	700	667	660	477	464	516	648	576	676	715
PEDEGAON	18 12'N	74 10'E	-	744	741	718	701	703	582	455	540	581	666	725	726
POONA	18 32'N	73 51'E	559	735	771	739	735	718	571	436	441	551	636	678	686
POWERKHERA	22 50'N	78 00'E	-	752	735	695	706	704	589	456	439	546	702	757	734
RAICHUR	16 12'N	77 12'E	-	746	748	732	711	665	524	503	553	553	641	730	727
SAKHARNAGAR	18 39'N	77 45'E	-	751	722	721	701	691	548	443	463	535	657	745	732
SAMALKOT	17 03'N	82 13'E	-	743	730	701	700	673	543	523	486	520	621	697	724
SHOLAPUR	17 40'N	76 00'E	-	752	736	740	700	693	530	434	474	522	663	762	749
SRINAGAR	34 05'N	74 50'E	1593	456	396	439	520	595	571	648	598	652	651	646	334
SURAT	21 12'N	72 52'E	-	742	745	723	726	728	626	481	462	647	728	734	724
TRIVANDRUM	8 29'N	76 58'E	-	683	709	670	558	603	464	462	544	555	518	540	686
VIRANGAM	23 02'N	72 07'E	-	755	738	709	740	725	705	520	472	701	731	744	668
						INDONESIA									
DJAKARTA	6 11'S	106 50'E	8	397	416	445	469	482	493	520	531	520	467	437	411
SOEMOBITO	7 32'S	112 20'E	16	461	455	426	460	519	539	547	515	530	510	469	388
						IRAN									
BABOLSAR	● 36 43'N	52 39'E	-21	043	043	034	075	034	054	058	048	034	041	044	034
ESFAHAN	● 32 37'N	51 40'E	1590	067	073	075	-	059	070	083	083	081	087	070	061
KERMANSHAH	● 34 19'N	47 07'E	1298	071	047	054	074	057	061	078	086	093	077	063	057
MESHHAD	● 36 16'N	59 38'E	985	058	059	028	070	056	082	086	084	087	075	054	044
PAHLAVI	● 38 05'N	46 17'E	1405	034	032	022	050	-	047	059	042	028	023	032	032
SHIRAZ	● 29 36'N	52 32'E	1530	070	068	077	069	070	084	083	080	087	090	077	071
TEHERAN	● 35 41'N	51 19'E	1191	065	050	054	074	049	072	080	079	083	075	066	063

STATION	LAT	LONG	ELEV	JAN	FEB	MAR	APR	MAY	JUN	JUL	AUG	SEP	OCT	NOV	DEC
IRELAND															
VALENTIA	51 56′N	10 15′W	14	407	378	411	486	505	479	402	430	403	353	330	343
ISRAEL															
DEAD SEA	31 15′N	35 25′E	-	584	597	638	659	673	716	720	716	-	678	620	583
JERUSALEM	31 46′N	35 15′E	789	610	614	622	680	712	752	750	749	732	698	620	588
LOD	32 00′N	34 54′E	40	580	668	681	676	713	739	722	713	701	684	628	635
ITALY															
ALGHERO	40 38′N	8 17′E	40	472	420	433	475	565	575	655	618	581	483	379	373
ANCONA	43 37′N	13 21′E	105	299	386	375	472	513	516	562	533	505	436	295	301
BARI	41 07′N	16 52′E	28	432	563	460	488	509	540	566	527	493	448	340	356
BOLOGNA	44 31′N	11 18′E	43	313	388	346	461	518	488	534	504	479	423	279	281
BOLZANO	46 28′N	11 19′E	237	381	425	450	480	507	456	470	466	490	460	369	337
BRINDISI	40 39′N	17 57′E	21	455	515	422	455	508	513	564	540	523	483	387	415
CAGLIARI	39 14′N	9 03′E	12	416	422	456	494	549	580	611	589	532	481	400	392
CAMPO IMPER. M.	42 27′N	13 34′E	2138	290	316	477	462	558	502	593	596	522	512	379	418
CAPO-PALINURO	40 01′N	15 16′E	185	463	516	488	504	562	573	591	508	582	531	428	458
COZZO SPADARO	36 41′N	15 09′E	46	-	-	-	677	572	656	675	665	578	-	-	433
CROTONE	39 00′N	17 05′E	154	428	502	438	443	556	551	573	583	520	471	337	412
ETNA C. C. M.	37 42′N	15 00′E	1884	476	457	589	401	565	605	699	602	544	469	451	468
FIRENZE	43 48′N	11 12′E	48	285	332	365	483	545	557	574	545	487	411	300	263
FOGGIA	41 26′N	15 33′E	82	405	490	415	433	454	468	506	507	478	418	341	368
GENOVA	44 24′N	8 58′E	98	345	365	382	440	444	493	557	525	497	459	351	322
GRAPPA M.	45 53′N	11 48′E	1776	517	547	633	677	489	441	528	486	495	447	496	492
MARSALA	37 49′N	12 27′E	2	425	427	498	515	582	624	693	630	553	503	416	411
MESSINA	38 12′N	15 33′E	54	394	440	470	477	544	576	613	584	522	461	388	387
MILANO	45 28′N	9 17′E	120	224	329	373	470	534	503	535	507	481	388	257	191
MODENA	44 39′N	10 44′E	64	447	490	391	393	526	575	623	565	553	525	314	353
MONTE CIMONE	44 12′N	10 42′E	2173	599	-	409	-	504	414	478	489	452	409	380	-
MONTE TERMINILLO	42 28′N	12 59′E	1875	505	511	381	387	444	428	526	491	490	503	360	373
NAPOLI	40 53′N	14 17′E	110	628	389	427	488	517	556	586	552	487	466	362	368
NAPOLI (I. U. N.)	40 50′N	14 15′E	25	342	369	448	527	534	573	571	561	520	487	397	393
OLBIA	40 56′N	9 30′E	2	449	458	432	460	511	519	567	540	512	418	371	388
PALLANZA	45 55′N	8 33′E	222	577	532	411	515	512	520	551	499	511	483	382	426
PANTELLERIA	36 49′N	11 57′E	254	432	428	424	445	474	477	502	486	469	410	414	403
PESCARA	42 26′N	14 13′E	16	417	492	388	450	534	533	616	552	511	445	319	349
PIANOSA	42 35′N	10 06′E	17	445	449	435	538	579	576	591	489	532	508	400	414
PIAN ROSA′M.	45 56′N	7 42′E	2448	477	580	586	639	612	575	570	528	532	548	491	477
PISA	43 41′N	10 24′E	11	469	452	380	480	530	503	542	530	537	534	429	390
PROCIDA	40 45′N	14 02′E	80	416	400	407	396	489	504	518	475	431	440	355	350
ROMA CIAMPINO	41 48′N	12 36′E	131	445	452	407	462	516	551	578	557	511	493	404	395
SAN REMO	43 49′N	7 50′E	113	455	484	452	526	563	531	584	550	537	520	414	427
SASSARI	40 43′N	8 33′E	512	289	246	401	518	566	573	624	577	565	471	406	352
SERPEDDI M.	39 22′N	9 18′E	1048	290	301	378	466	576	621	708	670	521	420	343	323
SIRACUSA	37 04′N	15 17′E	15	405	415	428	447	488	492	500	505	455	407	365	380
SORATTE M.	42 15′N	12 30′E	660	355	376	439	615	620	687	665	635	576	488	416	362
STROMBOLI	38 48′N	15 15′E	5	366	338	479	541	602	623	646	575	508	462	365	356
TARANTO	40 28′N	17 17′E	41	374	420	498	566	647	645	683	664	598	521	410	455
TORINO	45 12′N	7 39′E	282	374	419	378	468	469	469	512	471	460	428	321	329
TRIESTE	45 39′N	13 46′E	12	346	383	378	387	414	475	524	480	466	417	362	333
UDINE	46 02′N	13 11′E	92	439	419	441	414	477	432	523	502	493	488	396	379
USTICA	38 42′N	13 11′E	259	484	518	492	498	562	565	548	576	542	489	444	430

STATION	LAT	LONG	ELEV	JAN	FEB	MAR	APR	MAY	JUN	JUL	AUG	SEP	OCT	NOV	DEC
ITALY (CON'T)															
VENEZIA	45 26'N	12 23'E	17	328	375	407	466	534	504	538	515	493	456	337	288
VIESTE	41 53'N	16 11'E	67	292	312	411	574	671	662	673	678	593	501	360	413
VIGNA DI VALLE	42 05'N	12 13'E	270	383	383	388	496	584	610	654	612	540	477	371	353
JAPAN															
ABASHIRI	44 01'N	144 17'E	-	536	[illegible]	594	531	486	455	465	389	486	532	539	540
AKITA	39 43'N	140 06'E	9	413	469	483	508	502	465	450	501	484	495	426	370
AOMORI	40 49'N	140 47'E	4	467	496	529	496	491	470	459	490	473	520	455	418
ASAHIKAWA	43 46'N	142 22'E	-	351	401	489	463	417	436	434	383	429	411	348	348
ASHIZURI	32 43'N	133 01'E	-	597	609	408	499	364	396	466	525	422	422	555	588
ASOSAN	32 52'N	131 05'E	-	400	480	420	422	397	314	377	379	363	464	504	472
ESASHI	41 52'N	140 08'E	-	310	391	441	465	424	373	454	494	476	433	381	359
FIUKUOKA	33 35'N	130 23'E	2	378	396	417	417	389	338	358	408	386	458	463	410
FUKUSHIMA	37 45'N	140 28'E	-	503	536	484	503	438	369	365	466	397	450	490	558
HACHIJO-JIMA	33 06'N	139 47'E	-	370	341	372	329	345	260	373	441	407	360	361	366
HACHINOHE	40 32'N	141 32'E	-	490	459	423	461	410	383	397	414	389	453	458	450
HAKODATE	41 49'N	140 45'E	-	633	637	608	544	492	470	446	437	493	551	560	676
HAMADA	34 54'N	132 04'E	-	320	407	425	464	442	381	420	498	413	488	481	420
HAMAMATSU	34 42'N	137 43'E	-	544	436	436	404	353	279	329	394	342	330	363	427
HIKONE	35 16'N	136 15'E	-	486	532	483	521	524	411	453	510	469	499	571	496
HIROSHIMA	34 22'N	132 26'E	-	497	533	474	484	441	404	430	501	435	512	558	544
HOFU	34 03'N	131 32'E	-	512	572	497	507	448	382	434	543	485	581	623	630
IIDA	35 31'N	137 50'E	482	512	537	509	488	464	403	430	519	443	450	488	529
INAWASHIRO	37 34'N	140 07'E	-	599	639	603	517	555	472	512	552	487	538	522	540
ISHIGAKI-JIMA	24 20'N	124 10'E	-	406	368	361	358	415	395	456	466	580	501	518	457
ISHINOMAKI	38 23'N	141 18'E	-	513	516	444	529	419	402	322	438	413	371	545	487
IZUHARA	34 12'N	129 18'E	-	508	538	417	503	487	404	429	481	389	539	624	597
KAGOSHIMA	31 34'N	130 33'E	20	458	493	454	431	400	342	437	490	471	493	525	528
KOBE	34 41'N	135 11'E	58	426	415	399	384	376	319	367	404	353	382	409	417
KOCHI	33 34'N	133 33'E	-	562	557	469	471	383	355	393	483	437	498	578	570
KUMAMOTO	32 49'N	130 43'E	38	449	459	464	430	411	358	386	453	440	491	505	483
KUSHIRO	43 59'N	144 24'E	-	576	590	579	594	527	495	464	427	512	562	621	632
KUTCHAN	42 54'N	140 45'E	-	582	577	585	578	502	465	483	467	521	572	523	537
MAEBASHI	36 24'N	139 04'E	-	555	458	464	379	437	293	274	440	418	492	562	627
MAIZURU	35 28'N	135 23'E	-	412	429	387	472	435	411	454	487	416	407	508	485
MINAMI-DAITO-ZIMA	25 50'N	131 14'E	15	321	291	274	300	296	325	369	334	359	320	317	285
MITO	36 23'N	140 28'E	29	532	482	428	405	402	320	369	386	354	368	437	502
MIYAKO	39 39'N	141 58'E	-	580	561	482	510	434	383	367	419	443	467	574	581
MIYAZAKI	31 55'N	131 25'E	-	595	578	473	453	394	388	416	520	487	509	551	600
MIZUSAWA	39 08'N	141 08'E	-	457	494	454	460	432	366	379	407	426	453	458	432
MORIOKA	39 42'N	141 10'E	-	720	720	642	601	495	455	478	486	510	586	641	643
MURORAN	42 19'N	140 59'E	-	514	584	579	631	521	432	482	465	496	586	573	569
MUROTOMISAKI	33 15'N	134 11'E	-	695	706	574	599	511	486	568	666	593	577	706	882
NAGANO	36 40'N	138 12'E	418	533	537	533	510	488	432	450	494	435	471	518	534
NAGASAKI	32 44'N	129 53'E	-	329	403	402	381	401	372	456	551	421	473	498	431
NAGOYA	35 10'N	136 58'F	-	583	617	522	526	436	398	427	466	432	474	612	611
NAZE	28 23'N	129 30'E	-	329	332	338	355	311	401	486	461	466	390	351	336
NEMURO	43 30'N	145 35'E	26	556	585	547	493	450	411	387	399	435	498	525	540
OBIHIRO	42 55'N	143 13'E	-	576	600	595	532	450	423	369	397	456	524	598	598
OITA	33 14'N	131 37'E	5	525	481	464	443	419	364	402	452	428	471	487	530
OKI-DAITO-ZIMA	24 24'N	137 17'E	25	537	470	504	522	510	539	550	547	526	499	499	400
ONAHAMA	36 57'N	140 54'E	-	578	533	376	424	361	348	357	424	386	352	474	594
OSAKA	34 39'N	135 32'E	-	490	455	398	396	314	253	355	385	245	393	425	446

STATION	LAT	LONG	ELEV	JAN	FEB	MAR	APR	MAY	JUN	JUL	AUG	SEP	OCT	NOV	DEC
JAPAN (CON'T)															
OSHIMA	34 46'N	139 23'E	-	386	496	417	388	389	253	260	438	406	347	418	415
OWASH!	34 04'N	136 12'E	-	510	433	438	399	388	327	376	439	372	424	416	458
RUMOI	43 57'N	141 38'E	-	358	343	402	400	334	360	352	292	342	355	322	321
SAGA	33 15'N	130 18'E	-	453	518	459	459	403	328	388	495	447	550	597	527
SAIGO	36 12'N	133 20'E	-	488	538	547	592	604	484	528	617	551	626	624	540
SAKATA	38 54'N	139 50'E	-	367	396	395	467	420	407	452	412	495	412	405	381
SAPPORO	43 03'N	141 20'E	17	407	445	457	451	436	415	404	405	428	436	413	413
SENDAI	38 16'N	140 54'E	-	618	619	572	591	514	419	412	495	460	528	587	619
SHIMIZU	32 47'N	132 58'E	-	512	547	439	424	393	338	383	491	459	465	564	606
SHIMONOSEKI	33 57'N	130 56'E	-	308	375	390	392	353	317	348	459	374	447	425	365
SHIONOMISAKI	33 27'N	135 46'E	-	560	598	482	480	418	394	449	543	489	443	556	605
SHIRAKAWA	37 07'N	140 13'E	-	597	605	483	540	417	[illegible]	337	413	400	387	656	650
TADOTSU	34 17'N	133 46'E	-	414	350	378	387	429	368	401	440	-	-	-	-
TAKAMATSU	34 19'N	134 03'E	9	496	498	479	465	452	390	426	485	421	426	442	462
TATENO	36 03'N	140 08'E	6	599	529	523	515	514	448	407	493	420	439	485	569
TOHOKU UNIV.	38 15'N	140 52'E	48	471	452	439	471	419	355	291	314	295	389	436	399
TOKYO	35 41'N	139 46'E	4	443	420	385	363	356	301	340	372	327	327	389	427
TOMIE	32 37'N	128 46'E	-	270	315	356	288	245	224	229	315	289	463	447	381
TORISHIMA	30 29'N	140 18'E	[illegible]	407	382	350	336	299	326	396	441	483	453	394	433
TOTTORI	35 31'N	134 11'E	17	336	337	367	410	418	374	392	452	401	432	419	363
TOYAMA	36 42'N	137 12'E	-	373	434	420	448	472	383	396	473	412	360	426	337
TSUKUBASAN	36 13'N	140 06'E	-	624	525	489	471	496	396	368	414	377	435	515	622
URUKAWA	42 10'N	142 47'E	-	381	373	395	364	359	348	310	331	375	402	369	330
UTSUNOMIYA	36 33'N	139 52'E	120	619	569	518	474	454	358	370	415	393	438	523	593
WAKAMATSU	37 29'N	139 55'E	-	562	624	537	548	505	488	515	535	524	515	495	524
WAKKANAI	45 25'N	141 41'E	-	356	392	495	479	456	410	390	382	494	476	367	341
YAKUSHIMA	30 27'N	130 30'E	-	311	347	293	419	351	410	510	533	528	311	352	329
YAMAGATA	38 15'N	140 21'E	-	523	543	506	488	[illegible]	417	440	520	467	458	487	479
YONAGO	35 26'N	133 21'E	6	418	432	457	[illegible]	511	434	455	535	471	515	499	443
KENYA															
FORT ESSEX	00 42'S	36 42'E	2463	662	662	621	552	473	496	355	364	571	583	558	590
KERICHO	00 19'S	35 28'E	2042	657	666	663	544	554	574	503	496	530	501	530	612
MARIGAT	00 35'N	36 00'E	1219	795	776	784	726	760	767	642	754	793	789	699	742
MUGUGUA	01 12'S	36 38'E	2073	595	585	557	499	457	490	427	443	581	468	550	554
NAIROBI	01 18'S	36 45'E	1799	642	665	622	560	510	509	410	439	529	552	555	608
KOREA															
INCHON	37 29'N	126 38'E	69	534	544	516	504	510	506	475	498	508	530	523	524
KANGNUNG	37 45'N	128 54'E	26	590	529	518	505	478	455	465	498	550	516	527	530
PUZAN	35 06'N	129 02'E	71	696	634	604	580	569	489	464	539	554	561	632	670
PYONGYANG	39 01'N	125 49'E	-	566	547	544	522	500	485	454	455	503	530	526	530
SEOUL	37 34'N	126 58'E	86	535	526	517	505	510	506	465	475	509	531	501	498
TAIKYU	35 53'N	128 37'E	61	804	726	619	580	540	488	460	491	514	603	638	744
UNGGI	42 19'N	130 24'E	88	588	579	543	499	461	424	424	440	496	533	511	515
WONSAN	39 11'N	127 26'E	35	597	570	530	523	490	464	423	433	477	532	529	534
YOGAMPO	39 56'N	124 22'E	12	503	540	537	514	512	505	475	503	523	540	518	551
LEBANON															
KSARA OBSEVATORY	33 49'N	35 53'E	927	486	562	580	628	679	737	741	732	709	642	558	481

STATION	LAT	LONG	ELEV	JAN	FEB	MAR	APR	MAY	JUN	JUL	AUG	SEP	OCT	NOV	DEC
MACAU															
MACAU	22 12′N	113 33′E	65	445	280	337	419	441	482	564	561	550	635	642	579
MADEIRA ISLANDS															
FUNCHAL	32 38′N	16 54′W	58	531	521	571	564	571	537	578	583	599	566	489	543
PORTO SANTO	33 01′N	16 03′W	45	548	527	612	574	630	642	648	588	618	581	526	512
MALIGASY															
TANANARIVE	18 54′S	47 32′E	1310	520	539	564	617	630	624	631	682	697	683	645	585
MALAYA															
SINGAPORE	1 19′N	103 49′E	36	432	428	420	422	417	456	389	363	519	520	408	473
MALI															
GAO	16 16′N	0 03′W	270	645	617	603	611	599	567	580	575	588	603	633	607
TESSALIT	20 12′N	0 59′E	496	790	748	729	714	698	661	697	682	691	707	691	691
MALTA															
QRENDI	35 50′N	14 26′E	135	549	511	623	594	654	689	712	726	649	604	520	556
MARIANA ISLANDS															
SAIPAN	15 14′N	145 46′E	212	561	597	658	688	646	637	517	532	506	535	553	550
WOLEAI	7 22′N	143 55′E	2	545	571	611	582	584	504	525	502	498	538	546	571
MARSHALL ISLANDS															
JALUIT	• 5 55′N	169 39′E	2	056	060	048	048	051	050	051	050	056	049	050	048
PONAPE	• 6 58′N	158 13′E	30	042	047	043	040	040	041	045	048	043	045	043	038
MAURITANIA															
ATAR	20 31′N	13 04′W	227	700	724	706	736	698	713	686	682	610	644	649	680
FORT GOUROUD	22 41′N	12 42′W	297	732	705	719	740	726	695	669	637	617	566	629	732
NEMA	16 37′N	7 16′W	269	634	633	616	600	587	533	568	575	577	593	565	565
NOUAKCHOTT	18 07′N	15 56′W	5	743	713	742	745	714	712	672	672	673	691	681	693
PORT ETIENNE	20 56′N	17 03′W	8	706	714	709	726	718	722	674	681	682	673	669	669
MEXICO															
ALTOZOMONI	19 07′N	98 38′W	3975	618	847	817	525	317	400	497	619	544	666	697	-
CHIHUAHUA	28 38′N	106 05′W	1430	342	563	390	343	402	387	339	468	513	465	510	346
CIUDAD UNIV.	19 20′N	99 11′W	2268	546	706	786	595	555	461	461	518	503	502	557	594
TACUBAYA	19 24′N	99 06′W	2300	594	623	633	578	531	514	455	483	449	501	570	592
VERACRUZ	19 12′N	96 08′W	12	503	594	-	-	643	664	541	616	616	654	630	657
-	27 30′N	110 00′W	-	672	687	688	683	688	682	649	650	685	762	678	631
-	27 30′N	107 00′W	-	672	687	688	683	688	651	649	650	685	719	678	631
-	25 00′N	109 00′W	-	562	583	582	586	584	584	527	550	553	611	560	517
-	23 00′N	110 00′W	-	570	578	584	583	629	621	583	615	582	609	585	527
-	20 00′N	106 00′W	-	582	594	594	568	570	555	569	572	550	575	568	541

STATION	LAT	LONG	ELEV	JAN	FEB	MAR	APR	MAY	JUN	JUL	AUG	SEP	OCT	NOV	DEC
							MEXICO (CON'T)								
-	20 00'N	91 00'W	-	535	594	594	524	527	491	494	528	515	562	553	508
-	17 30'N	93 00'W	-	494	534	488	445	444	411	446	441	405	445	487	482
-	17 00'N	100 00'W	-	624	610	594	567	576	554	567	574	543	570	597	616
-	30 00'N	110 00'W	-	699	721	681	724	729	687	687	686	723	717	719	679
							MONGOLIA								
ULAN-BATOR	47 51'N	106 45'E	-	639	653	657	568	619	548	530	551	553	583	538	558
							MOZAMBIQUE								
BEIRA	19 08'S	34 08'E	7	566	516	629	640	614	665	637	676	601	574	593	532
LOURENCO MARQUEZ	25 58'S	32 36'E	59	572	593	610	639	672	690	669	657	555	484	515	506
LUMBO	15 00'S	40 07'E	10	559	534	571	635	640	614	660	708	731	716	718	585
							NETHERLANDS								
DE BILT	52 06'N	5 11'E	42	341	323	414	428	466	462	432	407	416	337	269	256
WAGENINGEN	52 00'N	5 36'E	20	305	306	392	424	444	425	393	398	412	338	258	267
							NEW GUINEA								
BALIEM	4 04'S	138 57'E	1615	-	-	607	637	626	659	625	629	547	659	629	570
HOLLANDIA	2 34'S	140 29'E	99	455	474	509	352	490	531	492	495	480	489	485	473
MERAUKE	8 28'S	140 23'E	3	523	516	489	485	480	360	451	502	547	542	558	458
RABUAL	4 00'S	152 00'E	6	517	503	529	516	565	592	520	556	548	534	510	486
							NEW ZEALAND								
INVERCARGILL	46 25'S	168 19'E	0	518	511	473	429	433	399	479	504	522	508	489	495
NANDI	17 45'S	177 27'E	16	650	612	541	556	599	646	657	652	644	640	616	609
OHAKEA	40 12'S	175 23'E	51	577	537	522	502	457	486	477	520	557	531	535	544
RAOUL ISLAND	29 15'S	177 55'W	49	590	545	565	532	566	478	535	520	563	553	596	658
WELLINGTON	41 17'S	174 46'E	126	549	502	506	483	420	455	435	486	542	513	502	494
WHENUAPAI	36 47'S	174 39'E	31	532	501	509	515	461	478	478	483	523	483	511	501
							NIGER								
AGADEZ	16 59'N	7 59'E	496	757	742	701	711	684	684	687	674	705	734	753	739
BILMA	18 41'N	12 55'E	362	674	692	625	645	637	656	605	661	640	683	702	669
NAIMEY	13 29'N	2 10'E	222	698	742	724	671	662	650	601	562	622	703	732	750
							NIGERIA								
BENIN CITY	6 33'N	5 37'E	109	394	441	452	441	429	414	339	330	367	433	464	458
ENUGU	6 28'N	7 33'E	137	501	508	462	494	496	567	400	378	419	453	516	538
IBADAN	7 26'N	3 54'E	228	508	512	486	481	481	445	373	342	385	456	521	519
IKEJA	6 35'N	3 20'E	38	503	571	565	559	501	454	432	402	430	484	607	528
ILORIN	8 29'N	4 35'E	287	586	601	556	545	530	635	460	429	419	504	593	598
JOS	9 52'N	8 54'E	1286	639	630	591	558	531	530	482	463	499	568	648	655
KADUNA	10 36'N	7 27'E	646	627	628	596	579	560	546	488	449	500	563	635	644
KANO	12 03'N	8 23'E	476	628	613	589	589	578	573	561	514	570	618	634	632
MAIDUGURI	11 51'N	13 05'E	354	653	636	568	600	601	585	540	503	570	629	659	644
MAKURDI	7 41'N	8 37'E	970	595	585	530	579	564	635	485	404	487	530	584	632

STATION	LAT	LONG	ELEV	JAN	FEB	MAR	APR	MAY	JUN	JUL	AUG	SEP	OCT	NOV	DEC
						NIGERIA (CON'T)									
MAMFE (Camaroon)	5 43'N	9 17'E	152	470	503	461	439	453	406	368	345	374	427	449	467
MINNA	9 37'N	6 32'E	260	585	577	562	571	569	478	411	407	492	563	644	627
PORT HARCOURT	4 51'N	7 01'E	20	452	452	437	440	433	386	347	359	362	390	420	485
SOKOTO	13 01'N	5 15'E	352	651	632	603	600	575	602	536	513	571	623	643	643
YOLA	9 14'N	12 28'E	175	626	630	570	580	576	553	516	497	533	592	636	642
							NORWAY								
BERGEN	60 24'N	5 19'E	44	301	301	507	387	487	427	361	369	298	232	233	202
BLINDERN	• 59 56'N	10 44'E	-	022	031	040	047	043	046	045	044	035	029	022	017
BRONNOYSUND	• 65 29'N	12 13'E	13	017	034	043	040	031	033	026	035	033	021	020	006
GJERMUNDNES	• 62 37'N	7 10'E	51	019	040	038	034	036	035	028	032	034	027	024	010
GREEN HARBOR	78 00'N	14 05'E	-	*	*	442	515	*	*	*	*	317	351	*	*
HAUGASTOL	• 60 31'N	7 52'E	988	026	033	048	054	048	047	040	036	036	031	029	019
HORNSUND	• 77 00'N	15 33'E	11	*	*	007	160	*	*	*	*	616	278	*	*
KJEVIK	• 58 12'N	8 05'E	15	026	032	041	052	049	057	049	047	043	032	022	022
LILLEHAMMER	• 61 06'N	10 29'E	228	019	034	051	050	045	041	038	038	036	032	026	018
MURCHISON BAY	80 03'N	18 15'E	7	*	*	576	648	*	*	*	*	372	*	*	*
SOLA	• 58 53'N	5 38'E	13	020	033	038	044	045	045	035	035	037	026	021	013
TROMSO	69 39'N	18 57'E	118	*	422	423	492	413	*	*	368	351	309	291	*
TRONDHEIM	• 63 25'N	10 27'E	123	016	039	040	035	039	036	030	036	033	026	018	015
ULLENSVANG	• 60 20'N	6 40'E	988	023	037	047	048	044	043	040	030	037	022	021	017
UTSIRA	• 59 18'N	4 53'E	56	017	029	037	046	044	044	033	035	035	024	020	014
							PAKISTAN								
KARACHI	24 54'N	67 08'E	-	630	653	670	614	574	542	409	449	472	605	634	642
MULTAN	30 12'N	71 26'E	-	607	609	557	590	566	579	573	546	570	599	530	547
PESHAWAR	34 00'N	71 31'E	-	556	641	552	569	546	594	559	555	595	638	565	530
QUETA	30 12'N	66 57'E	-	663	638	613	680	712	750	729	747	735	754	643	585
						PALAU ISLAND									
PALAU ISLAND	7 20'N	134 29'E	-	507	499	520	515	481	492	443	467	476	479	471	545
							PANAMA								
ALBROOK A. B.	8 39'N	79 34'W	6	505	572	596	554	459	390	428	422	508	457	478	554
							PERU								
HUANCAYO	12 02'S	75 19'W	3313	705	552	645	669	695	736	760	752	707	696	669	629
						PHILIPPINES									
QUEZON CITY	14 40'N	121 05'E	-	439	389	510	575	505	477	369	404	407	451	484	511
							POLAND								
BIALOWIEZA	52 42'N	23 51'E	200	346	352	-	501	513	-	475	-	-	422	207	222
BRWINOW	52 08'N	20 43'E	96	308	350	440	526	507	490	424	431	458	429	256	296
DANZIG	54 23'N	18 37'E	-	332	528	422	473	511	525	484	483	466	378	287	270
GDYNIA	54 30'N	18 36'E	-	296	379	433	448	494	516	465	451	429	366	300	232
KASPROWY-WIERCH	49 14'N	19 59'E	2007	517	405	596	506	466	358	380	364	419	541	515	422

STATION	LAT	LONG	ELEV	JAN	FEB	MAR	APR	MAY	JUN	JUL	AUG	SEP	OCT	NOV	DEC
							POLAND (CON'T)								
KOLOBRZEG	54 11'N	15 35'E	19	431	408	446	489	564	519	490	506	495	394	268	361
SUWALKI	54 06'N	22 57'E	165	467	432	576	551	595	560	539	546	511	447	282	366
SZCZAWNO-ZDROJ	50 48'N	16 16'E	441	424	378	420	414	475	475	413	469	429	412	305	405
SZRENICA	50 48'N	15 31'E	1364	-	-	-	328	359	323	353	310	337	344	373	-
WARSAW	52 19'N	20 59'E	113	246	326	395	418	468	363	406	406	385	322	228	187
WROCLAW	51 07'N	17 05'E	116	327	361	358	377	360	487	484	458	441	390	257	265
ZAKOPANE	49 17'N	19 58'E	486	415	508	468	426	365	-	315	491	484	498	402	387
							PORTUGAL								
BRAGANCA	41 49'N	6 46'W	725	427	558	499	617	620	672	744	691	632	600	573	422
CALDAS DA SAUDE	41 22'N	8 29'W	74	424	453	464	567	584	622	649	578	524	564	488	439
COIMBRA	40 12'N	8 25'W	141	503	582	481	614	592	595	627	618	591	618	565	509
EVURA	38 34'N	7 54'W	309	492	570	518	646	644	701	743	695	640	596	544	479
FARO	37 01'N	7 55'W	14	550	626	599	700	721	763	769	746	715	652	569	555
LISBOA	38 07'N	9 01'W	77	507	585	545	652	665	698	743	710	649	613	559	490
M. ESTORIL	38 07'N	9 06'W	31	559	563	590	676	673	710	751	695	650	629	603	510
PENHAS DOURADAS	40 25'N	7 33'W	1383	470	611	512	624	646	701	784	722	672	634	564	492
PORTO	41 08'N	8 36'W	96	435	523	509	655	659	664	685	644	614	589	533	431
VENDAS NOVAS	38 07'N	8 05'W	127	500	538	483	603	525	668	706	671	619	603	457	357
							PORT. GUINEA								
BISSAU	11 52'N	15 30'W	29	615	631	707	716	676	579	525	420	554	596	594	605
KANKAN	10 23'N	9 18'E	377	625	614	596	568	561	558	500	483	523	586	595	601
SIGUIRI	11 26'N	9 10'W	362	622	633	610	589	569	564	519	482	535	591	590	598
							PORT. TIMOR								
DILI	8 06'S	125 06'E	3	530	529	557	576	608	605	593	622	616	617	587	534
							PUERTO RICO								
SAN JUAN	18 28'N	66 06'W	26	655	661	697	675	600	659	695	632	630	636	623	679
							RHODESIA AND NYASALAND								
BULAWAYO	20 09'S	28 37'E	1330	552	539	625	668	706	696	718	723	676	622	556	502
ZOMBA	• 15 23'S	35 18'E	-	039	036	038	053	054	047	046	064	061	065	050	036
							SAMOA								
APIA	• 13 48'S	172 00'W	5	037	039	045	045	050	046	053	056	050	048	043	037
							SAO TOME								
ILHA DE	0 23'N	6 43'E	8	378	404	392	438	485	479	431	420	414	396	412	385
							SENEGAL								
DAKAR	14 43'N	17 26'W	17	563	594	631	629	610	594	503	424	476	517	550	536

STATION	LAT	LONG	ELEV	JAN	FEB	MAR	APR	MAY	JUN	JUL	AUG	SEP	OCT	NOV	DEC
SIERRA LEONE (CON'T)															
LUNGI	8 37'N	13 12'W	38	499	508	546	590	473	498	336	386	426	568	513	535
SPAIN															
ALMERIA	37 00'N	2 30'W	-	537	568	590	602	586	595	614	611	589	570	539	514
BADAJOZ	39 00'N	7 00'W	-	442	516	458	435	448	600	630	619	570	522	492	438
LAS ROZAS	40 30'N	3 30'W	-	449	540	513	582	567	580	626	616	558	518	470	443
SAN PABLO	37 30'N	6 00'W	-	392	531	530	572	565	573	592	571	552	503	446	425
SPANISH W. AFRICA															
CABO JUBY	27 56'N	12 55'W	6	585	583	574	570	550	506	491	529	540	564	544	539
SUDAN															
EL-FASHER	13 37'N	25 20'E	730	620	639	636	574	582	573	570	595	609	625	632	605
JUBA	4 52'N	31 37'E	457	557	553	522	537	593	583	628	565	589	604	582	580
KHARTOWN	15 36'N	32 33'E	380	649	650	650	627	613	576	574	570	589	611	639	647
PORT SUDAN	19 35'N	37 13'E	3	629	632	660	666	654	602	605	596	633	601	609	552
TOZI	12 30'N	34 00'E	440	570	572	580	531	550	524	500	516	547	558	550	566
WAD MEDANI	14 24'N	33 29'E	405	632	639	632	599	614	573	528	560	595	670	646	653
SWAN ISLAND															
SWAN ISLAND	17 24'N	83 56'W	18	657	632	692	680	652	571	609	585	625	543	587	582
SWEDEN															
ERKEN	59 50'N	18 38'E	-	363	486	512	473	483	483	474	422	436	316	210	233
FROSON	63 12'N	14 29'E	364	383	595	589	541	543	515	463	487	414	314	249	270
HARADS	66 05'N	20 57'E	-	267	400	400	364	350	406	501	409	360	248	171	829
KARLSTAD	59 22'N	13 28'E	47	362	456	509	448	527	567	485	476	460	326	208	246
KIRUNA	67 48'N	20 24'E	-	*	550	584	615	499	*	430	421	395	355	378	*
SANDVIKEN	60 37'N	16 48'E	-	255	419	445	488	533	472	494	450	438	329	256	254
STOCKHOLM	59 21'N	17 57'E	43	326	406	494	457	501	500	499	482	435	343	246	278
SVALOV	55 55'N	13 07'E	72	308	299	438	440	475	517	440	430	493	390	215	147
TEG	63 49'N	20 04'E	-	367	468	480	488	506	582	560	504	441	331	137	117
TORSLANDA	57 42'N	11 58'E	6	263	324	431	474	490	549	449	454	493	349	177	137
ULTUNA	59 49'N	17 49'E	-	325	476	566	474	467	464	429	449	309	284	275	286
VISBY	57 39'N	18 20'E	47	243	398	492	530	561	582	498	480	474	326	183	161
SWITZERLAND															
BASLE	47 35'N	7 35'E	317	390	486	385	437	515	457	-	-	500	316	206	316
DAVOS	46 48'N	9 49'E	1590	532	576	605	606	546	521	533	511	520	518	498	512
GENEVE	46 15'N	6 10'E	-	019	032	047	052	052	057	064	061	054	040	022	014
HOCHSERFAUS	47 13'N	8 17'E	1817	533	701	642	611	604	608	584	536	582	583	485	539
JUNGFRAUJOCH	46 32'N	7 58'E	3472	612	670	718	699	573	571	664	630	508	557	589	599
LOCARNO-MONTL	46 10'N	8 48'E	379	506	542	532	498	479	534	562	529	507	459	455	471
WEISSFLUHJOCH	46 50'N	9 48'E	2670	688	826	679	757	579	422	469	439	639	583	610	628
ZURICH	47 23'N	8 33'E	-	309	358	443	472	444	520	513	491	463	331	295	284

STATION	LAT	LONG	ELEV	JAN	FEB	MAR	APR	MAY	JUN	JUL	AUG	SEP	OCT	NOV	DEC
							THILAND								
BANGKOK	13 44′N	100 30′E	20	600	619	526	537	532	504	431	447	429	469	620	628
CHIANGMAI	18 47′N	98 59′E	-	603	596	509	550	547	478	395	503	522	578	631	663
NAKHON PHANOM	17 30′N	104 40′E	142	656	511	503	507	518	381	373	469	391	592	622	641
SONGKHLA	7 11′N	100 37′E	15	658	676	583	568	550	572	528	529	506	460	521	564
							TRINIDAD								
PORT-OF-SPAIN	10 38′N	61 24′W	-	587	647	674	562	518	503	507	587	613	570	555	587
							TUNISIA								
TUNIS-EL AOUINA	36 50′N	10 14′E	3	606	589	562	628	679	653	704	696	-	542	559	543
							UGANDA								
MOROTO	2 31′N	34 40′E	1372	716	672	660	642	674	676	559	644	664	793	687	691
							UNION OF SOUTH AFRICA								
ALEXANDER BAY	28 34′S	16 32′E	21	727	712	693	707	687	684	662	697	712	713	715	706
BLOEMFONTEIN	29 07′S	26 13′E	1422	635	617	609	663	658	695	710	734	716	670	685	645
CAPETOWN	33 54′S	18 27′E	19	712	681	675	607	527	594	586	589	640	646	687	696
CAPETOWN (WINGFIELD)	33 54′S	18 32′E	17	715	682	682	610	632	602	567	580	633	652	660	684
DURBAN	29 50′S	31 02′E	5	475	507	544	557	574	624	595	575	532	474	470	486
KEETMANSHOOP	26 34′S	18 07′E	1066	723	707	675	724	737	753	769	762	759	741	746	727
KIMBERLY	28 48′S	24 46′E	1197	592	608	595	645	640	671	676	724	711	693	684	659
MARION ISLAND	46 51′S	37 45′E	23	477	505	492	453	460	453	499	541	535	551	530	497
MAUN	19 59′S	23 25′E	945	536	524	575	589	645	660	692	708	682	613	588	547
PIETERSBURG	23 52′S	29 27′E	1230	613	594	620	648	703	717	658	678	625	632	635	581
PORT ELIZABETH	33 59′S	25 36′E	61	594	630	592	563	583	632	622	619	603	587	630	589
PRETORIA	25 45′S	28 14′E	1369	575	557	588	607	644	690	686	711	650	605	587	552
ROODEPLAAT	26 35′S	28 21′E	1189	514	606	606	641	676	696	663	705	634	615	613	558
SWAKOPMUND	22 41′S	14 31′E	-	603	585	619	609	601	643	552	631	607	641	656	620
UPINGTON	28 26′S	21 16′E	814	648	631	621	641	672	731	701	705	678	652	649	637
WINDHOEK	22 34′S	17 06′E	1217	638	609	615	680	714	758	787	778	740	698	683	669
							U. S. S. R.								
ARALSKOYE MORE	46 41′N	61 40′E	62	609	625	606	589	696	693	614	634	660	551	447	451
ARARAT PLAIN	40 11′N	44 24′E	-	534	485	481	560	654	693	704	706	677	694	512	434
ARKHANGLSK	64 30′N	40 42′E	4	347	350	512	574	414	473	500	462	311	272	216	422
CAPE CHELYUSKIN	77 43′N	104 17′E	12	*	*	595	672	*	*	*	*	356	462	*	*
CHETYREHSTOLBOVOY I	70 37′N	162 24′E	30	*	612	668	702	630	*	*	397	377	326	833	*
CHITA (TCHITA)	52 03′N	113 29′E	671	547	629	631	600	559	519	461	404	498	521	510	457
DIXON ISLAND	73 30′N	80 24′E	17	*	756	594	726	*	*	*	416	347	440	*	*
HAYES ISLAND	80 37′N	58 03′E	20	*	*	565	509	*	*	*	*	276	879	*	*
JAKUTSK	62 01′N	129 43′E	98	532	589	694	705	575	571	476	531	492	482	483	484
KAUNAS	54 56′N	23 59′E	71	322	350	515	471	501	503	496	463	433	352	205	261
KHARBOROVSK	48 31′N	135 07′E	86	605	651	590	482	497	479	458	468	509	478	535	569
KIEV	50 24′N	30 32′E	167	340	392	420	380	528	490	515	509	457	438	251	273
KICHINEV	49 00′N	28 51′E	90	425	455	471	468	555	542	611	570	540	528	298	384
KOTELNYI ISLAND	76 00′N	137 54′E	10	*	*	585	690	*	*	*	*	327	360	*	*
KUIBYCHEV	53 14′N	50 10′E	137	385	478	520	573	535	516	536	516	417	330	359	292
LENINGRAD	59 57′N	30 42′E	71	293	271	529	467	472	510	527	464	392	265	213	257

STATION	LAT	LONG	ELEV	JAN	FEB	MAR	APR	MAY	JUN	JUL	AUG	SEP	OCT	NOV	DEC
						U.S.S.R. (CON'T)									
NOVOSIBIRSK	54 54'N	82 57'E	130	516	554	594	503	513	505	493	495	494	332	324	390
ODESSA	46 26'N	30 46'E	43	350	399	460	462	577	537	598	579	535	517	288	328
OIMYAKON	63 16'N	143 09'E	740	634	686	752	740	600	510	496	567	496	515	603	647
OKHOTSK	59 22'N	143 12'E	6	584	696	741	610	520	449	358	480	452	522	516	591
OLENEK	68 30'N	112 26'E	127	*	587	664	697	578	*	*	419	364	428	578	*
OMSK	55 01'N	73 23'E	120	508	524	581	564	521	548	485	506	486	334	369	439
PREOBRAZHENIA ISLAND	74 40'N	112 50'E	24	*	919	586	617	*	*	*	373	308	302	*	*
SEMIPALATINSK	50 25'N	80 18'E	190	651	674	696	507	578	579	574	567	636	486	408	524
SVERDLOVSK	56 44'N	61 04'E	290	445	471	615	570	501	491	496	483	415	301	338	369
TASHKENT	41 20'N	69 18'E	478	394	422	435	485	566	618	653	649	638	528	467	402
TBILISI	41 43'N	44 48'E	403	389	466	406	499	514	522	584	580	518	488	355	390
TIKHAYA BAY	80 20'N	52 48'E	16	*	*	-	-	*	*	*	*	373	-	*	*
TURUKHANSK	65 47'N	87 57'E	38	575	561	593	685	569	497	510	479	293	378	399	*
UEDINENIA ISLAND	77 30'N	82 14'E	17	*	*	581	676	*	*	*	*	280	377	*	*
VERKHOYANSK	67 33'N	133 23'E	137	*	596	653	706	578	*	460	501	428	504	476	*
VLADIVOSTOK	43 16'N	132 03'E	80	605	641	584	495	518	413	434	388	551	540	597	555
WELLEN	66 10'N	169 53'E	6	488	477	600	649	601	529	442	354	262	353	239	973
WRANGEL ISLAND	70 58'N	178 32'E	3	*	581	658	692	561	*	*	359	311	388	*	*
YUZNO-SAKHALINSK	46 57'N	142 43'E	22	556	641	595	534	498	422	402	414	463	475	525	642
						UNITED ARAB REPUBLIC									
GIZA	30 02'N	31 13'E	21	580	623	672	670	656	671	667	664	659	626	570	565
						UNITED KINGDOM									
ABERPORTH	52 08'N	4 34'W	115	353	363	423	457	521	589	431	454	471	360	300	309
CAMBRIDGE	52 13'N	0 06'E	23	333	331	376	394	443	434	434	396	407	384	292	278
ESKDALEMUIR	55 19'N	3 12'W	246	406	297	355	410	433	371	379	368	385	352	275	264
GARSTON; WATFORD	51 42'N	0 23'W	85	235	279	322	372	394	388	375	367	367	300	228	215
KEW OBSER.	51 28'N	0 19'W	5	251	282	330	394	413	416	395	390	382	322	263	236
LERWICK OBSERV.	60 08'N	1 11'W	82	354	383	382	404	415	432	345	328	382	318	301	286
ROTHANSTED	51 48'N	0 21'W	128	312	344	374	408	429	425	386	379	376	324	272	243
						UNITED STATES									
AK ADAK	51 53'N	176 38'W	5	339	375	301	386	355	325	319	317	339	360	357	326
ANNETTE	55 02'N	131 34'W	34	341	380	415	448	451	405	414	400	385	324	312	291
BARROW	71 18'N	156 47'W	4	*	446	565	545	374	*	*	348	310	285	356	*
BETHEL	60 47'N	161 48'W	46	380	466	514	511	459	422	376	335	378	370	330	286
BETTLES	66 55'N	151 31'W	205	306	472	555	583	553	*	459	418	432	376	286	*
BIG DELTA	64 00'N	145 44'W	388	363	484	562	559	536	495	474	463	451	394	353	156
FAIRBANKS	64 49'N	147 52'W	138	315	471	552	544	517	486	454	425	427	373	328	056
GULKANA	62 09'N	145 27'W	481	368	472	555	568	514	489	472	462	445	421	336	239
HOMER	59 38'N	151 30'W	22	399	451	508	521	496	486	465	427	415	412	376	299
JUNEAU	58 22'N	134 35'W	7	321	350	391	428	402	392	371	349	325	284	280	228
KING SALMON	58 71'N	156 39'W	15	451	494	527	500	464	428	402	374	404	437	416	392
KODIAK	57 45'N	152 20'W	34	382	423	491	490	427	424	408	411	399	421	368	330
KOTZEBUE	66 52'N	162 38'W	5	236	447	535	560	535	*	449	406	416	385	225	000
MC GRATH	62 58'N	155 37'W	103	350	457	524	524	476	441	405	379	398	359	325	212
NOME	64 30'N	165 26'W	7	273	459	509	538	507	487	416	376	402	381	268	046
SUMMIT	63 20'N	149 08'W	733	370	459	537	551	523	454	414	390	406	399	365	206
YAKUTAT	59 31'N	139 40'W	9	324	356	415	438	397	373	351	338	332	323	287	233
AL BIRMINGHAM	33 34'N	86 45'W	192	425	464	490	531	532	529	508	521	507	520	470	427

STATION	LAT	LONG	ELEV	JAN	FEB	MAR	APR	MAY	JUN	JUL	AUG	SEP	OCT	NOV	DEC

UNITED STATES (CON'T)
=====================

STATION	LAT	LONG	ELEV	JAN	FEB	MAR	APR	MAY	JUN	JUL	AUG	SEP	OCT	NOV	DEC
MOBILE	30 41'N	88 15'W	67	457	495	513	538	536	519	483	493	492	531	485	446
MONTGOMERY	32 18'N	86 24'W	62	435	472	499	545	544	545	517	526	505	530	485	445
AR FORT SMITH	35 20'N	94 22'W	141	474	499	508	518	549	574	579	571	532	533	491	469
LITTLE ROCK	34 44'N	92 14'W	81	457	494	504	515	553	580	570	565	535	539	480	453
AZ PHOENIX	33 26'N	112 01'W	339	613	657	685	747	767	756	698	693	701	676	628	600
TUCSON	32 07'N	110 56'W	779	633	665	692	744	765	755	658	657	680	671	637	612
WINSLOW	35 01'N	110 44'W	1488	622	658	687	731	744	746	657	650	681	668	639	608
YUMA	32 40'N	114 36'W	63	642	678	718	762	782	777	689	703	709	687	650	627
CA ARCATA	40 59'N	124 06'W	69	418	460	479	531	534	536	506	492	507	468	411	409
BAKERSFIELD	35 25'N	119 03'W	150	490	551	619	673	720	756	752	736	706	649	545	468
CHINA LAKE	35 41'N	117 41'W	681	587	619	675	718	732	755	732	796	704	658	602	586
DAGGETT	34 52'N	116 47'W	588	602	632	682	728	744	761	730	723	708	667	617	593
EL TORO	33 40'N	117 44'W	116	572	594	610	613	594	605	663	652	606	584	564	564
FRESNO	36 46'N	119 43'W	100	440	524	619	678	714	750	752	741	714	653	535	417
LONG BEACH	33 49'N	118 09'W	17	563	586	611	616	592	590	645	635	594	573	554	552
LOS ANGELES	33 56'N	118 24'W	32	564	587	615	621	590	584	647	630	588	570	556	555
MOUNT SHASTA	41 19'N	122 19'W	1093	450	502	532	589	634	666	722	691	665	582	463	446
NEEDLES	3 46'N	114 37'W	270	322	423	554	711	848	922	833	719	619	476	362	304
OAKLAND	37 44'N	122 12'W	2	492	540	585	627	637	644	650	630	619	565	510	489
POINT MUGU	34 07'N	119 07'W	4	568	592	623	622	579	566	504	586	563	563	560	564
RED BLUFF	40 09'N	122 15'W	108	436	506	565	635	687	711	748	717	690	602	476	428
SACRAMENTO	38 31'N	121 30'W	8	427	509	593	657	702	735	753	729	699	622	498	420
SAN DIEGO	32 44'N	117 10'W	9	572	596	610	613	574	570	614	621	594	582	569	567
SAN FRANCISCO	37 37'N	122 23'W	5	490	534	583	626	641	651	669	649	633	570	508	483
SANTA MARIA	34 54'N	120 27'W	72	537	564	609	615	614	646	656	639	611	596	554	544
SUNNYVALE	37 25'N	122 04'W	12	507	546	593	632	655	672	683	664	637	578	518	493
CO COLORADO SPRINGS	38 49'N	104 43'W	1881	645	643	633	635	614	649	619	624	647	647	607	618
DENVER	39 45'N	104 52'W	1625	632	632	634	622	617	643	636	633	642	632	587	602
EAGLE	39 39'N	106 55'W	1985	565	602	621	639	652	686	668	645	656	634	575	566
GRAND JUNCTION	39 07'N	108 32'W	1475	580	616	637	655	687	711	690	674	677	645	597	586
PUEBLO	38 17'N	104 31'W	1439	635	630	633	641	623	667	647	647	651	641	603	605
CT HARTFORD	41 56'N	72 41'W	55	394	426	421	443	455	461	462	445	441	436	357	351
CU GUANTANAMO BAY	19 54'N	75 09'W	16	597	617	633	641	594	568	606	597	579	560	579	582
DC WASHINGTON	38 57'N	77 27'W	88	417	447	460	480	496	520	509	499	494	479	420	383
DE WILMINGTON	39 40'N	75 36'W	24	428	462	476	490	494	515	510	500	490	477	427	401
FL APALACHICOLA	29 44'N	85 02'W	6	458	497	532	585	599	556	512	506	518	553	516	466
DAYTONA BEACH	29 11'N	81 03'W	12	507	530	555	585	564	509	504	503	496	500	507	489
JACKSONVILLE	30 30'N	81 42'W	9	494	523	554	580	561	524	508	508	489	499	504	477
MIAMI	25 48'N	80 16'W	2	513	540	555	570	530	481	502	486	477	496	508	521
ORLANDO	28 33'N	81 20'W	36	520	537	563	588	571	511	510	500	500	516	529	510
TALAHASSEE	30 23'N	84 22'W	21	480	509	538	569	555	523	493	503	506	537	509	473

UNITED STATES (CON'T)

STATION	LAT	LONG	ELEV	JAN	FEB	MAR	APR	MAY	JUN	JUL	AUG	SEP	OCT	NOV	DEC
TALLAHASSEE	30 23′N	84 22′W	21	480	509	538	569	555	523	493	503	506	537	509	473
TAMPA	27 58′N	82 32′W	3	518	538	564	590	573	517	496	494	496	528	527	507
WEST PALM BEACH	26 41′N	80 06′W	6	495	514	543	558	530	479	505	496	467	471	491	501
GA ATLANTA	33 39′N	84 26′W	315	433	465	494	536	531	528	508	517	496	516	485	437
AUGUSTA	33 22′N	81 58′W	45	450	484	505	548	535	525	506	504	490	522	500	462
MACON	32 42′N	83 39′W	110	450	479	[illegible]	549	540	530	501	518	497	528	503	457
SAVANNAH	32 08′N	81 12′W	16	458	484	[illegible]	555	531	510	501	488	469	510	496	464
HI BARBERS POINT	21 19′N	158 04′W	10	529	550	547	555	573	582	584	587	579	559	540	533
HILO	19 43′N	155 04′W	11	475	465	442	433	453	481	473	475	490	484	446	450
HONOLULU	21 20′N	157 55′W	5	517	533	539	544	566	576	580	586	578	554	526	518
LIHUE	21 59′N	159 21′W	45	490	501	493	498	529	535	538	542	558	525	485	489
IA BURLINGTON	40 47′N	91 07′W	214	455	495	492	513	543	580	584	569	534	528	457	415
DES MOINES	41 32′N	93 39′W	294	470	508	504	523	542	581	588	571	545	541	466	435
MASON CITY	43 09′N	93 20′W	373	482	519	514	517	552	578	585	577	546	532	452	430
SIOUX CITY	42 24′N	96 23′W	336	479	510	508	534	553	581	595	579	547	537	470	438
ID BOISE	43 34′N	116 13′W	874	432	528	578	625	664	674	734	694	679	605	482	434
LEWISTON	46 23′N	117 01′W	438	349	422	478	505	542	551	658	621	584	493	357	334
POCATELLO	42 55′N	11 23′W	1365	465	543	601	619	664	678	729	705	685	630	514	457
IL CHICAGO	41 47′N	87 45′W	190	416	451	475	491	519	549	545	538	516	493	404	363
MOLINE	41 27′N	90 31′W	181	432	478	477	490	509	539	543	535	516	503	420	385
SPRINGFIELD	39 50′N	89 40′W	187	441	483	475	502	539	574	576	559	541	520	450	405
IN EVANSVILLE	38 03′N	87 32′W	118	404	440	464	490	513	543	538	533	512	510	428	381
FORT WAYNE	41 00′N	85 12′W	252	361	405	416	455	484	504	501	497	481	462	358	322
INDIANAPOLIS	39 44′N	86 17′W	246	372	[illegible]	430	463	488	511	506	509	493	475	384	343
SOUTH BEND	41 42′N	86 19′W	236	339	391	425	467	500	525	519	521	492	462	354	307
KS DODGE CITY	37 46′N	99 58′W	787	575	596	593	615	602	646	643	631	613	606	555	553
GOODLAND	39 22′N	101 42′W	1124	584	585	586	604	595	645	649	632	608	612	561	562
TOPEKA	39 04′N	95 38′W	270	498	517	515	541	553	582	596	590	560	549	500	466
WITCHITA	37 39′N	97 25′W	408	543	560	563	581	586	621	627	623	587	581	539	519
KY LEXINGTON	38 02′N	84 36′W	301	383	417	443	484	503	520	518	518	497	489	412	371
LOUISVILLE	38 11′N	85 44′W	149	386	424	446	480	495	521	514	517	497	490	411	375
LA BATON ROUGE	30 32′N	91 09′W	23	432	473	502	525	536	535	492	503	497	531	466	431
LAKE CHARLES	30 07′N	93 13′W	3	396	449	476	490	530	548	504	497	502	560	459	407
NEW ORLEANS	29 59′N	90 15′W	3	451	494	512	555	564	557	511	515	511	540	486	448
SHREVEPORT	32 28′N	93 49′W	79	444	486	500	509	540	571	566	566	536	550	494	454
MA BOSTON	42 22′N	71 02′W	5	400	429	441	448	471	497	491	466	484	459	367	376
MD BALTIMORE	39 11′N	76 40′W	47	431	463	477	490	495	514	510	494	492	479	430	401
PATUXENT RIVER	38 17′N	76 25′W	14	432	464	478	504	508	519	508	501	496	481	446	415
ME BANGOR	44 48′N	68 49′W	62	429	475	496	498	506	508	523	513	499	461	380	401
CARIBOU	46 52′N	68 01′W	190	443	510	537	500	465	481	497	484	452	400	324	373
PORTLAND	43 39′N	70 19′W	19	402	429	430	446	457	468	466	461	453	439	353	361
MI ALPENA	45 04′N	83 34′W	210	347	407	469	488	504	514	530	505	461	411	312	291
DETROIT	42 25′N	83 01′W	191	352	412	434	474	499	510	515	494	482	453	349	321
FLINT	42 58′N	83 44′W	233	331	392	419	456	483	496	504	489	463	434	321	296
GRAND RAPIDS	42 53′N	85 31′W	245	318	399	444	480	511	535	537	527	489	449	332	297
HOUGHTON	47 10′N	88 30′W	329	262	345	445	484	490	503	519	492	416	393	262	234
SAULT STE. MARIE	46 28′N	84 22′W	221	315	419	483	487	497	495	517	490	427	387	288	295
TRAVERSE CITY	44 44′N	85 35′W	192	292	371	454	486	506	523	537	512	463	413	303	271
MN DULUTH	46 50′N	92 11′W	432	409	473	489	485	484	484	523	498	449	421	336	349
INTERNATIONAL FAL	48 34′N	93 23′W	361	[illegible]	498	514	519	510	508	544	528	472	430	312	365
MINNEAPOLIS-ST. P	44 53′N	93 13′W	255	441	501	502	499	509	527	554	537	499	473	389	377
ROCHESTER	43 55′N	92 30′W	402	432	478	483	484	495	520	536	526	491	467	384	374
MO COLUMBIA	38 49′N	92 13′W	270	443	477	481	501	542	572	592	579	534	524	452	413
KANSAS CITY	39 18′N	94 43′W	315	478	495	495	520	541	569	589	575	527	526	482	453

STATION	LAT	LONG	ELEV	JAN	FEB	MAR	APR	MAY	JUN	JUL	AUG	SEP	OCT	NOV	DEC
UNITED STATES (CON'T) (CON'T)															
SPRINGFIELD	37 14 N	93 23'W	387	466	484	492	521	541	569	578	574	535	527	474	446
ST. LOUIS	38 45'N	90 23'W	172	453	482	491	514	540	573	574	560	537	522	461	418
MS JACKSON	32 19'N	90 05 W	101	436	478	510	539	556	560	536	537	520	535	478	439
MERIDIAN	32 20'N	88 45'W	94	431	472	494	524	533	543	512	524	501	529	475	433
MT BILLINGS	45 48'N	108 32'W	1088	484	517	551	533	562	595	671	648	593	557	472	474
CUT BANK	48 36'N	112 22'W	1170	471	518	555	534	559	561	647	619	569	534	463	451
DILLON	45 5'N	112 33'W	1588	505	560	584	569	583	586	672	645	607	567	492	486
GLASGOW	48 13'N	106 37'W	700	444	498	538	534	542	561	620	606	561	531	452	439
GREAT FALLS	47 29'N	111 22'W	1116	460	519	562	529	546	576	658	626	570	547	454	420
HELENA	46 36'N	112 00'W	1188	436	494	539'	524	548	558	658	621	577	535	456	430
LEWISTOWN	47 03'N	109 27'W	1264	448	491	536	511	533	564	646	614	564	529	449	441
MILES CITY	46 26'N	105 52'W	803	471	517	556	543	558	587	646	636	588	552	478	467
MISSOULA	46 55 N	114 05'W	972	329	405	465	489	526	529	657	607	557	473	364	322
NC ASHEVILLE	35 26'N	82 32'W	661	462	486	507	535	518	510	498	495	483	511	491	454
CAPE HATTERAS	35 16'N	75 33'W	2	436	475	513	569	563	560	538	519	521	504	502	452
CHARLOTTE	35 13'N	80 56'W	234	457	484	510	544	532	528	513	515	501	520	497	461
CHERRY POINT	34 54'N	76 53'W	11	476	507	534	574	552	533	513	496	504	515	516	487
GREENSBORO	36 05'N	79 57'W	270	468	494	514	543	537	536	522	517	506	514	495	466
RALEIGH	35 52'N	78 47'W	134	451	477	498	530	519	512	497	491	491	496	476	446
ND BISMARCK	46 46'N	100 45'W	502	490	544	552	515	545	564	616	605	554	526	447	444
FARGO	46 54'N	96 48'W	274	438	498	520	521	541	546	598	589	535	509	406	406
MINOT	48 16'N	101 17'W	522	439	487	510	524	548	541	593	586	535	515	415	409
NE GRAND ISLAND	40 58'N	98 19'W	566	523	532	535	566	571	613	621	604	570	568	512	496
NORTH OMAHA	41 22'N	96 01'W	404	510	524	521	523	543	580	590	580	521	529	453	454
NORTH PLATTE	41 08'N	100 41'W	849	551	559	566	577	576	620	638	620	592	591	530	531
SCOTTSBLUFF	41 52'N	103 36'W	1206	555	566	562	562	561	611	640	626	611	585	519	523
NH CONCORD	43 12'N	71 30'W	105	401	426	429	449	461	466	470	459	443	431	349	352
NJ LAKEHURST	40 02'N	74 20'W	37	425	450	462	483	484	485	477	475	471	467	417	396
NEWARK	40 42'N	74 10'W	9	431	457	467	483	489	491	493	487	479	472	410	391
NM ALBUQUERQUE	35 03'N	106 37'W	1619	643	666	682	714	728	737	697	696	697	683	648	632
CLAYTON	36 27'N	103 09'W	1515	638	637	650	659	628	664	639	640	646	651	613	618
FARMINGTON	36 45 N	108 14'W	1677	633	662	670	691	705	731	694	689	696	675	630	608
ROSWELL	33 24'N	104 32'W	1103	627	655	682	703	705	720	685	678	666	655	617	611
TRUTH OR CONSEQUE	33 14'N	107 16'W	1481	666	690	710	741	733	731	664	669	674	675	661	640
TUCUMCARI	35 11'N	103 36'W	1231	640	645	662	673	664	683	658	658	647	639	616	623
ZUNI	35 06'N	108 48'W	1965	625	644	652	695	710	716	634	632	670	662	623	609
NV ELKO	40 50'N	115 47'W	1547	541	598	618	634	667	693	735	721	713	659	561	534
ELY	39 17'N	114 52'W	1906	605	631	661	663	667	688	685	689	716	677	605	583
LAS VEGAS	36 05'N	115 10'W	664	641	681	714	748	760	763	725	718	728	694	640	623
LOVELOCK	40 04'N	118 33'W	1190	613	659	690	719	739	752	779	770	757	711	624	597
RENO	39 30'N	119 47'W	1341	596	639	681	714	729	739	754	744	741	692	601	575
TONOPAH	38 04'N	117 08'W	1653	646	682	717	736	742	764	756	749	745	713	647	633
WINNEMUCCA	40 54'N	117 48'W	1323	544	595	622	658	684	703	750	731	720	660	560	537
YUCCA FLATS	36 57'N	116 03'W	1197	644	662	700	729	741	750	743	729	729	695	631	624
NY ALBANY	42 45'N	73 48'W	89	390	421	430	453	457	473	484	471	452	426	319	338
BINGHAMTON	42 13'N	75 59'W	499	322	346	372	420	435	460	465	447	434	401	300	275
BUFFALO	42 56'N	78 44'W	215	301	326	389	447	465	493	498	476	446	411	301	272
MASSENA	44 56'N	74 52'W	63	372	408	445	465	473	486	492	472	447	406	314	315
NEW YORK (CN PRK)	40 47'N	73 58'W	57	393	416	438	455	474	468	473	462	457	446	367	349
NEW YORK (LGA)	40 46 N	73 54'W	16	429	458	471	486	490	493	500	493	482	473	408	394
ROCHESTER	43 07'N	77 40'W	169	317	346	397	456	468	497	500	479	450	411	303	271
SYRACUSE	43 07'N	76 07'W	124	335	354	391	451	460	486	493	474	453	409	300	276
OH AKRON-CANTON	40 55'N	81 26'W	377	338	376	408	454	483	503	500	497	480	453	349	307
CINCINNATI	39 04'N	84 40'W	271	366	406	421	461	483	503	496	504	484	474	382	345

UNITED STATES (CON'T) (CON'T)

	STATION	LAT	LONG	ELEV	JAN	FEB	MAR	APR	MAY	JUN	JUL	AUG	SEP	OCT	NOV	DEC
	CLEVELAND	41 24'N	81 51'W	245	313	353	393	453	488	504	512	494	471	438	329	282
	COUMBUS	40 00'N	82 53'W	254	349	381	408	449	476	496	491	508	478	462	360	322
	DAYTON	39 54'N	84 13'W	306	370	408	426	465	491	513	507	510	491	472	377	338
	TOLEDO	41 36 N	83 48'W	211	353	402	426	465	498	514	518	505	485	462	353	319
	YOUNGSTOWN	41 16'N	80 40'W	361	309	343	379	429	460	481	486	470	452	428	320	278
OK	OKLAHOMA CITY	35 24'N	97 36 W	397	512	528	543	554	551	589	596	593	551	548	521	500
	TULSA	36 12'N	95 54'W	206	481	499	512	517	524	555	569	569	527	525	490	469
OR	ASTORIA	46 09'N	123 53'W	7	319	374	404	440	473	445	492	481	480	407	332	299
	BURNS	43 35'N	119 03'W	1271	436	498	527	564	599	623	691	658	633	555	455	427
	MEDFORD	42 22'N	122 52'W	396	342	446	491	554	591	623	694	665	611	507	369	312
	NORTH BEND	43 25'N	124 15 W	5	387	440	467	516	542	545	592	563	537	473	399	374
	PENDLETON	45 41'N	118 51'W	456	345	414	482	524	566	587	674	638	605	511	368	327
	PORTLAND	45 36'N	122 36'W	12	306	373	413	456	488	485	574	535	489	406	324	285
	REDMOND	44 16'N	121 09'W	940	452	498	535	579	608	625	687	656	625	542	451	437
	SALEM	44 55'N	123 01'W	61	316	387	431	475	509	506	603	565	529	424	333	296
PA	ALLENTOWN	40 39'N	75 26'W	117	411	439	454	470	474	486	494	481	466	460	390	369
	ERIE	42 05'N	80 11'W	225	287	346	397	459	478	505	514	456	460	425	301	255
	HARRISBURG	40 13'N	76 51'W	106	410	438	453	469	478	494	494	481	474	459	390	376
	PHILADELPHIA	39 53'N	75 15'W	9	420	447	460	475	480	496	492	488	477	467	413	390
	PITTSBURG	40 30'N	80 13'W	372	329	358	396	438	463	482	473	469	454	443	344	295
	WILKES-SCRANTON	41 20'N	75 44'W	289	366	404	422	449	461	481	489	472	455	452	344	325
PN	KORROR ISLAND	7 20'N	134 29'E	33	480	502	500	513	487	463	456	458	469	477	487	471
	KWAJALEIN ISLAND	8 44'N	167 44'E	8	549	570	553	527	502	507	505	519	496	486	496	518
	WAKE ISLAND	19 17'N	166 39'E	4	567	583	593	590	600	595	562	558	550	552'	575	573
PR	SAN JUAN	18 26'N	66 00'W	19	548	563	581	570	531	531	549	549	528	528	540	531
RI	PROVIDENCE	41 44'N	71 26'W	19	414	438	442	462	481	485	475	469	461	461	383	378
SC	CHARLESTON	32 54'N	80 02'W	12	439	470	502	548	533	509	505	479	483	507	503	455
	COLUMBIA	33 57'N	81 07'W	69	464	493	515	557	543	536	516	515	503	524	510	473
	GREENVILLE	34 54'N	82 13 W	296	459	485	512	543	527	528	513	516	496	520	501	454
SD	HURON	44 23'N	98 13 W	393	452	481	501	528	547	575	613	601	560	537	458	420
	PIERRE	44 23'N	100 17'W	526	491	513	543	556	575	600	640	632	591	571	493	458
	RAPID CITY	44 03'N	103 04'W	966	494	528	550	546	551	583	625	622	597	573	505	485
	SIOUX FALLS	43 34'N	96 44'W	435	473	504	511	528	552	574	604	583	551	535	465	418
TN	CHATTANOOGA	35 02'N	85 12'W	210	398	426	454	496	497	504	486	495	472	489	441	395
	KNOXVILLE	35 49'N	83 59'W	299	402	436	464	515	518	522	505	507	493	502	444	399
	MEMPHIS	35 03'N	89 59'W	87	431	468	493	525	541	562	553	554	520	532	467	428
	NASHVILLE	36 07'N	86 41'W	180	380	419	443	498	524	539	530	530	499	502	420	369
TX	ABILENE	32 26'N	99 41'W	534	537	553	588	582	584	610	601	590	551	554	535	537
	AMARILLO	35 14'N	101 42'W	1098	611	620	631	648	635	658	639	639	623	622	593	598
	AUSTIN	30 18'N	97 42'W	189	472	503	519	501	525	576	593	579	544	542	496	479
	BROWNSVILLE	25 54'N	97 26'W	6	444	467	505	533	554	596	630	604	555	548	480	442
	CORPUS CHRISTI	27 46 N	97 30'W	13	458	488	505	507	536	586	620	595	560	554	494	455
	DALLAS	32 51'N	96 51'W	149	484	505	533	514	541	589	596	589	549	542	503	492
	KINGSVILLE	27 31'N	97 49'W	17	462	492	505	513	535	570	599	574	538	542	487	454
	LAREDO	27 32'N	99 28'W	158	485	506	534	533	560	581	604	600	565	549	490	476
	LUBBOCK	33 39'N	101 49'W	988	622	639	667	689	687	702	676	668	635	632	613	605
	LUFKIN	31 14'N	94 45'W	96	445	487	505	509	525	570	565	560	522	557	496	459
	MIDLAND-ODESSA	31 56'N	102 12'W	871	619	639	681	690	696	709	672	666	633	636	617	611
	PORT ARTHUR	29 57'N	94 01'W	7	432	475	489	502	536	559	521	521	516	534	475	433
	SAN ANGELO	31 22'N	100 30'W	582	541	552	591	581	582	606	597	591	549	553	539	537
	SAN ANTONIO	29 32'N	98 28'W	242	478	508	522	502	543	576	599	583	551	543	498	481
	SHERMAN	33 43'N	96 40'W	233	480	499	517	512	531	583	582	584	551	547	506	483
	WACO	31 37'N	97 12'W	155	472	504	527	507	508	585	599	589	548	541	498	486
	WICHITA FALLS	33 58'N	98 29'W	314	526	543	560	561	578	612	608	596	560	559	531	523

STATION	LAT	LONG	ELEV	JAN	FEB	MAR	APR	MAY	JUN	JUL	AUG	SEP	OCT	NOV	DEC
UNITED STATES (CON'T) (CON'T)															
UT BRYCE CANYON	37 42′N	112 09′W	2313	634	655	676	696	706	728	678	662	698	682	630	618
CEDAR CITY	37 42′N	113 06′W	1712	613	625	656	682	710	742	701	688	715	679	615	593
SALT LAKE CITY	40 46′N	111 58′W	1288	501	570	613	632	684	700	726	701	694	644	542	491
VA NORFOLK	36 54′N	76 12′W	9	457	483	508	544	543	549	519	514	503	496	491	456
RICHMOND	47 30′N	77 20′W	50	691	633	581	557	521	513	501	518	558	612	669	709
ROANOKE	37 19′N	79 58′W	358	452	472	493	514	507	516	503	496	492	499	468	439
VT BURLINGTON	44 28′N	73 09′W	104	358	393	424	447	461	473	484	468	444	403	298	295
WA OLYMPIA	46 58′N	122 54′W	61	285	355	401	444	481	464	540	500	475	371	302	267
SEATTLE-TACOMA	47 27′N	122 18′W	122	285	357	407	460	506	493	635	523	475	388	307	263
SPOKANE	47 38′N	117 32′W	721	348	439	501	532	567	570	666	630	595	500	365	322
WHIDBEY ISLAND	48 21′N	122 40′W	17	325	396	449	483	522	499	561	519	492	398	339	309
YAKIMA	46 34′N	120 32′W	325	379	464	528	563	592	594	665	635	605	514	388	347
WI EAU CLAIRE	44 52′N	91 29′W	273	428	492	496	494	492	512	531	516	476	455	364	362
GREEN BAY	44 29′N	88 08′W	214	420	469	498	496	503	522	531	515	482	447	370	364
LA CROSSE	43 52′N	91·15′W	205	434	465	491	489	500	521	534	527	487	463	383	372
MADISON	43 08′N	89 20′W	262	449	499	500	476	508	532	543	538	505	479	380	376
MILWAUKEE	42 57′N	87 54′W	211	414	454	477	491	515	541	550	541	508	476	392	363
WV CHARLESTON	38 22′N	81 36′W	290	355	381	409	444	472	486	471	466	466	459	389	342
HUNTINGTON	38 22′N	82 33′W	255	375	408	432	474	493	505	495	486	478	474	404	362
WY CASPER	42 55′N	106 28′W	1612	589	624	631	628	642	684	711	700	678	638	572	570
CHEYENNE	41 09′N	104 49′W	1872	610	623	608	593	578	618	625	613	631	623	574	590
ROCK SPRINGS	41 39′N	109 04′W	2056	599	645	655	654	680	704	714	700	698	663	588	585
SHERIDAN	44 46′N	106 58′W	1209	488	516	546	532	551	590	655	638	597	552	476	467
URUGUAY															
MONTEVIDEO	34 52′S	56 10′W	25	652	658	636	606	582	535	528	548	576	590	632	639
SAN JORGE	32 05′S	56 00′W	122	663	705	619	592	559	486	551	587	555	591	631	623
VENEZUELA															
BARCELONA	10 07′N	64 41′W	7	596	603	588	546	527	500	544	561	595	567	577	592
BARQUISIMETO	10 04′N	69 19′W	591	545	598	540	530	519	559	584	568	588	599	505	587
CALABOZO	8 48′N	67 27′W	100	579	613	602	558	512	545	509	522	431	552	566	554
CARACAS	10 30′N	66 53′W	862	594	647	612	573	479	503	536	561	564	522	529	576
CIUDAD BOLIVAR	8 09′N	63 33′W	50	562	572	554	543	541	485	547	584	607	574	563	588
CORO	11 25′N	69 41′W	20	678	690	705	641	602	630	673	663	678	621	639	656
GUIRIA	10 35′N	62 18′W	8	494	496	502	516	531	491	521	538	542	481	479	507
L ORCHILA	11 48′N	66 11′W	3	613	660	662	652	538	590	503	642	663	644	607	663
MAIQUETIA	10 36′N	66 59′W	43	594	661	564	496	475	617	661	636	675	598	596	609
MARACAIBO	10 39′N	71 36′W	40	580	562	510	535	468	511	553	575	687	538	576	631
MARACAY	10 15′N	67 39′W	442	715	725	689	645	514	589	619	637	674	570	622	652
MATURIN	9 45′N	63 11′W	70	518	536	508	475	461	415	441	495	474	487	474	487
MERIDA	8 30′N	71 15′W	1495	681	665	649	636	592	548	598	637	633	594	635	716
MORON	10 31′N	68 11′W	4	722	696	692	630	591	619	733	699	700	661	685	698
PUERTO AYACUCHO	5 41′N	67 38′W	124	551	532	481	508	393	421	406	497	483	499	512	514
SAN ANTONIO	7 51′N	72 27′W	404	566	567	466	416	493	476	507	522	517	522	533	556
SANTA ELENA	4 36′N	61 67′W	907	546	522	551	554	467	491	512	553	592	534	541	507
SAN FERNANDO	7 54′N	67 25′W	73	538	552	531	459	394	391	424	429	452	476	514	536
TUMEREMO	7 18′N	61 27′W	180	465	451	452	470	472	452	485	476	567	523	515	486
VIETNAM															
CHAPA	22 21′N	103 49′E	1570	395	442	574	376	404	363	403	378	439	389	478	607

STATION	LAT	LONG	ELEV	JAN	FEB	MAR	APR	MAY	JUN	JUL	AUG	SEP	OCT	NOV	DEC
							VIETNAM (CON'T)								
PHU-LEIN	20 48'N	106 38'E	125	305	-	234	384	474	493	492	-	-	-	505	450
							WAKE ISLAND								
WAKE ISLAND	19 17'N	166 39'E	12	679	708	688	694	694	694	685	686	685	687	716	644
							YUGOSLAVIA								
BANJA LUKA	44 47'N	17 13'E	153	366	420	404	488	576	513	559	536	575	470	167	278
BEOGRAD	44 47'N	20 32'E	243	394	439	459	452	504	528	550	498	522	478	339	344
HERCAGNOVI	42 28'N	18 31'E	34	299	372	343	402	502	511	575	565	508	439	290	242
LJUBLJANA	46 04'N	14 31'W	300	224	268	320	401	471	419	483	455	414	302	139	169
NEGOTIN	44 14'N	22 32'E	39	400	476	381	477	556	570	601	586	518	421	206	326
PARG	45 36'N	14 38'E	863	378	328	313	341	416	357	450	431	408	358	188	234
SKOPJE	41 59'N	21 28'E	240	314	472	394	465	553	556	601	582	528	431	303	270
SLJEME	45 54'N	15 37'W	999	347	366	384	427	492	407	489	461	454	382	231	276
SPLIT	43 31'N	16 26'E	122	403	417	405	464	488	458	552	539	511	441	313	310
ULOINJ	41 55'N	19 13'E	53	401	476	457	521	633	661	688	664	574	494	323	306
ZAGREB-GRIC	45 29'N	15 59'E	157	314	376	396	466	539	460	436	525	499	390	224	253
ZLATIBOR	43 44'N	19 43'E	1030	476	601	535	495	556	547	593	566	549	459	364	410

Average Radiation on Tilted Surfaces

In order to design solar heating and cooling systems, and also photovoltaic systems, it is necessary to estimate the average insolation falling on a solar collector, or a photovoltaic panel, each month of the year. This value, $\bar{H}_T$ (the subscript indicating a tilted surface) can be calculated as follows.

The insolation striking a tilted surface is the sum of three components: the direct beam insolation from the sun, the diffuse insolation from the sky, and the reflected insolation from the area in front of the tilted surface. Each component can be calculated; the resulting equation is

$$\bar{H}_T = (\bar{H} - \bar{H}_d)\,\bar{R}_b + \bar{H}_d\,\frac{(1 + \cos\beta)}{2} + \rho\,\frac{(1 - \cos\beta)}{2} \qquad (11)$$

where $\bar{R}_b$ = ratio of the monthly average daily beam radiation on the tilted surface to that on a horizontal surface

ρ = average reflectance of ground cover, usually taken as between 0.2 and 0.7 (fresh snow gives the high value)

β = the angle of tilt of the surface

$\bar{R}_b$ is found from the equation below, for surfaces sloped towards the equator (i.e. with zero azimuth)

$$\bar{R}_b = \frac{\cos L^* \cos\Delta \sin\Omega_{ST} + (\pi/180)\,\Omega_{ST} \sin L^* \sin\Delta}{\cos L \cos\Delta \sin\Omega_{SS} + (\pi/180)\,\Omega_{SS} \sin L \sin\Delta} \qquad (12)$$

where Ω_{ST} is the sunset hour angle (degrees) for the tilted surface, and is calculated from

$$\Omega_{ST} = \min\left[\cos^{-1}(-\tan L \tan\Delta),\ \cos^{-1}(-\tan L^* \tan\Delta)\right] \qquad (13)$$

Equations 12 and 13 apply to both hemispheres as long as L* is defined as

$$L^* = L - \beta \qquad \text{northern hemisphere}$$
$$L^* = L + \beta \qquad \text{southern hemisphere} \qquad (14)$$

The sequence of steps required to calculate the mean monthly daily insolation on a tilted surface, $\bar{H}_T$, is given below.

Step	Variable	Calculation
0.	-	Given: latitude: L surface tilt: β ground reflectance: ρ clearness index: $\bar{K}_T$
1.	Δ	Knowing the month and its day number (Table 1), calculate declination from Equation 2.

2. Ω_{ss} Find the sunset hour angle from Equation 5.

3. $\overline{H}_o$ Find the extraterrestrial insolation on a horizontal surface from Equation 8.

4. $\overline{H}$ Find the terrestrial insolation on a horizontal surface: $\overline{H} = \overline{H}_o \times \overline{K}_T$

5. $\overline{H}_d$ Find the diffuse radiation on the horizontal surface from Equation 10.

6. L* Find the equivalent latitude from Equation 14.

7. Ω_{sT} Find the sunset hour angle for the tilted surface from Equation 13.

8. $\overline{R}_b$ Find the ratio from Equation 12.

9. $\overline{H}_T$ Finally, calculate the monthly mean daily total radiation on the tilted surface from Equation 11.

Example 2

Determine the monthly mean daily insolation in Peshawar, Pakistan, on a south-facing flat plate solar collector tilted upwards at an angle equal to the latitude (34 00'N), during April. Ground reflectance is estimated as 0.2.

Solution

Following the steps outlined above:

1. Find Δ. The day number for April (Table 1) is n = 105 so the declination is given by

$$\Delta = 23.45 \sin [360 \times (284 + 105)/365] = 9.415°$$

2. Find Ω_{ss}. The sunset hour angle is found from Equation 5.

$$\cos \Omega = -\tan (9.415) \tan (34.0) = -0.1118$$
$$\Omega_{ss} = 96.4°$$

3. Find $\overline{H}_o$. The extraterrestrial insolation on a horizontal surface is calculated using Equation 8; take G_{sc} as 1353 W/m^2.

$$\overline{H}_o = \frac{24}{\pi} \times \frac{3600 \times 1353}{10^6} [1 + 0.033 \cos (360 \times 105/365)]$$

$$\times [\cos (34) \cos (9.415) \sin (96.4) + \frac{2\pi}{360} \times 96.4 \times \sin (34) \sin (9.415)]$$

$$= 35.69 \ MJ/m^2 \ day$$

4. Find $\overline{H}$. From Table 3, the clearness index, $\overline{K}_T$ for Peshawar in April is given as 0.569, so $\overline{H}$ is found from

$$\overline{H} = \overline{H}_o \times \overline{K}_T = 35.69 \times 0.569 = 20.31 \text{ MJ/m}^2 \text{ day}$$

5. Find $\overline{H}_d$. From Equation 10 we have:

$$\frac{\overline{H}_d}{\overline{H}} = 0.775 + 0.00653\ (96.4 - 90) - [0.505 + 0.00455\ (96.4 - 90)] \cos (115 \times 0.569 - 103) = 0.393$$

so $\overline{H}_d = 0.393\ \overline{H} = 0.393 \times 20.31 = 7.98 \text{ MJ/m}^2$ day

6. Find L*. For the northern hemisphere $L^* = L - \beta$

so $L^* = 34 - 34 = 0.$

7. Find Ω_{ST}. The sunset angle for the collector is found from Equation 13.

$$\Omega_{ST} = \text{minimum of } \cos^{-1} (-\tan 34 \tan 9.415) = 96.4° \text{ or } \cos^{-1} (-\tan 0. \tan 9.415) = 90°$$

so $\Omega_{ST} = 90°$

8. Find $\overline{R}_b$. This ratio follows from Equation 12

$$R_b = \frac{\cos 0.\ \cos 9.415 \sin 90. + (\pi/180) \times 90 \sin 0.\ \sin 9.415}{\cos 34.\ \cos 9.415 \sin 96.4 + (\pi/180)\ 96.4 \sin 34.\ \sin 9.415}$$

9. Find $\overline{H}_r$. The last step is to find $\overline{H}_T$ from Equation 11:

$$\overline{H}_T = (20.31 - 7.98) \times 1.02 + \frac{7.98}{2} (1 + \cos 34.) + \frac{0.2}{2} (1 - \cos 34.)$$

or $\underline{\overline{H}_T = 19.9 \text{ MJ/m}^2 \text{ day}}$

Calculations such as these, which are time-consuming and tedious to do by hand, can be performed very rapidly on a small computer.

References

1. Duffy, J.A., and W.A. Bechman, "Solar Engineering of Thermal Processes", John Wiley, New York, 1980.

2. Macomber, H.L., et al., "Photovoltaic Stand-Alone Systems", NASA-Lewis Research Center, Report #CR-165352, 1981.

HEAT TRANSFER

The design and analysis of solar energy conversion systems requires an understanding of the principal modes of heat transfer: conduction, convection, and radiation. In this set of notes we will examine these mechanisms and see how they may be combined to facilitate the thermal analysis of solar collectors and heat storage systems.

Conduction

Conduction is the only mode of heat transfer in opaque solid media. The rate of heat transfer is given by Fourier's law:

$$Q = -kA \frac{dT}{dx} \qquad (1)$$

where k is the thermal conductivity of the material, A is the area available for heat transfer, and dT/dx is the temperature gradient. The negative sign is required because dT/dx is itself negative since heat is transferred in the direction of decreasing temperature. If the thermal conductivity is independent of temperature, equation 1 may be integrated directly to give

$$Q = kA \frac{\Delta T}{\Delta x} \qquad (2)$$

where ΔT is the temperature difference and Δx is the thickness of the material through which heat is being conducted.

The units of thermal conductivity are Btu/hr ft°F or W/m K in S.I. units. The rate of heat transfer, Q, will then have units of Btu/hr or Watts (W). The following conversion factors apply.

1 Btu/hr = 0.2931 Watts
1 Btu/hr ft °F = 1.731 W/m K

Example 1

The glass cover of a solar collector has an area of 80 square feet and a thickness of 5/16 inches. The thermal conductivity of the glass is 0.5 Btu/hr ft°F. Determine the rate of heat transfer through the glass if the outside surface temperature is 50°F and the inside surface temperature is at 75°F.

Solution: The temperature difference, ΔT, is 25°F
also Δx = 5/16 inch
k = 0.5 Btu/hr ft °F
A = 32 ft^2

Hence from equation 2

$$Q = 0.5 \times 32 \times \frac{(75 - 50) \times 12}{5/16} = 15{,}360 \text{ Btu/hr}$$

For many substances k is, in fact, a linear function of temperature in which case the thermal conductivity should be evaluated at the mean temperature, i.e. at $(T_1 + T_2)/2$.

It is usual to determine conduction heat transfer rates by working in terms of the total resistance to the transfer of heat. One may then write:

$$Q = \frac{\Delta T_{overall}}{\Sigma R} \qquad (3)$$

where $\Delta T_{overall}$ is the temperature difference between inner and outer surfaces and ΣR is the sum of the resistances to the transfer of heat. From equation 2 it is clear that the resistances may be evaluated as

$$\Sigma R = \Sigma(\Delta x/kA) \qquad (4)$$

Example 2

The walls of a house are constructed as follows:

	material	thickness	conductivity
outside	brick	0.1 m	0.7 W/m K
	insulation	0.2 m	0.065 W/m K
inside	plaster board	0.03 m	0.48 W/m K

If the temperature difference across the inside and outside surfaces is 20°C, determine the rate of heat transfer due to conduction if the total wall area is 80 m^2.

The resistances are found as follows:

brick	R	= 0.1/0.7 X 80	= 0.00179 K/W
insulation	R	= 0.2/0.065 X 80	= 0.03846 K/W
plaster board	R	= 0.03/0.48 X 80	= 0.00078 K/W

so ΣR = 0.04103 K/W

The heat transfer is therefore

Q = 20/0.04103 = 487.4 Watts

The concept of a resistance to heat transfer is analogous to electrical resistance in an electric circuit. The wall structure of example 2 is an example of resistances in series. For some composite structures resistances may be also in parallel. For example, where there are two conductive routes between two surfaces the network may be presented as:

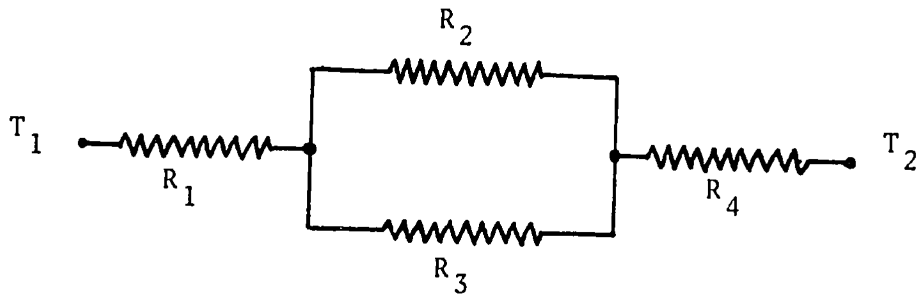

The overall resistance to heat transfer would then be calculated as

$$\Sigma R = R_1 + \frac{R_2 R_3}{R_2 + R_3} + R_4$$

This form of analysis may also be extended to cylinders or pipes where the resistance to conductive heat transfer is given by

$$R = \frac{\ln (r_o/r_i)}{2\pi k L} \qquad (5)$$

where r_i and r_o are the inner and outer radii of the relevant surface and L is the length of the pipe. The total conduction heat transfer is then found, as before, from equation 3.

Two further terms appear in the literature. The first is conductance, C, which is simply the reciprocal of resistance, i.e.

$$C = 1/R$$

but which may be given for a specified thickness of material on a unit area basis. The second is the overall heat transfer coefficient, U, which is simply the reciprocal of the sum of the resistances, i.e.

$$U = 1/\Sigma R$$

but which may also be given on a unit area basis in which case equation 3 is written as

$$Q = UA\Delta T \tag{6}$$

In all calculations it is important to closely examine the units of the relevant data to ensure that the appropriate equation is being used and that the calculation is dimensionally consistent.

Convection

Heat transfer takes place between a solid surface and a fluid whenever a temperature difference exists. If the fluid is in laminar motion then heat transfer is considered to take place largely by conduction. Even when the bulk of the fluid is in turbulent motion, the layer immediately adjacent to the wall is in laminar motion. Where mixing of the fluid particles occurs, the heat is transferred by convection. Convection may be either forced or natural (free) convection depending on whether the fluid motion is imposed or whether it occurs because of differences in density caused by temperature changes. A buffer layer exists between the laminar layer and the turbulent bulk. In this intermediate region the heat transfer is characterized by both conduction and convection.

Since the laminar layer presents a much greater resistance to heat transfer than either the buffer region or the turbulent bulk, most of the temperature resistance occurs across the laminar layer. The entire resistance to heat transfer is, for practical purposes, regarded as being concentrated in this thin layer. Thus the conductance term for a fluid is generally referred to as the film heat transfer coefficient.

The heat transfer brought about by convection is generally computed in a manner analogous to heat transfer by conduction. That is, one may write

$$Q = h_c A \Delta T \qquad (7)$$

where h_c = convective heat transfer coefficient, often called a film coefficient

A = area available for convective heat transfer

ΔT = temperature difference between the surface and the bulk of the fluid.

Convective heat transfer may also be treated within the framework of a thermal resistance network in a manner analogous to conduction. The thermal resistance to convection is given by

$$R_c = \frac{1}{h_c A} \qquad (8)$$

As an example, consider the heat transfer from the interior of a room at T_i through a wall to the air outside at temperature T_o. Heat is first transferred by free convection to the interior surface of the wall, then by conduction through the wall to the exterior surface, and finally from the exterior surface to the air outside. There are, therefore, three resistances to the transfer of heat. The total resistance R is given by:

$$R = \frac{1}{h_{ci}A} + \frac{x}{kA} + \frac{1}{h_{co}A}$$

where h_{ci}, h_{co} are the inner and outer convective film coefficients, x is the wall thickness, and k is the thermal conductivity of the wall material. The overall heat transfer is simply:

$$Q = \frac{T_i - T_o}{R}$$

Film Coefficients

Convective heat transfer film coefficients are generally determined experimentally and many correlations have been reported in the literature. The data are generally structured in terms of five dimensionless numbers. These are:

Nusselt number (Nu) = hL/k
Reynolds number (Re) = $\rho uL/\mu$
Prandtl number (Pr) = $\mu C_p/k$
Grasshof number (Gr) = $g\beta\Delta T\ L^3\rho^2/\mu^2$
Rayleigh number (Ra) = $g\beta\Delta T\ L^3\rho^2 C_p/\mu k$

where h = heat transfer coefficient
L = characteristic dimension
k = thermal conductivity
u = fluid velocity
ρ = fluid density
μ = viscosity
C_p = specific heat (constant pressure)
β = coefficient of expansion of the fluid
ΔT = temperature difference
g = acceleration due to gravity (9.81 m/s^2 or 32.2 ft/s^2)

All these terms are well defined except for the characteristic dimension L. This term will depend on the configuration of the system being examined. For ideal gases β is equal to the reciprocal of absolute temperature, i.e. $\beta = 1/T$. This is a good enough approximation for air.

In general, the Nusselt number, for convection, can be related to the other dimensionless numbers by equations of the form:

$Nu = C(Re^n Pr^m)$ forced convection
and $Nu = C(Gr^n Pr^m)$ free convection

where C, n, m are empirical constants which must be determined experimentally. Once the Nusselt number has been determined for the system under consideration, the film coefficient follows directly from

$$h = (Nu)k/L \qquad (9)$$

The following correlations are applicable for common system configurations found in solar energy systems.

1. Laminar Flow in Pipes and Ducts

$$Nu = 1.86 \left(Re.Pr.\frac{D_h}{L}\right)^{1/3} \left(\frac{\mu_b}{\mu_w}\right)^{0.14} \qquad (10)$$

applicable for $Re.Pr.D_h/L > 10$
and $Re < 2100$
D_h is the hydraulic diameter of the pipe or duct, given by

$$D_h = \frac{4 \times \text{flow area}}{\text{wetted perimeter}} \qquad (11)$$

μ_b is the viscosity at the bulk (mean) temperature of the fluid (use this temperature for Pr also); μ_w is the viscosity of the fluid at the wall temperature.

also $Nu = hD_h/k$
$Re = \rho u D_h/\mu_b$

and L is the length of the pipe or duct.

If the conduit is short, i.e. $L/D_h < 60$, Nu may be multiplied by a factor equal to

$$1 + (D_h/L)^{0.7}$$

2. Turbulent Flow in Pipes and Ducts

When the Reynolds number is above 6000 then fluid flow is fully turbulent and heat transfer is enhanced. The Nusselt number may be estimated as

$$Nu = 0.023\, Re^{0.8} Pr^{1/3} \left(\frac{\mu_b}{\mu_w}\right)^{0.14} \qquad (12)$$

applicable for $Re > 10{,}000$
$0.7 < Pr < 7000$

and properties based on bulk temperatures.

If the tube is short increase Nu by

$$1 + (D_h/L)^{0.7}$$

3. Turbulent Flow Between Flat Plates

One side heated:

$$Nu = 0.0196\, Re^{0.8} Pr^{1/3} \qquad (13)$$

where Re and Nu are based on the hydraulic diameter.

4. Flow in a Helical Coil

For flow in a helical coil the value of the heat transfer coefficient calculated for a straight tube should be multiplied by

$$1 + 3.5 \left(\frac{\text{tube diameter}}{\text{coil diameter}}\right)$$

5. Free Convection from Surfaces

a) Vertical surfaces, L = vertical dimension, < 3 ft

$$\begin{aligned} Ra < 10^4, \quad & Nu = 1.36\ Ra^{0.2} \\ 10^4 < Ra < 10^9, \quad & Nu = 0.59\ Ra^{0.25} \\ Ra > 10^9, \quad & Nu = 0.13\ Ra^{1/3} \end{aligned} \qquad (14)$$

b) Horizontal Cylinder, L = diameter, < 8 ins

$$\begin{aligned} 1 < Ra < 10^4, \quad & Nu = 1.09\ Ra^{0.2} \\ 10^4 < Ra < 10^9, \quad & Nu = 0.53\ Ra^{0.25} \\ Ra > 10^9, \quad & Nu = 0.13\ Ra^{1/3} \end{aligned} \qquad (15)$$

c) Horizontal Flat Surfaces

$$\begin{aligned} 10^4 < Ra < 10^7, \quad & Nu = 0.76\ Ra^{0.25} \\ 10^7 < Ra < 10^{10}, \quad & Nu = 0.15\ Ra^{1/3} \end{aligned} \qquad (16)$$

The characteristic length, L, is four times the area divided by the perimeter.

d) Sphere, L = diameter

$$Nu = 2 + 0.45\ Ra^{0.25} \qquad (17)$$

In all the above correlations fluid properties are to be evaluated at temperature, T_f, where

$$T_f = 1/2\ (\text{surface temperature} + \text{ambient temperature})$$

6. Free Convection Between Two Parallel Surfaces

For air, the Nusselt number may be found as:

$$Nu = 1 + 1.44\ [1 - 1708/B]^+ \left\{1 - \frac{1708}{B} (\sin 1.8\beta)^{1.6}\right\}$$

$$+ [(B/5830)^{1/3} - 1]^+ \qquad (18)$$

where the meaning of the + exponent is that only the positive values of the term in the square brackets are to be used (i.e. use zero if the term is negative).

In equation (18) $B = Ra \cos \beta$ where Ra is the Rayleigh number and β is the angle between the surfaces and the horizontal. Ra is based on $L = d$, the distance between the plates. Equation 18 is valid for β between zero and 75°.

For inclinations between 75° and 90° the recommended relation for air is

$$Nu = \max [\, 1,\ 0.288\ (A\ Ra \sin \beta)^{1/4},\ 0.039\ (Ra \sin \beta)^{1/3}] \qquad (19)$$

The constant A in equation 19 is the aspect ratio of the air layer, defined as the ratio of the thickness to the length along the layer measured along either surface in the upslope direction.

7. Air Flow over a Flat Surface

The calculation of heat transfer coefficients for flat heated surfaces exposed to wind does not appear to be well established. For smooth surfaces a rough approximation is given by the dimensional equations:

$$h = 4.5 + 2.9u \ ; \qquad h = W/m^2\,K\ , \qquad u = m/s$$
$$\text{or}\quad h = 0.8 + 0.23u \ ; \qquad h = Btu/hr\ ft^2\,°F\ , \qquad u = mph$$

Radiation

All heated bodies emit thermal electromagnetic radiation whose wavelengths and intensities are dependent upon the temperature of the body and its optical characteristics.

Thermal radiation is usually considered to lie within that part of the electromagnetic wave spectrum with a wavelength between 0.1 to 100 μm (microns). Solar radiation has most of its energy in the range between 0.1 and 3 μm. The visible part of the spectrum is between about 0.4 - 0.7 μm.

It can be shown that the energy density at a given wavelength is related to the monochromatic radiation emitted by a perfect radiator, usually called a black body, according to the relation.

$$E_{b\lambda} = \frac{C_1}{(e^{C2/\lambda T} - 1)\,\lambda^5} \ W/m^2 \cdot \mu m \qquad (21)$$

where $C_1 = 3.7405 \times 10^8 \ W.\ \mu m^4/m^2$
$C_2 = 1.43879 \times 10^4 \ \mu m.K$

E_b is the monochromatic emissive power of a blackbody, defined as the energy emitted by a perfect radiator per unit wavelength, at the specified wavelength λ, per unit area and per unit time at the specified temperature T (in degrees Kelvin).

The total energy emitted by a blackbody can be obtained by integration over all wavelengths:

$$E_b = \int_0^\infty E_{b\lambda} d\lambda = \sigma T^4 \ W/m^2 \qquad (22)$$

where σ is called the Stefan-Boltzmann constant and is equal to 5.67×10^{-8} $W/m^2\ K^4$.

It is also of interest to know the wavelength corresponding to the maximum intensity of blackbody radiation. This may be determined from Wien's displacement law:

$$\lambda_{max} T = 2897.8 \ \mu m \qquad (23)$$

For example, we can estimate the wavelength of the maximum intensity of the radiation emitted from the human body.

Taking the body temperature as 98.4°F or 37°C, we have

$$\lambda_{max} = \frac{2897.8}{37 + 273} = 9.34 \ \mu m$$

Table 4 Fraction of Blackbody Radiant Energy Between Zero and λT for even increments of λT

λT, μm K	$f_{0-\lambda T}$	λT, μm K	$f_{0-\lambda T}$
1000	0.0003	6200	0.7541
1100	0.0009	6300	0.7618
1200	0.0021	6400	0.7692
1300	0.0043	6500	0.7763
1400	0.0077	6600	0.7831
1500	0.0128	6700	0.7897
1600	0.0197	6800	0.7961
1700	0.0285	6900	0.8022
1800	0.0393	7000	0.8080
1900	0.0521	7100	0.8137
2000	0.0667	7200	0.8191
2100	0.0830	7300	0.8244
2200	0.1009	7400	0.8295
2300	0.1200	7500	0.8343
2400	0.1402	7600	0.8390
2500	0.1613	7700	0.8436
2500	0.1831	7800	0.8479
2700	0.2053	7900	0.8521
2800	0.2279	8000	0.8562
2900	0.2506	8100	0.8601
3000	0.2732	8200	0.8639
3100	0.2958	8300	0.8676
3200	0.3181	8400	0.8711
3300	0.3401	8500	0.8745
3400	0.3617	8600	0.8778
3500	0.3829	8700	0.8810
3600	0.4036	8800	0.8841
3700	0.4238	8900	0.8871
3800	0.4434	9000	0.8899
3900	0.4624	9100	0.8927
4000	0.4829	9200	0.8954
4100	0.4987	9300	0.8980
4200	0.5160	9400	0.9005
4300	0.5327	9500	0.9030
4400	0.5488	9600	0.9054
4500	0.5643	9700	0.9076
4600	0.5793	9800	0.9099
4700	0.5937	9900	0.9120
4800	0.6075	10000	0.9141
4900	0.6209	11000	0.9318
5000	0.6337	12000	0.9450
5100	0.6461	13000	0.9550
5200	0.6579	14000	0.9628
5300	0.6693	15000	0.9689
5400	0.6803	16000	0.9737
5500	0.6909	17000	0.9776
5600	0.7010	18000	0.9807
5700	0.7107	19000	0.9833
5800	0.7201	20000	0.9855
5900	0.7291	30000	0.9952
6000	0.7378	40000	0.9978
6100	0.7461	50000	0.9988

From reference 3

It is also useful to know what fraction of the total radiated energy is being emitted over a range of wavelengths. Table 4 shows the fraction of blackbody radiant energy emitted between zero and λT for increments of λT.

For example, we can determine the fraction of the sun's radiative energy output that lies within the visible part of the electromagnetic spectrum. The temperature of the surface of the sun is about 6000 K. The visible part of the EM spectrum lies approximately between 0.4 and 0.7 microns.

From Table 4 we have:

$$\lambda T = 0.7 \times 6000 = 4200 \qquad f\,(<4200) = 0.516$$
$$\lambda T = 0.4 \times 6000 = 2400 \qquad f\,(<2400) = 0.140$$

Fraction between = 0.376

so about 38% of the sun's output is visible.

Absorptance, Emittance and Reflectance

The absorptance, α, is the fraction of incident light of a given wavelength that is absorbed when light strikes an absorbing surface. The absorptance of a surface is therefore a function of the wavelength intensity distribution of the incident light.

The emittance, ε, is the fraction of the emittance of a perfect blackbody at a given wavelength emitted by a heated surface.

When radiation strikes a body some is reflected, some absorbed, and if the material is translucent, some is transmitted. It is clear that

$$\alpha + \tau + r = 1$$

α = fraction absorbed
τ = fraction transmitted (24)
r = fraction reflected

If a body is opaque then $\tau = 0$

The reflection of radiation can be specular or diffuse. When the angle of incidence is equal to the angle of reflection, the reflection is called specular. If the reflected radiation is uniformly distributed in all direction it is said to be diffuse. A real surface exhibits both kinds of reflection. A highly polished surface approaches specular reflection, a rough surface generally reflects diffusely.

At a particular wavelength, absorptance is equal to emittance. This relationship is essentially Kirchhoff's law:

$$\alpha_\lambda = \varepsilon_\lambda$$

For an opaque surface therefore

$$\varepsilon_\lambda = 1 - r_\lambda$$

and

$$\alpha_\lambda = 1 - r_\lambda$$

The subscript λ is important to note because, for most materials, α, ε , and r vary significantly with wavelength over the range of interest in solar energy systems. The few materials for which they do not vary with λ are termed gray bodies, and those with $\alpha = \varepsilon = 1$ for all wavelengths are termed blackbodies.

Infrared Radiation Heat Transfer Between Gray Surfaces

The majority of heat-transfer problems in solar energy applications involve radiation between two surfaces. For this situation and assuming:

1. The surfaces are gray and reflection is diffuse.
2. Surface temperatures are uniform.

The radiative heat transfer between the surfaces is given by

$$Q = \frac{\sigma(T_2^4 - T_1^4)}{\frac{1 - \varepsilon_1}{\varepsilon_1 A_1} + \frac{1}{A_1 F_{12}} + \frac{1 - \varepsilon_2}{\varepsilon_2 A_2}} \qquad (25)$$

where subscripts 1 and 2 refer to the two surfaces, ε is the emittance, T is absolute temperature (Kelvin), A is area, and F_{12} is the view factor.

For the special case of radiation between two large parallel plates (i.e. as in flat-plate collectors) the areas A_1 and A_2 are equal, and F_{12} is unity. Equation 25 therefore reduces to:

$$Q = \frac{A\sigma(T_2^4 - T_1^4)}{\frac{1}{\varepsilon_1} + \frac{1}{\varepsilon_2} - 1} \qquad (26)$$

Equation 26 also applies to radiation between two concentric long cylinders forming an annulus when the diameter ratio approaches unity.

The second special case is for a small body (surface 1) surrounded by a large enclosure (surface 2). Under these conditions, the area ratio A_1/A_2 approaches zero, F_{12} is again unity, and equation 25 becomes

$$Q = \varepsilon_1 A_1 \sigma(T_2^4 - T_1^4) \qquad (27)$$

The result is independent of the surface properties of the large enclosure since virtually none of the radiation leaving the small object is reflected back from the large enclosure. The large enclosure effectively absorbs all radiation from the small body and thus acts like a black body. Equation 27 applies in the case of a flat plate radiating to the sky.

The sky can be considered as a black body at some equivalent sky temperature, T_s. The net radiation to a surface with emittance ε and temperature T is therefore found from

$$Q = \varepsilon A \sigma (T_s^4 - T^4) \qquad (28)$$

Several relations have been proposed to relate T_s, for clear skies, to other measured meteorological variables. One simple relation is:

$$T_s = 0.0552\ T_a^{1.5} \qquad (29)$$

where T_a is the local air temperature in degrees Kelvin.

It is possible to define heat transfer coefficients such that equations 26 and 27 reduce to simple form of equation 7. That is, we have

$$h = \frac{\sigma}{1/\varepsilon_1 + 1/\varepsilon_2 - 1} (T_2 + T_1)(T_2^2 + T_1^2) \qquad (30)$$

or

$$h = \varepsilon_1 \sigma (T_2 + T_1)(T_2^2 + T_1^2) \qquad (31)$$

derived from equations 26 and 27 respectively.

Radiation Transmission Through Covers

The transmittance, reflectance, and absorption of solar radiation by translucent solar collector covers are functions of the incoming radiation, and the thickness, refractive index, and extinction coefficient of the material. Generally, the refractive index, n, and the extinction coefficient, K are functions of the wavelength of the radiation. However, for glass these properties may be taken as independent of wavelength.

Reflectance

For smooth surfaces the reflection of unpolarized radiation on passing from a medium 1 with a refractive index n_1 to medium 2 with refractive index n_2 is given by

$$r_\perp = \frac{\sin^2(\Theta_2 - \Theta_1)}{\sin^2(\Theta_2 + \Theta_1)} \tag{32}$$

$$r_\parallel = \frac{\tan^2(\Theta_2 - \Theta_1)}{\tan^2(\Theta_2 + \Theta_1)} \tag{33}$$

$$r(\Theta_1) = \frac{I_r}{I_i} = 1/2\,(r_\perp + r_\parallel) \tag{34}$$

where Θ_1 and Θ_2 are the angles of incidence and refraction as shown in Figure 1.

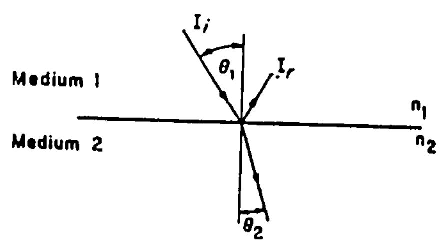

Figure 1 Angles of incidence and refraction in media having refractive indices n_1 and n_2. [3]

Equation 30 represents the perpendicular component of unpolarized radiation $r_\perp$ and equation 31 represents the parallel component of unpolarized radiation, $r_\parallel$. Equation 32 then gives the reflection of unpolarized radiation as the average of the two components. The angles θ_1 and θ_2 are related to the indices of refraction by Snell's law

$$\frac{n_1}{n_2} = \frac{\sin\Theta_2}{\sin\Theta_1} \tag{35}$$

Thus if the angle of incidence and refractive indices are known, equations 32 through 35 are sufficient to calculate the reflectance of the single interface.

For radiation at normal incidence ($\Theta_1 = \Theta_2 = 0$) equations 34 and 35 may be combined to yield

$$r(0) = \frac{I_r}{I_i} = \left[\frac{(n_1 - n_2)}{(n_1 + n_2)}\right]^2 \qquad (36)$$

Refractive indices for some common translucent materials are given below:

TABLE 5 Refractive Index for Various Substances in the Visible Range Based on Air

Material	Index of refraction
Air	1.000
Clean polycarbonate (PCO)	1.59
Diamond	2.42
Glass (solar collector type)	1.50–1.52
Plexiglass (polymethyl methacrylate, PMMA)	1.49
Mylar (polyethylene terephthalate, PET)	1.64
Quartz	1.54
Tedlar (polyvinyl fluoride, PVF)	1.45
Teflon (polyfluoroethylenepropylene, FEP)	1.34
Water–liquid	1.33
solid	1.31

Example 3

Calculate the reflectance of one surface of glass at normal incidence and at 60°. The average index of refraction of glass for the solar spectrum is 1.526 (for air $n \approx 1$).

At normal incidence, equation 36 may be written for $n_1 = 1$ as

$$r(0) = \left(\frac{n - 1}{n + 1}\right)^2$$

or

$$r(0) = \left(\frac{1.526 - 1}{1.526 + 1}\right)^2 = 0.0434$$

At an incidence angle of 60°, equation 35 gives the refraction angle Θ_2 as

$$\Theta_2 = \sin^{-1}\left(\frac{\sin 60}{1.526}\right) = 34.58°$$

Then from equation 34 the reflectance is

$$r(60) = \frac{1}{2}\left[\frac{\sin^2(34.58 - 60)}{\sin^2(34.58 + 60)} + \frac{\tan^2(34.58 - 60)}{\tan^2(34.58 + 60)}\right]$$

$$= \frac{1}{2}(0.185 + 0.001) = 0.093$$

Transmittance

For a single cover the average transmittance after reflection losses is given by

$$\tau_r = \frac{1}{2}\left[\frac{1 - r_{\parallel}}{1 + r_{\parallel}} + \frac{1 - r_{\perp}}{1 + r_{\perp}}\right] \quad (37)$$

For a system of N covers, all of the same material, the average transmittance after reflection losses are accounted for is given by

$$\tau_r = \frac{1}{2}\left[\frac{1 - r_{\perp}}{1 + (2N - 1)r_{\perp}} + \frac{1 - r_{\parallel}}{1 + (2N - 1)r_{\parallel}}\right] \quad (38)$$

Example 4

Calculate the transmittance of two covers of nonabsorbing glass at normal incidence and at 60°.

At normal incidence the reflectance of one interface $r(0) = 0.0434$ (see example 3). From equation 38 with $r_{\perp} = r_{\parallel}$ we have

$$\tau_r(0) = \frac{1 - r(0)}{1 + 3r(0)}$$

$$= \frac{1 - 0.0434}{1 + 3(0.0434)} = 0.85$$

At a 60° incidence angle equations 32 and 33 give

$$r_{\perp} = 0.185$$

$$r_{\parallel} = 0.001$$

and from equation 38 we then have

$$\tau_r(60) = \frac{1}{2}\left[\frac{1 - 0.001}{1 + 3(0.001)} + \frac{1 - 0.185}{1 + 3(0.185)}\right]$$

$$= \underline{0.76}$$

Figure 2 below shows the effect of multiple glass nonabsorbing covers on overall transmittance. Table 6 lists the average refractive indices of some common cover materials.

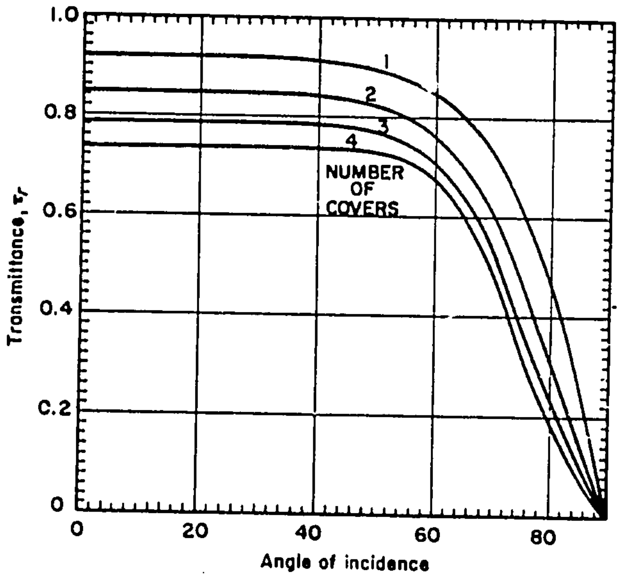

Figure 2. Transmittance of 1, 2, 3, and 4 nonabsorbing covers having an index of refraction of 1.526. [3]

Table 6. Average Refractive Index in Solar Spectrum of Some Cover Materials [3]

Cover Material	Average Refractive Index
Glass	1.526
Polymethyl methacrylate	1.49
Polyvinylfluoride	1.45
Polyfluorinated ethylene propylene	1.34
Polytetrafluoroethylene	1.37
Polycarbonate	1.60

Absorptance

The absorption of radiation in translucent media is described by Bouguer's law, which leads to an estimate of absorptance as

$$\alpha = 1 - \exp^{-KL} \tag{39}$$

where K is the extinction coefficient and L is the distance that the radiation travels, i.e.

$$L = \frac{\text{cover thickness}}{\cos \Theta_2}$$

The overall transmittance of a single cover is then given by

$$\tau = (1 - \alpha)\tau_r \tag{40}$$

and the reflectance r from the simple identity:

$$r = 1 - \alpha - \tau \tag{41}$$

The extinction coefficients for some common transparent materials are listed below.

TABLE 7. Extinction Coefficients for Transparent Materials [4]

Polyvinyl fluoride (Tedlar)	1.4 cm^{-1}
Fluorinated ethylene propylene (Teflon)	0.59
Polyethylene terephthalate (Mylar)	2.05
Polyethylene	1.65
Ordinary window glass	~0.3
White glass (<0.01% Fe_2O_3)	~0.04
Heat-absorbing glass	1.3-2.7

Example 5

Calculate the transmittance, reflectance, and absorptance of a single glass cover 2.3 mm thick at an angle of 60°. The extinction coefficient of the glass is 32 m^{-1}.

Assuming for this glass n = 1.526 then from Example 3 we have

$$\Theta_2 = 34.58°$$
$$r_\perp(60) = 0.185$$
$$r_\parallel(60) = 0.001$$

then from equation 39

$$\alpha = 1 - \exp(-32 \times 0.0023/\cos 34.58)$$
$$= 0.085$$

From equation 37 we have

$$\tau_r = 1/2\left[\frac{1 - 0.001}{1 + 0.001} + \frac{1 - 0.185}{1 + 0.185}\right]$$

$$= 0.843$$

It follows then that

$$\tau = (1 - 0.085) \times 0.843 = 0.771$$

and $$r = 1 - 0.085 - 0.771 = 0.144$$

Although equations 39, 40 and 41 were derived for a single cover they also apply to identical multiple covers, except that τ_r should now be evaluated using equation 38 and the value of L used in euqation 39 should be equal to the total cover system thickness.

Wavelength Variation of Transmission

Most transparent media transmit selectively. Transmittance is a function of the wavelength of the incident radiation. Glass, the material most commonly used as a cover material in solar collectors, may absorb little of the solar energy spectrum if its Fe_2O_3 (iron oxide) content is low. If the Fe_2O_3 content is high, it will absorb in the infrared portion of the solar spectrum. The transmittance of several glasses of varying iron content is shown in Figure 3.

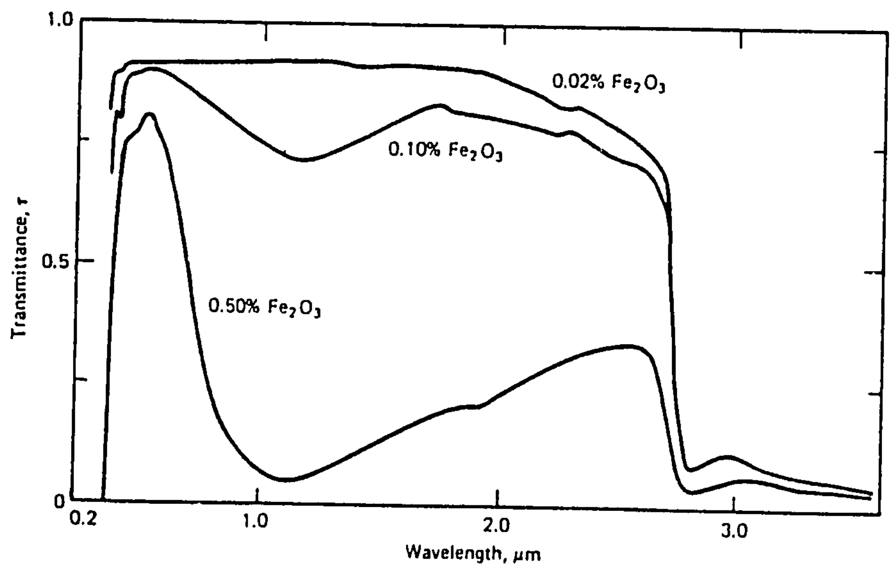

Figure 3 Spectral transmittance of 6 mm thick glass with various iron oxide contents. [3]

It is apparent that "water glass" (low iron) glass has the best transmission; glasses with high Fe_2O_3 content have a greenish appearance and are relatively poor transmitters. Note that the transmission is not a strong function of wavelength in the solar spectrum except for the high iron content glass. Glass becomes substantially opaque at wavelength longer than 3 μm and can be considered as opaque to longwave radiation (i.e. thermal infrared). This useful characteristic is the principal reason that glass is such an attractive material for covering flat-plate solar collectors.

Plastics are generally more transparent than glass. Like glass, they absorb in the untraviolet but they have variable transmittance in the infrared depending on the thickness and the molecular bonds present in the particular plastic. Simple plastics like polyethylene have few absorption bands at certain wavelengths.

The infrared absorption of plastics is important in collector behavior. Glass being opaque to the thermal infrared, traps heat radiation. Some plastics, being relatively transparent, allow thermal radiation to escape. If plastic windows are used, the plastic must either be thick enough tc absorb the thermal radiation or be instrinsically opaque to it. The transmittance - wavelength curves of a number of plastics of importance for solar energy collectors are shown below and overleaf. [5]

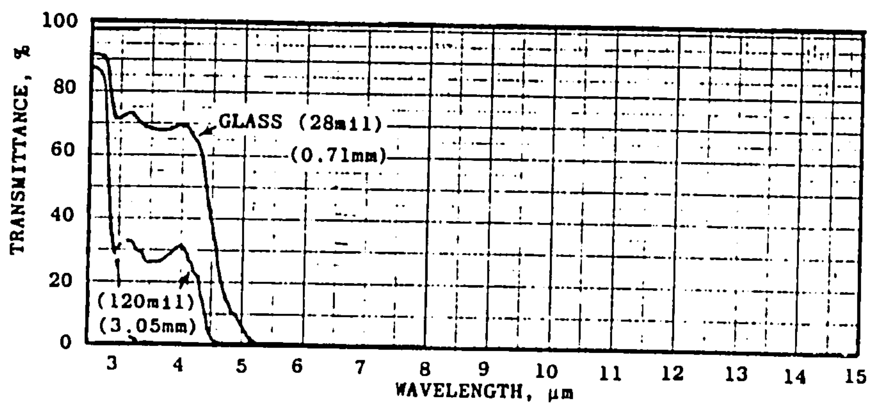

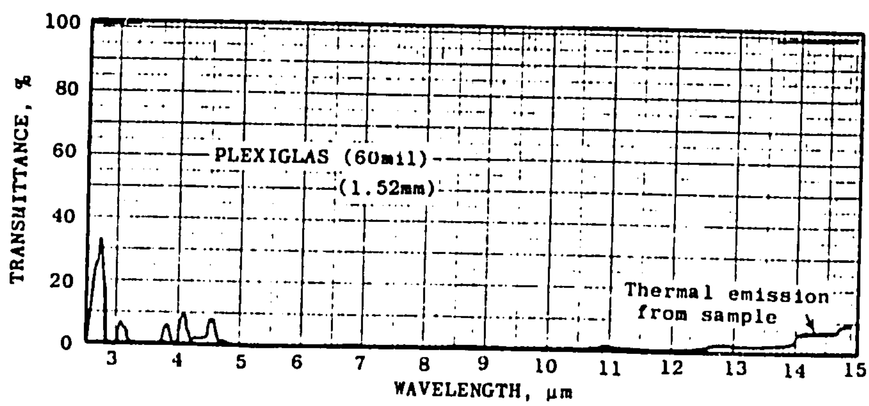

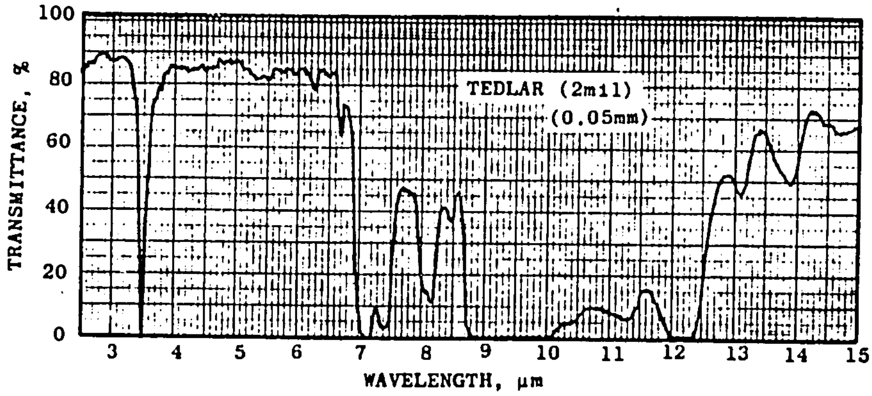
TEDLAR (2mil)
(0.05mm)
TRANSMITTANCE, %
WAVELENGTH, µm
100
80
60
40
20
0
3
4
5
6
7
8
9
10
11
12
13
14
15

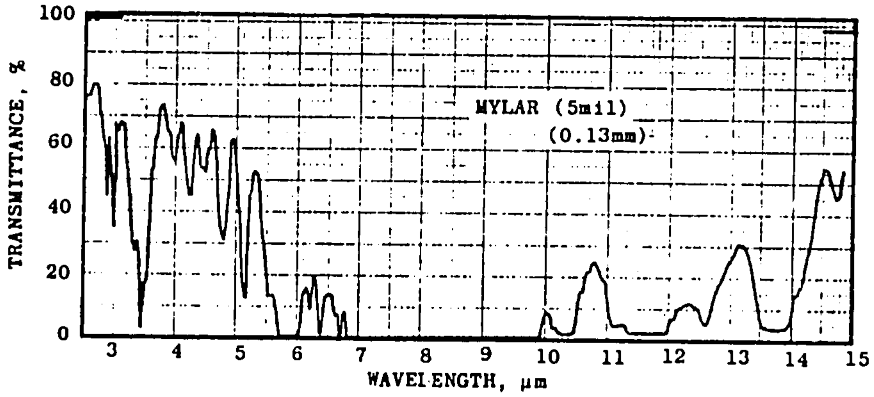
MYLAR (5mil)
(0.13mm)
TRANSMITTANCE, %
WAVELENGTH, µm
100
80
60
40
20
0
3
4
5
6
7
8
9
10
11
12
13
14
15

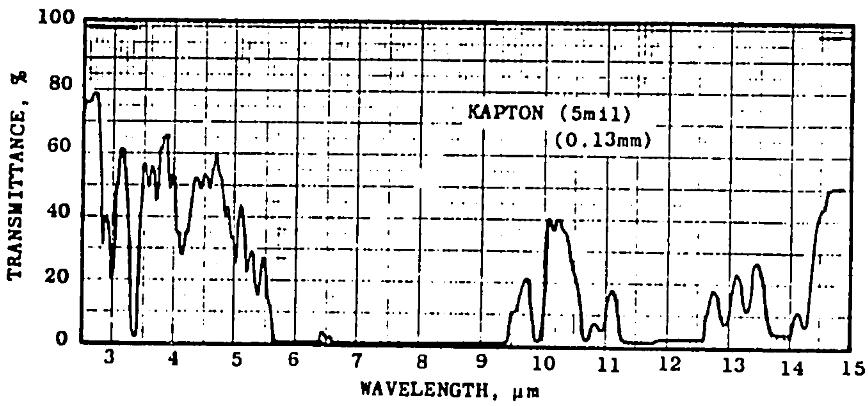
KAPTON (5mil)
(0.13mm)
TRANSMITTANCE, %
WAVELENGTH, µm
100
80
60
40
20
0
3
4
5
6
7
8
9
10
11
12
13
14
15

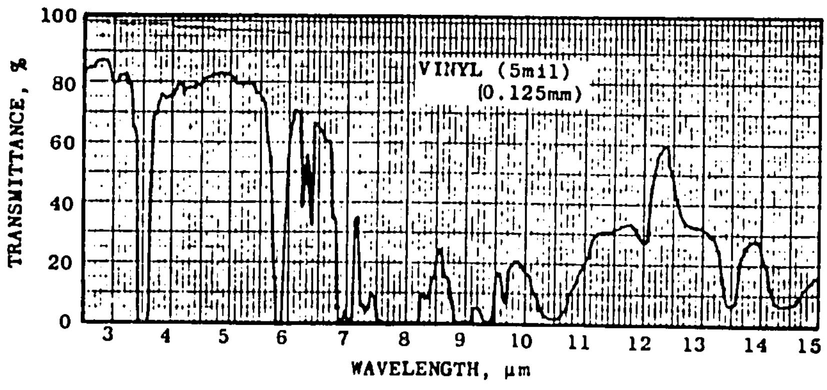
VINYL (5mil)
(0.125mm)
TRANSMITTANCE, %
WAVELENGTH, µm
100
80
60
40
20
0
3
4
5
6
7
8
9
10
11
12
13
14
15

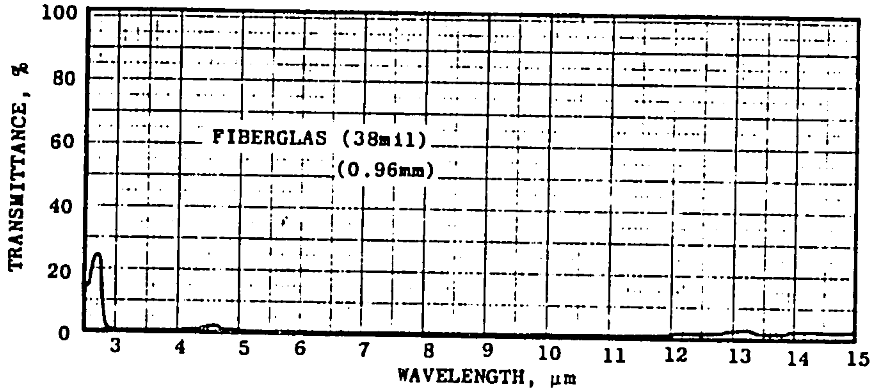

100
80
60
40
20
0
TRANSMITTANCE, %
FIBERGLAS (38mil)
(0.96mm)
3 4 5 6 7 8 9 10 11 12 13 14 15
WAVELENGTH, μm

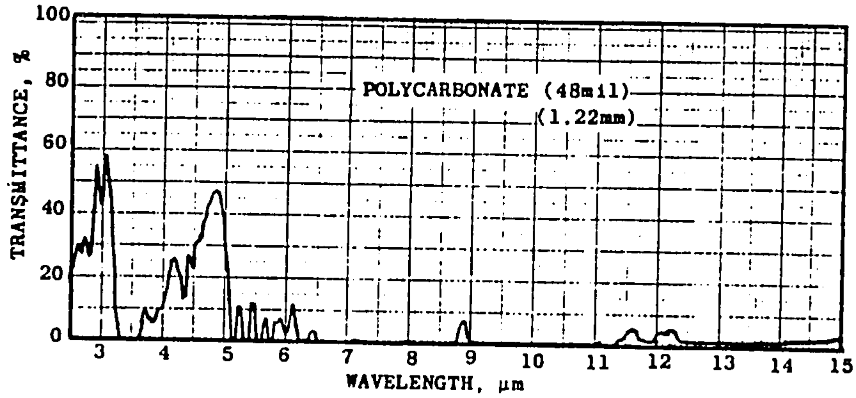

100
80
60
40
20
0
TRANSMITTANCE, %
POLYCARBONATE (48mil)
(1.22mm)
3 4 5 6 7 8 9 10 11 12 13 14 15
WAVELENGTH, μm

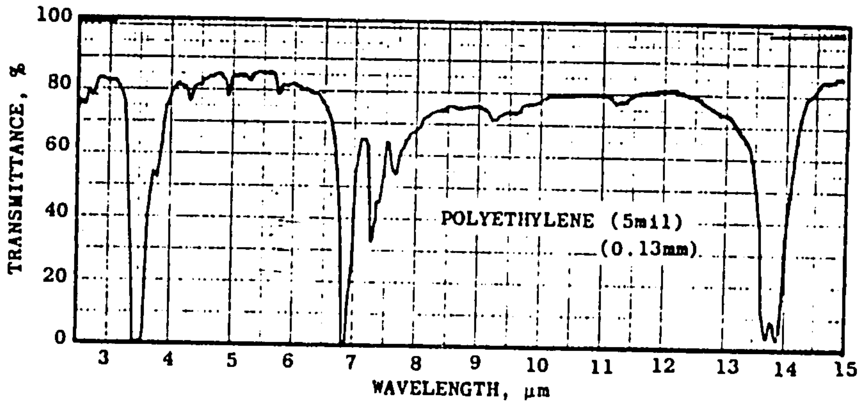

100
80
60
40
20
0
TRANSMITTANCE, %
POLYETHYLENE (5mil)
(0.13mm)
3 4 5 6 7 8 9 10 11 12 13 14 15
WAVELENGTH, μm

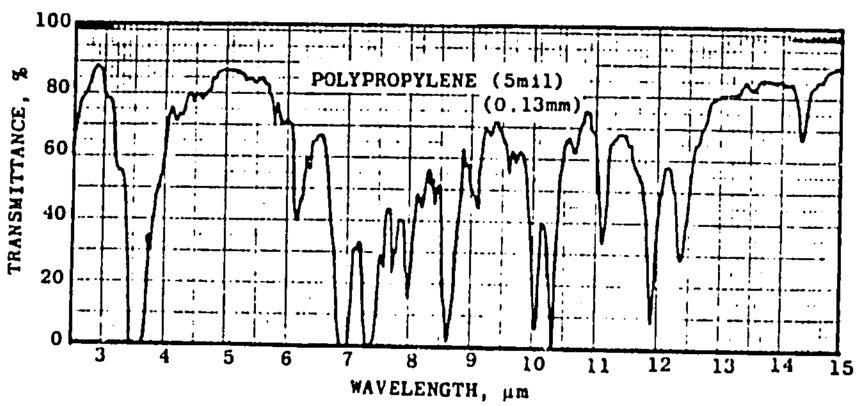

100
80
60
40
20
0
TRANSMITTANCE, %
POLYPROPYLENE (5mil)
(0.13mm)
3 4 5 6 7 8 9 10 11 12 13 14 15
WAVELENGTH, μm

In the transmittance curves, the thickness shown are typical for solar collector systems. Plastic films are very thin and are used in tension for window coverings. Their thinness tends to make them transparent, whereas the thicker plastics used for rigid window coverings are thick enough to be almost totally opaque in the thermal infrared. Plexiglas and Fiberglas are more opaque than glass, but polycarbonate shows some transmission out to 6 microns.

Selective Surfaces

The problem of minimizing heat losses from a solar collector brings us to an examination of the optical properties of the absorber surface and the transparent windows. It is clear that we want as much radiant energy from the sun as possible to reach the absorber, while at the same time we wish to reduce to a minimum the thermal infrared energy radiating from the hot parts of the collector. Optical properties which vary widely from one spectral region to another produce what is termed selectivity. Figure 4 below illustrates the essential characteristics of selective surfaces.

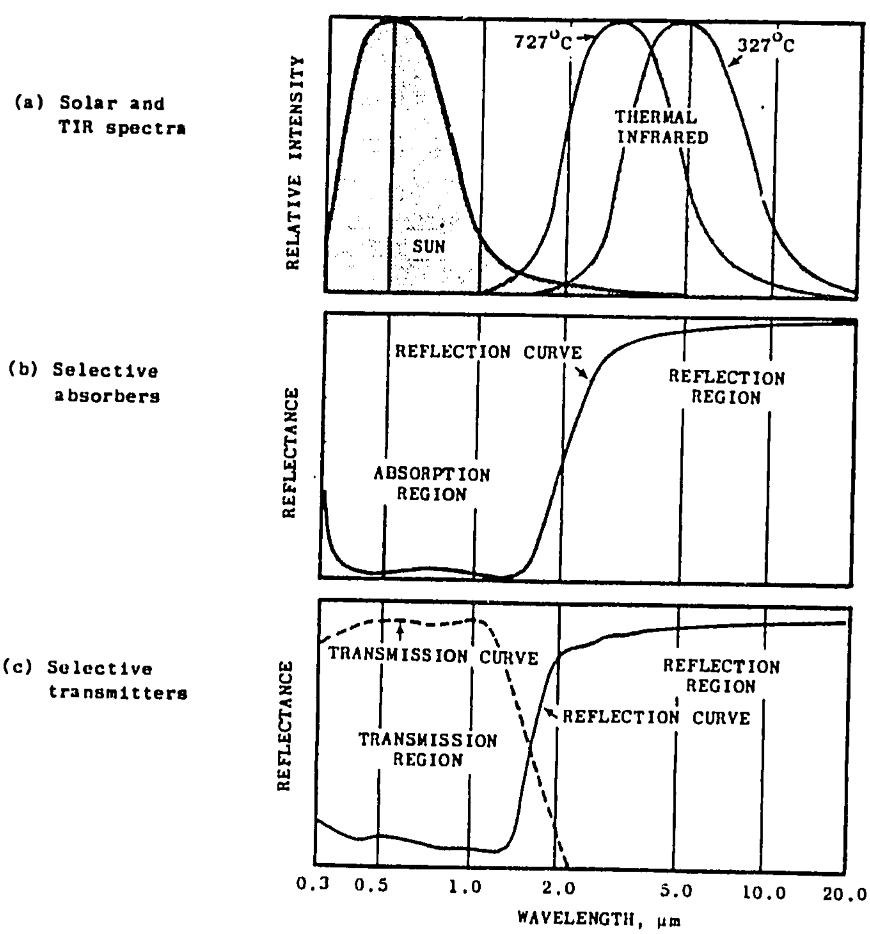

Fig. 4. Three diagrams illustrating the basic physics of selective surfaces. The top diagram shows radiant energy curves for the sun and for a hot surface radiating mainly in the thermal infrared; the middle diagram shows a typical curve for a selective absorber; the bottom diagram shows a typical curve for a selective transmitting surface. [5]

There are basically two types of selective surface of use in solar collectors:

1) Selective absorbing surfaces, where the surface is black to sunlight, making the transition from absorptive to reflective behavior in the region between 1.5 and 3 microns. By Kirchoff's law a reflective surface is a poor emitter, the value of the emittance being $\varepsilon = 1 - r$, where r is reflectivity of the surface. A highly selective surface is therefore one that has the highest possible reflectance in the thermal infrared. The measure of selectivity is the ratio of the absorptance for sunlight divided by the emittance for thermal infrared at the temperature of the projected use of the selective surface. This ratio, α/ε, can therefore vary with temperature, depending on the exact variations of both absorptance and emittance with wavelength.

2) Selective transmitting surfaces, where the surface is transparent to sunlight, making the transition from transmissive to reflective behavior in the region between 1.5 and 3 microns. The function of such surfaces is to let sunlight into a collector but to inhibit the loss of thermal infrared from the absorber.

TABLE 8. Properties of Some Selected Plated Coating Systems[a]

Coating[b]	Substrate	$\bar{\alpha}_s$	$\bar{\epsilon}_l$	Durability: Breakdown temperature (°F)	Durability: Humidity-degradation MIL STD 810B	Estimated manufactured cost per ft² (U.S.)
Black nickel on nickel	Steel	0.95	0.07	>550	Variable	0.30
Black chrome on nickel	Steel	0.95	0.09	>800	No effect	0.35–0.15
Black chrome	Steel	0.91	0.07	>800	Completely rusted	0.10
	Copper	0.95	0.14	600	Little effect	0.10
	Galvanized steel	0.95	0.16	>800	Complete removal	0.10
Black copper	Copper	0.88	0.15	600	Complete removal	0.10
Iron oxide	Steel	0.85	0.08	800	Little effect	0.05
Manganese oxide	Aluminum	0.70	0.08			0.10
Organic overcoat on iron oxide	Steel	0.90	0.16		Little effect	0.15
Organic overcoat on black chrome	Steel	0.94	0.20		Little effect	0.15

[a]From U.S. Dept. of Commerce, "Optical Coatings for Flat Plate Solar Collectors," NTIS No. PB-252-383, Honeywell, Inc., 1975.

[b]Black nickel coating plated over a nickel-steel substrate has the best selective properties ($\bar{\alpha}_s = 0.95$, $\bar{\epsilon}_l = 0.07$) but degraded significantly during humidity tests. Black chrome plated on a nickel-steel substrate also had very good selective properties ($\bar{\alpha}_s = 0.95$, $\bar{\epsilon}_l = 0.09$) and also showed high resistance to humidity. [4]

References

1. Perry, R.H., and Chilton, C.H., "Chemical Engineers' Handbook", 5th edition, McGraw-Hill Book Co., New York, 1973.

2. Baumeister, T., et. al., "Marks' Standard Handbook for Mechanical Engineers", 8th edition, McGraw-Hill Book Co., New York, 1978.

3. Duffie, J.A. and W.A. Bechman, "Solar Engineering of Thermal Processes", John Wiley, New York, 1980.

4. Kreith, F., and J.F. Kreider, "Principles of Solar Engineering", McGraw-Hill Book Co., New York, 1978.

5. Meinel, A.D., and M.P. Meinel, "Applied Solar Energy",

ANALYSIS OF FLAT PLATE COLLECTORS

Although solar energy is sometimes portrayed as a 'simple' technology, the thermal analysis of a solar collector is, in fact, quite complex. Flat plate collectors can be designed for applications requiring energy at moderate temperatures, up to about 100°C. They absorb both beam and diffuse solar radiation, do not need to track the sun, and generally require little maintenance.

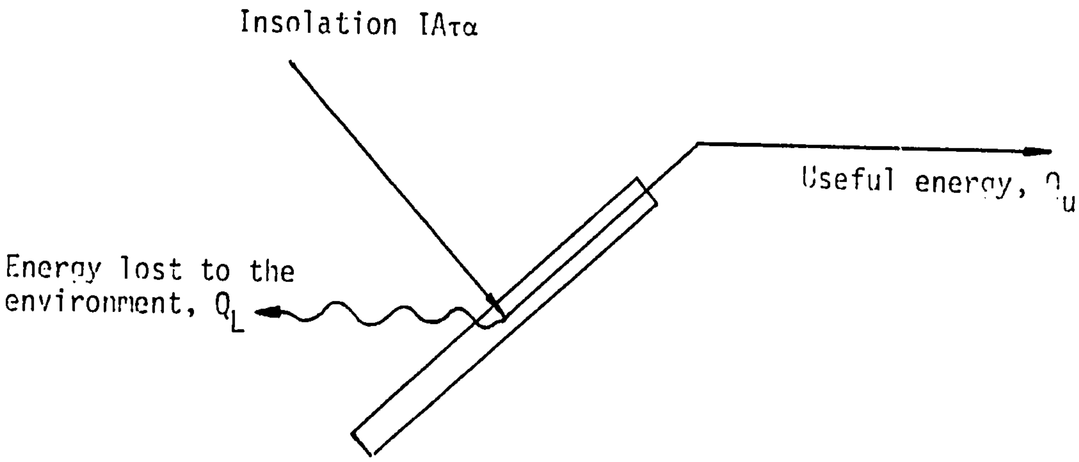

Figure 1. Energy balance over collector.

In the steady state, the heat balance over the collector may be written

$$Q_u = IA\tau\alpha - Q_L \qquad (1)$$

where Q_u = useful energy transferred from the absorber plate to the working fluid.

Q_L = heat losses from the collector.

I = incident solar radiation.

A = area of the collector.

τ = overall transmittance of the collector covers.

α = absorptance of the absorber surface.

The instantaneous efficiency of the collector, η , would then be defined as

$$\eta = \frac{Qu}{IA} \tag{2}$$

In practice, this is not a useful parameter since it varies continually with time. The average efficiency $\bar{\eta}$ is then:

$$\bar{\eta} = \frac{\int Q_u dt}{\int AIdt} \tag{3}$$

In Equation (1) the heat losses from the collector Q_L can be written as a function of the overall heat loss coefficient U_L as follows:

$$Q_L = U_L A(T_p - T_a) \tag{4}$$

where T_p is the mean plate temperature and T_a is the ambient temperature. Equation (1) becomes

$$Q_u = A[I\tau\alpha - U_L(T_p - T_a)] \tag{5}$$

The problem here is that the temperature of the absorber plate T_p is difficult to calculate or measure since it is a function of the collector design, the incident solar radiation, and the entering fluid conditions.

To help in the thermal analysis of flat plate collectors, and to get around the fact that the absorber plate temperature T_p in Equation (5) is not known, it is conventional practice to introduce two new variables into the analysis. These variables are the Collector Efficiency Factor and the Heat Removal Factor.

Collector Efficiency Factor

The collector efficiency factor F' is given by the following expression

$$F' = \frac{1/U_L}{W\left[\frac{1}{U_L[D + (W - D)F]} + \frac{1}{C_B} + \frac{1}{\pi D_i h_f}\right]} \qquad (6)$$

where
U_L = the collector overall heat loss coefficient.
W = the distance between tubes centres on the absorber plate.
D = the outside diameter of the tubes.
F = the fin efficiency.
C_B = the bond conductance.
D_i = the inside diameter of the tubes.
h_f = the inside convective film coefficient for the fluid.

Figure 2 below may be used to estimate the fin efficiency, F, or it may be calculated directly from

$$F = \frac{\tanh\,[m(W - D)/2]}{m\,(W - D)/2} \qquad (7)$$

where $m = \sqrt{U_L/k\,\delta}$ (8)

where
δ = absorber plate thickness.
k = thermal conductivity of the plate.

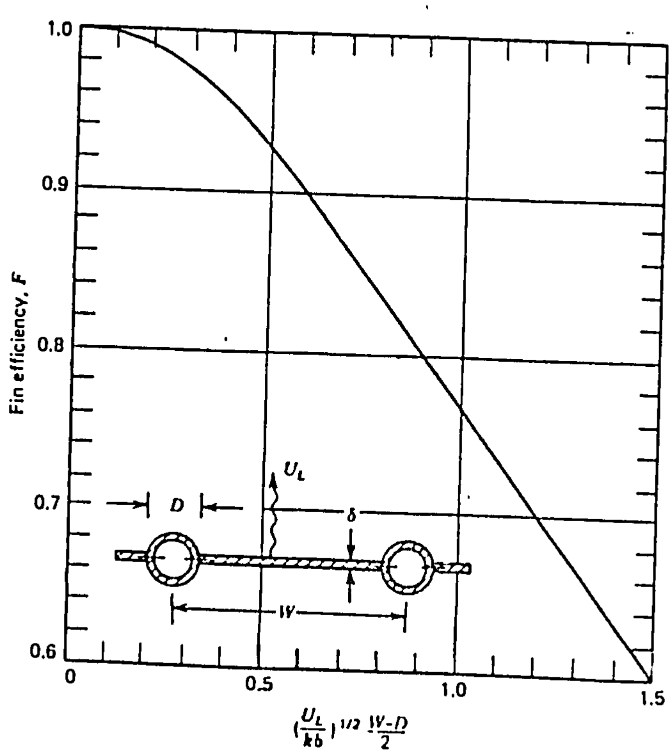

Figure 2 Fin efficiency for tube and sheet solar collectors. [3]

The bond conductance, C_B, can be estimated from a knowledge of the bond thermal conductivity, k, the bond average thickness, , and the bond width, B. On a per unit length basis

$$C_B = \frac{kB}{\gamma} \qquad (9)$$

The bond conductance can be very important in accurately describing collector performance. Simple wiring or clamping of the tubes to the absorber plate may result in a significant loss of performance.

The collector efficiency factor is essentially a constant for any collector design and fluid flow rate.

Collector Heat Removal Factor

The collector heat removal factor, F_R, may be determined from the following expression.

$$F_R = \frac{\dot{m}C_p}{U_L} \left(1 - e^{-1/C} \right) \qquad (10)$$

where C is a dimensionless collector capacitance equal to

$$C = \frac{\dot{m}C_p}{U_L F'} \qquad (11)$$

$\dot{m}$ = fluid mass flow rate, per unit area kg/m^2s
C_p = specific heat of the fluid, J/kg K
U_L = overall heat loss coefficient, W/m^2 K
F' = collector efficiency factor

It now becomes possible to write a simple expression for the useful energy collected by a flat plate collector.

$$Q_u = F_R A \left[I\tau\alpha - U_L(T_{in} - T_a) \right] \qquad (12)$$

This is a much more useful expression than Equation 5, since both T_{in}, the inlet temperature of the fluid, and the ambient temperature, T_a, are usually known. The heat removal factor, F_R, may be computed once U_L has been determined, and $I\tau\alpha$, the radiation striking the absorber plate, will also be available.

Example 1

Calculate the collector efficiency factor, F', and the collector heat removal factor, F_R, for the following system:

Overall loss coefficient	8 W/m^2 K
Tube spacing	150 mm
Tube I.D.	10 mm
Plate thickness	0.5 mm
Plate conductivity	385 W/m K
Heat transfer coefficient inside tubes	300 W/m^2 K
Bond resistance	0
Flow rate	0.03 kg/s
Specific heat of water	4190 J/kg K
Dimension	1 X 2 m

Solution

Determine the fin efficiency, F, from Equations 7 and 8.

$$m = \left(\frac{8}{385 \times 5 \times 10^{-4}}\right)^{1/2} = 6.45$$

$$F = \frac{\tan h \ [6.45(0.15 - 0.01)/2]}{6.45(0.15 - 0.01)/2}$$

$$= 0.937$$

The collector efficiency factor, F', is then given by Equation 6.

$$F' = \frac{1/8}{0.15\left[\frac{1}{8(0.01 + 0.14 \times 0.937)} + \frac{1}{\pi \times 0.01 \times 300}\right]}$$

$$= 0.34$$

To find the heat removal factor, F_R, we first determine the dimensionless capacitance, C, from Equation 11.

$$C = \frac{0.03 \times 4190}{2 \times 8 \times 0.84} = 9.35$$

so from Equation 10

$$F_R = \frac{0.015 \times 4190}{8} [1 - \exp(-1/9.35)]$$

$$= \underline{\underline{0.797}}$$

The Calculation of the Overall Loss Coefficient U_L

A basic calculation is to determine the overall collector heat transfer coefficient U_L. The thermal network for a two-cover flat plate collector is shown overleaf in Figure 3. It is clear that

$$R_1 = \frac{1}{h_{c2} + h_{r2}} \tag{13}$$

$$R_2 = \frac{1}{h_{c1} + h_{r1}} \tag{14}$$

$$R_3 = \frac{1}{h_{cp} + h_{rp}} \tag{15}$$

$$R_4 = \Delta x/k \tag{16}$$

$$R_5 = \frac{1}{h_{cb} + h_{rb}} \tag{17}$$

$$\text{and } U_L = \frac{1}{R_1 + R_2 + R_3} + \frac{1}{R_4 + R_5} \tag{18}$$

In some texts, a 'top loss' coefficient, U_t, and a 'back loss' coefficient U_b are specified, where

$$U_t = \frac{1}{R_1 + R_2 + R_3} \tag{19}$$

$$U_b = \frac{1}{R_4 + R_5} \tag{20}$$

In general, it is possible to assume R_5 is zero and that all resistance to heat flow is due to the insulation. However, it may also be necessary to consider edge losses. In a well designed system the edge loss should be small. It is recommended that edge insulation should be about the same thickness as that on the back of the collector. In this case edge losses can be included with the back loss to give

$$U_b = \frac{k}{x}(1 + A_e/A_c) \tag{21}$$

where A_e is area of the edge. This formulation assumes R_5 is zero and that the back and edges are insulated in a similar manner. Edge losses for well constructed large collector arrays are usually negligible, but for small collectors the edge losses may be significant.

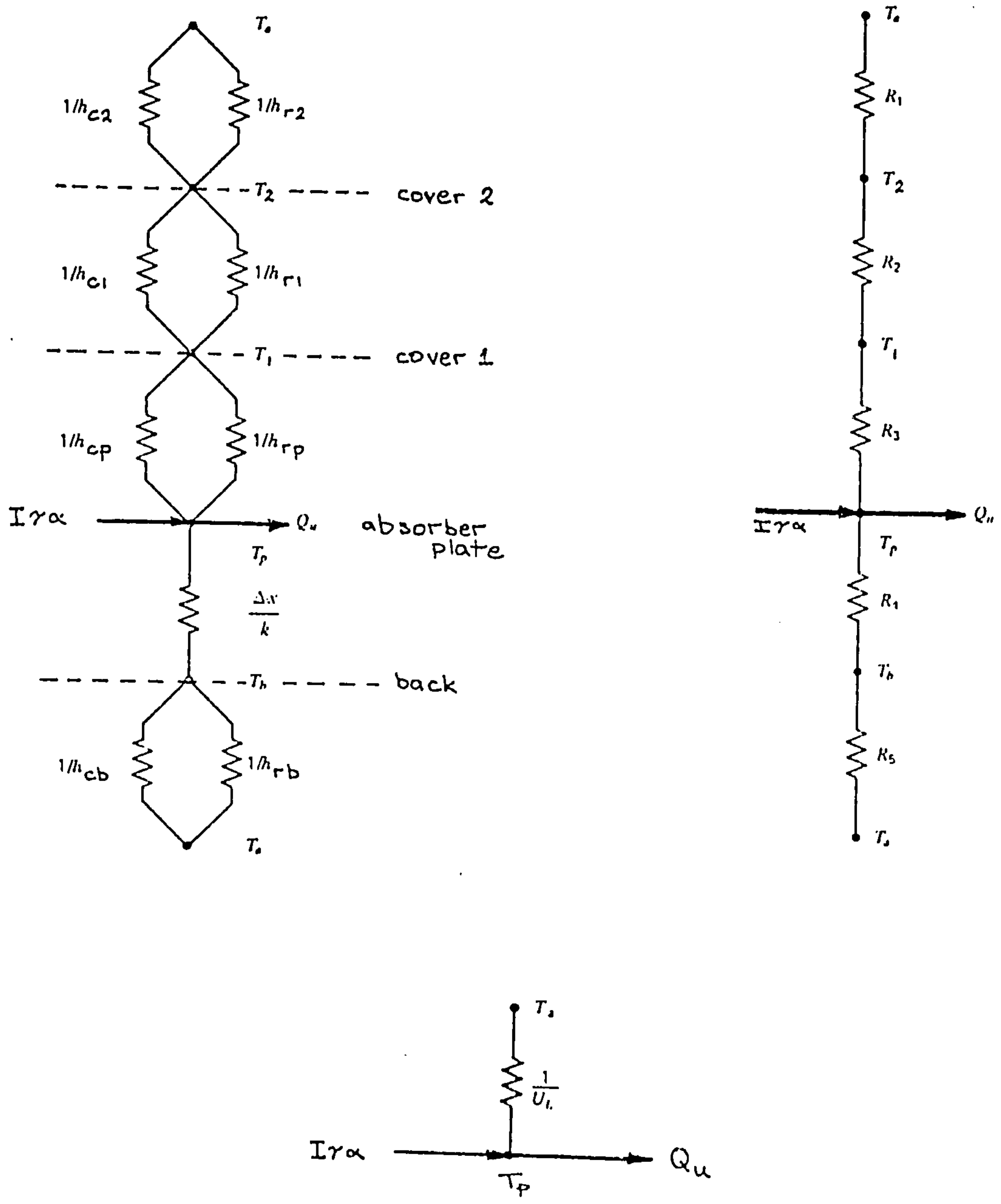

Figure 3. Thermal network for a two-cover flat-plate collector, (a) in terms of conduction, convection, and radiation resistances, (b) in terms of resistances between plates, (c) in terms of an overall heat transfer coefficient. [3]

h_c = convective heat transfer coefficient

h_r = radiative heat transfer coefficient

The procedure for determining the loss coefficient U_L is an iterative process. First, a guess is made of the unknown absorber plate and cover temperatures. This permits the calculation of the heat transfer coefficients and therefore the resistances to heat transfer. The value of U_L then follows from Equation 18. The absorber plate temperature is then recalculated from

$$T_p = T_{in} + \frac{Q_u/A}{U_L F_R}(1 - F_R) \tag{22}$$

A new temperature is then calculated for the first cover. This cover temperature is used to find the next cover temperature and so on. For any two adjacent covers, the new temperature of cover 2 can be expressed in terms of cover 1 as

$$T_2 = T_1 - \frac{U_t(T_p - T_a)}{h_{c1} + h_{r1}} \tag{23}$$

When the absorber plate temperature and the cover temperatures have been recalculated, the overall loss coefficient, U_L, is calculated once again. This iterative procedure continues until calculated and estimated plate and cover temperatures remain the same.

However, the calculation of U_L depends on estimating the radiative and convective heat transfer coefficients (h_r and h_c respectively) for the heat transfer between the absorber plate and the first cover, between the covers if there is more than one, and between the outer cover and the environment. The equations used to determine these coefficients are given below.

A) PLATE TO COVER

Radiation:

$$h_r = \frac{\sigma(T_p^2 + T_1^2)\cdot(T_p + T_1)}{1/\varepsilon_p + 1/\varepsilon_1 - 1} \quad W/m^2K \tag{24}$$

where T_p = absorber plate temperature, K
T_1 = innermost cover temperature, K
ε_p = absorber plate emittance
ε_1 = cover emittance
σ = Boltzmann's constant
= 5.67×10^{-8} W/m^2K^4

Convection:

$$h_c = \frac{k}{d} N \quad W/m^2K \tag{25}$$

where k = thermal conductivity of air, Wm/K
d = distance between the surfaces
N = a dimensionless number (the Nusselt number) which may be determined here as

$$N = 1 + 1.44\,[1 - z]^+[1 - z(\sin 1.8\beta)^{1.6}] + [0.664z^{-1/3} - 1]^+ \tag{26}$$

In this equation the meaning of the + exponent is that only the positive values of the term in the square brackets are to be used, (i.e. a value of zero is used if the term is negative).

Also $z = 1708/R \cos\beta$ (27)

where β is the angle between the collector and the horizontal; R is another dimensionless number, the Rayleigh number and is given by

$$R = g\Delta T\, d^3 \rho^2\, C_p/\mu k T \qquad (28)$$

and here
- g = acceleration due to gravity, 9.81 m/s^2
- ΔT = temperature difference between the surfaces, K
- d = distance between the surfaces, m
- ρ = density of air, kg/m^3
- C_p = specific heat of air at constant pressure, J/kg K
- μ = viscosity of air, kg/m.s
- k = thermal conductivity of air, Wm/K
- T = the average temperature of the air between the surfaces, K

B) COVER TO COVER

Radiation: Same as Equation (24) except that the equation is now applied to the two cover surfaces.

Convection: Same as for the plate-to-cover situation.

C) OUTER COVER TO SKY

Radiation: $h_r = \varepsilon\sigma(T_2^2 + T_s^2)(T_2 + T_s)$ (29)

where
- ε = emittance of outer cover
- T_2 = cover temperature, K
- T_s = sky temperature, K
- σ = Boltzmann's constant = 5.67×10^{-8} W/m^2K^4

Convection: $h_c = 4.5 + 2.9\,u$ W/m^2K (30)

The calculation of heat transfer coefficients for flat heated surfaces exposed to wind is not yet well established. For smooth surfaces Equation (30) is a reasonable approximation. The average wind speed, u, must be in metres per second.

Example 2

Calculate the overall loss coefficient for a collector (single cover) with the following specifications:

Plate to cover spacing	25 mm
Plate emittance	0.95
Ambient air and sky temperature	10°C (283 K)
Wind heat transfer coefficient	10 W/m^2 K
Mean plate temperature	100°C (373 K)
Collector tilt	45°
Glass emittance	0.88
Back insulation thickness	50 mm
Insulation conductivity	0.045 W/m.K
Collector array dimensions	10 X 3 X 0.075 m

Solution

Estimate the cover temperature as 35°C (308 K). In this example the absorber plate temperature has been specified.

A) PLATE TO COVER

Radiation: From Equation (24),

$$h_{rp} = \sigma \frac{(T_p{}^2 + T_1{}^2)(T_p + T_1)}{1/\varepsilon_p + 1/\varepsilon_1 - 1}$$

$$= 5.67 \times 10^{-8} \times \frac{(373^2 + 308^2)(373 + 308)}{1/0.95 + 1/0.88 - 1}$$

$$= \underline{7.60 \text{ W/m}^2 \text{ K}}$$

Convection: $h_{cp} = kN/d$ where Equations 26, 27 and 28 are to be used.

$$R = \frac{g\ \Delta T\ d^3 \rho^2 C_p}{\mu k T}$$

from Table 1 at $T = \frac{100 + 35}{2} = 67.5°C$

$= 340.5$ K

$\rho = 1.032$ kg/m^3
$C_p = 1.0084 \times 10^3$ J/kg K
$\mu = 2.0575 \times 10^{-5}$ kg/ms
$k = 0.02931$ W/m K
$\Delta T = 100 - 35 = 65$ K
$d = 0.025$ m

so $R = \dfrac{9.81 \times 65 \times 0.025^3 \times 1.032^2 \times 1008.4}{2.0575 \times 10^{-5} \times 0.02931 \times 340.5}$

$= 52110$

From Equation 27, $Z = 1708/52110 \times \cos 45° = 0.0464$

and $(\sin 1.8\beta)^{1.6} = 0.98$

so $N = 1 + 1.44\,[1 - 0.0464][1 - 0.0464(0.98)] + [0.664(0.0464)^{-1/3} - 1]$

$= 3.159$

hence $h_{cp} = 3.159 \times \dfrac{0.02931}{0.025} = \underline{3.70 \text{ W/m}^2\text{ K}}$

B) COVER TO SKY

Radiation: $h_{r1} = \varepsilon\sigma(T_1{}^2 + T_s{}^2)(T_1 + T_s)$

$= 0.88 \times 5.67 \times 10^{-8}(308^2 + 283^2)(308 + 283)$

$= \underline{5.16 \text{ W/m}^2\text{ K}}$

Convection: $\underline{h_{c1} = 10 \text{ W/m}^2\text{ K}}$ (given)

so resistance, plate to cover $= \dfrac{1}{7.60 + 3.70}$

$= 0.0885 \text{ m}^2\text{ K/W}$

and resistance, cover to sky $= \dfrac{1}{5.16 + 10}$

$= 0.0660 \text{ m}^2\text{ K/W}$

so $U_t = \dfrac{1}{0.0885 + 0.0660} = 6.47 \text{ W/m}^2\text{ K}$

This is the first estimate of the top loss coefficient. We now check the first estimate of the cover temperature. From Equation 23

$$T_1 = T_p - \frac{U_t(T_p - T_a)}{h_{cp} + h_{rp}}$$

$$= 100 - \frac{6.47(100 - 10)}{7.6 + 3.70}$$

$$= 48.5°C$$

The procedure now is to recompute all the film coefficients using this new estimate of the cover temperature. We do not repeat the calculations here, but the results are:

$$h_{rp} = 8.03 \text{ W/m}^2 \text{ K}$$
$$h_{cp} = 3.52 \text{ W/m}^2 \text{ K}$$
$$h_{r1} = 5.53 \text{ W/m}^2 \text{ K}$$
$$h_{c1} = 10 \quad \text{W/m}^2 \text{ K} \qquad \text{as before}$$

so $$U_t = \left(\frac{1}{8.03 + 3.52} + \frac{1}{5.53 + 10}\right)^{-1}$$
$$= \underline{6.62 \text{ W/m}^2\text{K}}$$

The third estimate of the cover temperature, T_1, is therefore

$$T_1 = 100 - \frac{6.62(100 - 10)}{8.03 + 3.52}$$
$$= \underline{48.4°\text{C}}$$

so the calculation is acceptable.

Once the top loss coefficient has been determined, the back loss coefficient can be quickly found.

from Equation 21 $$U_b = \frac{k}{x}\left(1 + \frac{A_e}{A_c}\right)$$

so $$U_b = \frac{0.045}{0.05}\left[1 + \frac{2(10 + 3) \text{ X } 0.075}{10 \text{ X } 3}\right]$$
$$= 0.96 \text{ W/m}^2 \text{ K}$$

so $$U_L = U_t + U_b = 6.62 + 0.96$$
$$= \underline{7.58 \text{ W/m}^2 \text{ K}}$$

The charts overleaf give top loss coefficients for typical flat plate collectors under a variety of environmental conditions.

Top Loss Coefficients for Flat Plate Collectors With a Plate Emittance of 0.95 [3]

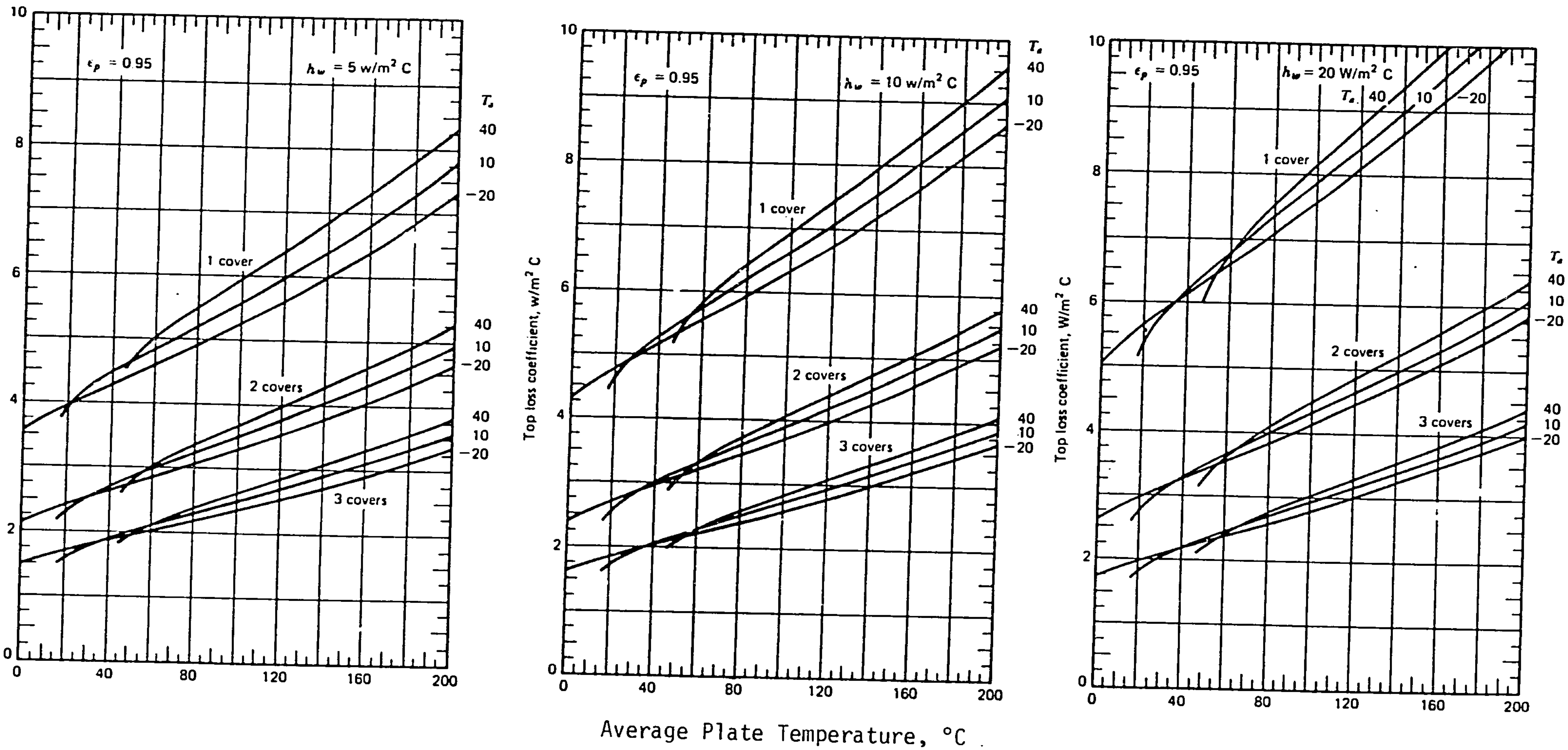

Top Loss Coefficients for Flat Plate Collectors With a Plate Emittance of 0.1 [3].

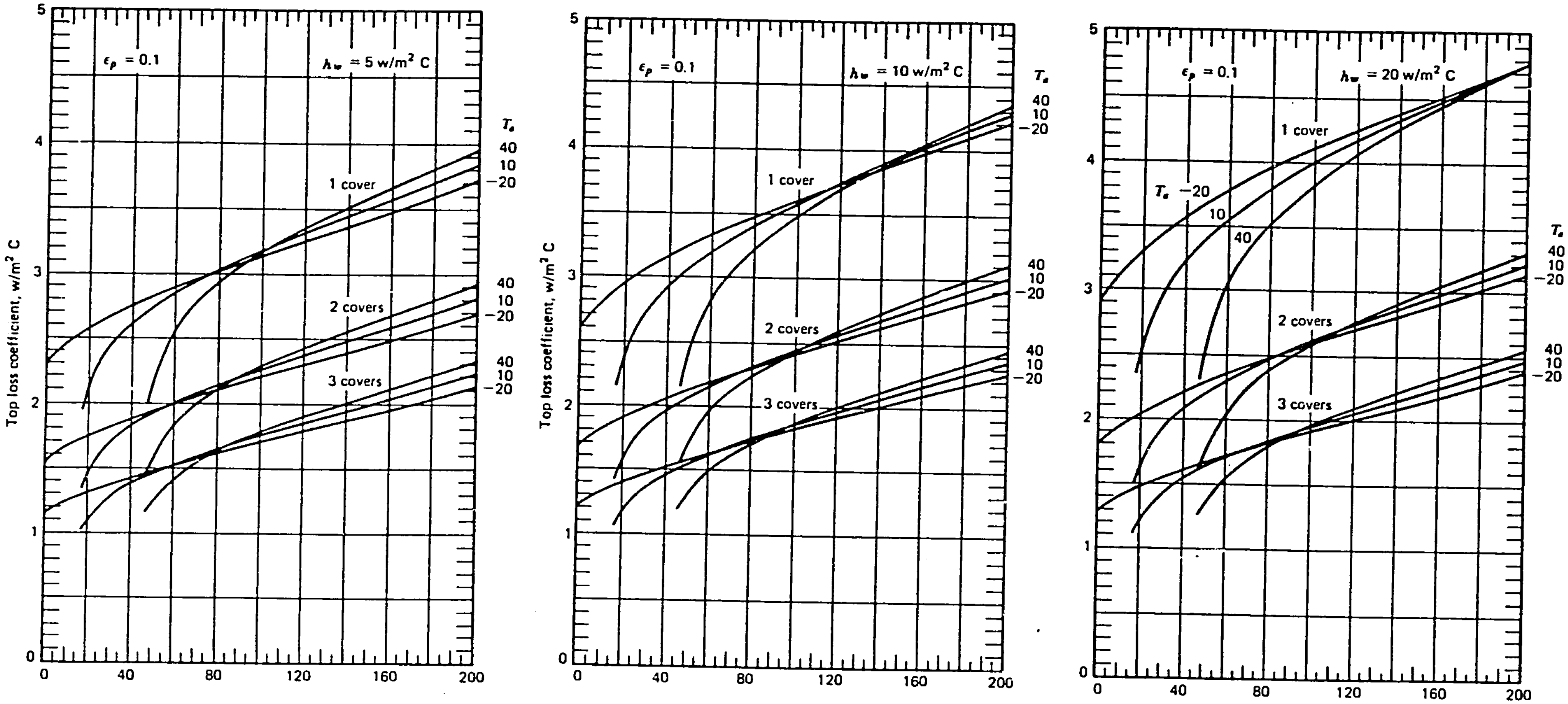

Average Plate Temperature, °C

Minimizing Thermal Losses

Assuming the collector to be adequately insulated (including the edges), there remain two principal modifications to further reduce heat losses from the collector. The first is to add additional covers or glazings, the second is to incorporate a selective absorber plate. Figure 4 below shows the effect on thermal losses of double glazing and selective surfaces. The cover temperatures and the heat flux by convection and radiation are shown for one and two glass covers and for selective and non-selective absorber plates. Note that radiation between the inside surfaces is the dominant mode of heat transfer in the absence of a selective surface. When a selective surface having an emittance of 0.10 is used, convection is the dominant heat transfer mode between the selective surface and the cover, but radiation is still the largest term between the two covers in the double-glazed system.

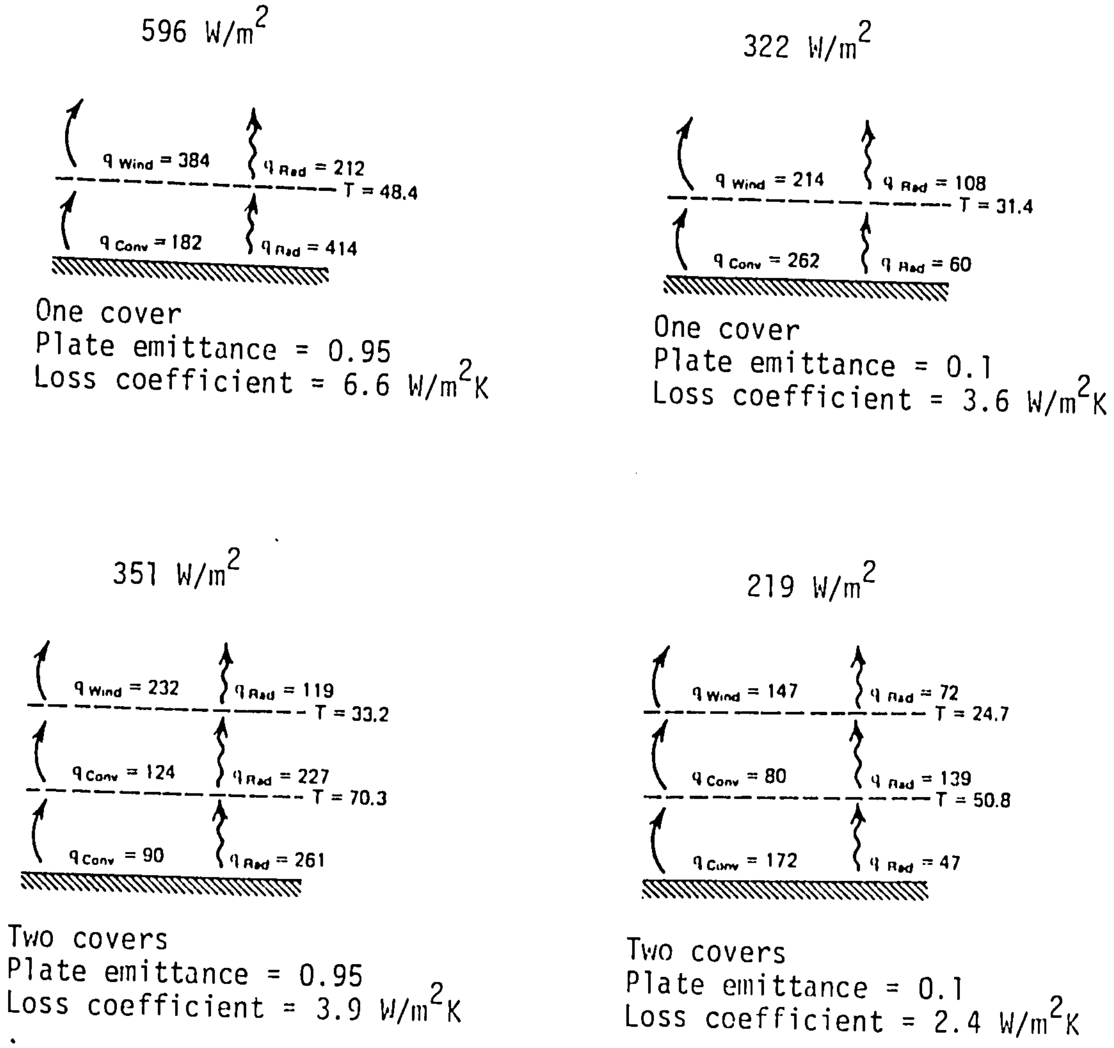

Figure 4. Data for flat plate collectors operating at 100°C with ambient and sky temperatures of 10°C, cover spacing of 25 mm, tilt of 45°, and a wind loss coefficient of 10 W/m K. [ref. 3]

Energy Gain from Flat Plate Collectors

It is now possible to evaluate all the terms necessary to compute the amount of useful energy delivered by a flat plate collector. This quantity, Q_u watts, is found from Equation 12, after F_R and U_L have been determined in the manner illustrated by Examples 1 and 2. However, equation 12 is time-dependent since I, the incident solar radiation, obviously varies through the day. In order to determine, therefore, the useful energy delivered by the collector and its mean efficiency, it is necessary to compute Q_u for short time increments over the period of a day. The procedure is illustrated by the following example.

Example 3

Calculate the daily useful gain and efficiency of a bank of 10 solar collectors installed in parallel. The hourly radiation on the plane of the collector, I, and the hourly ambient temperature, T_a, are given in the table below. Assume that the combined $\tau\alpha$ coefficient is 0.8 the overall loss coefficient, U_L, is 6.6 W/m^2K, and the heat removal factor is 0.8. Each collector is 2 m^2 in area. If the fluid inlet temperature is 40°C and the flow rate through each collector is 0.03 kg/s, what is the fluid temperature rise and how does it vary during the day?

Time	T_a (°C)	I (W/m^2)
7 - 8	20	5.6
8 - 9	24	119.4
9 - 10	25	275.0
10 - 11	28	788.9
11 - 12	31	833.3
12 - 1	33	913.8
1 - 2	31	866.7
2 - 3	30	644.4
3 - 4	29	336.1
4 - 5	26	13.9
		4797.1 W hr/m^2

Solution

We wish to calculate the useful energy delivered from Equation 12 and the mean efficiency from Equation 3. For each time increment we have:

Time	$I\tau\alpha$ (W/m^2)	$U_L(T_{in} - T_a)$ (W/m^2)	Q_u/A (W/m^2)
7 - 8	4.5	132.0	0
8 - 9	95.5	105.6	0
9 - 10	220.0	99.0	96.8
10 - 11	631.1	79.2	441.5
11 - 12	666.6	59.4	485.8
12 - 1	731.0	46.2	547.8
1 - 2	693.4	59.4	507.2
2 - 3	515.5	66.0	359.6
3 - 4	268.9	72.6	157.0
4 - 5	11.1	92.4	0
			2595.7 W hr/m^2

the mean efficiency $\bar{\eta} = \frac{\Sigma Q_u/A}{\Sigma I}$

$$= \frac{2595.7}{4797.1} = 0.54$$

The energy delivery by the 20 m^2 array over the day is

$$2595.7 \times 20 \times 3600 = \underline{\underline{186.9 \text{ MJ}}}$$

The temperature rise for the water will vary according to the period. The smallest positive temperature rise is between 9 and 10; the highest between 12 and 1.

taking $C_p = 4195$ J/kg K

and $\dot{m} = 0.03$ kg/s for each 2 m^2 collector.

then $\Delta T = \frac{Q_u}{\dot{m}C_p}$

so from 9 - 10: $\Delta T = \frac{96.8 \times 2}{0.03 \times 4195} = 1.5°C$

and from 12 - 1: $\Delta T = \frac{547.8 \times 2}{0.03 \times 4195} = 8.7°C$

Performance Characteristics

The performance characteristics of flat-plate collectors are often presented graphically.

Since the instantaneous efficiency is given by

$$\eta = \frac{Q_u}{IA}$$

and since $Q_u = F_R A[I\tau\alpha - U_L(T_{in} - T_a)]$

the efficiency may be expressed as a function of the fluid inlet temperature, T_{in}, as

$$\eta = -F_R U_L\left(\frac{T_{in} - T_a}{I}\right) + F_R\tau\alpha \qquad (31)$$

If η is plotted against $(T_{in} - T_a)/I$ then a straight line results with a negative slope of $F_R U_L$. The intercept on the abscissa is equal to $F_R\tau\alpha$. A number of typical plots are shown overleaf. It is clear that, in practice, there is considerable data scatter and that, moreover, the plots are slightly non-linear. However, a straight line drawn through the data points and intercepting the abscissa presents a very convenient indication of collector performance. It will be necessary to calculate or estimate the transmittance of the covers, τ, and the absorptance of the collector plate surface α. The intercept divided by the product, $\tau\alpha$, gives the value of F_R, the collector heat removal factor. The slope of the line divided by F_R then gives U_L, the overall heat loss coefficient.

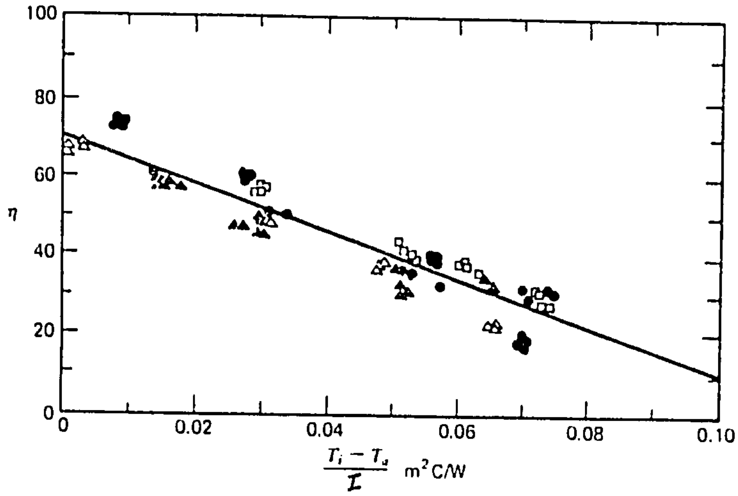

Experimental collector efficiency data measured for a type of liquid heating collector with one cover and a selective absorber. Sixteen points are shown for each of five test sites. The curve represents the theoretical characteristic derived from points calculated for the test conditions. [3]

Efficiency curve for a double-glazed flat-plate liquid-heating solar collector with a selective coating on the absorber. $\dot{m}$ = 0.0136 kg/sec · m²; T_a = 29°C; T_{in} = 38–101°C; I = 590–977 W/cm²; wind ≈ 3.1 m/sec. (The tests were run indoors using a solar simulator.) [4]

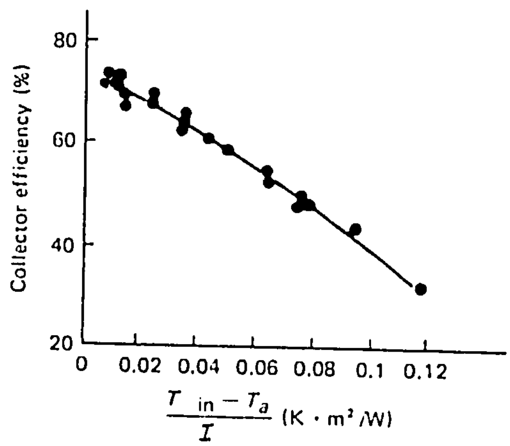

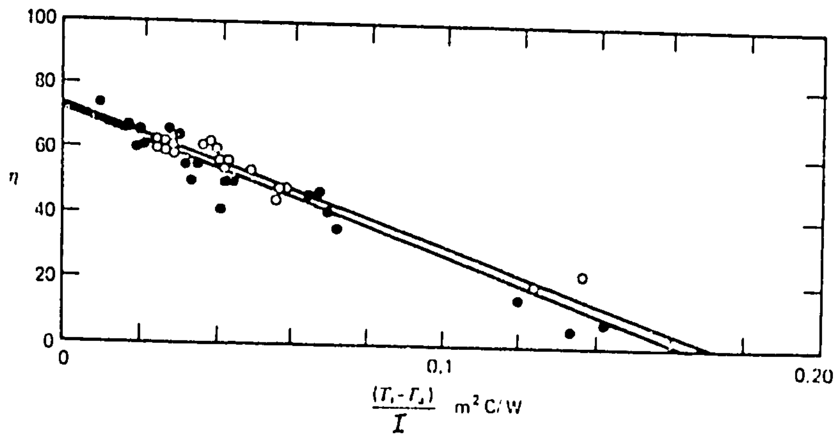

Experimental thermal efficiency curves for two air heaters operated outdoors. Absorbing surface was flat black paint. [3]

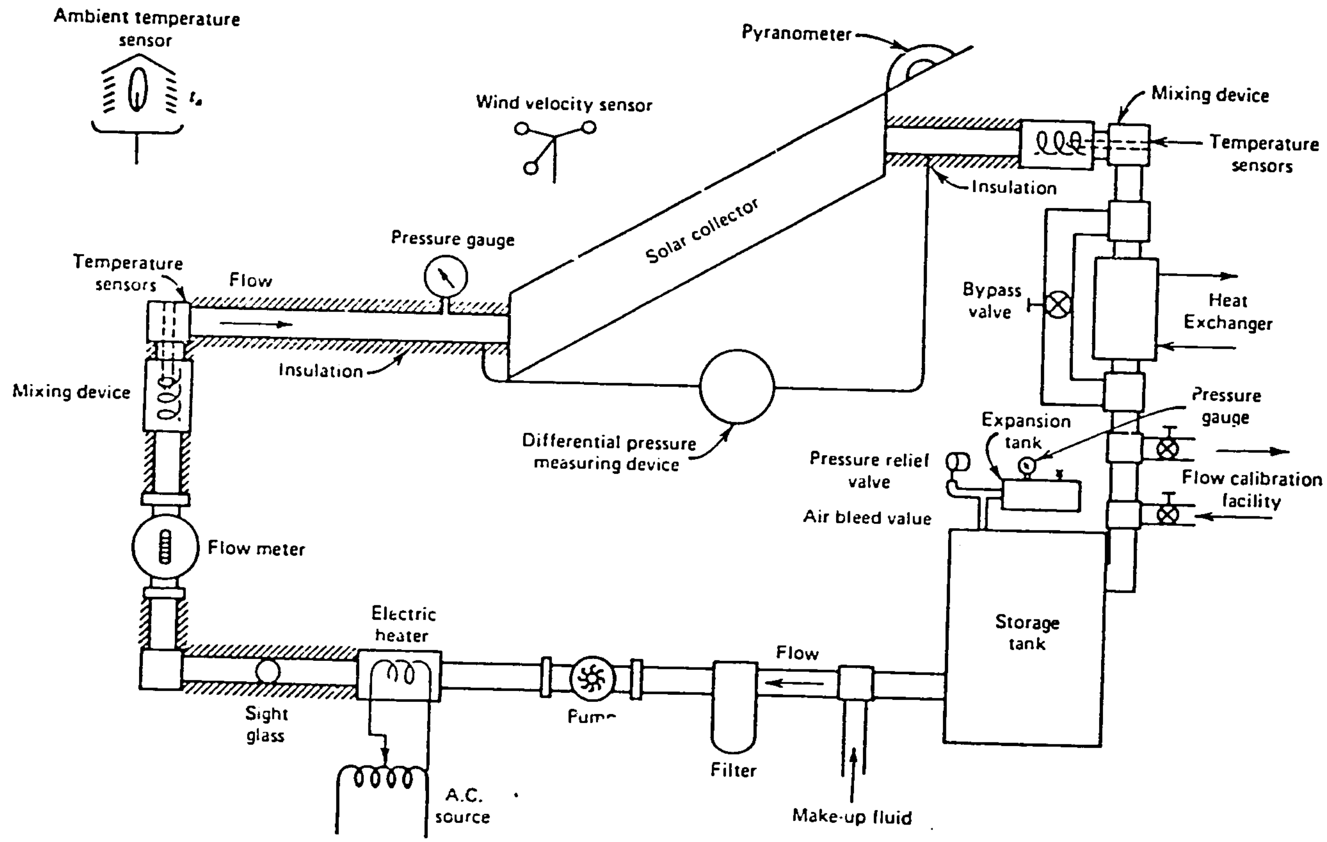

PERFORMANCE TESTING OF FLAT PLATE COLLECTOR

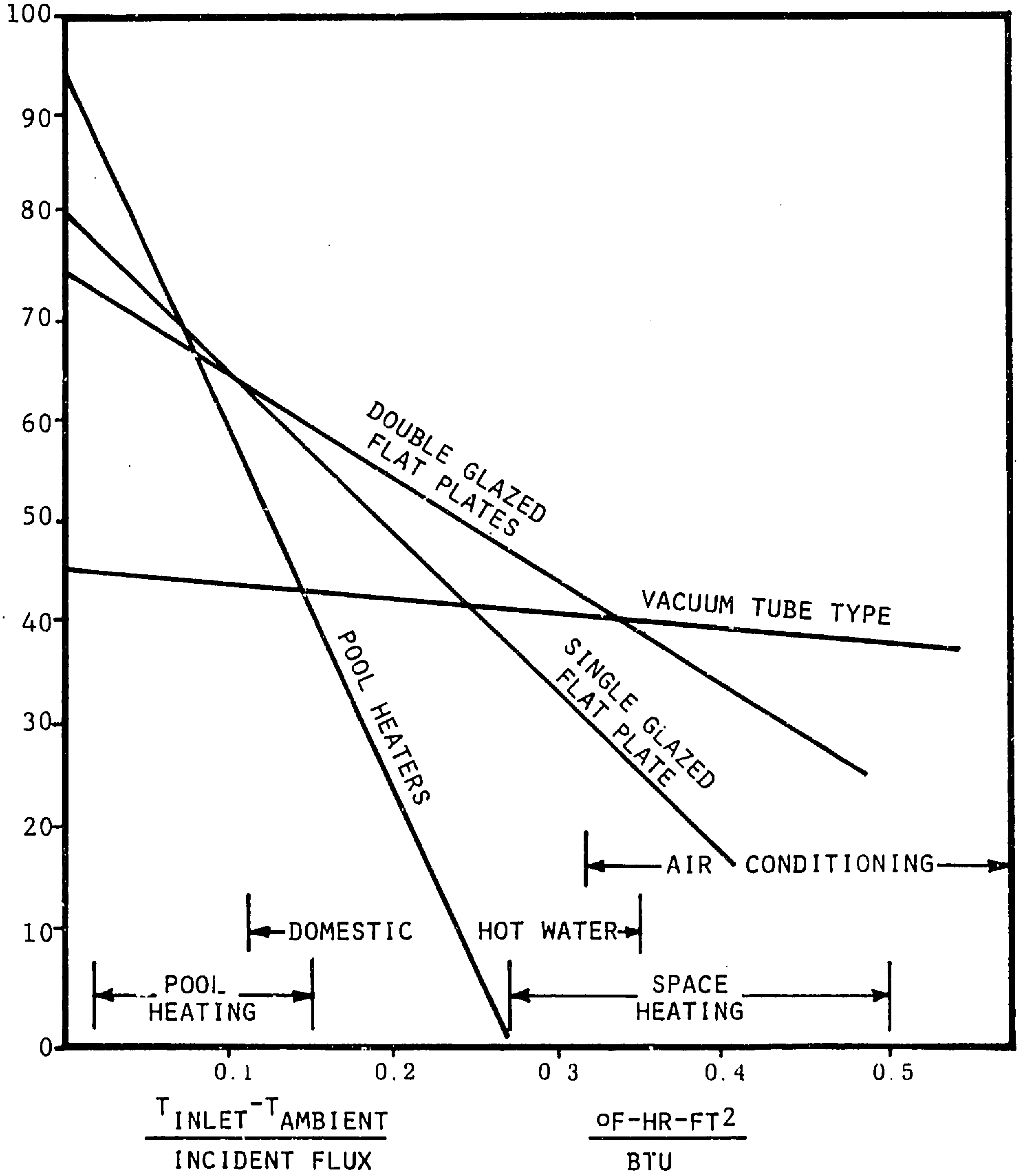

Collector Efficiencies of Various Liquid Collectors

References

1. Perry, R.H., and Chilton, C.H., "Chemical Engineers' Handbook", 5th edition, McGraw-Hill Book Co., New York. 1973.

2. Baumeister, T., et. al., "Marks' Standard Handbook for Mechanical Engineers", 8th edition, McGraw-Hill Book Co., New York, 1978.

3. Duffie, J.A. and W.A. Bechman, "Solar Engineering of Thermal Processes", John Wiley, New York, 1980.

4. Kreith, F., an dJ.F. Kreider, "Principles of Solar Engineering", McGraw-Hill Book Co., New York, 1978.

5. Meinel, A.D., and M.P. Meinel, "Applied Solar Energy",

SOLAR THERMAL SYSTEMS

Solar thermal systems designed to utilize solar radiation for heating or cooling are generally composed of a number of basic subsystems. These are:

1. Solar collector system
2. Thermal energy storage system
3. Fluid circulation system
4. Heat exchanger system
5. Control system

The solar collection part of the system has been examined in a previous section. In this set of notes we want to look at the remaining components of a solar thermal system: thermal energy storage, fluid circulation, heat exhangers and control.

Thermal Energy Storage

Solar energy is a time-dependent and variable resource. This characteristic makes thermal energy storage virtually a mandatory component of any solar thermal system. Thermal storage is used to dampen out diurnal and meteorological variations in the level of insolation and provide a more nearly constant heat source for the system load. The optimal size of the storage system depends on a number of considerations: the insolation and meteorological characteristics of the area where the system is located, the nature of the system load, and the economics of the total system.

Water is by far the most common thermal storage medium for solar powered thermal systems requiring a temperature of less than 100°C. Water has a number of very attractive properties as a thermal storage medium. It is cheap, non-toxic and non-flammable; it has a high specific heat, high density and excellent transport properties.

For some applications heat storage in solid med is a possibility, particularly when air is used to collect and transport thermal energy. Solid-phase storage has a number of advantages: they generally permit larger temperature variations and higher operating temperatures, they stratify thermally, and they are durable and reliable systems. Table 1 shows thermal properties for a number of liquids and solids.

It is clear that on both a mass and a volumetric basis, water is an excellent thermal storage medium.

An alternative method of thermal energy storage takes advantage of the fact that a considerable amount of heat is absorbed or evolved during a change of phase. A thermal energy storage system that uses solid-liquid phase changes in the storage medium to store heat is called a phase-change storage system.

There are two kinds of solid-liquid phase change storage systems. The first is simple melting and freezing; the second involves the chemical reaction between water and salt hydrates. When the hydrate is heated, the salt dissolves in its water of crystallization and absorbs heat. On cooling the anhydrate becomes hydrated and crystallizes with the evolution of heat. Table 2 gives the melting point and heat of fusion for a number of phase change materials.

Although phase-change storage has great potential, it suffers from a lack of reliability and durability, particularly with salt hydrate systems. After many cycles, the rehydration (crystallization) phase change requires progressively more subcooling before it takes place. The isothermal behavior, therefore, deteriorates. In addition, since the phase change is not a true melting, density differences between component compounds may occur which exacerbates the subcooling problem.

Table 1. Properties of Heat Storage Materials

Material	Specific heat kJ/kg K	Density kg/m^3	Heat capacity kJ/m^3 K
Water	4.2	1000	4200
Isobutanol	3.0	808	2420
Propanol	2.5	800	2000
Scrap iron	0.50	7850	2748
Magnetite	0.75	5126	2691
Scrap aluminum	0.96	2723	1830
Concrete	1.13	2240	1772
Stone	0.88	2720	1676
Brick	0.84	2240	1317

Note: The volumetric heat capacity for the solid materials assumes a 30% void fraction.

Table 2. Properties of Phase Change Materials

Material	Melting point °C	Heat of fusion kJ/kg
Calcium chloride hexahydrate	30	168
Sodium carbonate decahydrate	33	267
Disodium phosphate dodecahydrate	40	279
Calcium nitrate tetrahydrate	47	153
Sodium sulfate decahydrate (Glauber's salt)	32	241
Sodium thiosulphate pentahydrate (STP)	45	95
Naphthalene	80	149
Naphthol	95	163
Paraffin	74	230
P-116 wax	47	209

Water Storage Systems

Water is a good storage medium. A typical system is shown in Figure 1.

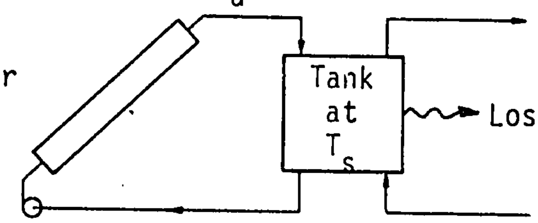

Figure 1. Typical collector and storage system

For a well mixed tank of water it is not too difficult to accurately model the system. An energy balance over the tank yields the equation

$$M_s c_p \frac{dT_s}{dt} = Q_u - Q_L - L \tag{1}$$

where M_s = mass of water in storage, kg,
c_p = specific heat of water, J/kgK,
T_s = temperature of stored water,
t = time,
Q_u = heat added to the storage, Watts,
Q_L = heat lost from the system, Watts,
L = heat extracted by the load, Watts.

Since the thermal losses, Q_L, can be expressed as a linear function of temperature difference, $T_s - T_a^*$, where T_a^* is the ambient temperature close to the storage system, Equation 1 can be rewritten as

$$M_s c_p \frac{dT_s}{dt} = Q_u - (UA)_s(T_s - T_a^*) - L \tag{2}$$

where $(UA)_s$ is the loss coefficient for the storage system. This term can be readily estimated by determining conduction, convection, and radiation losses from the storage tank. The example below shows how this equation can be used to estimate the storage temperature as a function of time by the use of a simple numerical integration procedure.

Example 1

A well-mixed water tank storage system containing 1,500 kg of water has a loss coefficient of 11.1 W/K. The tank commences a 24 hour day at a temperature of 45°C and is in a room at 20°C. Energy Q_u is added and energy L is extracted as indicated on an hourly basis below. Calculate the temperature of the tank over the 24-hour period using numerical integration.

Hour	Energy Added Q_u, MJ/hr	Energy Extracted L, MJ/hr
1	-	12
2	-	12
3	-	11
4	-	11
5	-	13
6	-	14
7	-	18
8	-	21
9	21	20
10	41	20
11	60	18
12	75	16
13	77	14
14	68	14
15	48	13
16	25	18
17	2	22
18	-	24
19	-	18
20	-	20
21	-	15
22	-	11
23	-	10
24	-	9

Solution

The differential equation of Equation 2 can be approximately solved by rewriting it as:

$$T_s^+ = T_s + \frac{\Delta t}{M_s c_p} [Q_u - (UA)_{\_} (T_s - T_a^*) - L]$$

The starting temperature (T_s) of 20°C is used to estimate the tank temperature after 1 hr, T_s^+. This calculated temperature then becomes the tank temperature, T_s, and a new temperature T_a^+ is estimated by recursively applying the above equation. Substituting the given constants reduces the equation to:

$$T_s^+ = T_s + \frac{\Delta t}{1500 \times 4190} [Q_u - 11.1 \times 3600 (T_s - 20) - L]$$

$$\text{or } T_s^+ = T_s + \frac{\Delta t}{6.285 \times 10^6} [Q_u - 39,960 (T_s - 20) - L]$$

The temperature profile may now be estimated as follows. After one hour:

$$T_s = 45 + \frac{1}{6.285 \times 10^6} [0 - 39,960 (45-20) - 12 \times 10^6]$$

or $T_s^+ = 42.9°C$

After 2 hours:

$$T_s^+ = 42.9 + \frac{1}{6.285 \times 10^6} [0 - 39,960 (42.9 - 20) - 12 \times 10^6]$$

or $T_s^+ = 40.9°C$

This recursive procedure is continued through the 24 hour period to produce the approximate time variation of the storage temperature. The calculated temperatures are shown below.

Hour	Q_u MJ/hr	L MJ/hr	T_s °C
0	-	-	45
1	-	12	42.9
2	-	12	40.9
3	-	11	39.0
4	-	11	37.1
5	-	13	35.0
6	-	14	32.6
7	-	18	29.7
8	-	21	26.3
9	21	20	26.4
10	41	20	29.7
11	60	18	36.3
12	75	16	45.6
13	77	14	55.5
14	68	14	63.8
15	48	13	69.1
16	25	18	69.9
17	2	22	66.4
18	-	24	62.3
19	-	18	59.2
20	-	20	55.7
21	-	15	53.1
22	-	11	51.2
23	-	10	49.4
24	-	9	47.8

Equation 2 may be extended by introducing the relationship between Q_u, the energy gain from the solar collector, the temperature of the storage system T_s, the insolation characteristics, and the collector overall loss coefficient, U_L. We can write

$$Q_u = F_R A \left[I\tau\alpha - U_L (T_s - T_a) \right] \qquad \text{Watts} \qquad (3)$$

where F_r = collector heat removal factor
A = collector area, m^2
T_a = ambient temperature, °C
τ = transmissivity of the collector covers
α = absorptance of the absorber.

If Q_u is to be calculated from Equation 3 from hourly insolation and temperature data, it should be recalled that it is the function of the system control devices to pump fluid through the collector loop only when there is an energy gain. This occurs when the insolation has increased to the point where $I\tau\alpha$ is greater than $U_L (T_s - T_a)$.

Example 2

Determine the hourly performance of the large solar heating installation indicated below

Area of collectors	= 100 m^2
Storage volume	= 7.5 m^3
Collector overall loss coefficient	= 5.2 W/m^2K
Storage losses	= negligible

The heat removal factor, F_R, is estimated as 0.8, $\tau\alpha$ as 0.85. The load over the period is constant at 25 kW. The insolation levels and ambient temperatures are shown below. Assume the initial storage temperature is 70°C.

Time	I (W/m^2)	T_a (°C)
8	157.6	20
9	516.9	24
10	740.7	25
11	870.0	28
12	914.1	31
13	870.0	33
14	740.7	32
15	516.9	31
16	157.6	29

Solution

The heat balance over the storage system, Equation 2, reduces to

$$7500 \times 4190 \frac{dT_s}{dt} = Q_u - 25{,}000 \qquad \text{Watts}$$

$$\text{where } Q_u = 80 \left[0.85I - 5.2 (T_s - T_a) \right] \qquad \text{Watts} \qquad (4)$$

The differential equation can be solved numerically by rewriting it as

$$T_s^+ = T_s + \frac{\Delta t}{31.43 \times 10^6} [Q_u - 25,000]$$

or for Δt = 1 hr = 3,600s

$$T_s + = T_s + 1.145 \times 10^{-4} [Q_u - 25,000] \qquad (5)$$

The calculation proceeds as follows:

Time = 0800 hrs, I = 157.6 W/m^2, T_a = 20°C, T_s = 70°C

From Equation 4 Q_u = 80 [0.85 X 157.6 - 5.2 X 50]
= - 10,083 Watts

Therefore there is no energy gain from the collectors at this point. With Q_u = 0, (no flow through the collectors) Equation 5 becomes

$$T_s^+ = T_s + 1.145 \times 10^{-4} [-25,000]$$

or

$$T_s^+ = 70 - 2.9 = \underline{67.1°C}$$

Time = 0900 hrs, I = 516.9 W/m^2, T_a = 24°C, T_s = 67.1°C

From Equation 4 Q_u = 80 [0.85 X 516.9 - 5.2 X 43.1]
= 17,220 Watts

From Equation 5 T_s+ = 67.1 + 1.145 X 10^{-4} [17,220 - 25,000]

T_s+ = 66.2°C

This calculation procedure can be continued in this manner to produce the table shown below.

Time	I W/m^2	T_a °C	Q_u KW	L KW	T_s °C
8	157.6	20	0	25	67.1
9	516.9	24	17.2	25	66.2
10	740.7	25	33.2	25	67.1
11	870.0	28	42.9	25	69.1
12	914.1	31	46.3	25	71.5
13	870.0	33	43.1	25	73.6
14	740.7	33	33.4	25	74.6
15	516.9	31	17.0	25	73.7
16	157.6	29	0	25	70.8
	5.48 kWh/m^2		233.1 KWh	225 KWh	

The data used in this example are realistic and show some interesting characteristics. The mean collector efficiency can be estimated for the $100m^2$ array as

$$\frac{233.1}{5.48 \times 100} = 43\%$$

which is on the low side. The low collector efficiency is due to the high fluid temperatures at which the collector operates.

The energy collected over the course of the day is:

233.1 kWh = 839.2 MJ

equivalent to 8.39 MJ/m^2 day
or 739 Btu/ft^2 day

These figures are close to the convenient solar 'rule of thumb' for a flat plate collector:

Energy collected = 700 - 1000 Btu/ft^2 day
= 8 - 11 MJ/m^2 day

The other thermal characteristic indicated here is temperature swing. In this example the storage temperature fluctuates between about 66°C and 75°C. These variations can be important depending on the load characteristics. For example, if the solar thermal system is driving an absorption chiller, temperatures of at least 60°C will be required in the generator of the chiller. The coefficient of performance of the cooling system will drop off sharply if such a temperature is not maintained. It is therefore important that the thermal storage system is designed with the load thermodynamic requirements in mind.

Design Guidelines

Computer simulations, experimental investigations, and a great deal of practical experience have yielded some general guidelines for sizing flat plate collectors and thermal storage systems.

The optimum storage size for an active solar thermal system will fall in the range of 0.2 to 0.4 MJ/°C m^2, equivalent to 10-20 Btu/°F ft^2. These ranges are for thermal capacity per unit area of collector, i.e.

$$0.2 < M_s c_p / A < 0.4 \text{ MJ/°C m}^2$$

For water as the storage medium (C_p = 4190 J/kg K) these figures produce the rule of thumb that thermal storage should be 45-90 litres/m^2 or 1.2 - 2.4 gal/ft^2.

Flow rates through forced-circulation systems are generally based on 0.02 - 0.04 gpm/ft^2 of collector, equivalent to 0.015 - 0.03 litre/m^2s.

As we have previously mentioned, the collector array can be roughly sized based on its ability to collect about 8-11 MJ/m^2 day or 700-1000 Btu/ft^2 day. These design guidelines permit the rapid sizing of solar thermal systems to drive a specified load. An approximate design based on these rules of thumb provides a convenient and often quite accurate starting point for more detailed analyses and simulations of system performance. For example, consider again Example 2. Suppose we were told the system load and asked to roughly size the solar collectors and thermal storage requirements for the system. The load extracts an amount of energy equal to

$$9 \times 25 \text{ kWh} \times 3.6 \text{ MJ/kWh} = 810 \text{ MJ/day}$$

knowing the relatively high storage temperature requirements we would estimate collector energy gain at the lower end of the 8-11 MJ/m^2 day scale. Estimating collector area as

$$810 \frac{\text{MJ}}{\text{day}} \cdot \frac{\text{m}^2 \text{ day}}{8 \text{ MJ}} \approx 100 \text{ m}^2 \text{ collector}$$

Storage requirements would be about 75 litres/m^2 which gives us an estimated storage volume of 7.5 cubic metres.

Stratified Storage

When heated fluid from the collector does not mix with the bulk of the fluid in the storage system, the storage system is said to be stratified. This phenomena is made possible because most fluids become less dense as they become hotter. The incoming fluid therefore has a tendency to remain at the top of the tank above the colder fluid below. If the fluid flowing to the collector is taken from the bottom of the tank in a perfectly stratified system the collector inlet temperature will remain constant until one tank volume of fluid has passed through the collectors, at which time the collector inlet temperature will show a step rise in temperature.

In practice, perfect thermal stratification is impossible since the inlet fluid velocity always causes some local fluid mixing and also because in mid to late afternoon, as insolation levels decrease, the tank inlet water temperature may actually be less than the highest fluid temperatures at the top of the tank. The fluid therefore descends into the body of the tank again producing a degree of mixing.

With a well-mixed storage tank, on the other hand, the temperature of the tank is uniform and will rise slowly throughout the day as the solar collectors absorb solar energy. As the storage temperature rises, the efficiency of the collectors decreases. However, compensating for this disadvantage with well-mixed storage systems is the rather higher heat transfer attained by using a more rapid flow rate than is consistent with an attempt to maintain thermal stratification in the storage tank.

In practice, there is little to choose between the two design concepts for liquid systems. It is useful and convenient to take advantage of the degree of stratification that always exists in any liquid thermal storage tank in the absence of a stirring device or excessively high inlet flow rates. Hot fluid is added or withdrawn from the top of the tank, cold fluid cold fluid added or withdrawn from the bottom.

Rock Bed Storage

Rock bed storage units have been successfuly used to store heat for many years. Hot air from solar collectors flows through a bed of pebbles and heat is transferred from the air to the rocks. The air leaves the storage unit at a temperature very close to the temperature of the pebbles adjacent to the outlet plenum. This is the charging mode. To remove heat from the storage system, the flow of air is reversed: cold air enters the cold end of the unit and is heated as it passes through the bed. Since there can be no mixing of the storage media in a rock storage unit the system is always thermally stratified when charged. This means that the collectors always operate with the coolest available incoming air, which helps to increase their efficiency. However, it should be noted that in rock bed storage systems, unlike liquid storage systems, heat cannot be added and removed from storage simultaneously. A typical rock bed thermal storage unit is shown in Figure 2. In general, the air flow is downward during charging, and upward during discharging. Although it is not essential that this flow pattern is adopted, such a design minimizes heat losses to the ground since the bottom of the storage is at the lowest temperature.

Rock bed storage units have several advantages. They are inexpensive, stable, and easy to construct; they will not freeze or boil; they are virtually maintenance free, and they will last a long time. Their disadvantages include their incompatibility with hot fluid systems, their relative large volume (approximately three times the volume of a water system of equal thermal capacity), and possible problems with dust and particle entrainment.

Thermal Stratification

One of the principal advantages of rock bed storage units is that, if properly designed, they exhibit a high degree of thermal stratification. The small size of the pebbles provides a large surface area for heat transfer so that the average temperature of a particular rock is close to local air temperature. When hot air is blown into the bed a well-defined thermal wave moves through the bed in the direction of the air flow. Figure 3 shows typical bed temperature profiles during the charging mode. The rock bed in this figure was initially at 21°C; the incoming air was at 65.5°C. Note that the outlet temperature of the air remains constant at the initial bed temperature of 21°C until, at about 9 hours after charging begins, the leading edge of the thermal wave reaches the bottom of the bed.

In a real system charged with hot air from a solar collector, the temperature of the air entering the rock bed varies during the day, typically reaching a maximum temperature around noon or soon after depending on the location and configuration of the collector (and assuming a clear day). During the afternoon the temperature of the air entering the rock bed will be decreasing. The effect of this daily temperature variation is to drive a temperature peak through the bed, a peak that continually flattens as it moves down through the layers of rock. This phenomenon can clearly be seen in Figure 4 which shows measured time-lapsed cross-sectional temperature profiles through a rock bed storage system over a 22-hour period.

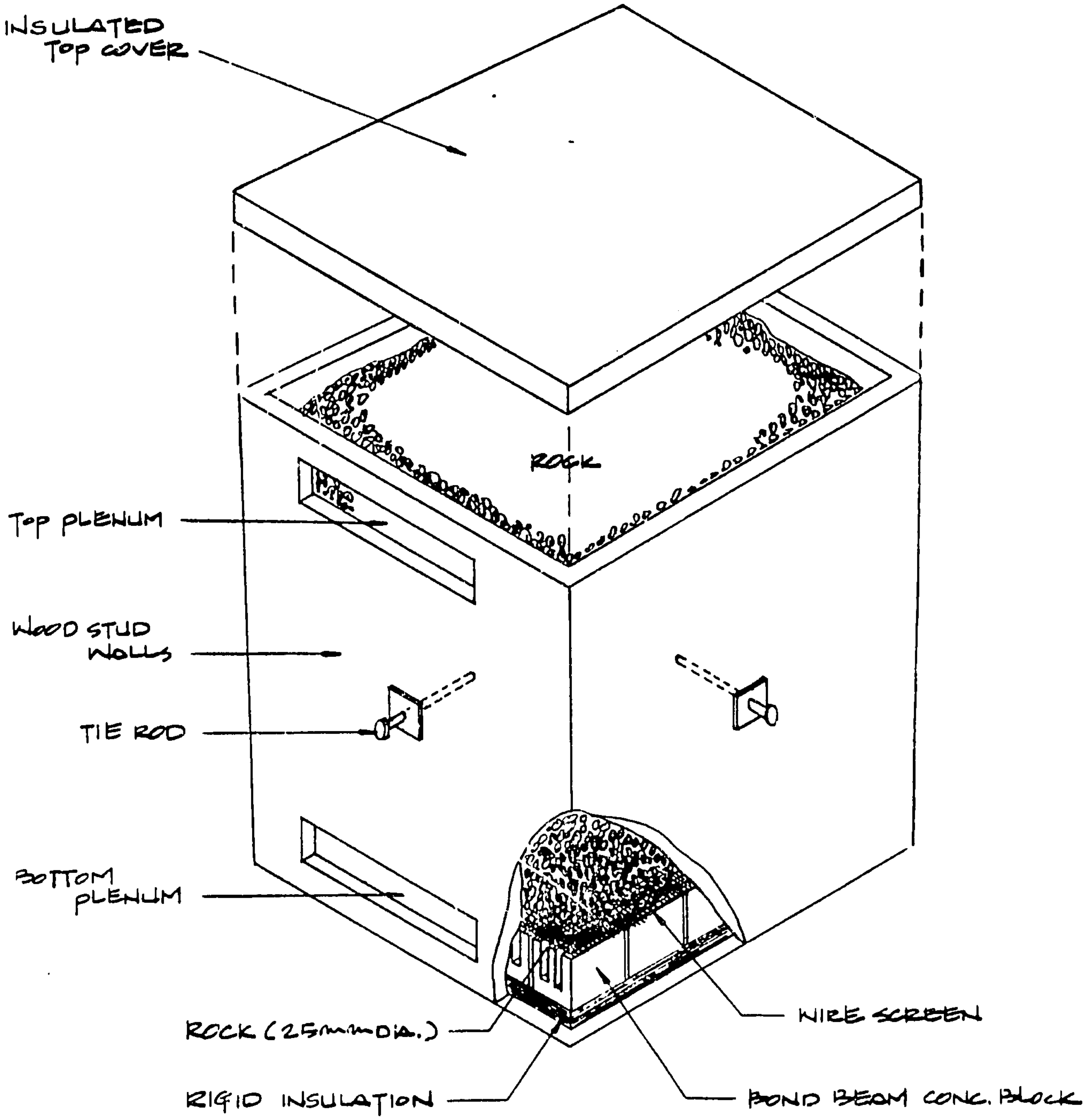

Figure 2. Typical Rock Bed Thermal Storage Unit

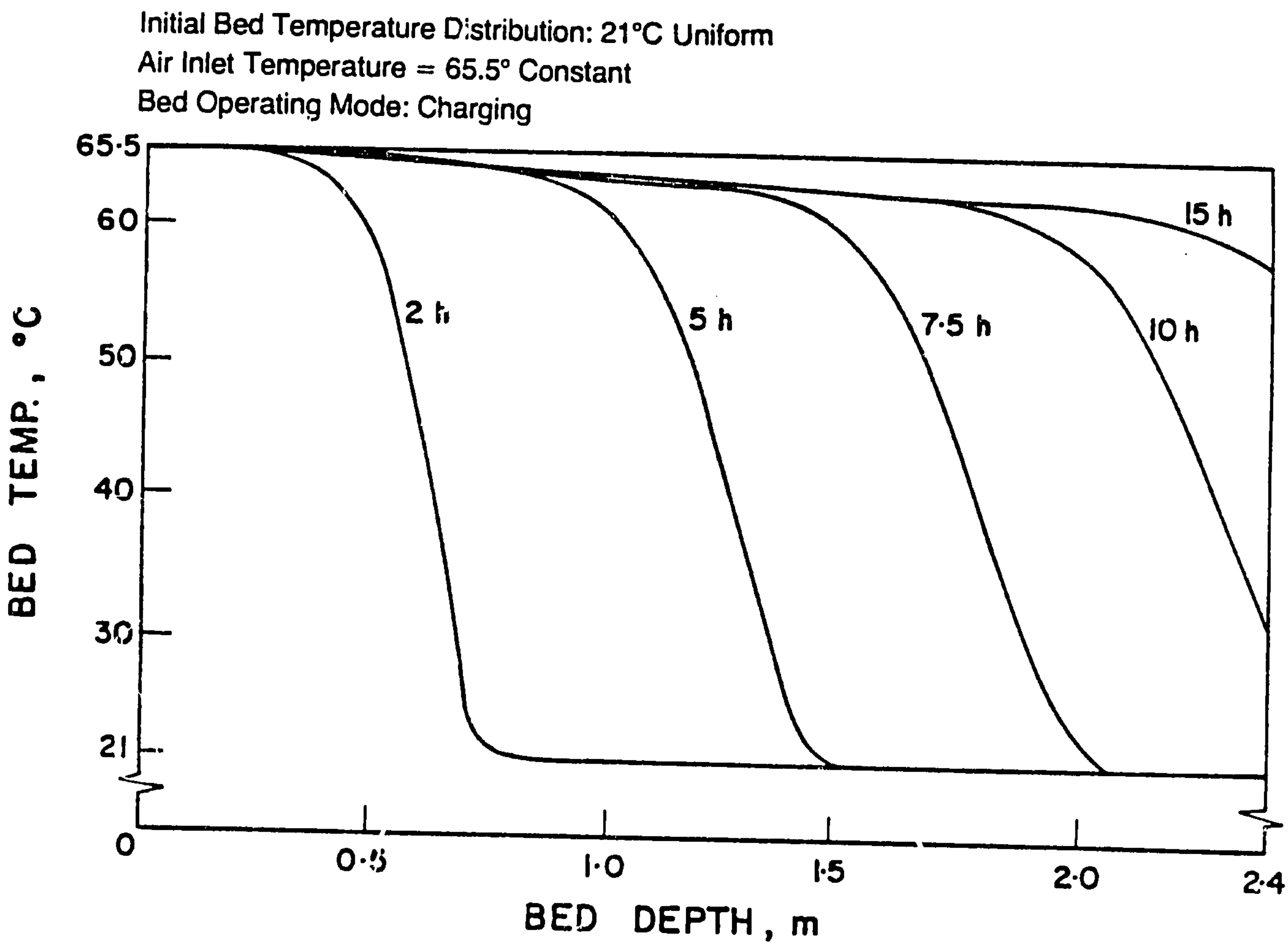

Figure 3. Rock Bed Temperature Profiles During Charging.

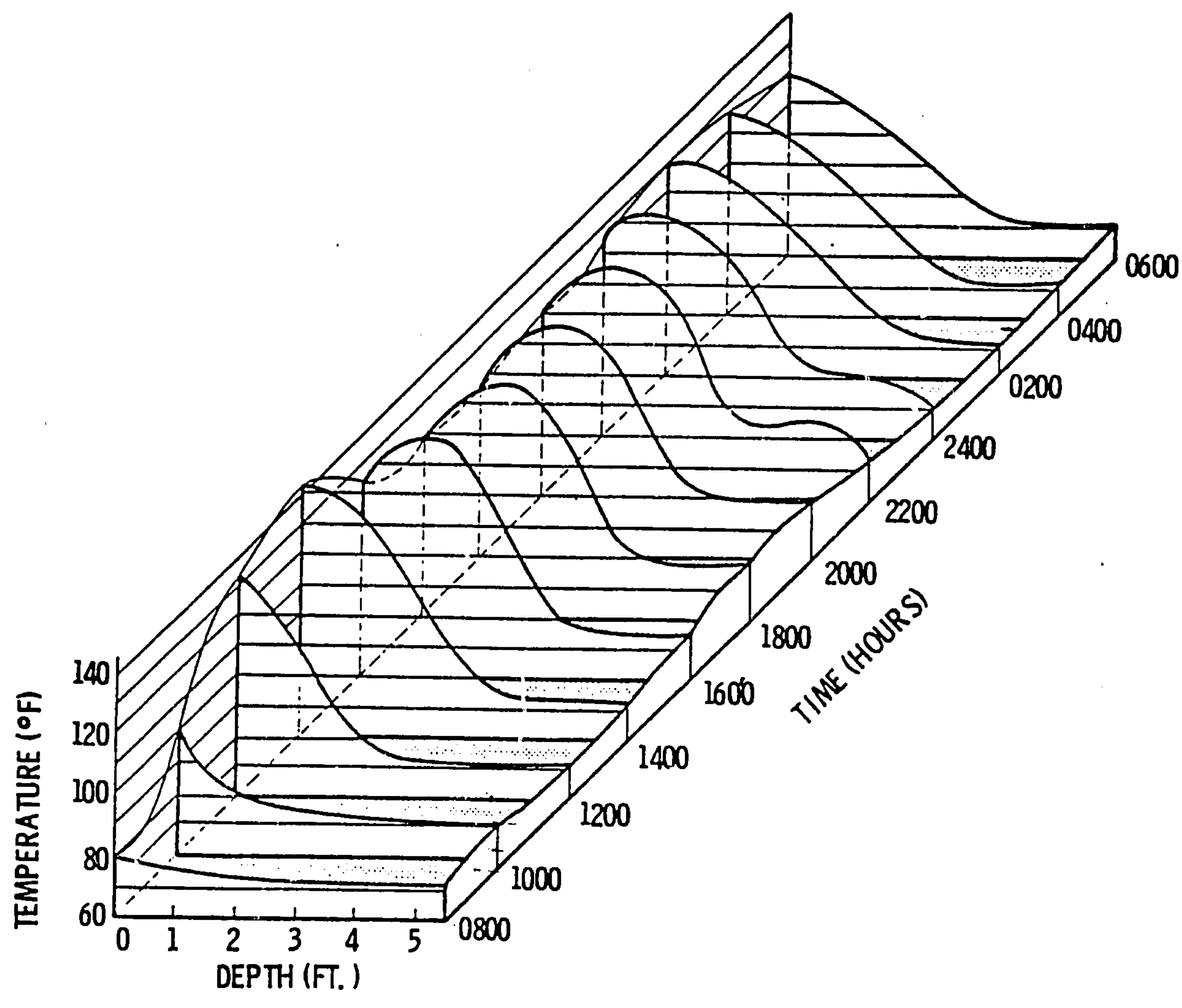

Figure 4. **Propagation of Pebble-Bed Temperature Profile (During Heat Storage Charge-Discharge Cycle),**

The time required for a thermal wave to traverse a rock bed is important to the performance of solar heating systems. The rock bed size and air flowrate should be selected so that the air returned to the collector remains at the minimum temperature for most of the heat collection period, thus maximizing the efficiency of the solar collector. The time taken for the thermal wave to traverse the rock bed should not be longer than the heat collection period since this would mean that a part of the bed would remain unused. The time taken, t, for the thermal wave to traverse the rock bed can be estimated from

$$t = \frac{Lc_s}{Vc_a} \quad \text{seconds} \tag{6}$$

where

L = rock bed length in direction of flow, metres
c_s = rock storage heat capacity, MJ/m^3 K.
c_a = heat capacity of air, MJ/m^3 K
V = rock bed face velocity, m/s

The heat capacity of a rock bed storage system is generally about 1.4 MJ/m^3 K. This figure assumes a typical 40% void fraction. The kind of rock used does not markedly affect the heat capacitance of the storage system.

If left undisturbed, a thermally stratified rock bed will progressively destratify until the bed reaches a uniform temperature. This decay of the thermocline is undesirable since it both raises the temperature of the air flowing to the collectors during charging, thereby reducing their efficiency, and lowers the temperature of the air going to load during the discharge cycle. However, the rate of thermal destratification is typically quite slow. It takes several days for an undisturbed rock bed to reach a uniform temperature. Figure 5 shows rock bed temperature profiles as a function of time. Reasonably good thermal stratification was maintained for at least three days in this experiment. Thus, decay of thermal stratification in rock bed storage units has only a minor effect on system performance. Charging the bed from the bottom as opposed to the top also has little impact on performance.

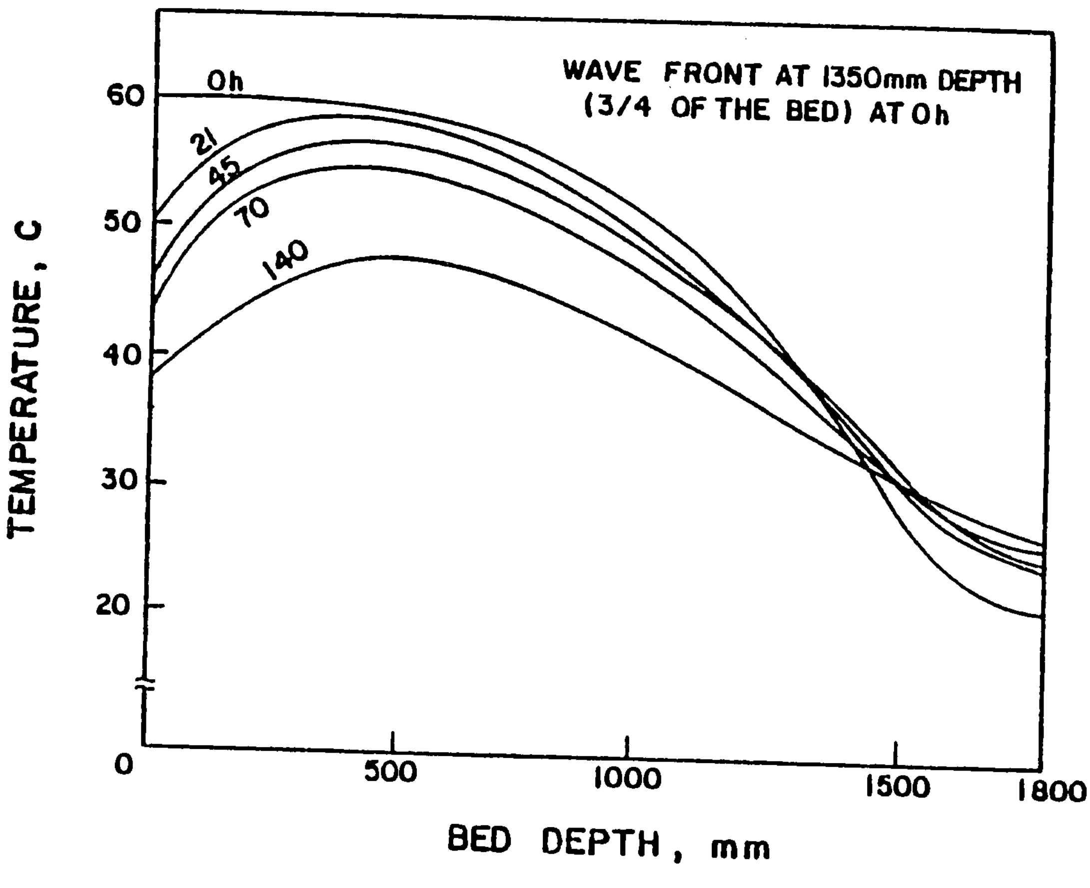

Figure 5. Stratified Rock Bed Temperature Profiles
- Variation with Time in Hours.

Sizing the Rock Bed

Studies suggest [5] that system performance improves as the rock bed storage volume increases up to about 0.2 cubic metres of storage volume for for each square metre of flat plate collector (m^3/m^2). Above this value the performance of the system does not change markedly with additional storage volume. The volume of storage recommended for air systems is 0.15 to 0.3 m^3/m^2 (0.5 - 1.0 ft^3/ft^2 collector).

If storage sizes greater than this range are used, the performance of the system may actually decrease because heat losses from the storage system will increase, and the temperature of the air going to the system load will decrease.

To minimize heat losses and material costs, the shape of the rock bed should be such that its surface area is minimal. However, in practice, rock bed storage units are usually constructed as square or rectangular bins with the air passing vertically through the pebbles as shown in Figure 2. A maximum depth of about 2.5 m is recommended to limit the pressure drop through the bed. For active solar systems, the flow rate of air through the rock bed is determined by the collector area. The design value is typically 0.01 m^3/s per square metre of collector. Combined with the recommended storage volume of 0.15 - 0.3 m^3/m^2, these figures indicate a flowrate of 0.03 - 0.07 m^3/s per cubic metre of rock storage, with 0.05 m^3/s a good rule-of-thumb. For a bed depth of 1.5 to 2.5 metres, the bed face velocity should be approximately 0.075 to 0.1 m/s regardless of the size of the storage system.

Rock bed storage systems with horizontal flow can be constructed if vertical space is limited. However, horizontal flow rock beds are not recommended because of problems with air flow distribution and channeling. When the bed is loaded, smaller pebbles tend to move to the bottom of the bed creating greater resistance to the horizontal flow of air through the lower portion of the bed. The air therefore has a tendency to channel through the upper part of the bed causing a loss in storage capacity and a reduction in system performance. Attempts have been made to ameliorate these problems as shown in Figures 6 and 7. Baffles can be installed perpendicular to the air flow or, alternatively, horizontal sheets of impervious materials such as plastic sheets can be used to encourage uniform horizontal flow.

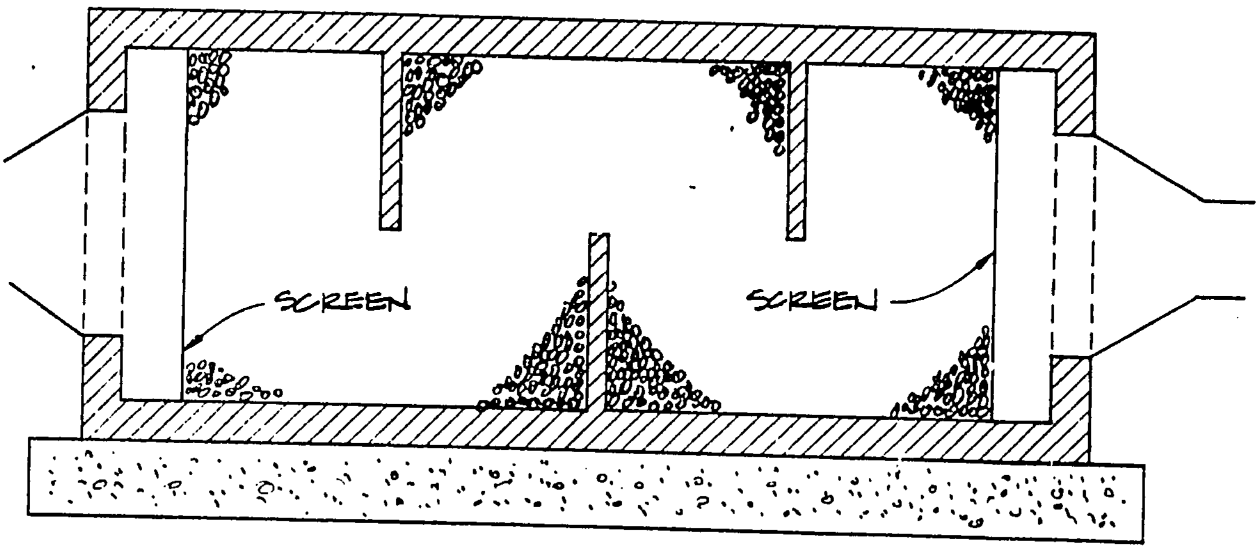

Figure 6. Horizontal Flow Rock Bed (Alternative 1) [5]

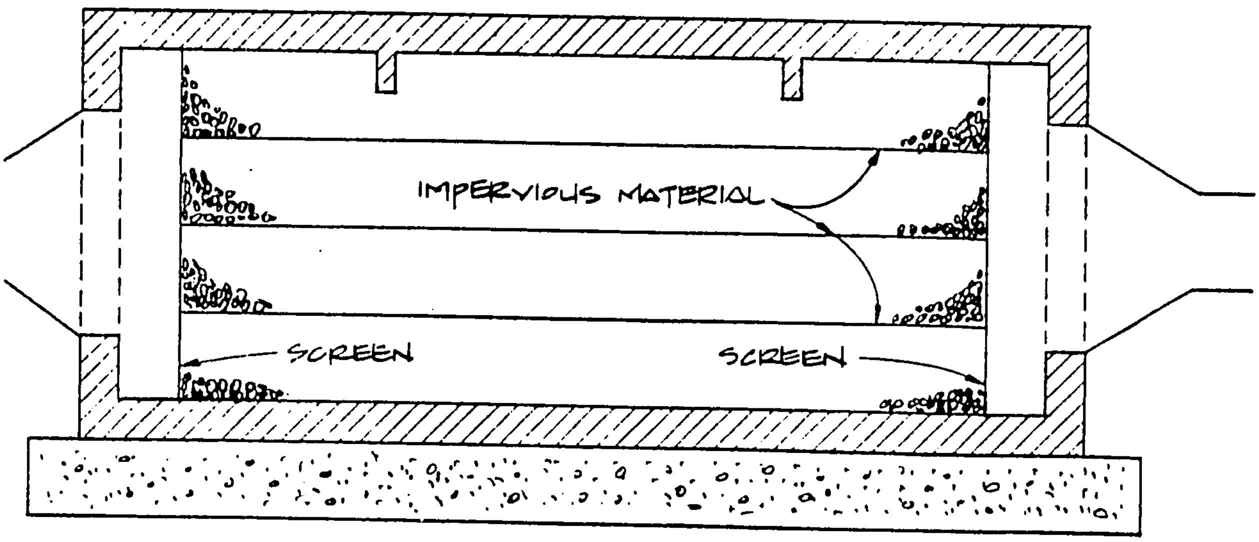

Figure 7. Horizontal Flow Rock Bed (Alternative 2) [5]

Rock Bed Pressure Drop

The size of the pebbles or rocks used in the bed affects two important design parameters. Decreasing the rock size increases the rate of heat transfer but also increases the pressure drop across the bed. The rock diameter should be small enough to ensure that heat is conducted into the centre of the rock as fast as heat is transferred to the rock from the air flow. For typical flow rates a rock diameter of 25 mm or less is recommended.

Too high a pressure drop across the bed means high system electrical energy consumption, whereas too low a pressure drop makes uniform flow distribution difficult. A pressure drop of 30 to 50 Pa across the bed is considered acceptable (0.0044-0.0073 psi, or 0.12-0.2 inches water). Accurate prediction of rock bed pressure drop, however, is never very precise since it varies according to how the storage container is filled. Differences in pressure drop of up to 20% have been measured in laboratory tests of the same rocks in the same container [9]. The shape of the rocks also has an effect on the bed pressure drop. Generally, one can distinguish three varieties of rock bed fill:

(1) Round stones; obtained from gravel pits, no sharp edges.
(2) Crushed stones; obtained by crushing round stones, sharp and round edges.
(3) Crushed rock; obtained from quarries, no round edges - all sharp.

These varieties are screened. The grade classified as 'clear' is the appropriate type for rock bed storage units since the clear grade has only a narrow range of particle sizes [5].

Nine samples of different kinds of rocks and stones were tested for their pressure drop characteristics [9]. The results are shown in Figure 8. The curves shown in this figure are for randomly packed beds and for clean, washed rocks. Unwashed rocks can have twice the pressure drop of clean rocks.

Fan Requirements

In order to select the size of fan required for the system, the designer must determine the overall pressure drop through the rock bed-collector loop. The total static pressure drop is the sum of the pressure drops through the rock bed, plenums, ducting and solar collectors. The pressure drop through the solar collectors can usually be obtained from the manufacturer. As a rule-of-thumb, fan power requirements will be approximately 2.5 Watts per square metre of collector area.

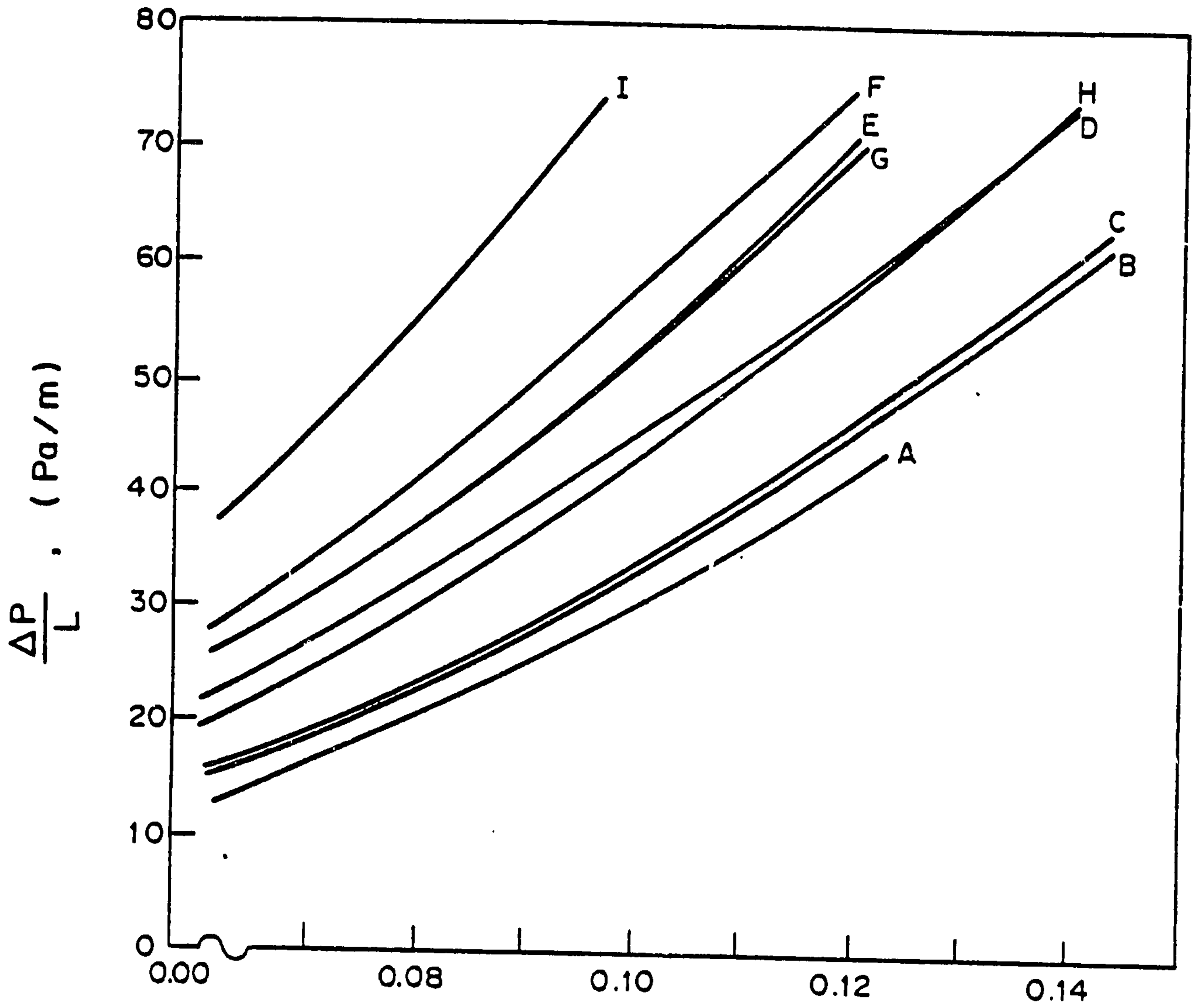

Figure 8. Plot of Rock Bed Pressure Drop Versus Face Velocity.

where P is static pressure loss (Pa)
L is rock bed length in the flow direction (m)
V is rock bed face velocity (m/s) (total flow rate divided by bed cross-sectional area)

A 19 mm Rounds (clear)
B 19 mm Crushed Rock (clear)
C 19 mm Crushed Stone (clear)
D HL4 Crushed Stone
E HL1 Crushed Stone
F 12.7 mm Rounds (clear)
G HL6 Crushed Rock
H HL1 Crushed Rock
I 9.5 mm Rounds (clear)

Note: Although this figure is an approximation based on a very limited sampling, it is entirely adequate for the purpose of ensuring a pressure drop that leads to a uniform flow. [5]

Pump Selection

In an active solar hot water system a pump will be required to circulate a fluid within the system. It is important that the pump selected for this task is carefully chosen. Pumps are selected by matching their performance curves with the pressure drop-flowrate characteristics of the systems itself. A typical performance curve for a small centrifugal pump is shown below in Figure 9. The curve indicates that this pump will lift water to a maximum height of 8 feet, but at this point there is no flow. As the head against which the pump is working falls, so the flowrate increases up to a maximum of about 1300-1700 gallons per hour depending on the size of the fittings. In actual operation, the pump will operate somewhere between these two extremes at a point which depends on the system curve.

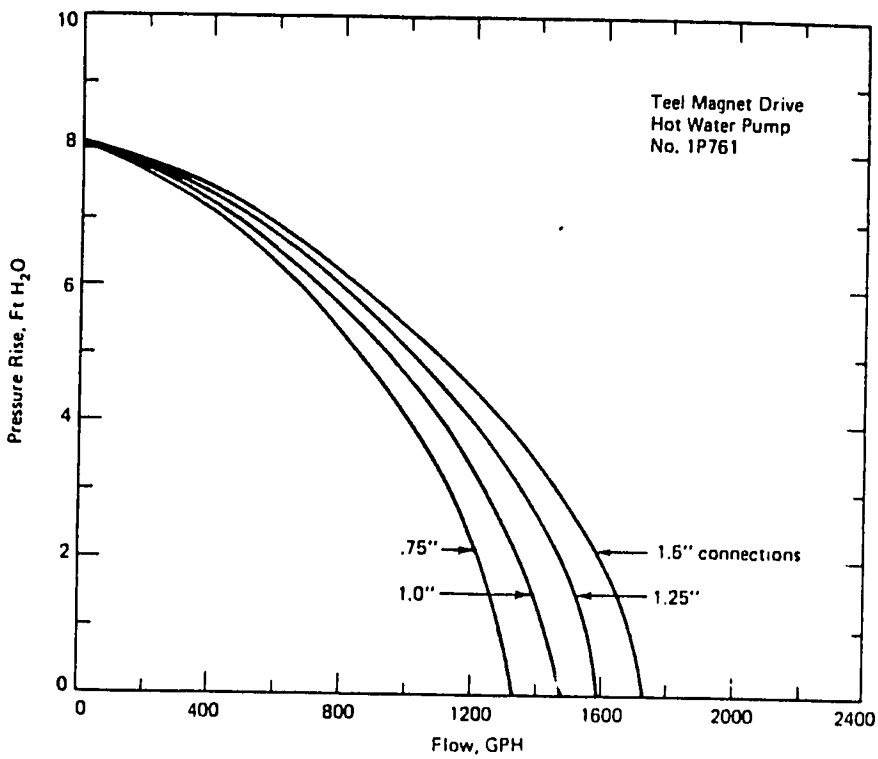

FIGURE 9. Pressure-flow characteristic curve for a magnetic drive centrifugal pump. [1]

To construct the system curve it is necessary to calculate the system pressure drop at the design flowrate. The system curve then follows from the relationship between flowrate and system pressure drop:

$$\frac{H_1}{H_2} = \left(\frac{Q_1}{Q_2}\right)^2 \tag{7}$$

where:

H = pressure drop or head,
Q = volumetric flow rate.

A system curve is shown in Figure 10. Where the system curve intersects the pump performance curve defines the operating point of the system. A pump is therefore selected so the estimated operating point is at a system flow rate close to the design value.

It should be noted that the system curve shown is for a closed-loop system where the pump is required only to overcome fluid friction at the design flowrate. In open-loop systems, the pump must also lift the fluid to an elevation which will depend on the system configuration. The system curve will be displaced upwards on the graph by a head equal to the lift required of the pump.

Figure 11 shows performance curves for several small pumps frequently used in solar heating systems. This figure illustrates how the shape of the performance curve can vary. Centrifugal pumps used in closed loop piping circuits should be selected for a mid-curve operating condition, and should have relatively flat performance curves. Pumps with a steep- curve characteristic should not be used because they tend to limit system flow rates.

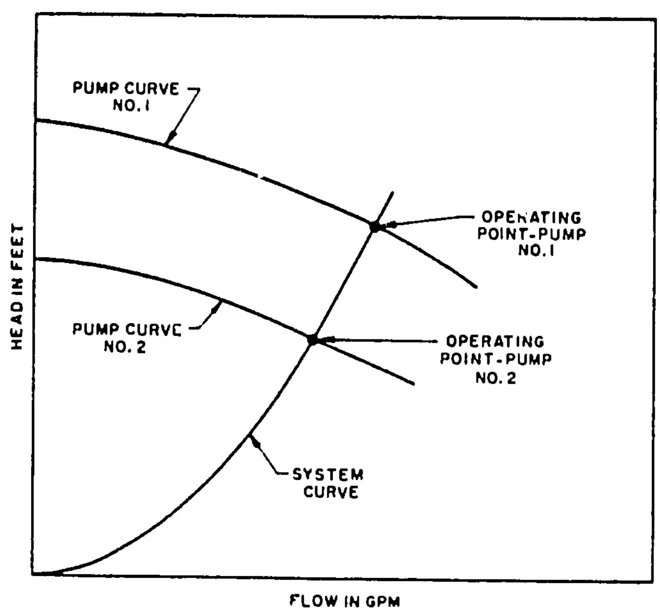

Fig 10. Typical System Curve for a Closed-Loop System. [15]

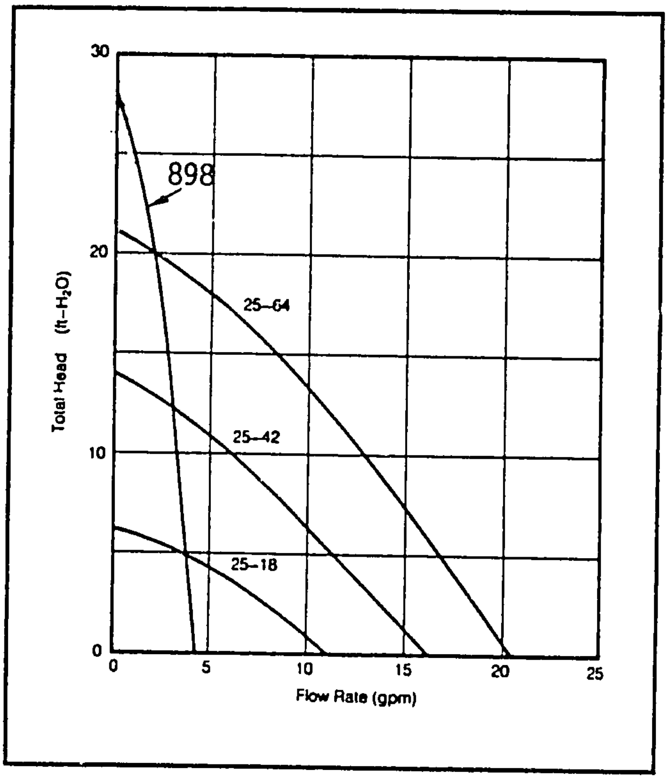

Figure 11 Example pump curves (25-64, 25-42, and 25-18 are Grundfos; 898 is a Richdel pump). [16]

Parallel Pumping

Pumps are often used in parallel. For parallel operation, each pump operates at the same head and provides one half the system flowrate. The pump curve for parallel operation can be established by doubling the flow rate of the single pump curve as shown in Figure 12. The operating point for both single and parallel operation can be determined by drawing in the system curve as indicated in Figure 13. When only a single pump is in operation the system flow rate is reduced, not by half, but by an amount dependent on both the characteristics of the pumps and the system. When only a single pump is operating, the flowrate is higher than that through each pump when they are operated together in parallel. When possible, the pumps should be selected to permit single-pump operation. This allows single-pump operation in the event one of the pumps fails.

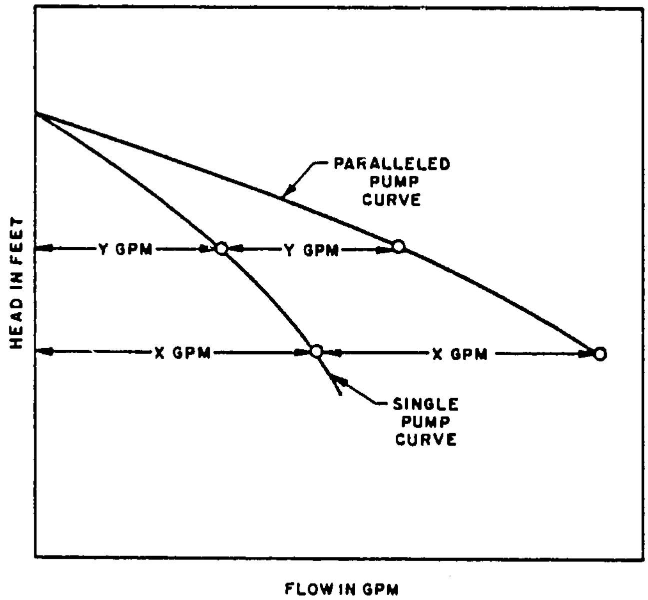

Fig. 12. Pump Curve for Parallel Operation [15]

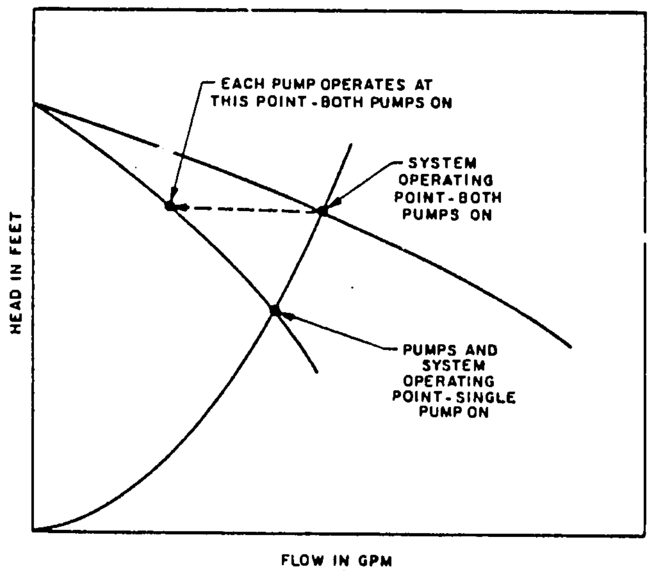

Fig. 13 Operating Conditions for Parallel Pump Installation [15]

Pumps in series

When pumps are placed in series, each pump provides one half the total system pumping head at equal pumping rates. The pump curve for pumps in series can be constructed from the performance curve of a single pump by doubling the head at each point of the curve as shown in Figure 14. Figure 15 shows the system curve drawn in and the system operating point. It should be noted that each pump draws maximum power during the series operation. During single-pump operation, the pump draws minimum power.

It should be emphasized that both parallel and series configurations require close attention to pump and system characteristics in order to accurately determine the expected operating points. The use of safety factors, the use of improper or inaccurate pressure drop charts, inadequate pressure drop calculation, etc., may lead to inappropriate pump selection and consequent operational difficulties.

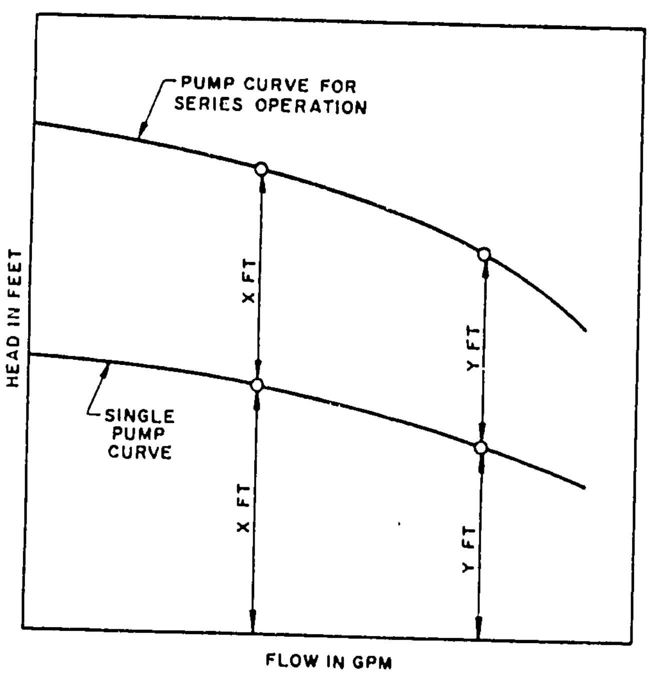

Fig. 14 Pump Curve for Series Operation [15]

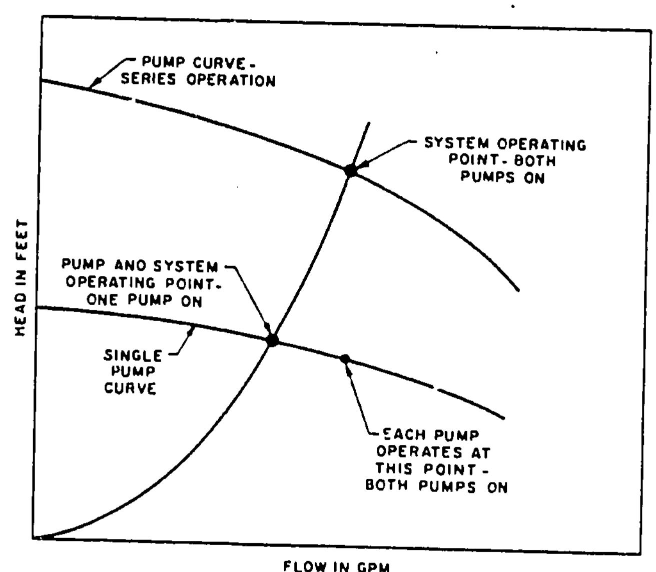

Fig. 15 Operating Conditions for Series Pump Installation [15]

System Pressure Drop

In order to establish the system curve it is necessary to determine the system pressure drop at the design flowrate. The volumetric flowrate is determined from heat transfer considerations, but the system pressure drop will depend on fixing the diameter of the pipework and accounting for all fittings, bends, and other equipment in the piping system. The pipe diameter can be determined by observing some simple design criteria. The general range of pipe friction losses in hydronic systems is between 1 and 5 ft. of head per 100 ft. of pipe length. A value of 2.5 ft/100 ft. is a mean value to which many systems are designed [10]. A further constraint is velocity. Closed loop hydronic systems are generally sized so that the fluid velocity does not exceed 4 fps (1.2 m/s). Above this velocity the system becomes noisy and erosion can start to become a problem especially at elbows.

It is also recommended that fluid velocity should not fall below 2 fps (0.6 m/s). These limits on fluid velocity and pressure drop closely constrain the selection of an appropriate pipe diameter. The central area of Figure 16 shows the region of permissible pipe sizes for a specified fluid flow. One would generally select the smallest available pipe diameter that falls within this central region.

For valves, bends, functions, and other elements, pressure drop is usually listed in elbow equivalents. The elbow equivalent is then used to estimate an equivalent pipe length from Table 3. Elbow equivalents for valves and fittings for iron and copper pipes are shown in Table 4.

Table 3. Equivalent Length in Feet of Pipe for 90-Deg Elbows

Vel. Fps	Pipe Size														
	½	¾	1	1¼	1½	2	2½	3	3½	4	5	6	8	10	12
1	1.2	1.7	2.2	3.0	3.5	4.5	5.4	6.7	7.7	8.6	10.5	12.2	15.4	18.7	22.2
2	1.4	1.9	2.5	3.3	3.9	5.1	6.0	7.5	8.6	9.5	11.7	13.7	17.3	20.8	24.8
3	1.5	2.0	2.7	3.6	4.2	5.4	6.4	8.0	9.2	10.2	12.5	14.6	18.4	22.3	26.5
4	1.5	2.1	2.8	3.7	4.4	5.6	6.7	8.3	9.6	10.6	13.1	15.2	19.2	23.2	27.6
5	1.6	2.2	2.9	3.9	4.5	5.9	7.0	8.7	10.0	11.1	13.6	15.8	19.8	24.2	28.8
6	1.7	2.3	3.0	4.0	4.7	6.0	7.2	8.9	10.3	11.4	14.0	16.3	20.5	24.9	29.6
7	1.7	2.3	3.0	4.1	4.8	6.2	7.4	9.1	10.5	11.7	14.3	16.7	21.0	25.5	30.3
8	1.7	2.4	3.1	4.2	4.9	6.3	7.5	9.3	10.8	11.9	14.6	17.1	21.5	26.1	31.0
9	1.8	2.4	3.2	4.3	5.0	6.4	7.7	9.5	11.0	12.2	14.9	17.4	21.9	26.6	31.6
10	1.8	2.5	3.2	4.3	5.1	6.5	7.8	9.7	11.2	12.4	15.2	17.7	22.2	27.0	32.0

Table 4. Iron and Copper Elbow Equivalents

Fitting	Iron Pipe	Copper Tubing
Elbow, 90-deg	1.0	1.0
Elbow, 45-deg	0.7	0.7
Elbow, 90-deg long turn...	0.5	0.5
Elbow, welded, 90-deg....	0.5	0.5
Reduced coupling	0.4	0.4
Open return bend........	1.0	1.0
Angle radiator valve......	2.0	3.0
Radiator or convector	3.0	4.0
Boiler or heater	3.0	4.0
Open gate valve	0.5	0.7
Open globe valve	12.0	17.0

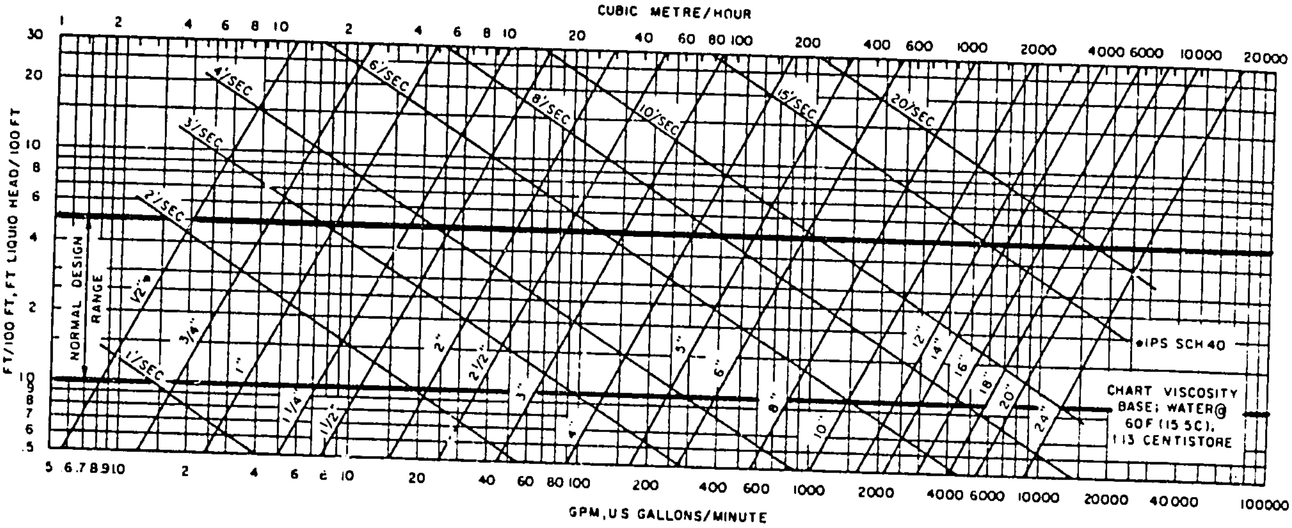

Fig. 16 Friction Loss for Water in Commercial Steel Pipe (Schedule 40) [12]

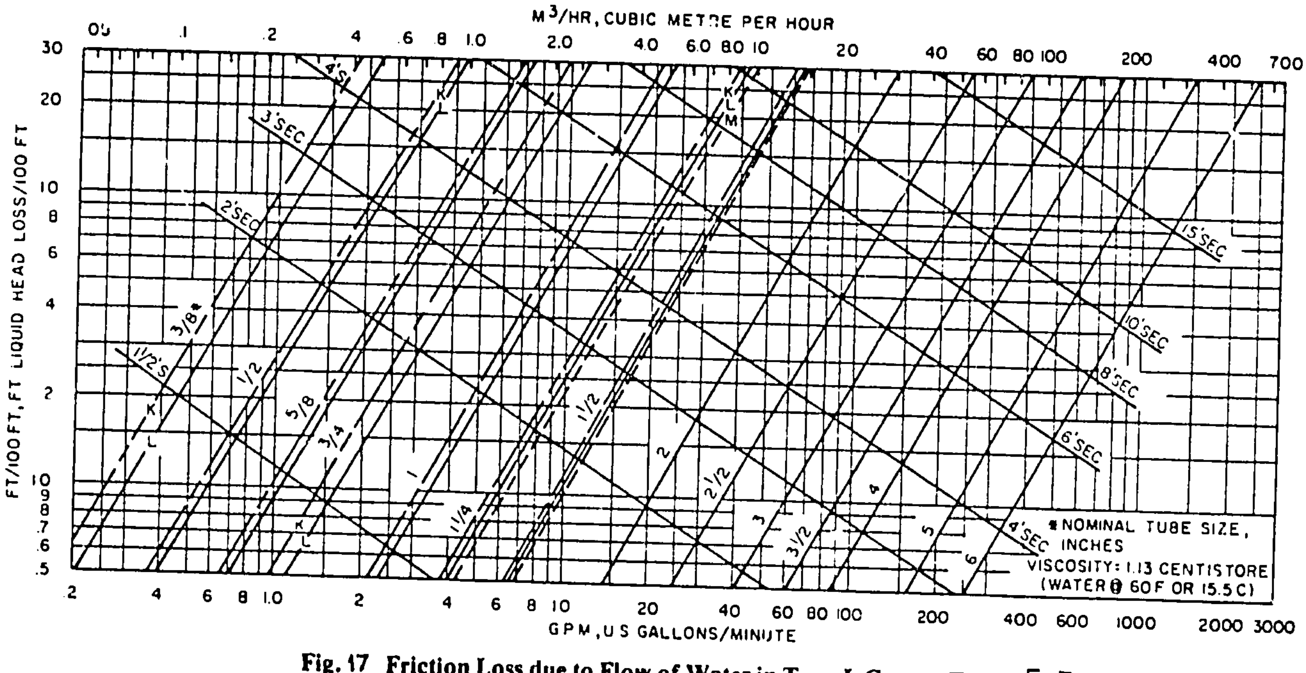

Fig. 17 Friction Loss due to Flow of Water in Type L Copper Tube [12]

1
11

Example 3

Determine the pressure drop for a 1-inch open gate valve and 20 ft. of 1-inch type L copper pipe at a flow velocity of 2.5 fps.

Solution

From Table 4, an open gate valve is equivalent to 0.7 elbows. From Table 3, a 1-inch elbow at 2.5 fps fluid velocity is equivalent to 2.6 feet of 1 inch pipe. Therefore, the gate valve is equivalent to 0.7 x 2.6 = 1.8 feet of pipe.

The pressure drop for the system is therefore based on 20 + 1.8 = 21.8 feet of 1-inch type L copper pipe. From Figure 17, the pressure drop at 2.5 fps can be estimated as 3 feet of water per 100 ft. of pipe. For 21.8 feet of pipe the pressure drop would be

$$\frac{3}{100} \times 21.8 = 0.65 \text{ ft } H_2O$$

$$= 0.28 \text{ psi}$$

The following rule of thumb is often used: the equivalent length of pipe for an elbow (in feet of pipe) is approximately twice the nominal pipe diameter in inches. Thus, a 1-inch elbow is equivalent to 2 feet of 1-inch pipe, a 4-inch elbow is equivalent to 8 feet of 4-inch pipe, etc.

Pressure drop through pipe tees varies with flow through the branch. Pressure drops through the functions for tees of equal inlet and outlet sizes are shown in Figure 18.

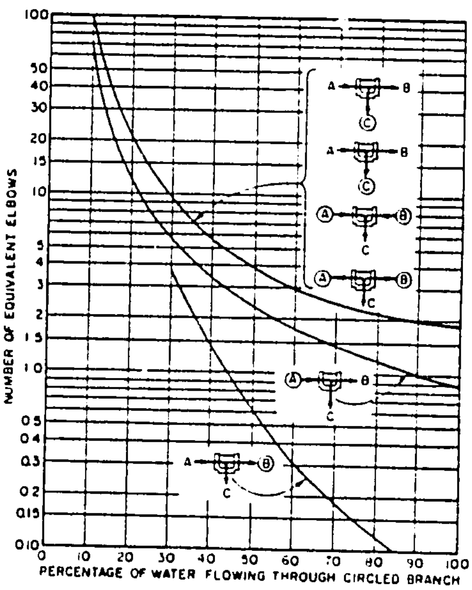

Notes: 1. The chart is based on straight tees, that is, branches A, B, and C are the same size.

2. Pressure loss in desired circuit is obtained by selecting proper curve according to illustrations, determining the flow at the circled branch, and multiplying the pressure loss for the same size elbow at the flow rate in the circled branch by the equivalent elbows indicated.

3. When the size of an outlet is reduced the equivalent elbows shown in the chart do not apply. Therefore, the maximum loss for any circuit for any flow will not exceed 2 elbow equivalents at the maximum flow (gpm) occurring in any branch of the tee.

4. The top curve of the chart is the average of 4 curves, one for each of the tee circuits illustrated.

Fig. 18 Elbow Equivalents of Tees at Various Flow Conditions [12]

System Control and Configuration

The function of the control system is to control the solar thermal system in such a way that the collection and storage of heat is accomplished as effectively as possible. The basic components of the control system are the temperature sensors, the differential temperature controller, and the output system. The differential controller starts the pump whenever a temperature sensor on the absorber plate of the collector indicates a temperature a few degrees higher than the temperature in the middle or at the bottom of the storage tank. The controller turns the pump off when the temperature differential falls below a preset level. Typical differentials are 15°F (8°C) for turn on, 5°F (3°C) for turn off. It is important that the collector sensor be mounted to a section of the absorber where it is thermally buffered from the temperature drop caused by the flow through the collector when the pump is first switched on. Otherwise, the pump may cycle on-off for a considerable period of time. Temperature sensors may also be used to monitor both freezing conditions and excessive storage temperatures. In each case the control system is designed so that the differential controller makes an appropriate response to the signals it receives from the sensors.

The output system delivers the appropriate control voltages from the differential controller to tne pumps, valves, fans, or dampers that control the fluid circulation.

A typical system configuration is shown in Figure 21. This is a drain-down system, which means that in the event of freezing conditions the system is designed to drain away to a sewer. The vacuum breaker above the collectors permits air to enter the system while draining. Horizontal piping is avoided. When the temperature rises sufficiently the solenoid valves isolating the storage tank open, the dump valve closes, and the system is refilled from the cold water supply. The air vent on top of the system allows air to escape as the collectors fill with water. This kind of system is exposed to main line pressures and must be designed accordingly. The biggest disadvantage with this design, however, is that drainage is dependent on the combined action of an electrical dump-valve and a differential controller. If either fail in freezing conditions the system is likely to be damaged.

Figure 22 shows a similar system except that here the system drains back into the storage tank. This configuration is called a drain-back system. Whenever the circulation pump is off the fluid in the collectors drains back into the storage tank. The storage tank is vented to permit air to enter the system. Note that the collector loop is not exposed to main supply pressure which would prevent the system from draining. The collector return line must enter the storage tank above the fluid level in order for the system to drain.

Figure 23 shows a typical closed-loop solar thermal system. Since the collector loop is closed an expansion tank becomes necessary. If freezing is a potential problem the heat transfer fluid must be a water/glycol mixture or some other freeze resistant fluid. Figure 24 shows a similar closed-loop system, this time employing two tanks. This system will return cooler water to the collector thereby improving their efficiency. However, thermal losses from storage will be greater.

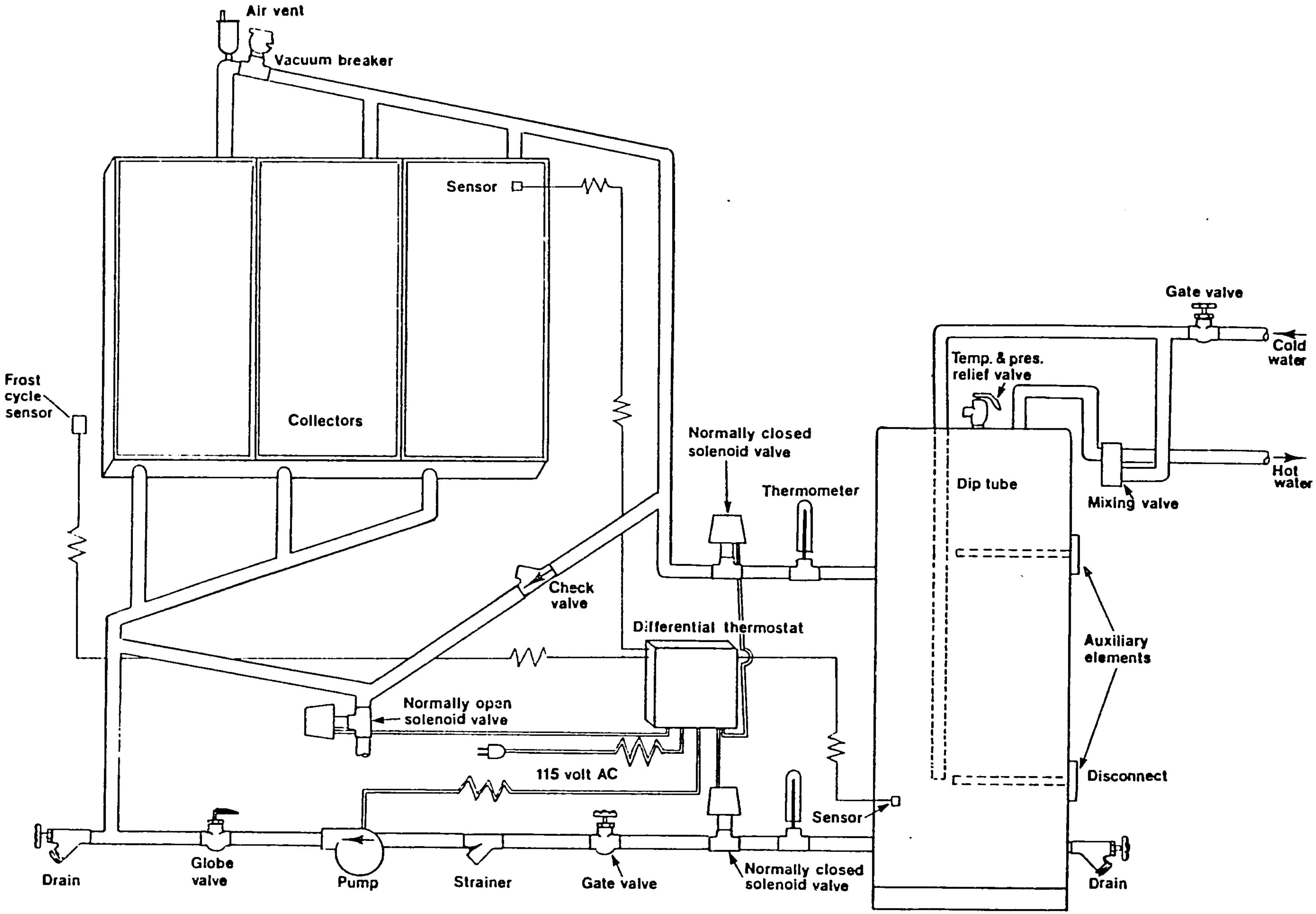

Figure 21. Drain-Down System [7]

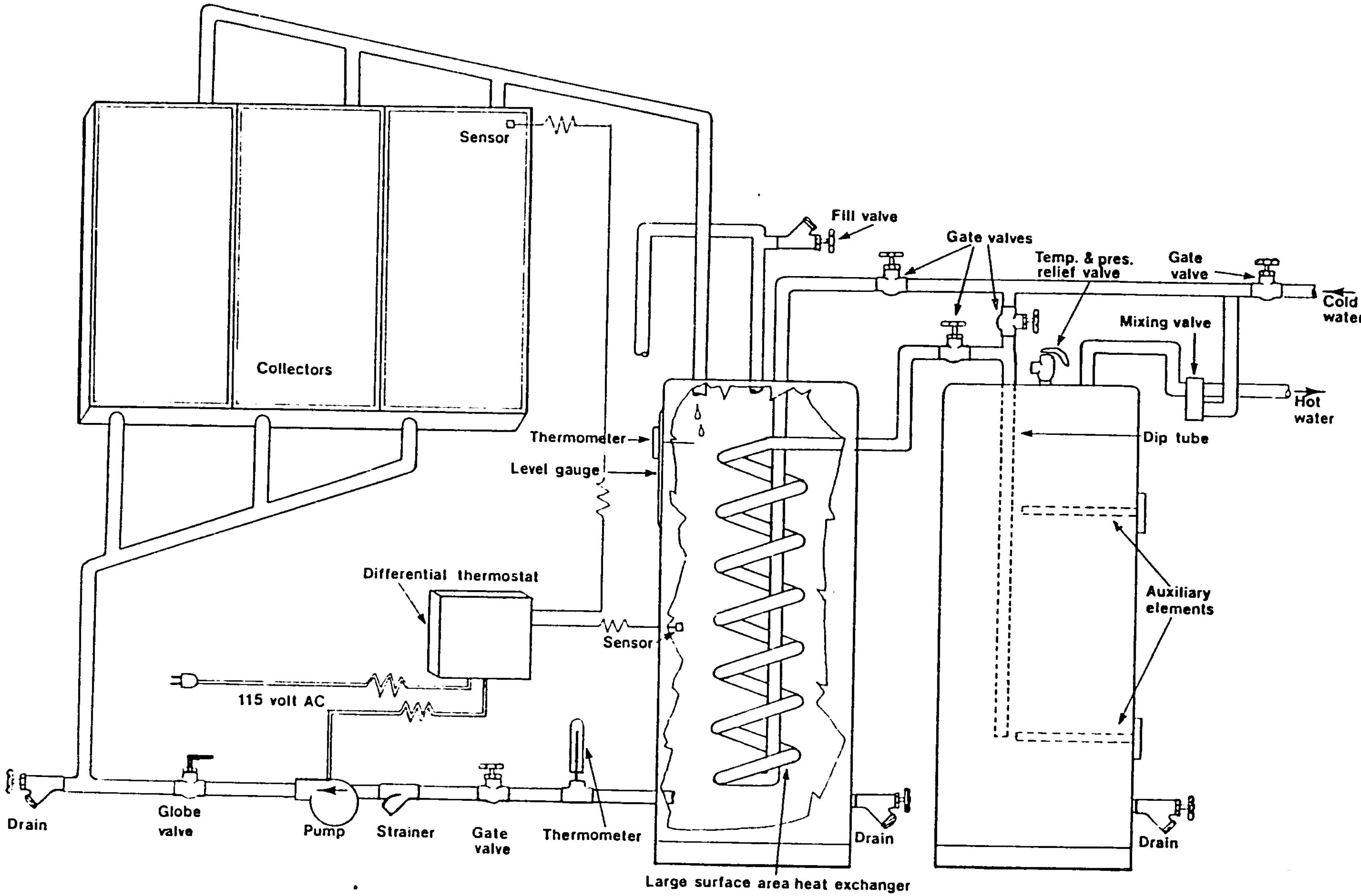

Figure 22. Drain-Back System [7]

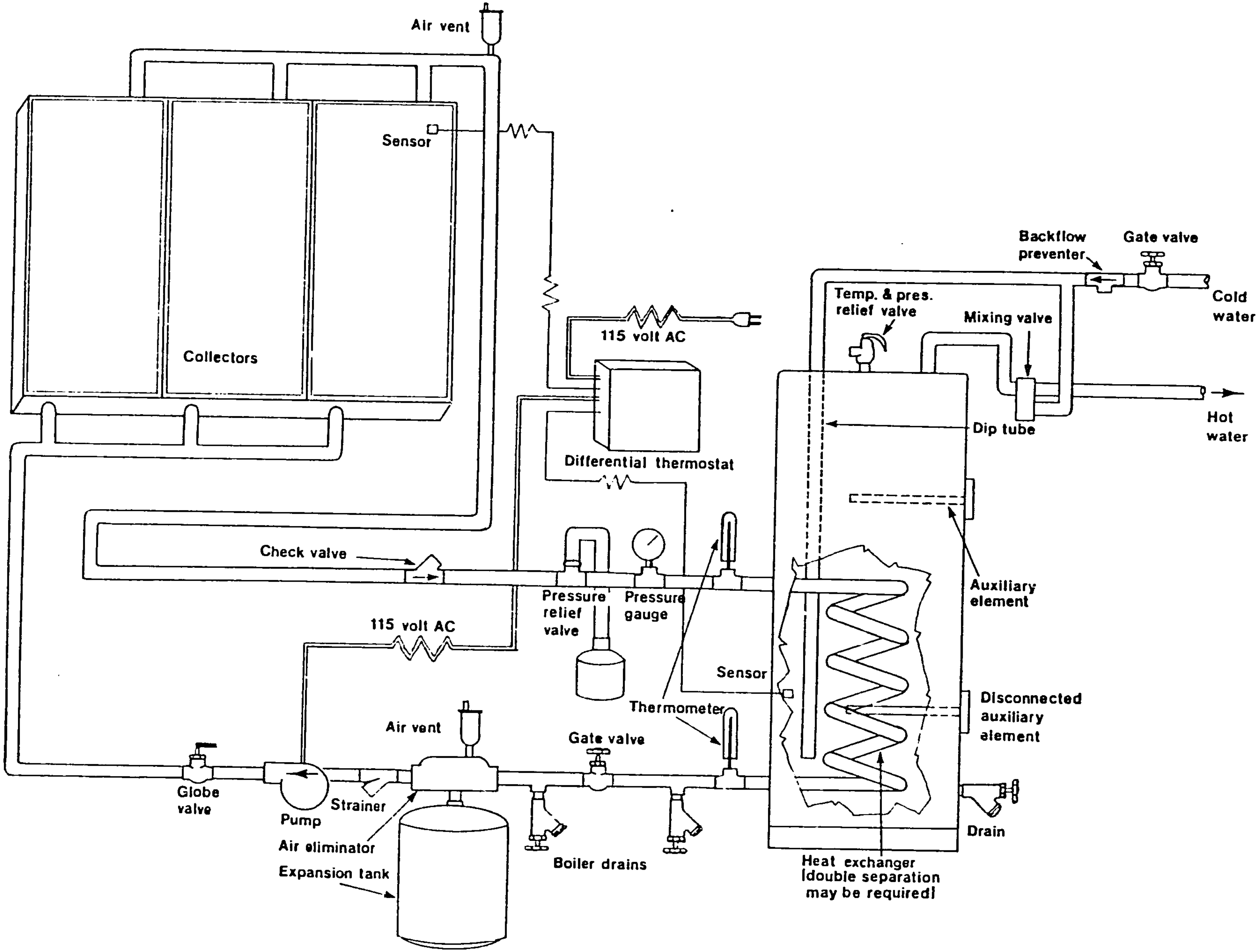

Figure 23. Closed-Loop System -- One Tank [7]

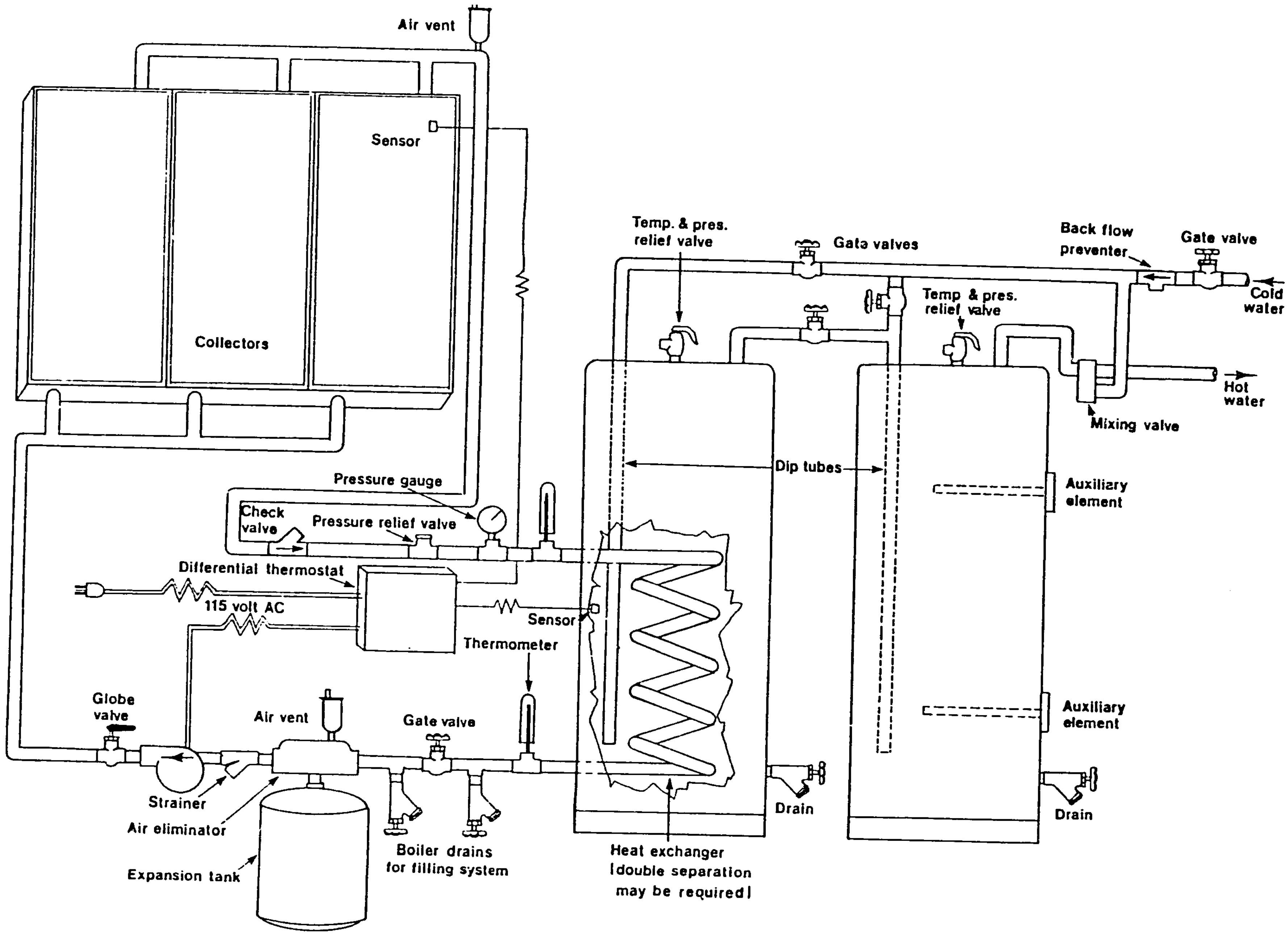

Figure 24. Closed-Loop System -- Two Tanks [7]

By far the simplest solar thermal system is the thermosyphon system. Figure 25 shows a typical system. No control system is required. However, the storage system must be at a higher elevation than the collectors. This is often an impractical arrangement with large solar thermal systems.

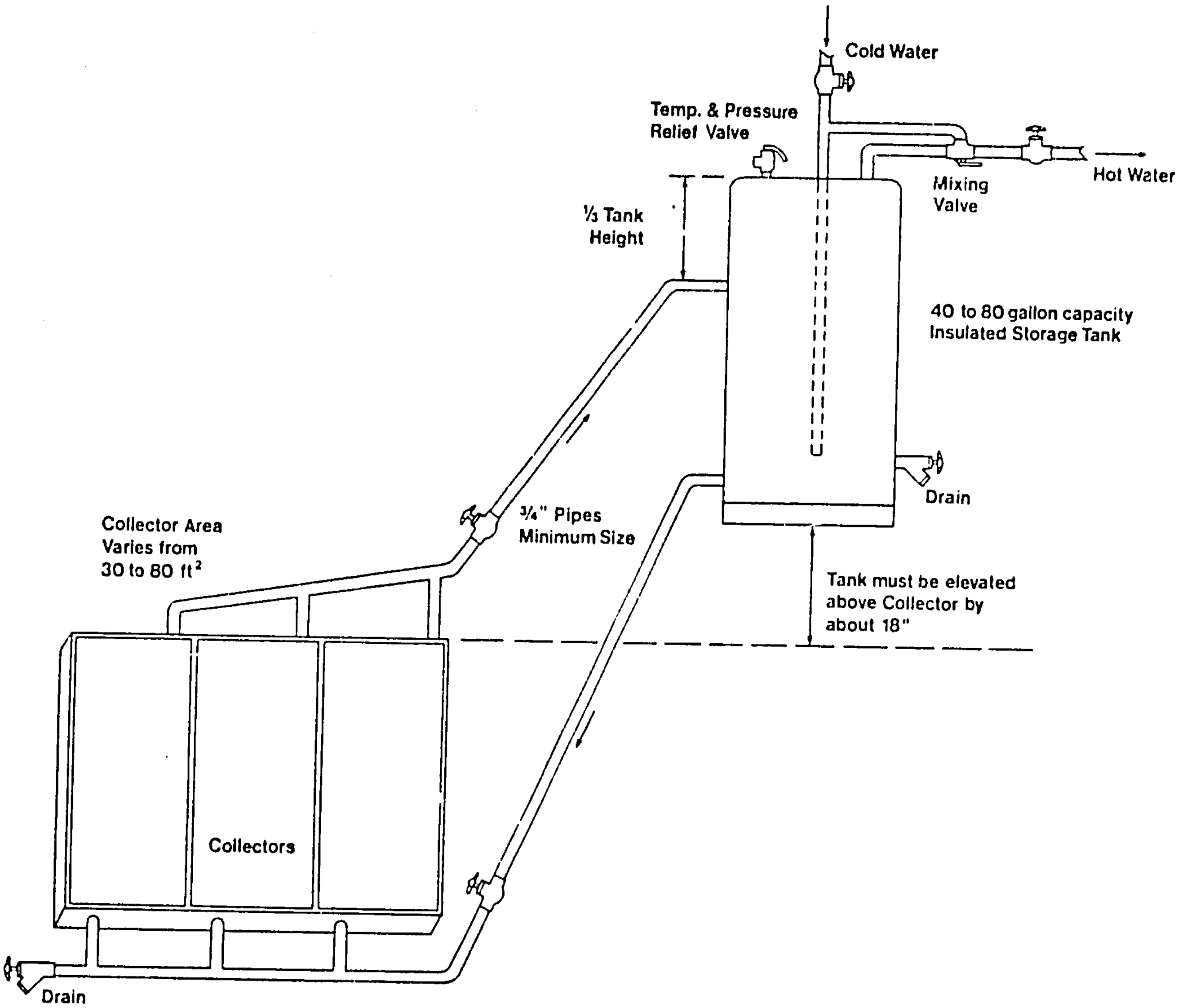

Figure 25. Thermosyphon System [7]

References

1. Lunde, P.J., "Solar Thermal Engineering", Wiley, Toronto, 1980.

2. Duffie, J.A. and Beckman, W.A , "Solar Engineering of Thermal Processes," Wiley, Toronto, 1980.

3. Duffie, J.A. and Beckman, W.A. "Solar Energy Thermal Processes", Wiley, Toronto, 1974.

4. Tully, G.F., "Solar Heating Systems", McGraw-Hill, New York. 1981.

5. "A Guide to Rock Bed Storage Units", Report No. STOR-10, National Research Council Canada, Ottawa, Canada, 1981.

6. "Introduction to Solar Heating and Cooling Design and Sizing", U.S.D.O.E., Office of Solar Applications, August 1978, DOE/CS, 0011.

7. "Installation Guidelines for Solar DHW Systems", U.S. Dept. of Housing and Urban Development, Office of Policy Development and Research, May 1980, HUD-POR-407 (2).

8. "Solar Heating and Cooling of Residential Buildings: Sizing, Installation and Operation of Systems", U.S. Dept. of Commerce, Economic Development Administration, September 1980.

9. Sullivan, H.F., and Hollands, K.G.T., "Rock Bed Thermal Energy Storage", National Research Council of Canada, Report STOR-8, Ottawa, 1980.

10. Sullivan, H.F., et. al., "Loss of Thermal Stratification with Time in Rock Bed Storage Units", Proceedings of the 1981 SESCI Conference, Montreal, 1981.

11. ASHRAE Guide and Data Book-Systems, 1970.

12. ASHRAE Handbook of Fundamentals, 1981.

13. Kreith, F., and Kreider, J.F., "Principles of Solar Engineering", McGraw-Hill, New York, 1978.

14. DeWinter, F., "Heat Exchanger Penalties in Double Loop Solar Water Heating Systems", Solar Energy, 17: 335 (1975).

15. ASHRAE Systems Handbook, 1980.

16. Leckie, J., et. al., "Other Homes and Garbage: Designs for Self-Sufficient Living", Sierra Club Books.

Solar Thermal Electric Systems

There are two basic techniques for converting the sun's radiation into electrical power: (1) direct conversion by transfer of the energy to the electrons of a solid--the photovoltaic effect; (2) conversion of the radiation to heat which is then used to power a thermodynamic cycle from which energy is extracted and converted to electricity. In this section of the text we look at systems designed to convert the sun's energy to electricity using the second approach.

Thermodynamic processes which use source temperature differences to produce work (shaft power) are limited in efficiency by what is known as the Carnot efficiency. The efficiency of a heat engine converting thermal energy to work cannot exceed the Carnot efficiency, η_c, of the system which is defined as

$$\eta_c = \frac{T_{hot} - T_{cold}}{T_{hot}}$$

T_{hot} is the absolute temperature of the thermodynamic working fluid at its highest level, and T_{cold} is the absolute temperature of the working fluid at its lowest level, at the point where heat is rejected from the cycle.

It can be seen from this expression that the Carnot efficiency increases with increasing source temperatures. Actually it is temperature difference which governs the efficiency but in practice T_{cold} is generally fixed by the temperature of the local cooling water. As an example, consider a flat plate collector boiling a freon-type fluid used in a thermodynamic cycle producing work. If the fluid boils at 80° C and cooling water is available at 30° C the absolute maximum efficiency of the cycle is (353 - 303)/353 = 0.14 or 14 percent. Since a real system is considered acceptable if it attains an efficiency of half the Carnot limit, a Rankine cycle process using flat plate collectors would only achieve a thermodynamic efficiency of perhaps 7 percent. If the thermal and other losses from the solar collector are included, the overall system efficiency, i.e. insolation to mechanical work, will be only about 3 to 4 percent assuming that the efficiency of the collector is about 50%.

If electricity is to be produced from sunlight using thermodynamic processes, it is therefore clearly advantageous to generate the highest possible temperatures at the hot side of the cycle. Concentrating solar collectors, or systems using reflectors to focus sunlight, are therefore much more efficient at converting the sun's radiation to electricity than flat plate collector systems.

Solar thermal electric systems that employ concentrating collectors include the following design concepts.

1. Central receiver ("power tower") systems (CRS) which are composed of a field of heliostats (mirrors) which are controlled to reflect incoming direct solar rays to a common absorber (receiver) elevated above the field by a central tower. The energy, in the form of heat, is transferred from the absorber to a working fluid (steam, air, helium, sodium potassium eutectic or salts), which in turn is the source of heat for a thermodynamic cycle (Rankine, Brayton, or combined Rankine/Brayton) to convert the heat to electricity.

2. Line concentrators which are fields of distributed (discrete) parabolic concentrating collectors which focus direct insolation upon a line with single axis tracking and an open or cavity receiver or absorber. The heat is transported from the array via the absorber pipeline and is transferred to the working fluid of a Rankine power cycle.

3. Point concentrators which are fields of distributed (discrete) paraboloidal concentrating collectors which focus direct sun rays at a point, with dual axis tracking and a cavity receiver (absorber). The heat is transported from the array in one concept via steam, oils, or chemical mixtures to a central Rankine power conversion system. An alternate concept is to use individual power converters (Brayton or Stirling engines) for each collector module, to produce electricity, and then transport electric current to the power conditioning facility, then to the busbar.

DISTRIBUTED COLLECTOR SYSTEMS (DCS)

1. COOLIDGE

An experimental solar irrigation project sponsored by the U.S. DOE and run by the University of Arizona has been in operation since 1980. It provides electricity to pump water from three 91 m deep wells at Coolidge, Arizona to irrigate cotton crops. The power plant uses 2140 m^2 of parabolic trough concentrating collectors to focus sunlight on receiver tubes within which circulates the primary circuit heat transfer fluid: Caloria HT-43, a synthetic oil stable at high temperatures. The primary fluid vapourizes a low-boiling point secondary fluid (toluene) that drives a Rankine-cycle turbine that generates electricity.

Electrical power is fed into local electric-utility lines, from which power is drawn as needed to pump about 5300 litres per minute from the three wells, each of which requires about 50 KW. Maximum power output is rated as 175 KW of which approximately 25 KW is for power plant pumps and motors. Figure 1 shows schematically the elements of the system. The Acurex collectors raise the temperature of the Caloria HT-43 oil to around 290°C. The oil is then circulated through a 30,000 gallon (114 m^3) thermal storage tank. A disadvantage with this particular thermodynamic cycle is that the pressure in the condenser is below atmospheric, thus raising the possibiity of air leaking into the system. Toluene forms explosive mixtures with air at low concentrations.

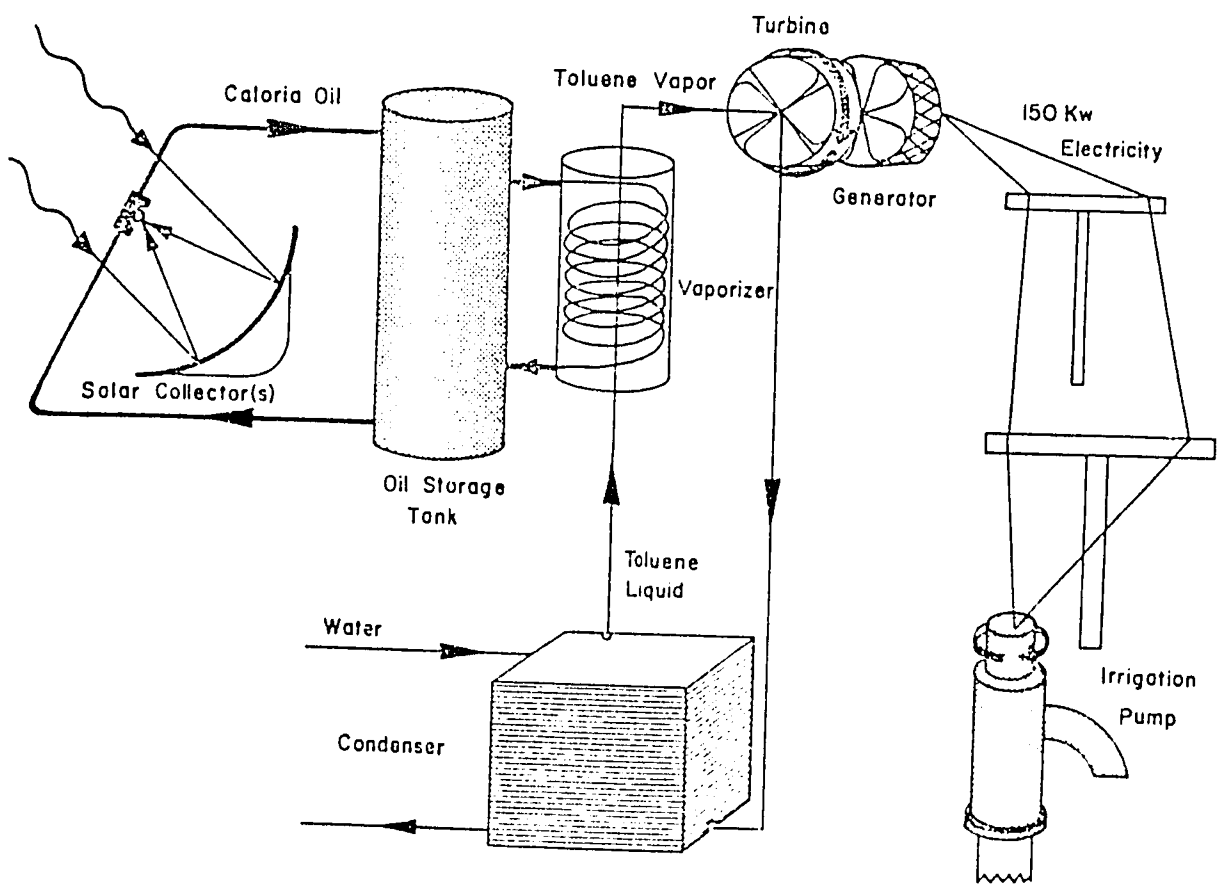

Figure 1. Diagram of Coolidge Pumping System

2. ALMERIA

As another example of a DCS system we look at the Small Solar Power Systems Project (SSPS) initiated by the International Energy Agency (IEA). Supported and funded by eight European countries and the U.S., the SSPS is part of the IEA Research and Development program which is aimed at applying and demonstrating those new or improved energy technologies that offer significant potential for contributing to future energy needs.

The principal objective of the SSPS project is to examine in some detail the feasibility of using solar radiation to generate electric power for possible application either in established grids or in communities whose geographical situation renders conventional electrical supply techniques difficult and costly. Evaluation is to be performed with respect to two dissimilar engineering approaches. A solar farm or DCS using parabolic trough collectors is to be located adjacent to a central receiver system (CRS) using a field of heliostats.

The technical and operational objectives are to compare both technological concepts, based on the same design philosophy and operated under the same environmental conditions. The SSPS-DCS plant, which has a rated output of 500 KWe, utilizes the pilot-system experience of Acurex in building irrigation plants in New Mexico and Arizona, as well as of the German company M.A.N. in operating similar systems in Spain, Mexico, and Australia. The plant has two collector fields of approximately equal size (see Table 1). One field is made up of 10 loops of [illegible]0 collectors manufactured by Acurex; the other field consists of 1[illegible] loops of 6 collector modules developed by M.A.N. Both of these collector designs are line-focusing parabolic trough types.

The Acurex collector is arranged to track the sun in a single-axis mode, the rotational axis being oriented in the east-west direction. The M.A.N. collector modules employ two-axis tracking for orientation in azimuth and elevation. Application of the two design concepts in the same location offers the opportunity to compare life-cycle costs versus annual energy output under realistic conditions.

The heat transfer and power conversion systems of the DCS have been designed with three heat transfer loops.

1) The first loop takes low temperature oil, Caloria HT-43 at 225°C, from the bottom of a thermal storage tank, circulates it through the collector fields, and returns it at a temperature of 295°C to the top of the storage tank.

2) In a second loop, a boiler takes the hot oil from the storage tank, discharges the thermal energy to the steam loop, and returns the oil to the thermal storage tank.

3. The third loop circulates water through the boiler and then expands the generated steam through a turbine generating electricity. The low-enthalpy steam is condensed and pumped back to the boiler.
Figure 2 shows a simplified diagram of the DCS process flow.

Table 1. SSPS Distributed Collector System—Performance Data [3]

Design point:	day 80, 12:00 (equinox noon) solar insolation	 0,92 kW/m²
Collector fields:	ACUREX collector, model 3001 60 groups in 10 loops	2674 m²
	MAN collector, model 3/32, "HELIOMAN" 84 modules in 14 loops	 2688 m²
	total aperture area concentration ratio land-use-factor (ACUREX/MAN)	5362 m² ca. 40 0,27/0,32
	heat transfer medium collector inlet temperature collector outlet temperature	thermal-oil (HT-43) 225°C 295°C
Thermal storage:	one-tank-thermocline, storage medium capacity equivalent to hot/cold temperature	 thermal-oil (HT-43) 0,8 MWh_e 295°C/225°C
Steam generator:	HT-43 inlet temperature HT-43 outlet temperature steam outlet temperature steam pressure	295°C 225°C 285°C 25 bar
Power (at design point):	solar insolation thermal gross electric net electric	4933 kW 2580 kW 577 kW 500 kW
Efficiencies (at design point):	thermal/gross electric thermal/net electric insolation/net electric	22,4% 19,4% 10,1%

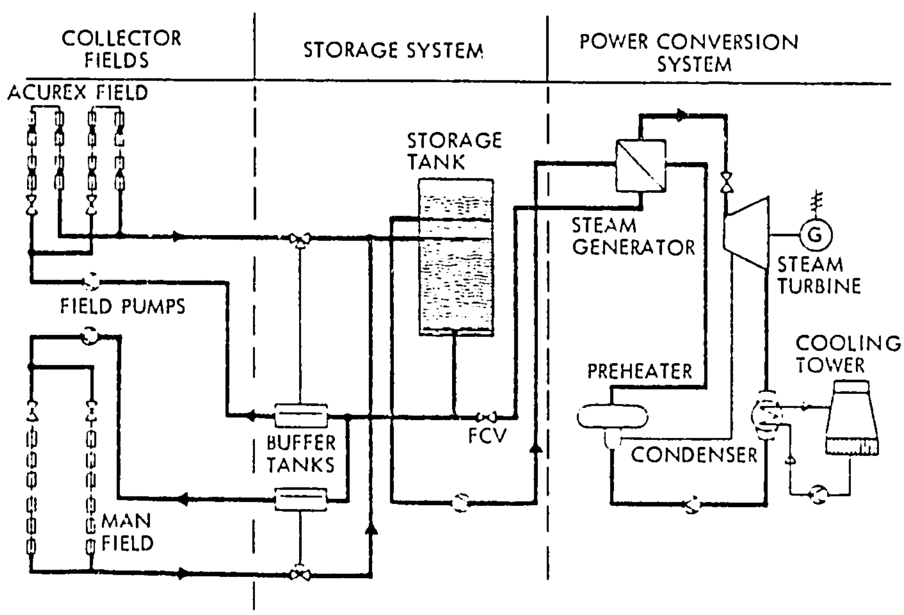

Fig. 2. *Simplified schematic diagram of DCS process flow* [1]

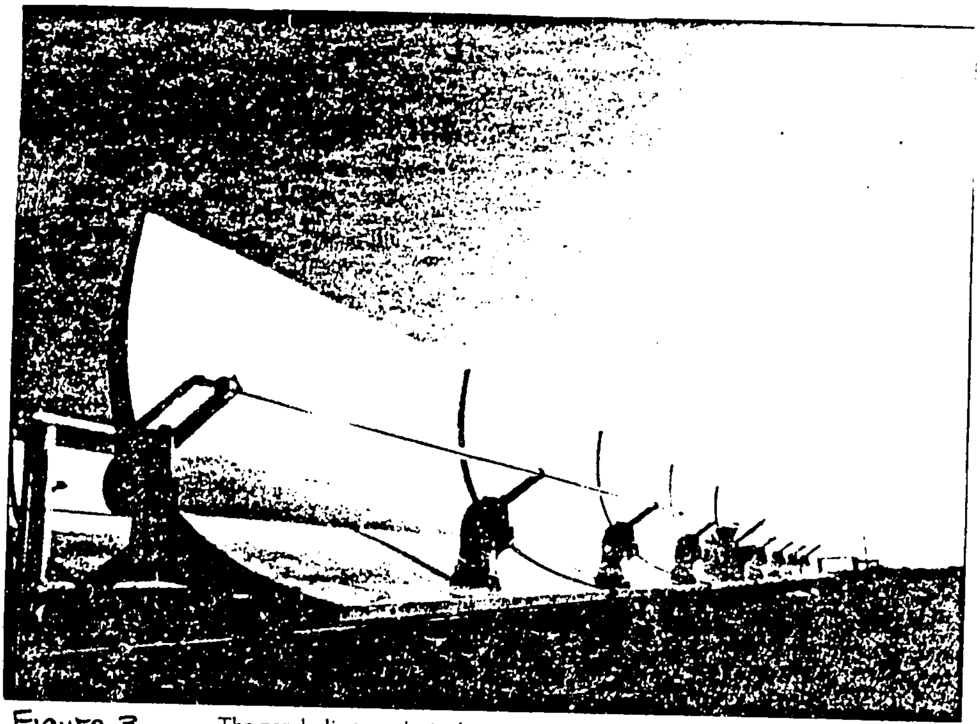

Figure 3. The parabolic-trough single-axis tracking collector by Acurex. [3]

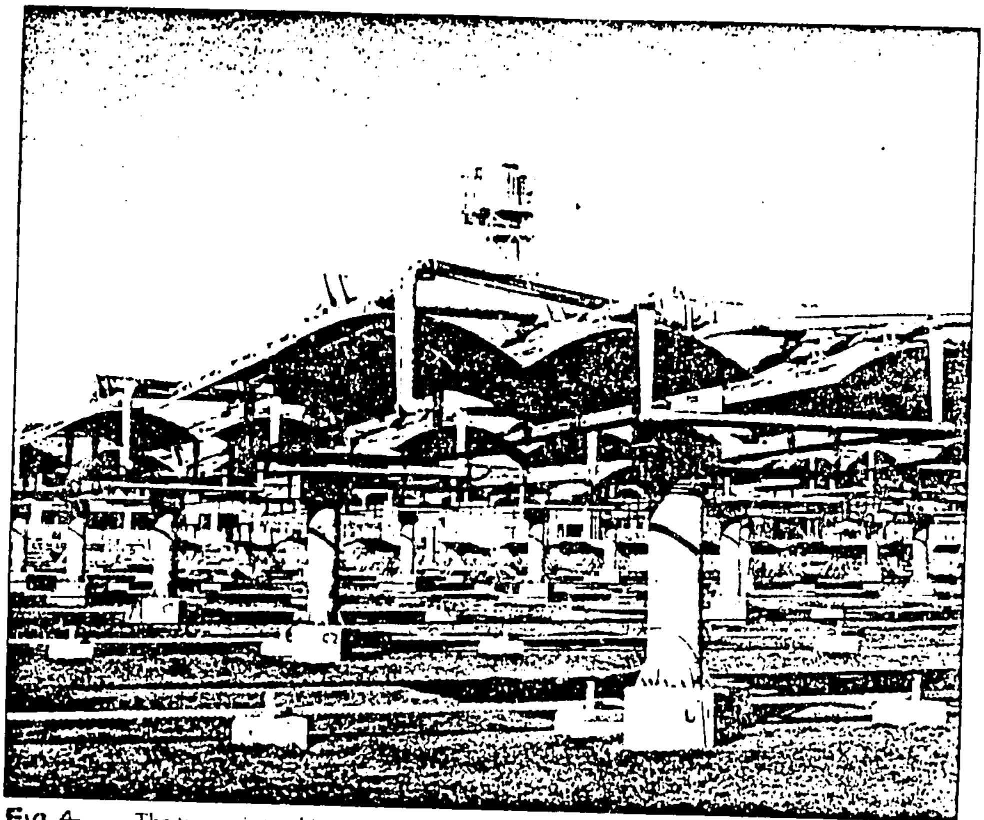

Fig 4. The two-axis tracking concentrator by M.A.N., in stow position with faces down. [3]

CENTRAL RECEIVER SYSTEMS

Eight central receiver system experiments and pilot plants are now in operation or under construction throughout the world, each with the output power of one megawatt or more of thermal energy. Two of these systems are now operating in the United States and France, and six more--located in the United States, France, Italy, Japan, and Spain--are under construction. All told, they represent an investment of at least Ω250 million.

One of the first relatively large systems, a 1 MWt solar furnace constructed by the French at Odeillo in the Pyreness Mountains, was converted in the late 1970's to generate electricity for demonstration purposes. In this application, the thermal power was removed from the receiver by means of a hot-oil heat-transfer loop to thermal storage, or directly to an oil-to-steam heat exchanger to operate a steam turbine coupled to an electric generator.

As a solar furnace, the Odeillo plant develops temperatures up to 3,000°C without the need for direct flame-firing of test specimens or use of heat-exchanger enclosures. Sixty-three heliostat mirrors, controlled by computers, reflect the sun's radiation onto a parabolic mirror which in turn concentrates the radiation on the fixed-focus area.

The Central Receiver Test Facility (CRTF) installed in 1977 at Sandia National Laboratories in New Mexico is a test bed for components and subsystems for the Barstow, California, pilot electric plant. Its sophisticated tower contains three test bays served by an elevator. The field consists of 222 heliostats which can focus five megawatts of thermal power into a test bay.

The recently completed 10MWe Barstow steam plant is connected to the Southern California Edison utility grid, and could potentially serve the needs of a community of 6,000. Its storage system is designed to provide 7 MWe for four hours.

A two-megawatt electric plant is under construction at Targasone, near Odeillo. Two towers will allow the testing of one receiver subsystem while another subsystem is being installed or modified. Molten salt will be used as the heat-transfer fluid and also as the thermal-storage material.

A third Spanish plant, a 1 MWe facility to be built at the Almeria site, is receiving assistance from the United States in the use of newly-developed design methodologies and computer programs. All three plants are expected to be operational by 1982.

Under Japan's Project Sunshine program, two pilot plants with different design approaches have been constructed at Nio, Kagawa Prefecture, on Shikoku, one of Japan's major southern island. Capable of producing 1,000 kWe each, the two plants are now operational.

Figure 5 shows the basic components of a central receiver system.

FIGURE 5.

CENTRAL RECEIVER SOLAR THERMAL POWER SYSTEM

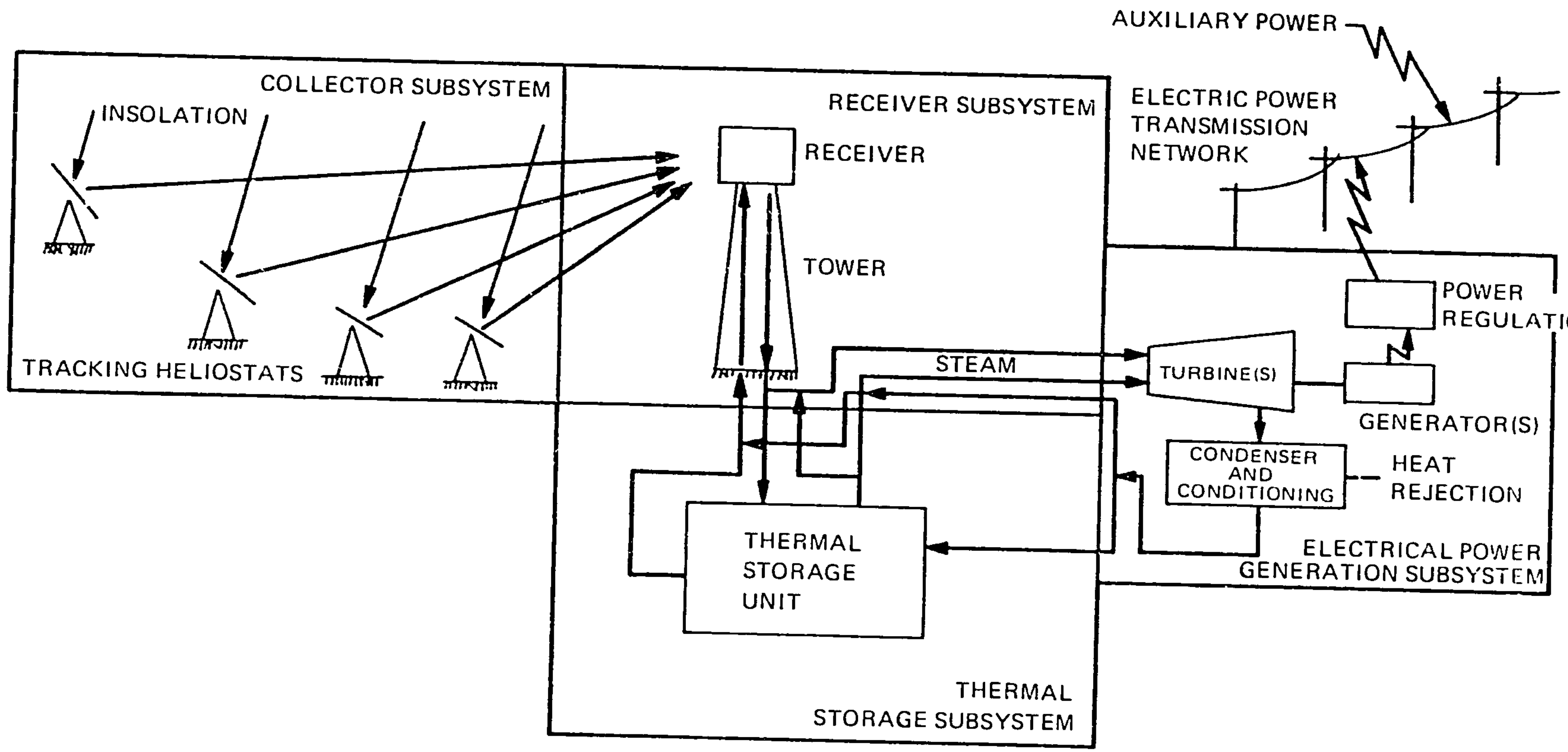

Source: ERDA, Central Receiver Solar Thermal Power System – Phase I, 10 MWe Pilot Plant, Washington, D. C., 1976.

1. ALMERIA

The SPSS - CRS plant has a rated output of 500 kWe. Solar radiation is concentrated about 450 times by a heliostat field with approximately 4000 m^2 of reflective surface. The Martin Marietta first-generation heliostats track the sun both in asimuth and elevation, with a maximum pointing error of about 2 mrad whenever the wind speed is less than 13 km/h. The field is designed to survive wind speeds of up to 144 km/h, seismic activities of 0.6 m/s^2, and the impact of 20 mm hail at 20 m/s. Additional performance data is indicated below in Table 2.

Table 2. SSPS Central Receiver System—Performance Data [3]

Design point:	day 80, 12:00 (equinox noon)	
	solar insolation	0,92 kW/m²
Heliostat field:	total reflective surface area	4000 m²
	concentration ratio	450
	land-use-factor	0,22
Cavity receiver:	heat transfer medium	Sodium
	aperture size	9 m²
	active heat transfer surface	16,9 m²
	inlet temperature	270°C
	outlet temperature	530°C
Thermal storage:	two-tank-system, storage medium	Sodium
	capacity equivalent to	1,0 MWhe
	hot storage temperature	530°C
	cold storage temperature	275°C
Steam generator:	sodium inlet temperature	525°C
	sodium outlet temperature	275°C
	steam outlet temperature	510°C
	steam pressure	100 bar
Power (at design point):	solar insolation	3675 kW
	thermal	2283 kW
	gross electric	600 kW
	net electric	517 kW
Efficiencies (at design point):	thermal/gross electric	26,3%
	thermal/net electric	22,6%
	insolation/net electric	14,1%

Transfer of thermal energy in the sodium cooled system is performed at high temperature (530°C) and low pressure (4 bar). The incoming energy (2.7 MWt at the design point), which produces peak fluxes on the tube bundle of the receiver of 0.63 MW/m^2, is passed through a storage system to the boiler. The third loop generates steam and delivers it to the turbines at 510°C and 100 bar.

The German designed cavity-type receiver has a vertical octagonal aperture of 9.7 m^2. Sodium flows in six horizontal parallel tubes which wind back and forth from the bottom to the top of the cavity. Sodium enters the inlet header at 270°C at the bottom of the panel and leaves the outlet header at 530°C near the top. The receiver is mounted on top of a 43 m high steel tower with a concrete foundation.

A cold sodium vessel and a hot sodium vessel, each having a volume of 70 m^3, provide storage for the CRS. Sodium enters the hot storage vessel from the receiver at 530°C, is pumped to the helical-tube steam generator, then is returned to the cold sodium vessel at 275°C. The power conversion unit is a steam-driven five-piston motor coupled to a three-phase generator. The operating conditions of this unit are indicated below.

Thermal input (steam)	2200 kWt
Inlet pressure	100 - 102 bar
Inlet temperature	500 - 520°C
Back pressure	0.3 bar
Speed	1000 rpm
Motor	845 Hp
Gross output	600 kWe
Net output	562 kWe
Efficiency (gross/thermal)	27.3 %
Efficiency (net/thermal)	25.5 %

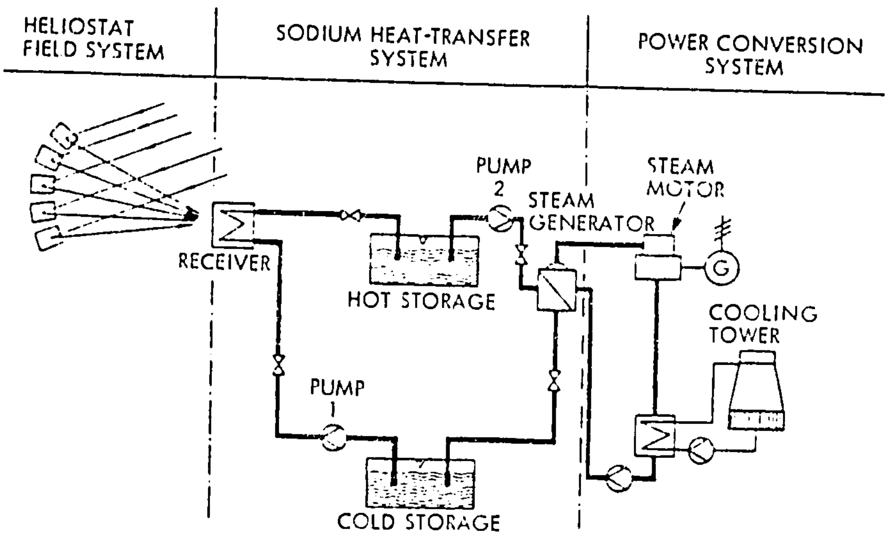

Fig 6. *Simplified schematic diagram of CRS process flow* [1]

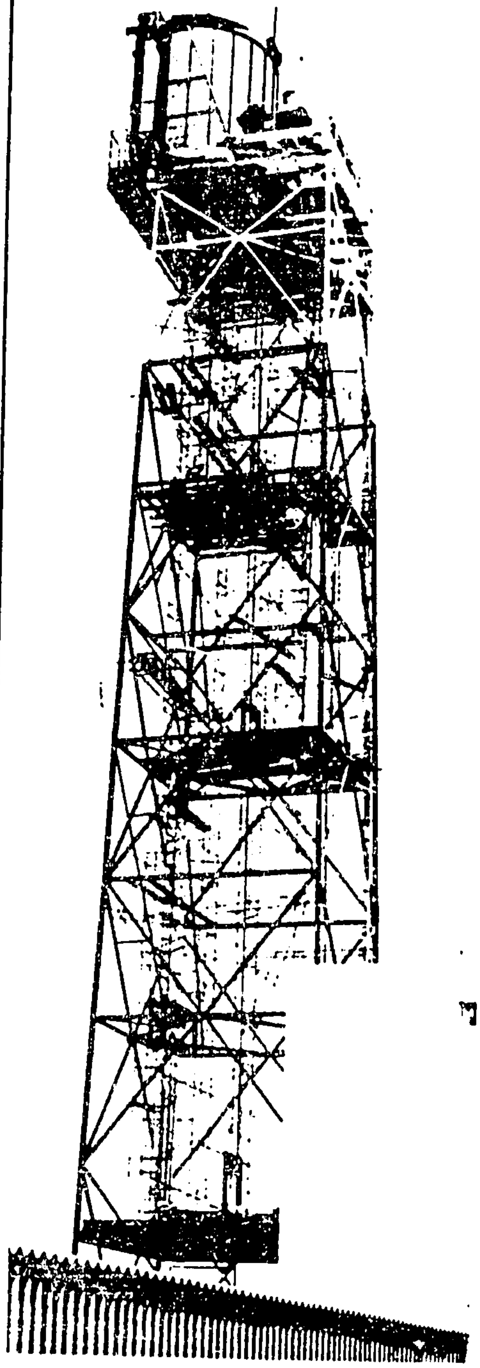

The 43-meter-high receiver tower as seen from the ground, with a view of the back of the sodium receiver. [1]

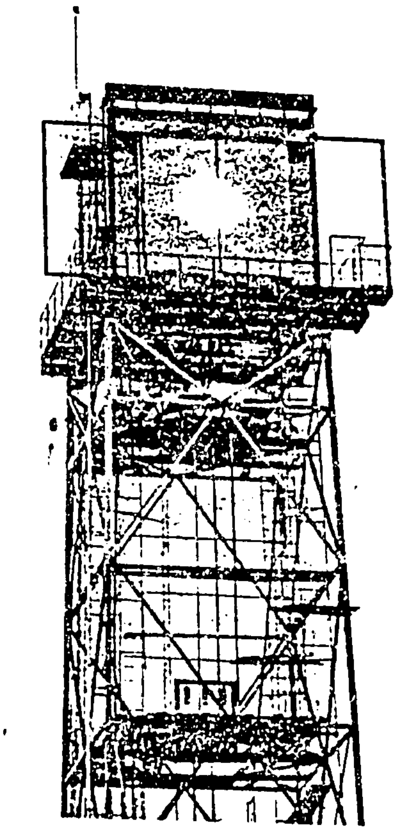

The cavity-type sodium receiver of the CRS is shown mounted on the receiver tower. In this photograph, the receiver doors are closed, showing a single heliostat image. [1]

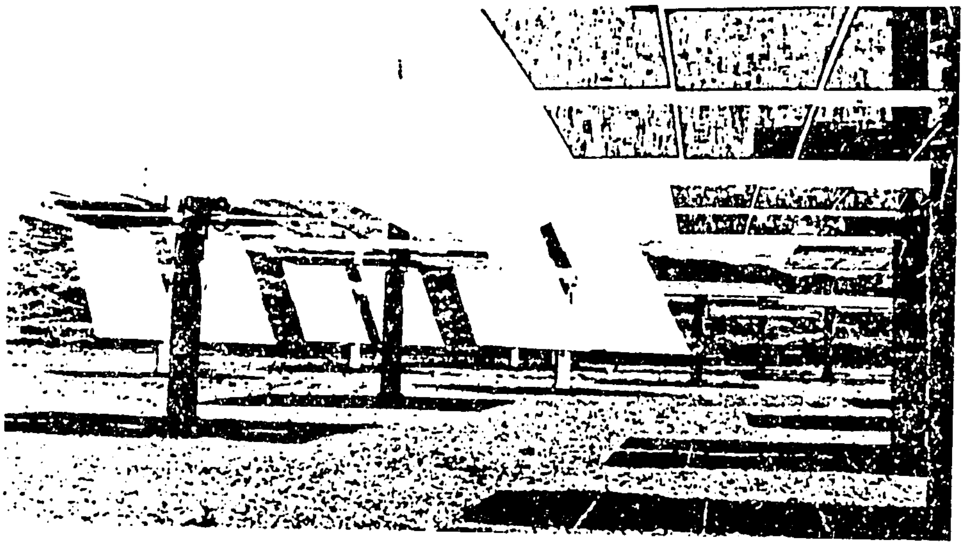

Closeup of the CRS heliostat field shows the Martin Marietta first-generation-type heliostats, some of which are in the stowed position with the reflecting surface facing downward (foreground). [1]

2. BARSTOW

A central receiver pilot plant capable of generating 10 MWe is in operation near Barstow, California. This project is the first of its kind in the U.S. and will be a pilot operation for judging the feasibility of central receiver systems.

Seven major systems are involved in total plant operation: the collector, receiver, thermal storage, master control, plant support, beam characterization, and electric power generating systems. (The first six of these make up the solar facility.) The heliostats of the collector system reflect solar energy onto the receiver mounted on a 90.8 m (298 ft) tower. In the receiver, water is boiled and converted to high-pressure steam (516°C and 10.3 MPa; 960°F and 1465 psia), which is then converted to electrical energy by the turbine/generator. Any steam from the receiver in excess of the energy required (35.7 MWt) for the generation of 10 MWe net power to the utility grid is diverted to thermal storage for use when output from the receiver is under that needed for rated electrical power.

When the turbine operates directly on steam from the receiver, the pilot plant's rated output is 10 MWe plus 1.8 MWe parasitic loads (internal plant loads). When operating from the thermal storage system alone (274°C and 2.7 MPa; 525°F and 385 psia), the net electrical output is 7 MWe. Overall efficiency of the system ranges from 13.5% (full insolation day) to 11.1 % (full energy storage operation).

Collector System

The collector field, consisting of 1818 Martin Marietta sun-tracking heliostats, has a total reflecting area of 72,538 m^2 (781,740 ft^2) and is divided into four quadrants. Each heliostat is made of 12 slightly concave mirror panels totaling 40 m^2 (430 ft^2) of mirrored surface that focus the sun's rays on the receiver. The mirror assembly is mounted on a geared drive unit for azimuth and elevation control.

There are a total of 1240 heliostats in the two northern quadrants and 578 heliostats in the two southern quadrants. In the southern quadrants, the heliostats are focused on each of the 6 preheat panels under optimum conditions. In the northern quadrants, the heliostats are focused on each of the 18 boiler panels so that the heat is distributed over the length of the panels.

The collector control subsystem consists of a micro-processor in each heliostat, a heliostat field controller for groups up to 32 heliostats, and a central computer called the heliostat array controller. The annual and diurnal sun position information for pointing each heliostat are stored within this control subsystem. The heliostats can be controlled individually or in groups in either manual or automatic modes. The heliostat array controller is located in the plant control room and is functionally tied into the master control system. The plant operator can control the collector field through either the heliostat array controller or the master control system.

The heliostats are designed to operate in winds up to 36 mph and will be stowed in a mirror-down position in higher winds. Design specifications include survivability in a stowed position in winds up to 90 mph. Several heliostats have satisfactorily passed tests in which wind-induced structural loads were simulated.

Receiver System

The receiver system consists of a single-pass to superheat boiler with external tubing, a tower, pumps, piping, wiring, and controls necessary to provide the required amount of steam to the turbine. Steam demand can be varied from the control room by the operator, or the receiver system can react to a demand from the electric power generating system up to the receiver's rated output.

The receiver is designed to produce 516°C (960°F) steam at 10.3 MPa (1465 psia) at a flow rate of 112,140 lb/h. The receiver has 24 panels (6 preheat and 18 boiler), each approximately 0.9 m (3 ft) wide and 13.7 m (45 ft) long. The panels are arranged in a cylindrical configuration with a total surface area of 330 m^2 (3252 ft^2). Each panel consists of seventy Incoloy 800 tubes through which water is pumped and boiled. The external surface temperature of the receiver tubes at rated output will be approximately 621°C (1150°F). Each receiver tube is 0.69 cm (0.27 in.) inside diameter and 1.27 cm (0.5 in.) outside diameter. These boiler tubes are made with thick walls and special metal in order to withstand the effects of diurnal cycling, wich can cause premature metal fatigue. In contrast to a solar boiler, conventional boilers are kept heated even when steam and/or electrical demand is low. In a solar receiver, the heat source disappears when the sun is obscured or not shining, and the boiler cools. When insolation returns, the boiler is reheated.

Within each panel, all tubes are welded to the adjacent tubes for their full length on the outside surface only. The receiver panel exterior is painted with a special black paint ("Pyromark") to increase thermal energy absorption. The interior surface of the receiver panels is insulated.

The tower, holding the receiver 90.8 m (298 ft) above the desert floor, has a 7.6 m (25 ft) deep footing and a 1500 ton concrete base. The tower is equipped with a temporary crane for installation of the receiver panels. The wide area of the tower beneath the receiver houses air-conditioned rooms where the receiver computer controls and some of the beam characterization system are located.

Thermal Storage System

The thermal storage system provides for storage of thermal energy to extend the plant's electrical power generating capability into nighttime or during periods of cloud cover. It also provides steam for keeping selected portions of the plant warm during non-operating hours and for starting up the plant the following day. Sealing steam is required in the turbine casing even when it is not running. Even though the primary source for this turbine sealing steam is thermal storage, a small auxiliary electric boiler is standing by in case the thermal storage system is depleted or not operating.

The storage tank is 13.7 m (45 ft) high, 19.8 m (65 ft) in diameter (inner), and built on a special lightweight, insulating concrete for reducing heat loss to the ground. The walls are made of steel and 30.5 cm (1 ft) of insulation and the roof is aluminum plus 61 cm (2 ft) of insulation. The 3581 m^3 (946,000 gal) capacity tank, filled with rock, sand and about 908 m^3 (240,000 gal) of thermal oil (Caloria HT 43), acts as a heat storage vessel or unit.

Desuperheated steam from the receiver is routed through dual heat exchangers in which thermal storage oil is heated. The heated oil is pumped back into the tank and thermal energy is transferred to the rock and sand. When fully charged, the temperature of the thermal storage mixture (oil, rock, and sand) will be approximately 302°C (575°F). When discharging, the heated oil is pumped through another heat exchanger to boil water. Steam at 274°C (525°F) and 2.7 MPa (385 psia) can be delivered to the turbine at a rate of 105,000 lb/h. The rated electrical capacity of the plant operating on thermal storage energy is 28 megawatt-hours (28 MWe-h) net output, i.e., 7 MWe power for 4 hours. After discharging, sufficient thermal energy will be available for heating, sealing steam, and restarting the plant the next day.

As do other plant systems, the thermal storage system has its own controls and also can be controlled both manually and automatically through the master control system.

View of the tower with the boiler receiver mounted at its apex. A man is standing beneath and to the left of the receiver behind the railing. [2]

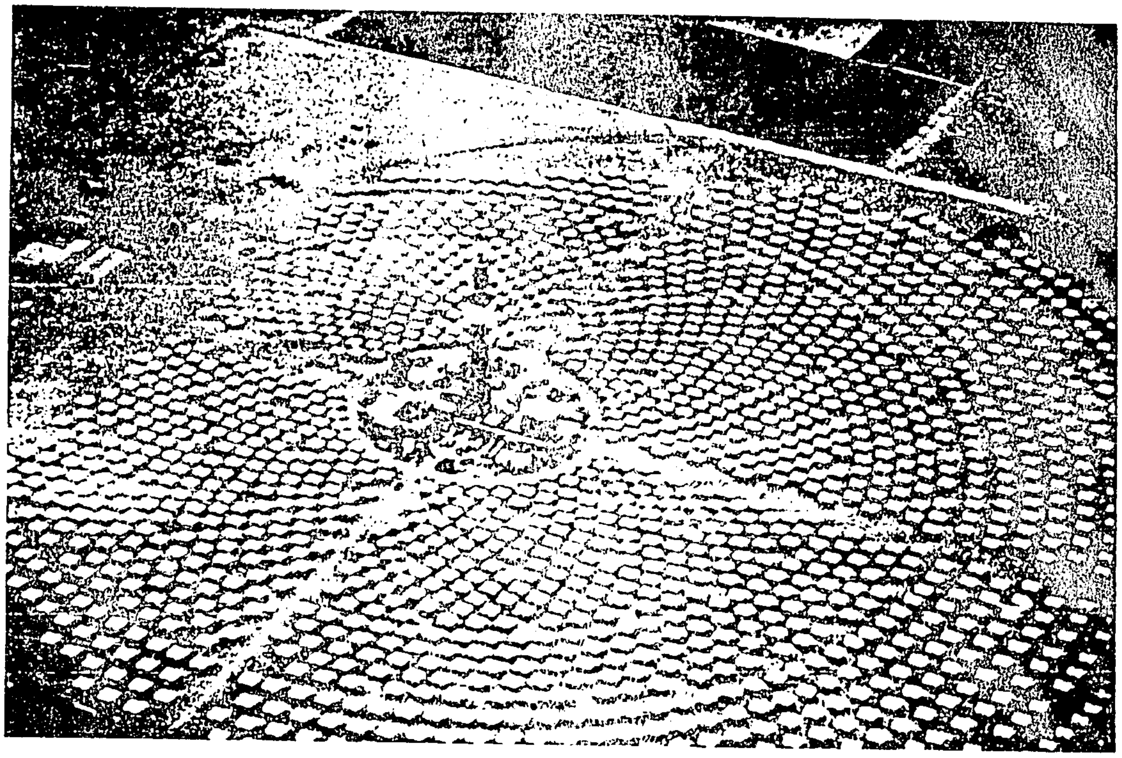

The 10 MWe Solar One Central Receiver System in California. Over 1800 heliostats focus sunlight onto the receiver.

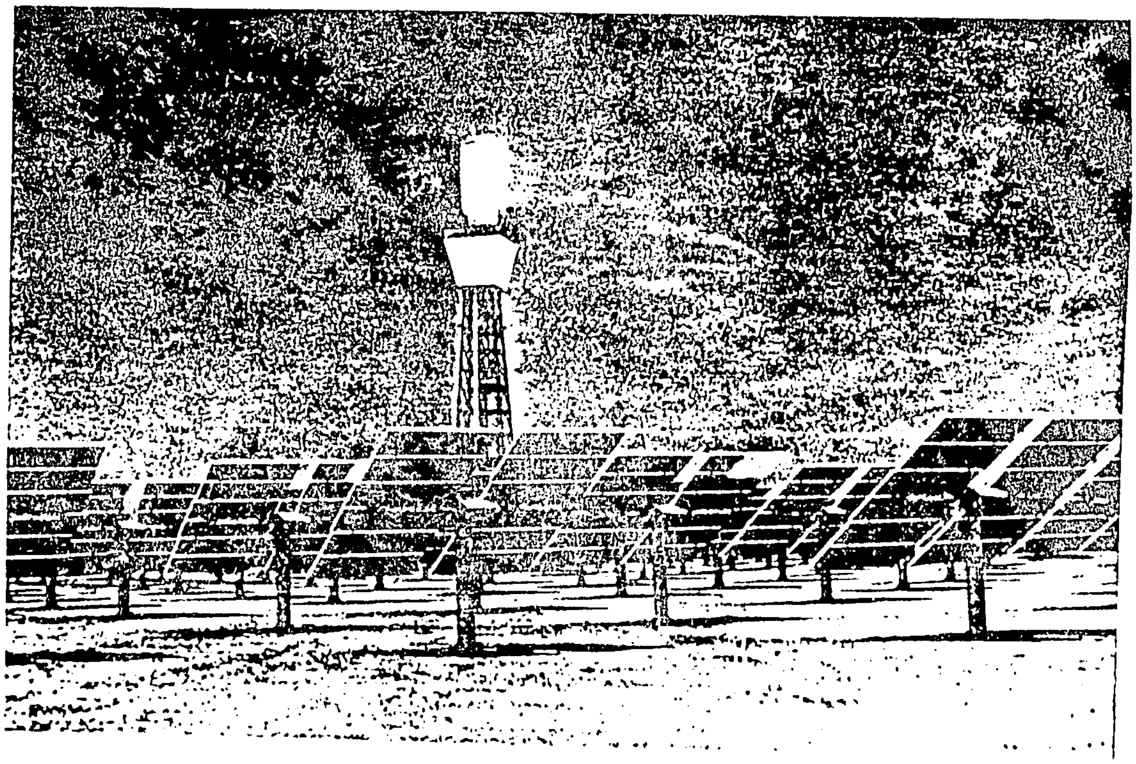

The receiver under load. About 70 MW of energy is focused on the absorber in the center of the field.

The capital cost of the Barstow 10 MWe CRS plant is estimated at 141 M$. Annual operating and maintenance costs are estimated as 3.7 M$. Construction took 5 years. These data permit us to make an estimation of the cost of the electricity that will be produced by the plant.

The capital cost of 141 M$ does not include interest charges on the loan. Construction costs are 141/5 = 28.2 M$/yr for 5 years. We assume interest is charged at 15% annually. The total capital cost, including capital charges, is therefore given by:

$$I = \frac{(1 + 0.15)^5 - 1}{0.15} \times 28.2 = 190.14 \text{ M\$}$$

The capital recovery factor (CRF) for this debt, based on 15% interest rate and a 40 yr lifetime, would be:

$$\text{CRF }(0.15,\ 40) = \frac{0.15}{1 - (1 + 0.15)^{-40}} = 0.15056$$

So the amount paid annually in capital charges is 190.14 x 0.15056 = 28.63 M$/yr.

Operation and maintenance costs are 3.7 M$/yr, so total annual costs may be estimated as 32.33 M$/yr.

How much electricity will the plant produce? This is very difficult to estimate at this stage in the development and demonstration of CRS plants.

Data for California suggest that the direct insolation is about 3200 kWh/m^2 per year. Using this figure and the total heliostat area of 72,538 m^2, the gross insolation is about 232.12 x 10^6 kWh/yr.

The efficiency of the Almeria CRS plant is estimated as about 14% (insolation kWh to net electric kWhe). So an approximate estimate of net electric output for the Barstow 10 MWe plant would be:

$$0.14 \times 232.12 \times 10^6 = 32.5 \times 10^6 \text{ kWhe/yr}$$

Assuming that all routine maintenance is performed at night, so that the daytime plant factor is 100%, the cost of electricity produced by the system is approximately:

$$\frac{32.33 \times 10^6 \text{ \$/yr}}{32.5 \times 10^6 \text{ kWhe/yr}} = 0.995 \text{ \$/kWhe}$$

or very nearly $1 per kWhe.

References

1. The Solar Thermal Report, Sandia National Laboratories, Vol. 2, No. 7, September 1981.

2. The Solar Thermal Report, Sandia National Laboratories, Vol. 2, No. 9, December 1981.

3. Sunworld, Vol. 5, No. 3, Pergamon Press, 1981.

4. Scheinberg, R.N., and J.N. Reeves, "10 MWe Solar Thermal Central Receiver Pilot Plant", US Dept. of Energy, 1981.

BIBLIOGRAPHY

1. **Fundamentals of Solar Energy Conversion**, by Edward Anderson, University of Nebraska - Lincoln. Published by Addison-Wesley Publishing Company, Reading, Massachusetts; 636 p, 1983.

2. **Solar Energy Thermal Processes**, by John Duffie and William Beckman, University of Wisconsin. Published by John Wiley and Sons, New York; 386 p, 1974.

3. **Solar Engineering of Thermal Processes**, by John Duffie and William Beckman, University of Wisconsin. Published by John Wiley and Sons, New York; 762 p, 1980.

4. **Principles of Solar Engineering**, by Frank Kreith and Jan Kreider. Published by McGraw-Hill Book Company, New York; 778 p, 1978.

5. **Solar Thermal Engineering**, by Peter J. Lunde. Published by John Wiley and Sons, New York; 612 p, 1980.

6. **Solar Energy**, by Donald Rapp. Published by Prentice-Hall Inc., Englewood Cliffs, New Jersey; 516 p, 1981.

7. **Solar Energy Handbook - Theory and Applications**, prepared by Power Systems Group, AMETEK Inc. Published by the Chilton Book Company, Radnor, Pennsylvania; 180 p, 1979.

8. **Applications of Solar Energy for Heating and Cooling of Buildings**, edited by R.C. Jordan and B.Y.H. Liu. Available from ASHRAE, Atlanta, Georgia; 206 p, 1977.

9. **Installation Guidelines for Solar Domestic Hot Water Systems in One and Two-Family Dwellings**, 2nd edition. Available from the US Government Printing Office (S/N 023-000-00520-4), Washington, D.C.; 107 p, 1980.

10. **Solar Heating and Cooling of Residential Buildings - Sizing, Installation and Operation of Systems**, 2nd edition, prepared by Solar Energy Applications Laboratory, Colorado State University. Available from the US Government Printing Office, Washington, D.C.; September 1980.

11. **Handbook of Experience in the Design and Installation of Solar Heating and Cooling Systems**, by Dan Ward and Harjinder Oberoi. Available from ASHRAE, Atlanta, Georgia; 238 p, July 1980.

12. **Introduction to Solar Heating and Cooling Design and Sizing.** Available from NTIS (DOE/CS-0011), Springfield, Virginia; 460 p, August 1978.

13. **Final Reliability and Materials Design Guidelines for Solar Domestic HotWater Systems**, prepared by Argonne National Laboratory. Available from NTIS (DE82016180), Springfield, Virginia; 220 p, October 1979.

14. **Solar Energy for Buildings Handbook**, by David Christensen, University of Alabama. Available from NTIS (ORO-5361-T1), Springfield, Virginia; 222 p, October 1979.

15. **Application of Solar Technology to Today's Energy Needs**, Volume I, prepared by The Office of Technology Assessment and available from the US Government Printing Office (S/N 052-003-00539-5), Washington, D.C., 526 p, June 1978.

16. **Solar Energy for the Villages of Tanzania**, proceedings of the workshop held in Dar es Salaam, August 1977. Available from the National Academy of Sciences, Board on Science and Technology for International Development, Washington, D.C.; 167 p, 1978.

17. **Thermal and Economic Analysis of Solar Assisted Heat Pumps for Low-Temperature Industrial Process Heat Applications**, by S.K. Chaturvedi and L.M. Murphy, Solar Energy Research Institute. Available from NTIS (SERI/TR-632-880), Springfield, Virginia; 76 p, October 1981.

18. **Flat Plate Thermal Solar Collectors: A Physical Background**, by Per Isakson, Swedish Council for Building Research. Available from NTIS (PB81135741), Springfield, Virginia; 104 p, 1980.

19. **Methods of Testing to Determine the Thermal Performance of Solar Collectors**, ASHRAE Standard 93-77. Available from ASHRAE, Atlanta, Georgia; 50 p, 1977.

20. **Direct Use of the Sun's Energy**, by Farrington Daniels. Published by Ballantine Books, New York; 270 p, 1964.

21. **Solar Selective Surfaces**, by O.P. Agnihotri and B.K. Gupta. Published by John Wiley and Sons, New York; 215 p, 1981.

22. **Application of Solar Energy to Industrial Dehydration**, prepared by California Polytechnic State University, San Luis Obispo, for the US Department of Energy. Final report second phase; 85 p, September 1978.

23. **Low Temperature and Solar Grain Drying Handbook**, prepared by the Midwest Plan Service. Available from MPS, Iowa State University, Ames, Iowa 50011; 86 p, 1980.

24. **Demonstration of Collectors and Instrumentation for Application to Solar Drying of Peanuts, Tobacco and Forage**, prepared by the Georgia Institute of Technology, Atlanta, Georgia. Final report; 262 p, 1979.

25. **Solar Ponds for Residential Heating-Heat Extraction from a Salt Gradient Solar Pond**, by H.C. Bryant, University of New Mexico. Available from NTIS (PB80-108624), Springfield, Virginia; 33 p, 1979.

26. **Solar Energy,** International Journal for Scientists, Engineers and Technologists in Solar Energy and Its Application. Published monthly by Pergamon Press, Elmsford, New York.

27. **Solar Age,** (journal); published monthly by Solar Vision Inc., Church Hill, Harrisville, New Hampshire.

28. **Sunworld,** journal of the International Solar Energy Society. Published bimonthly by ISES, Victoria, Australia.

29. **The Trade-Off Between Collector Area, Storage Volume, and Building Conservation in Annual Storage Solar Heating Systems,** by Sanford Sillman, Solar Energy Research Institute. Available from NTIS (SERI/TR-721-907), Springfield, Virginia; 126 p, March 1981.

30. **Solar Collector Performance Manual,** prepared by A.B. Newton and S.H. Gilman. Available from ASHRAE, Atlanta; 201 p, 1978.

31. **Solar Energy for Domestic Heating and Cooling - A Bibliography with Abstracts and a Survey of Literature and Information Sources,** by A. Eggers-Lura, European Helio Centre. Published by Pergamon Press, Elmsford, New York; 400 p, 1979.

32. **Proceedings of the Meeting of the Expert Group on the Use of Solar and Wind Energy,** Energy Resources Development Series No. 16. Available from the United Nations (Sales No. E.76.II.F.13), New York; 147 p, 1976.

33. **Solar Domestic and Service Hot Water Heating Systems Manual,** published by ASHRAE, Atlanta, Georgia; 180 p, 1983.

34. **Methods of Testing to Determine the Thermal Performance of Solar Domestic Water Heating Systems.** ASHRAE Standard 95-1981; published by ASHRAE, Atlanta, Georgia; 23 p, 1981.

35. **The Availability of Solar Energy in Thailand,** by R.H.B. Exell, Asian Institute of Technology. Available from the National Technical Information Service (PB80 193907), Springfield, Virginia; 85 p, 1979.

36. **A Treatise on Solar Energy,** by H.P. Garg, IIT, New Delhi. Published by John Wiley, New York; 400 p, 1982.

37. **Solar Energy Handbook,** by J. Kreider and F. Kreith. Published by McGrawHill Book Company, New York; 1120 p, 1980.

38. **Solar Heating and Cooling,** 2nd edition, by J. Kreider and F. Keith. Published by McGraw-Hill Book Company, New York; 384 p, 1982.

39. **An Introduction to Solar Radiation,** by M. Iqbal, University of British Columbia. Published by Academic Press, New York; 1983.

40. **Solar Energy Engineering**, edited by A.A.M. Sayigh, Riyadh University, Saudi Arabia. Published by Academic Press, New York; 506 p, 1977.

41. **Solar and Wind Technology** (journal). A new journal published by Pergamon Press in 1984.

42. **Solar Power Tower Design Guide: Solar Thermal Central Receiver Power Systems**, by K.W. Battleson, Sandia National Laboratories. Available from NTIS (DE81026584), Springfield, Virginia; 166 p, April 1981.

43. **Assessment of the Potential of Solar Thermal Small Power Systems in Small Utilities**, by P. Steitz et. al. Available from NTIS (DOE/JPL-1060-14), Springfield, Virginia; November 1978.

44. **End-Use Matching for Solar Industrial Process Heat**, by K.C. Brown et. al., Solar Energy Research Institute. Available from NTIS (SERI/TR-34091), Springfield, Virginia; 220 p, October 1979.

45. **Central Receiver Test Facility (CRTF) Experiment Manual**, by John Holmes et. al. Sandia National Laboratories. Available from NTIS (SAND77-1173), Springfield, Virginia; 89 p, October 1979.

46. **The Effects of Regional Insolation Differences Upon Advanced Solar Thermal Electric Power Plant Performance and Energy Costs**, by A.F. Latta et. al., Jet Propulsion Laboratory. Available from NTIS (DOE/JPL-1060-17), Springfield, Virginia; 85 p, March 1979.

47. **Preliminary Definition and Characterization of a Solar Industrial Process Heat Technology and Manufacturing Plant for the Year 2000**, prepared by Los Alamos Scientific Laboratory. Available from NTIS (DOE/EV-0100), Springfield, Virginia; 27 p, September 1980.

48. **Medium and High Temperature Solar Processes**, by Jan Kreider. Published by Academic Press, New York; 346 p, 1979.

49. **Thermal Storage and Heat Transfer in Solar Energy Systems**, edited by Frank Keith, Solar Energy Research Institute. Available from the American Society of Mechanical Engineers, New York; 79 p, 1978.

50. **Thermal Storage**, by T.S. Dean, University of Kansas. Published by the Franklin Institute Press, Philadelphia, Pennsylvania; 61 p, 1978.

51. **Thermal Energy Storage for Solar Applications: An Overview**, by Charles Wyman, Solar Energy Research Institute. Available from NTIS (SERI/TR-34089), Springfield, Virginia; 116 p, 1979.

52. **Low Temperature Thermal Energy Storage, A State of the Art Survey**, by F. Baylin, Solar Energy Research Institute. Available from NTIS (SERI/RR-54164), Springfield, Virginia; 107 p, 1979.

53. **Sensible Heat Storage For a Solar Thermal Power Plant**, by Thomas Baldwin et. al., Lawrence Berkeley Laboratory. Available from NTIS (LBL-9321), Springfield, Virginia; 183 p, July 1979.

54. **Methods of Testing Thermal Storage Devices Based on Thermal Performance.** ASHRAE Standard 94-77; available from ASHRAE, Atlanta, Georgia; 22 p, 1977.

55. **Thermal Stratification in Liquid Storage Tanks - A State of the Art Review and Literature Survey**, by S.M. Han and D.L. Chrsitensen. NASA Technical Brief Vol. 5, No. 2, MFS-25416; 29 p, January 1980.

56. **Melting in Phase-Change Thermal Storage Media**, by E.M. Sparrow and J.W. Ramsey, University of Minnesota. Available from NTIS (COO-2993-1), Springfield, Virginia; 86 p, 1976.

57. **A Survey of Sensible and Latent Heat Thermal Energy Storage Projects**, by F. Baylin and M. Merino, Solar Energy Research Institute. Available from NTIS (SERI/RR-355-456), Springfield, Virginia; 339 p, May 1981.

58. **High Temperature Thermal Energy Storage**, by Robert Turner, California Institute of Technology. Published by the Franklin Institute Press, Philadelphia, Pennsylvania; 91 p, 1978.

59. **Fundamentals of Energy Storage**, by J. Jensen and B. Sorensen. Published by John Wiley, New York; 368 p, 1983.

60. **Thermal Energy Storage and Regeneration**, by F. Schmidt and A. Willmott. Published by McGraw-Hill Book Company, New York; 384 p, 1981.

APPENDICES

93-77

ANSI B198.1-1977

ASHRAE STANDARD

Methods of Testing TO DETERMINE THE THERMAL PERFORMANCE OF SOLAR COLLECTORS

Approved by the ASHRAE Standards Committee February 1977; approved by the Board of Directors for publication February 1977; effective date as of February 1977.

ASHRAE Standards are updated on a five-year cycle; the date following the Standard number is the year of approval. The latest copies may be purchased from the ASHRAE Publications Sales Department, 345 E. 47th Street, New York, NY 10017.

Corrected Printing, 1978

1978

The American Society of Heating, Refrigerating, and Air-Conditioning Engineers, Inc.

345 East 47th Street, New York, N.Y. 10017

FOREWORD

This Standard has been prepared by a Committee drawn primarily from the membership of ASHRAE Technical Committee on Solar Energy Utilization, TC 6.7. The Committee's objective was to formulate a test procedure whereby solar energy collectors can be tested both indoors and outdoors, to rate the collectors in accordance with their thermal performance, and to determine their time constant and the variation of their efficiency with changes in the angle of incidence between the sun's direct rays and the normal to the collector aperture.

Standard 93-77 is based upon the Interim Report NBSIR 74-635, prepared for the National Science Foundation/Energy Research and Development Administration by James E. Hill and Tamami Kusuda of the Center for Building Technology, National Bureau of Standards. Following an organizational meeting at ASHRAE's Annual Meeting in Dallas in 1976, Committee 93 held many day-long sessions during which each section of NBSIR 74-635 was carefully reviewed. Task Groups formed by the Committee formulated revised versions of each section of the report, and added a considerable amount of new material which provided for methods of indoor and outdoor testing, for determination of the collector time constant and the variation of collector efficiency with changing angle of incidence. Instrumentation also received special attention. Provisions for testing both concentrating and flat-plate collectors are included.

NOMENCLATURE

- a, b = constants used in incident angle modifier equation, dimensionless
- A = cross-sectional area, $m^2(ft^2)$
- A_a = transparent frontal area for a flat-plate collector or aperture area for a concentrating collector, $m^2(ft^2)$
- A_g = gross collector area, $m^2(ft^2)$
- A_n = area of nozzle, $m^2(ft^2)$
- A_r = absorbing area of a flat-plate collector or the receiving area of a concentrating collector, $m^2(ft^2)$
- b_o = constant used in incident angle modifier equation, dimensionless
- C_A = effective heat capacity of the solar collector, J/°C(Btu/F)
- C_n = nozzle coefficient of discharge, dimensionless
- c_p = specific heat of the transfer fluid, J/(kg·°C) (Btu/(lbm·F))
- D_n = nozzle throat diameter, m(ft)
- f_t = temperature factor for calculation of nozzle Reynolds number, dimensionless
- F' = absorber plate efficiency factor, dimensionless
- F_R = solar collector heat removal factor, dimensionless
- I = solar irradiation, $W/m^2(Btu/(hr \cdot ft^2))$
- I_D = direct solar irradiation component $W/m^2(Btu/(hr \cdot ft^2))$
- I_{DN} = direct normal solar irradiation, $W/m^2(Btu/(hr \cdot ft^2))$
- I_d = diffuse solar irradiation incident upon the aperture plane of collector, $W/m^2(Btu/(hr \cdot ft^2))$
- I_{sc} = solar constant, 1 353 W/m^2(429.2 $Btu/(hr \cdot ft^2)$)
- I_t = total solar irradiation incident upon the aperture plane of collector, $W/m^2(Btu/(hr \cdot ft^2))$
- K = factor defined by equation (8.7), dimensionless
- $K_{\alpha\tau}$ = incident angle modifier, dimensionless
- LST = local standard time, decimal hours
- LSTM = local standard time meridian, deg
- AST = apparent solar time, decimal hours
- m = air mass, dimensionless
- $\dot{m}$ = mass flow rate of the transfer fluid, kg/s (lbm/hr)
- N_{Re} = Reynolds number, dimensionless
- P_{th} = theoretical power required to move the transfer fluid through the collector, W(hp)
- p_n = absolute pressure at the nozzle throat, $Pa(lbf/in.^2)$
- p_v = velocity pressure at the nozzle throat or the static pressure difference across the nozzle, $Pa(lbf/in.^2)$
- Δp = pressure drop across the collector, $Pa(lbf/in.^2)$
- Δp_n = pressure drop across the nozzle, $Pa(lbf/in.^2)$
- Q_{mi} = measured air flow rate, $m^3/s(ft^3/min)$
- Q_s = standard air flow rate, $m^3/s(ft^3/min)$
- q_u = rate of useful energy extraction from the collector, W(Btu/hr)
- t_a = ambient air temperature, °C(F)
- t_f = average fluid temperature, °C(F)
- $t_{f,e}$ = temperature of the transfer fluid leaving the collector, °C(F)
- $t_{f,e,initial}$ = temperature of transfer fluid leaving the collector at the beginning of a specified time period, °C(F)
- $t_{f,e,T}$ = temperature of the transfer fluid leaving the collector at a specified time, °C(F)
- $t_{f,i}$ = temperature of the transfer fluid entering the collector, °C(F)
- t_p = average temperature of the absorbing surface for a flat-plate collector, °C(F)
- t_r = average temperature of the absorbing surface for a concentrating collector, °C(F)
- Δt = temperature difference, °C(F)
- U_L = solar collector heat transfer loss coefficient, $W/(m^2 \cdot °C)$ $(Btu/(hr \cdot ft^2 \cdot F))$
- V_a = velocity of the air at the nozzle throat, m/s (ft/min)
- v_n = specific volume of the air at the nozzle at standard barometric pressure, m^3/kg dry air (ft^3/lbm dry air)
- v_n' = specific volume of air at the nozzle per unit mass of air-water vapor mixture, m^3/kg (ft^3/lbm)
- w = density, kg/m^3 (lbm/ft^3)
- W_n = humidity ratio at the nozzle, kg H_2O/kg dry air (lbm H_2O/lbm dry air)
- α = absorptance of the collector absorber surface for solar radiation
- Γ = fraction of specularly reflected radiation from the reflector or refracted radiation which is intercepted by the solar collector absorbing surface
- γ = collector-solar azimuth, deg
- θ = angle of incidence between direct solar rays and the normal to the collector surface or to the aperture, deg
- β = solar altitude angle, deg
- ϕ = solar azimuth angle, deg
- ψ = collector azimuth angle, (measured from the south in the horizontal plane), deg
- η_g = collector efficiency based on gross collector area, %
- λ = wavelength, μm
- ρ = specular reflectance of the solar collector reflector
- T = time, decimal hours or seconds
- τ = transmittance of the solar collector cover plate, dimensionless (if no cover plate is used, $\tau = 1.0$)
- $(\tau\alpha)_e$ = effective transmittance-absorptance product, dimensionless
- $(\tau\alpha)_{e,n}$ = effective transmittance-absorptance product at normal incidence
- T_1, T_2 = time at the beginning and end of a test period, decimal hours
- Σ = collector tilt from the horizontal, deg

1. PURPOSE

1.1 The purpose of this standard is to provide test methods for determining the thermal performance of solar energy collector modules (hereinafter called solar collectors) which heat fluids for use in thermal systems.

2. SCOPE

2.1. This standard applies to non-concentrating and concentrating solar collectors in which a fluid enters the collector through a single inlet and leaves the collector through a single outlet.

2.1.1 Collectors containing more than one inlet and more than one outlet may be tested according to this standard provided that the external piping or ducting can be connected so as to provide effectively a single inlet and a single outlet.

2.2 The heat transfer fluid (hereinafter called the transfer fluid) may be either a liquid or a gas but not a mixture of the two phases.

2.3 This standard contains methods for conducting tests outdoors under natural solar irradiation and for conducting tests indoors under simulated solar irradiation.

2.4 This standard provides test methods and calculation procedures for determining steady state and quasi-steady state thermal performance, time and angular response characteristics of solar collectors.

2.5 This standard is not applicable to those collectors in which the thermal storage unit is an integral part of the collector to such an extent that the collection process and the storage process cannot be separated for the purpose of making measurements of these two processes.

3. DEFINITIONS

3.1 *Absorber.* The absorber is that part of the solar collector which receives the incident radiation energy and transforms it into thermal energy. It may possess a surface through which energy is transmitted to the transfer fluid; however, the transfer fluid itself can be the absorber.

3.2 *Absorber Area.* The absorber area is the total heat transfer area from which the absorbed solar irradiation heats the transfer fluid, or the area of the absorber medium if both transfer fluid and solid surfaces jointly perform the absorbing function.

3.3 *Air Mass.* The air mass is the ratio of the mass of atmosphere in the actual earth-sun path to the mass which would exist if the sun were directly overhead at sea level.

3.4 *Angle of Incidence.* The angle of incidence is the angle between the direct solar irradiation and the normal to the aperture plane.

3.5 *Aperture Area.* The aperture area is the maximum projected area of a solar collector through which the unconcentrated solar radiant energy is admitted.

3.6 *Area, Gross Collector.* Gross collector area is the maximum projected area of the complete collector module including integral mounting means.

3.7 *Collector, Concentrating.* A concentrating collector is a solar collector which uses reflectors, lenses or other optical elements to concentrate the radiant energy passing through the aperture onto an absorber of which the surface area is smaller than the aperture area.

3.8 *Collector, Flat-Plate.* A flat-plate collector is a non-concentrating solar collector in which the absorbing surface is essentially planar.

3.9 *Concentration Ratio.* The concentration ratio of a concentrating solar collector is the ratio of the aperture area to the absorber area.

3.10 *Cover, Collector.* The collector cover is the material covering the aperture to provide thermal and environmental protection.

3.11 *Irradiation, Instantaneous.* Instantaneous irradiation is the quantity of solar radiation incident on a unit surface area in unit time, measured in W/m^2($Btu/(hr \cdot ft^2)$).

3.12 *Irradiation, Integrated Average.* The average integrated irradiation is the solar radiation incident on a unit surface area during a specified time period divided by the duration of that time period.

3.13 *Instantaneous Efficiency.* The instantaneous efficiency of a solar collector is the amount of energy removed by the transfer fluid per unit of gross collector area during the specified time period divided by the total solar radiation incident on the collector per unit area during the same test period, under steady state or quasi-steady state.

3.14 *Pyranometer.* A pyranometer is a radiometer used to measure the total solar radiation incident upon a surface per unit time per unit area. This energy includes the direct radiation, the diffuse sky radiation and the solar radiation reflected from the foreground.

3.15 *Pyrheliometer.* A pyrheliometer is a radiometer used to measure the direct radiation on a surface normal to the sun's rays.

3.16 *Quasi-Steady State.* Quasi-steady state describes the state of the solar collector test when the flow rate and temperature of the fluid entering the collector are constant but the exit fluid temperature changes due to the normal change in irradiation that occurs with time for clear sky conditions.

3.17 *Solar Collector.* A solar collector is a device designed to absorb incident solar radiation and to transfer the energy to a fluid passing through it.

3.18 *Standard Air.* Standard air is air weighing 1.2 kg/m³(0.075 lbm/ft³), and is equivalent in density to dry air at a temperature of 21.1°C (70F) and a barometric pressure of 1.01 × 10⁵ Pa (29.92 in. Hg).

3.19 *Standard Barometric Pressure.* Standard barometric pressure is 1.01 × 10⁵ Pa (29.92 in. Hg).

3.20 *Temperature, Ambient Air.* Ambient air temperature is the temperature of the air immediately surrounding the solar collectors being tested.

3.21 *Time Constant.* The time constant is the time required for the fluid leaving a solar collector to attain 63.2% of its steady state value following a step change in irradiation or inlet fluid temperature.

3.22 *Total Incident Irradiation.* Total incident irradiation is the total solar radiant energy incident upon a unit surface area during a specified time period, expressed in (W·hr)/m²(Btu/ft²).

3.23 *Transfer Fluid, Heat.* The heat transfer fluid is the medium, such as air, water or other fluid, which passes through the solar collector and carries the absorbed thermal energy away from the collector.

4. CLASSIFICATIONS

4.1 Solar collectors may be classified according to their collecting characteristics, the way in which they are mounted (i.e., stationary or sun tracking) and the type of transfer fluid which they employ.

4.1.1 **Collecting Characteristics.** A non-concentrating or flat-plate collector is one in which the solar radiation absorbing surface is essentially flat and in which the aperture and the absorber are similar in area and geometry. A concentrating collector is one which usually contains reflectors or other optical means to concentrate the energy entering through the aperture to be incident upon a heat absorber of surface area smaller than the aperture.

4.1.2 **Mounting.** A solar collector can be mounted in a stationary position with a fixed azimuth and tilt angle (measured from the horizontal) or it may be adjustable as to tilt angle to follow the annual changes in solar declination; it may also be designed to track the sun in altitude and azimuth (altazimuth mounting) or in its apparent daily rotation about the earth (polar or equatorial mounting).

4.1.3 *Type of Fluid.* A collector may use either a liquid or a gas as the transfer medium.

5. REQUIREMENTS

5.1 Solar collectors shall be tested in accordance with the provisions set forth in this Section and in Section 8.

5.1.1 The collector whose thermal performance is to be tested in accordance with this document shall be preconditioned prior to initiation of the test. Preconditioning shall consist of stagnation heat in a non-operational mode in a dry condition for three days in which the cumulative mean incident solar radiation measured in the plane of the collector shall be not less than 4722 (W·hr)/(m²·day) (1500 Btu/(ft²·day)). The exposure angle shall be the angle of test specified herein.

5.1.2 Testing of full scale modules is preferred. The size of collector to be tested shall be large enough so that the performance characteristics determined will be indicative of those that would occur when the collector is part of an installed system. If the collector is modular and the test is being done on one module, it should be mounted and insulated in such a way that the back and edge losses will be characteristic of those that will occur during operation on a structure.

5.1.3 For tests conducted outdoors to determine thermal efficiency, the collector shall be mounted in a location such that there will be no significant energy reflected or reradiated onto the collector from surrounding buildings or any other surfaces in the vicinity of the test stand for the duration of the test(s). This requirement will be satisfied if the ground and immediately adjacent foreground surfaces are diffuse reflectors with a reflectance of less than 0.20. If significant reflection can occur, provision shall be made to shield the collector by the use of a nonreflective shield. In addition, the test stand shall be located so that no shadow will be cast onto the collector by any obstruction at any time during the test period.

5.1.4 For tests conducted outdoors to determine thermal efficiency, the tests shall be conducted at times having weather conditions such that the integrated average irradiation measured in the plane of the collector or aperture, reported, and used for the computation of instantaneous efficiency values shall be not less than 630 W/m²(200 Btu/(hr·ft²)). Specific irradiation values that can be expected for clear sky conditions are shown in Tables A1 through A6 taken from Reference 1. More accurate estimates can be made using the Tables in conjunction with Clearness Numbers (see Reference 2, p. 26.9, Fig. 3)

5.1.5 For tests conducted to determine thermal efficiency at near-normal incidence conditions, the orientation of the collector shall be such that the incident angle (measured from the normal to the collector surface or aperture) is less than 30° during the period in which test data are being taken. Angles of incidence may be estimated from Tables A7 through A12 taken from Reference 3. More accurate estimates can be made using the procedures outlined in Reference 2, p. 26.3; Reference 4, pp. 282-292; and Reference 5, Chapter 58.

5.1.6 For tests conducted to determine thermal efficiency and incident angle modifier for a flat plate collector, the air velocity across the collector surface shall be measured and recorded as part of the test data. The velocity measurement shall be made in the immediate vicinity of the collector, at a height corresponding to the mid-height of the collector, and at a location where the velocity sensor is not shielded from the wind and the sensor does not cast a shadow on the collector during the tests. Wind direction during each test shall also be determined and reported.

5.1.7 For tests conducted outdoors to determine collector thermal efficiency, the range of ambient temperatures for all reported test points comprising the efficiency curve shall be less than 30°C (54F).

5.1.8 The transfer fluid used in the solar collector shall have a known specific heat which varies by less than 0.5% over the temperature range of the fluid during a particular test period. The density of the transfer fluid shall also be known and it shall not vary by more than 0.5% over a particular test period.

6. INSTRUMENTATION

6.1 Solar Radiation Measurement

6.1.1 A pyranometer shall be used to measure the total short wave radiation from both the sun and the sky and a pyrheliometer shall be used to measure the direct normal irradiation. The instruments shall have the following minimum characteristics, which are consistent with current practice and/or the requirements of a first class pyranometer or pyrheliometer as classified by the World Meteorological Organization (WMO) [4,6,8]*.

6.1.1.1 Change of Response Due to Variation in Ambient Temperature. The instruments shall be equipped with a built-in temperature compensation circuit and have a temperature sensitivity of less than ± 1% over the range −20 to +40°C (−4 to +104F).

6.1.1.2 Variation in Spectral Response. Pyranometer and pyrheliometer errors caused by a departure from the required spectral response of the sensor shall not exceed ± 2% over the range of interest. The WMO specification for a first class pyranometer is ± 1%.

6.1.1.3 Nonlinearity of Response. Unless the pyranometer was supplied with a calibration curve relating the output to the irradiation, its response shall be within ± 1% of being linear over the range of irradiation existing during the tests.

6.1.1.4 Time Response of Pyranometer and Pyrheliometer. The time constant of the pyranometer, defined as the time required for the instrument to achieve a reading of $1 - 1/e = 63.2\%$ of its final reading after a step change in irradiation, shall be less than 5 seconds. The time constant for the pyrheliometer shall be less than 25 seconds.

6.1.1.5 Variation of Response with Angle of Incidence. Ideally the response of the pyranometer is proportional to the cosine of the incident angle of the direct solar radiation and is constant at all azimuth angles. The pyranometer's deviation from a true cosine response shall be less than ± 1% for the incident angles encountered during the test(s).

6.1.1.6 Precautions for Effects of Humidity and Moisture. The pyranometer shall be provided with a means of preventing accumulation of moisture that may condense on surfaces within the instrument and affect its reading. An instrument with a desiccator that can be inspected is required. The ambient relative humidity and condition of the desiccator should be observed prior to and following any daily measurement sequence.

6.1.2 The pyranometer shall be calibrated for solar response within 12 months preceding the collector test(s) against another pyranometer whose calibration uncertainty relative to recognized measurement standards is known. Any change of more than ± 1% over a year period shall warrant the use of more frequent calibration or replacement of the instrument. If the instrument is damaged in any significant manner, it shall be recalibrated or replaced.

Summary of Performance Specifications for Solar Radiometers

	Sensitivity mW/cm²	Stability %	Temperature Compensation, %	Spectral Selectivity, %	Linearity %	Time Constant	Cosine Response, %
Pyrheliometer	± 0.4	± 1.0	± 1.0	± 2.0	± 1.0	<25 s	—
Pyranometer	± 0.1	± 1.0	± 1.0	± 2.0	± 1.0	<5 s	± 1

6.1.3 When a pyrheliometer is available, it may be used to determine the direct component of the irradiation incident on a tilted pyranometer. The diffuse component may also be determined by shading the tilted pyranometer from the direct irradiation. (See Section 8.3.2 and Ref. 8). At non-horizontal attitudes, ground features which can affect readings shall be noted and their effect on calibration shall be documented.

6.2 Temperature Measurements

6.2.1 Temperature measurements shall be made in accordance with ASHRAE Standard 41.1-74 [9].

6.2.2 The accuracy and precision of the instruments including their associated readout devices shall be

*Numbers in brackets denote the references in Section 10 within the limits as follows:

	Instrument Accuracy*	Instrument Precision**
Temperature	± 0.5°C (± 0.9F)	± 0.2°C (± 0.36F)
Temperature Difference	± 0.1°C (± 0.18F)	± 0.1°C (± 0.18F)

*The ability of the instrument to indicate the true value of the measured quantity.
**Closeness of agreement among repeated measurements of the same physical quantity.

6.2.3 Temperature Difference Measurements Across the Solar Collector. The temperature difference of the transfer fluid across the solar collector may be measured with one of the following [10]:

a. A type T thermopile (See Section 7.2.5)

b. Calibrated resistance thermometers connected in two arms of a bridge circuit (recommended only when transfer fluid is a liquid).

c. Precision thermometers.

d. Calibrated thermistors.

e. Calibrated matched type T thermocouples.

6.2.4 In no case should the smallest scale division of the instrument or instrument system exceed 2 times the specified precision. For example, if the specified precision is ± 0.1°C (± 0.18F), the smallest scale division shall not exceed 0.2°C (0.36F).

6.2.5 The instruments shall be configured and used in accordance with Section 7 of this standard.

6.3 Liquid Flow Measurements

6.3.1 The accuracy of the liquid flow rate measurement, using the calibration if furnished, shall be equal to or better than ± 1.0% of the measured value in mass units per unit time.

6.4 Integrators and Recorders

6.4.1 Strip chart recorders used shall have an accuracy equal to or better than ± 0.5% of the full scale reading and have a time constant of 1 second or less. The peak signal indication shall be between 50 and 100% of full scale.

6.4.2 Electronic integrators used shall have an accuracy equal to or better than ± 1.0% of the measured value.

6.4.3 The input impedance of recorders shall be greater than 1000 times the impedance of the sensors.

6.5 Air Flow Measurements

When air is used as the transfer fluid, the air flow rate shall be determined as described in Section 7, using instrumentation for mixing and sampling as described in References 9 and 11.

6.6 Pressure Measurements

6.6.1 Nozzle Throat Pressure. The pressure measurement at the nozzle throat shall be made with instruments which shall permit measurements of pressure to within ± 2.0% of the absolute pressure and whose smallest scale division shall not exceed 2 times the specified accuracy [12].

6.6.2 Air Flow Measurements. The static pressure across the nozzle and the velocity pressure at the nozzle throat shall be measured with manometers or pressure transducers which have been calibrated and found to have an accuracy to within ± 1.0% of the reading. The smallest manometer scale division shall not exceed 2.0% of the reading [12].

6.6.3 Pressure Drop Across Collector. The static pressure drop across the solar collector shall be measured with a manometer having an accuracy of ±2.5 Pa (0.01 in. H_2O) for air heating collectors and ±25 Pa (0.10 in. H_2O) for liquid heating collectors.

6.7 Time and Mass Measurements

For calibration purposes, time measurements and mass measurements shall be made to an accuracy of ± 0.20% [12].

6.8 Wind Velocity

The wind velocity shall be measured with an instrument and associated readout device that can determine the integrated average wind velocity for each test period to an accuracy of ± 0.8 m/s (± 1.8 mph).

7. APPARATUS AND METHOD OF TESTING

7.1 Liquid as the Transfer Fluid

The test configurations for testing solar collectors employing liquid as the transfer fluid are shown in Figures 1, 2 and 3 which are representative rather than exact and are not drawn to scale. Any of these configurations is acceptable provided that the test conditions specified herein are satisfied. When the circulating transfer fluid is susceptible to evaporation losses as shown in Figure 3, care should be taken to minimize and to account for the evaporation losses.

7.1.1 Solar Collector. The solar collector shall be rigidly mounted to the test rack at the predetermined tilt angle (for stationary collectors) with backing (if required) determined in accordance with the provisions of Section 5.1.2. It is essential that the test rack, whether fixed or movable, be unaffected by strong gusts of wind.

7.1.2 Ambient Temperature. The ambient temperature sensor shall be housed in a well-ventilated instrumentation shelter with its bottom 1.25 m (4.1 ft) above the ground and with its door facing north, so that the sun's direct beam cannot fall upon the sensor when the door is opened. The instrument shelter shall be painted white outside and shall not be closer to any

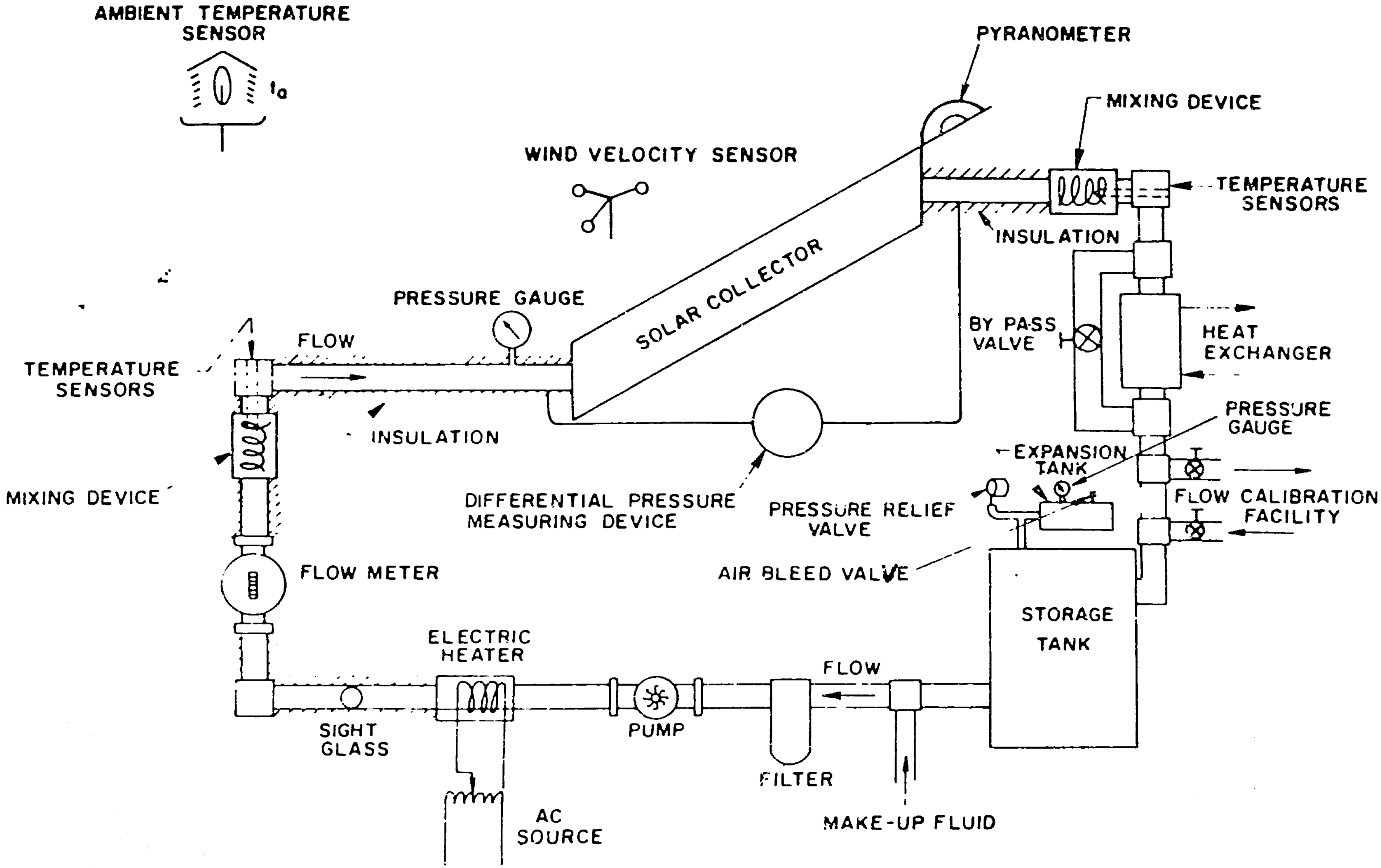

Fig. 1 Closed-Loop Testing Configuration for the Solar Collector when the Transfer Fluid is a Liquid

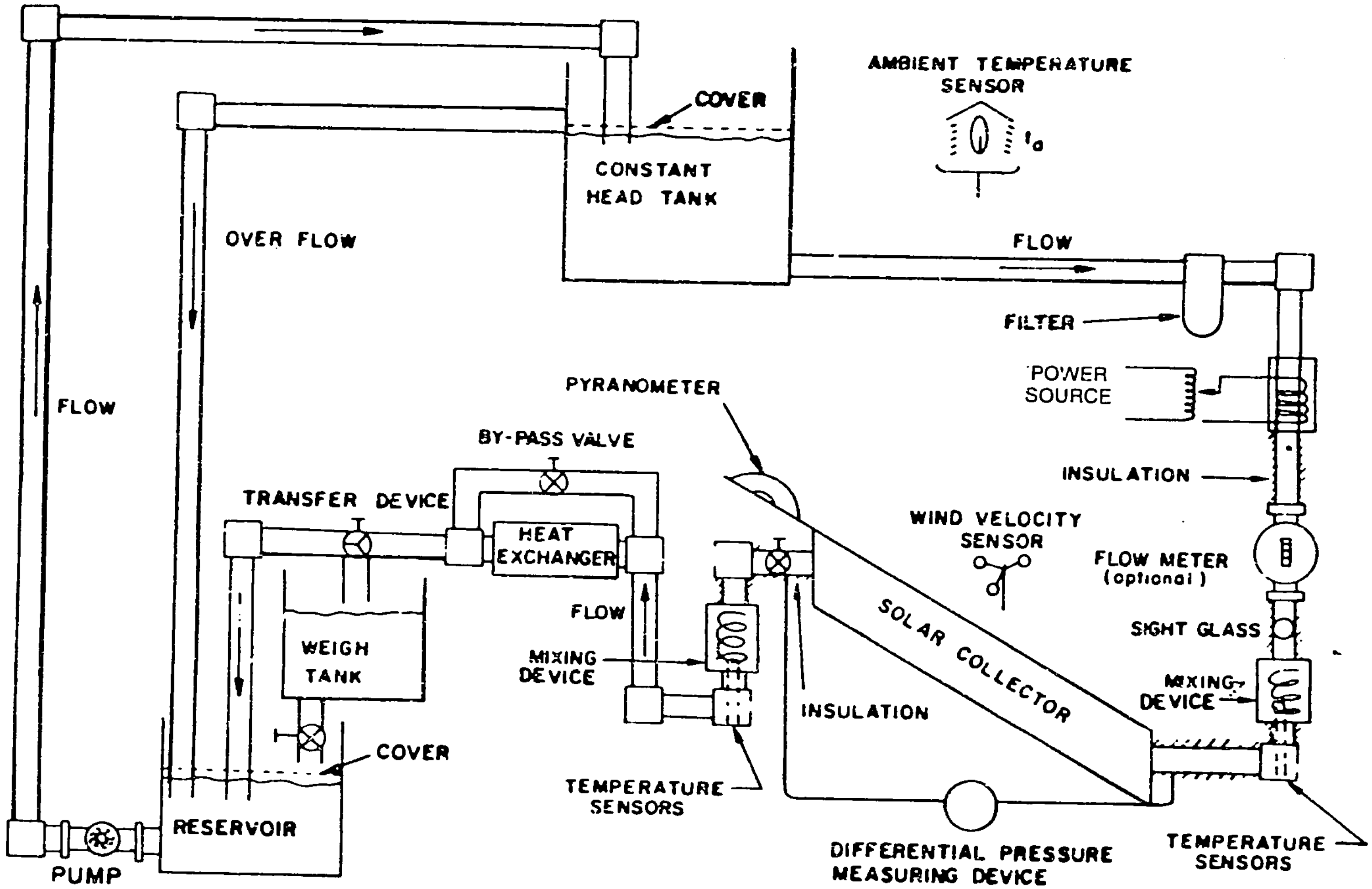

Fig. 2 Open-Loop Testing Configuration for the Solar Collector when the Transfer Fluid is Liquid

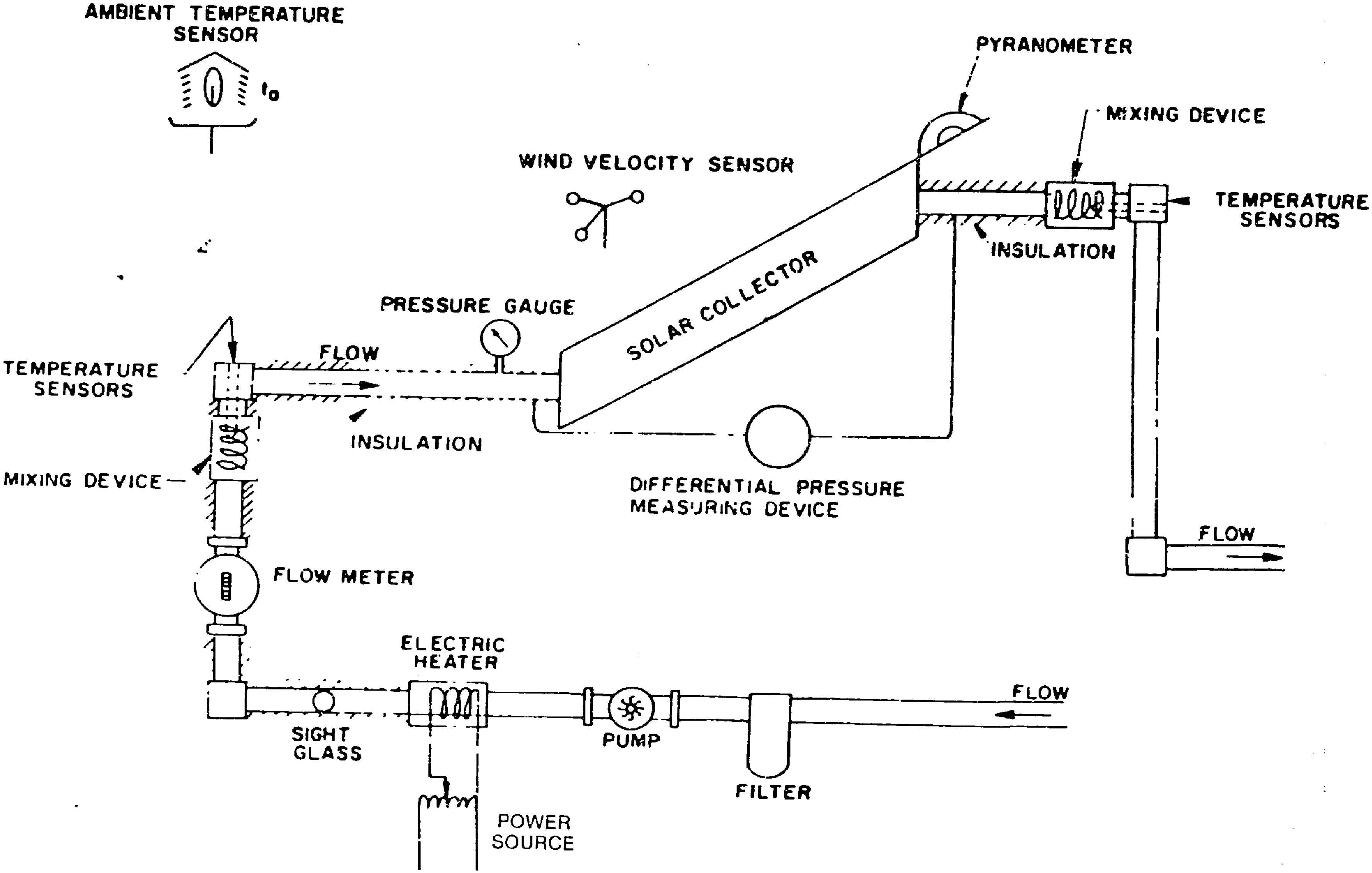

Fig. 3 Open-Loop Testing Configuration for Use when Fluid is Supplied Continuously

obstruction than twice the height of the obstruction itself (i.e., trees, fences, building, etc.) [13].

7.1.3 Solar Radiation. Irradiation measurements shall be reported in terms of apparent solar time for the test site (see Appendix A).

A pyranometer for measuring the total irradiation and a suitable method for determining the direct component shall be utilized for all collector tests. The pyranometer shall meet the requirements specified in Section 6.1.1 and shall be mounted such that its sensor is coplanar with the plane of the collector aperture. It shall not cast a shadow onto the collector aperture at any time during the test period. The pyranometer shall not be mounted so as to receive a percentage of terrestrial radiation that is disproportionate with that received by the collector. It is recommended that the pyranometer be mounted near the upper-half periphery of the collector, and in the upper center of the collector array. The pyranometer should be oriented so that the emerging leads or the connector are located north of the receiving surface (in the Northern Hemisphere), or are otherwise shaded to minimize solar heating of the electrical connections.

A pyrheliometer shall be utilized to determine the direct component of solar radiation when testing concentrating collectors that do not accept diffuse radiation.

Care should also be taken to minimize reflected and reradiated energy from the solar collector onto the pyranometer. Some pyranometers are supplied with shields. Pyranometers not supplied with a shield may be susceptible to error due to reflections of radiation that originate below the plane of the sensor.

Collectors that accept diffuse radiation shall have the direct component of the solar radiation determined for each data point. This measurement can be made utilizing the shading-disk or the shade-band method using a pyranometer (see Section 8.3.2). However, a preferable method involves the use of a pyrheliometer that measures the direct component.

7.1.4 Temperature Difference Measurements Across the Solar Collector. The temperature difference of the transfer fluid between entering and leaving the solar collector shall be measured in accordance with Sections 6.2.2 and 6.2.3.

To minimize temperature measurement error, each probe shall be located as close as possible to the inlet or outlet of the solar collector and shall be inserted into a mixing device located as shown in Figures 1, 2 and 3. In addition, the piping between the mixing device and the collector shall be insulated in such a manner that the calculated heat loss or gain from the ambient air will not cause a temperature change for any test of more than 0.05°C (0.09F) between each mixing device and the collector.

7.1.5 Additional Temperature Measurements. The temperature of the transfer fluid at each of the two positions cited above shall also be measured by inserting appropriate sensors into the mixing devices (except for the case where precision thermometers are employed to determine temperature difference). Reference 9 should be followed in making these measurements.

7.1.6 Pressure Drop Across the Solar Collector. The pressure drop across the solar collector shall be measured using static pressure tap holes and either a manometer or a differential-pressure transducer. The edges of the holes on the inside surface of the pipe should be free of burrs and should be as small as practical and should not exceed 1.6 mm (1/16 in.) in diameter. The thickness of the pipe wall should be 2.5 times the hole diameter. Provision shall be made for determining the absolute pressure of the entering transfer fluid [14].

7.1.7 Reconditioning Apparatus. As shown in Fig. 1, the use of a closed-loop test facility requires that a heat exchanger be employed to cool the transfer fluid and an adjustable in-line electrical resistance heater be used to control the inlet temperature to the prescribed test values. This combination of equipment or its equivalent shall control the temperature of the fluid entering the collector to within ±0.5°C (±0.9F) at all times during the tests.

A heat exchanger is also recommended when employing an open-loop test facility similar to Fig. 2 to cool the outlet liquid to minimize evaporation losses and thus minimize weighing errors in the gravimetric determination of mass flow rate. Figure 3 shows an open-loop system in which the fluid is not recirculated.

7.1.8 Additional Equipment. A pump and a means of adjusting the flow rate of the transfer fluid shall be provided at the relative locations shown in Figures 1, 2 and 3. Depending upon the test apparatus design, an additional throttle valve may be required in the line just preceding the solar collector for proper control. When using the open-loop configuration in Figures 2 and 3, a throttle valve should be used in the exit line as close as possible to the collector. This valve is required to control the internal pressure (absolute) of the collector when testing at inlet temperatures and/or at flows that result in boiling.

A storage tank, expansion tank, air vent and a pressure relief valve should be installed in the closed-loop test configuration as shown in Fig. 1 to stabilize the flow and allow the transfer fluid to expand and contract freely in the system.* Depending upon the design, an expansion tank and relief valve are sometimes inserted between the pump and the collector in an open-loop test facility.

*Figure 1 should not be interpreted to mean that the relief valve and expansion tank must necessarily be located below the collector.

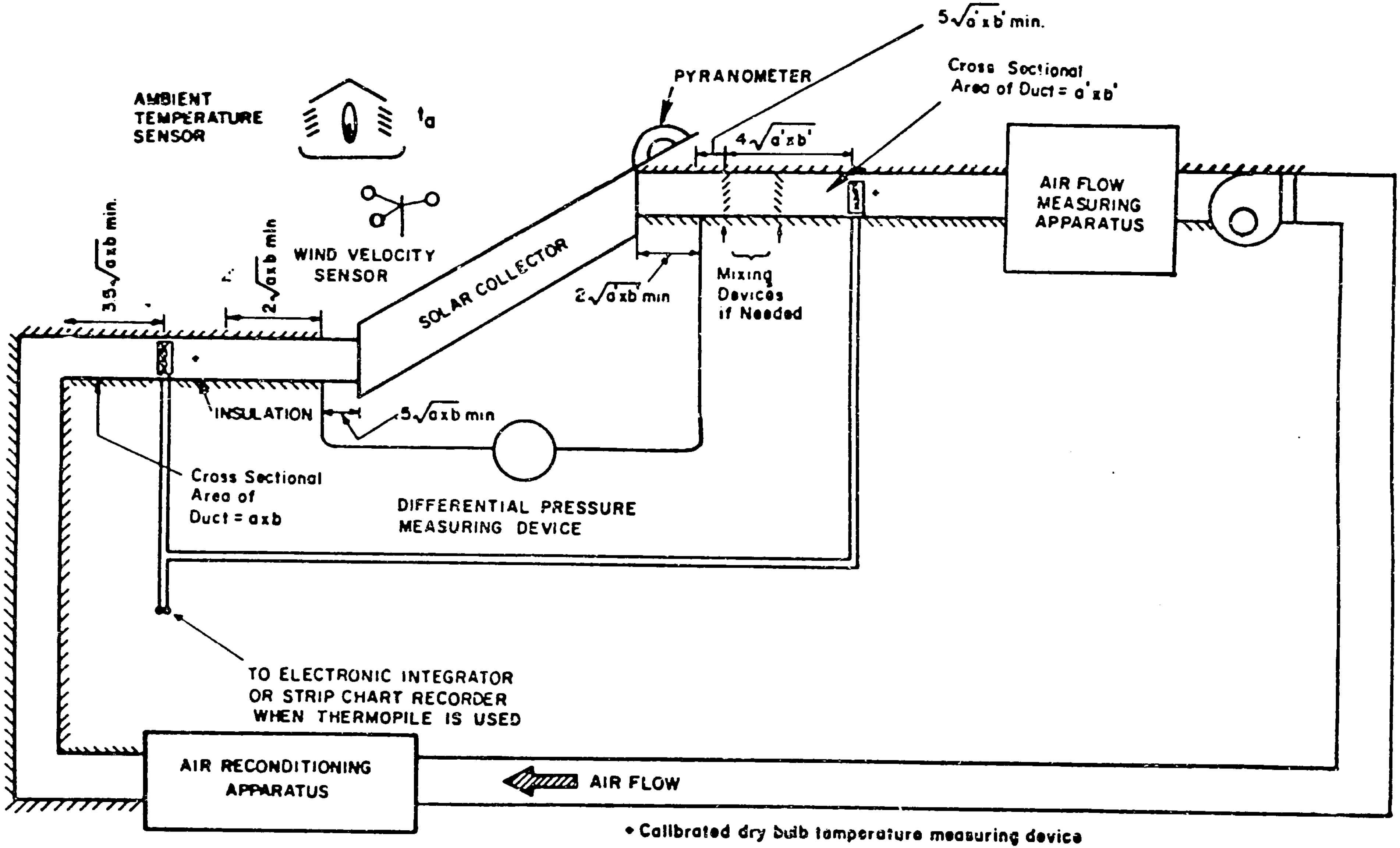

Fig. 4 Testing Configuration for the Solar Collector when the Transfer Fluid is Air

Filters and a sight glass should be installed within the apparatus to ensure that the transfer fluid passing through the collector is free of contaminants, including air bubbles.

7.2 Air as the Transfer Fluid

The test configuration for the solar collector employing air as the transfer fluid is shown in Fig. 4. The recommended apparatus consists of a closed-loop configuration. An open-loop configuration is an acceptable alternative provided that the test conditions specified herein can be satisfied.

7.2.1 Solar Collector (see Section 7.1.1)

7.2.2 Ambient Temperature (see Section 7.1.2)

7.2.3 Solar Radiation (see Section 7.1.3)

7.2.4 Test Ducts

The air outlet duct between the air flow measuring apparatus and the solar collector shall have the same dimensions as the air inlet duct leading to the solar collector.

7.2.5 Temperature Difference Measurement Across the Collector. If a thermopile is used to measure the difference between the outlet and the inlet temperatures, the thermopile shall be made from calibrated thermocouple wire taken from a single spool. Extension wires to the recording device shall also be made from that same spool. The wire diameter must be no larger than 0.51 mm (24AWG) and the thermopile shall be fabricated as shown in Fig. 5. There shall be a minimum of six junctions in the air inlet test duct and six junctions in the air outlet test duct. These junctions shall be located at the centers of equal cross-sectional areas.

During all tests, the variation in temperature at a given cross section of the air inlet and air outlet test ducts shall be less than ±0.5°C (±0.9F) at the location of the temperature sensors. The variation shall be checked prior to testing, utilizing instrumentation and procedures outlined in Reference 9. If the variation exceeds the above limits, mixing devices shall be installed to achieve this degree of temperature uniformity. Reference 11 discusses the positioning and performance of several types of air mixers. The temperature sensors should be located as near as possible to the inlet and outlet of the solar collector. The air inlet and air outlet ducts shall be insulated in such a manner that the calculated heat loss or gain to or from the ambient air would not cause a temperature change for any test of more than 0.3°C (0.5F) between the temperature measuring locations and the collector.

7.2.6 Temperature Measurements. Sensors and read-out devices meeting the accuracy requirements of Section 6.2.2 shall be used to measure the temperature at the locations in the air inlet and air outlet ducts shown in Fig. 4. Reference 9 should be followed in making these measurements.

7.2.7 Duct Pressure Measurements. The static pressure drop across the solar collector shall be measured using a differential pressure measuring device as shown in Figures 1-4 [12]. Each side of this device shall be connected to four externally manifolded pressure taps on the air inlet and air outlet ducts as shown in Fig. 6. The pressure taps should consist of 6.4 mm (1/4 in.) nipples soldered to the duct and centered over 1 mm (0.04 in.) diameter holes. The edges of these holes on the inside surfaces of the ducts should be free of burrs and other surface irregularities [14].

7.2.8 Air Flow Measuring Apparatus. Where the air flow rate is sufficiently large, it shall be measured with the nozzle apparatus discussed in Section 7 of Reference 12. As shown in Fig. 7 this apparatus consists basically of a receiving chamber, a discharge chamber and an air flow measuring nozzle. The distance from the center of the nozzle to the side walls shall not be less than 1.5 times the nozzle throat diameter, and the diffusion baffles shall be installed in the receiving chamber at least 1.5 nozzle throat diameters upstream of the nozzle and 2.5 nozzle throat diameters downstream of the nozzle. The apparatus should be designed so that the nozzle can be easily changed and the nozzle used on each test shall be selected so that the throat velocity is between 15 m/s (2960 fpm) and 35 m/s (6900 fpm). When nozzles are constructed in accordance with Fig. 8 and installed in accordance with this section of this standard, the discharge coefficient may be assumed to be as follows:

Reynolds Number N_{Re}	Discharge Coefficient C_n
20,000	0.96
50,00	0.97
100,000	0.98
150,000	0.98
200,000 and above	0.99

If the throat diameter of the nozzle is 0.13 m (5 in.) or larger, the discharge coefficient may be assumed to be 0.99. For nozzles smaller than 0.05 m (2 in.) and where a more accurate discharge coefficient than given above is desired, the nozzle should be calibrated. The area of the nozzle shall be determined by measuring its diameter to an accuracy of ±0.2% in four places approximately 45 degrees apart around the nozzle in each of two planes through the nozzle throat, one at the outlet and the other in the straight section near the radius [12].

Where the nozzle apparatus is used, an exhaust fan capable of providing the desired flow rates through the solar collector shall be installed as shown in Figure 4. The dry and wet bulb temperatures of the air entering the nozzle shall be measured in accordance with Reference 9. The velocity of the air passing through the nozzle shall be determined by either measuring the velocity head by means of a commercially available pitot tube or by measuring the static pressure drop

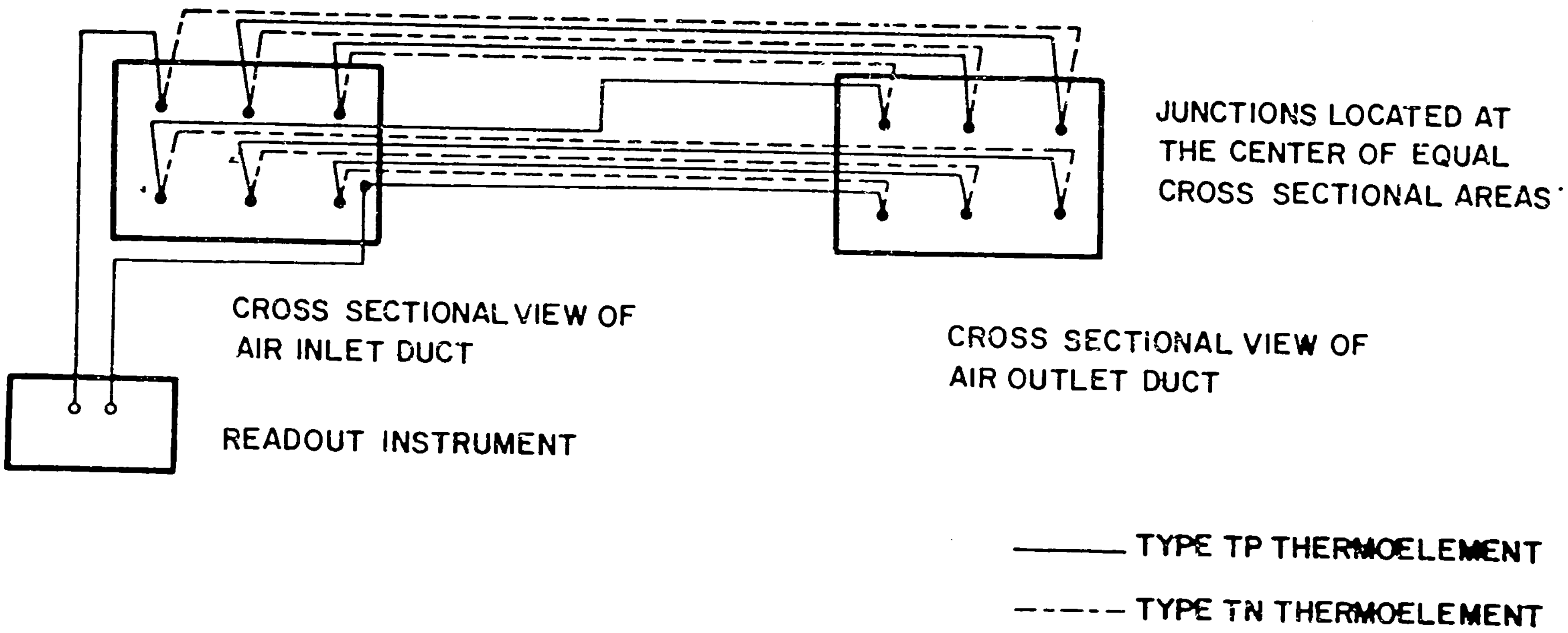

Fig. 5 Schematic of the Thermopile Arrangement Used to Measure the Temperature Difference Across the Solar Collector

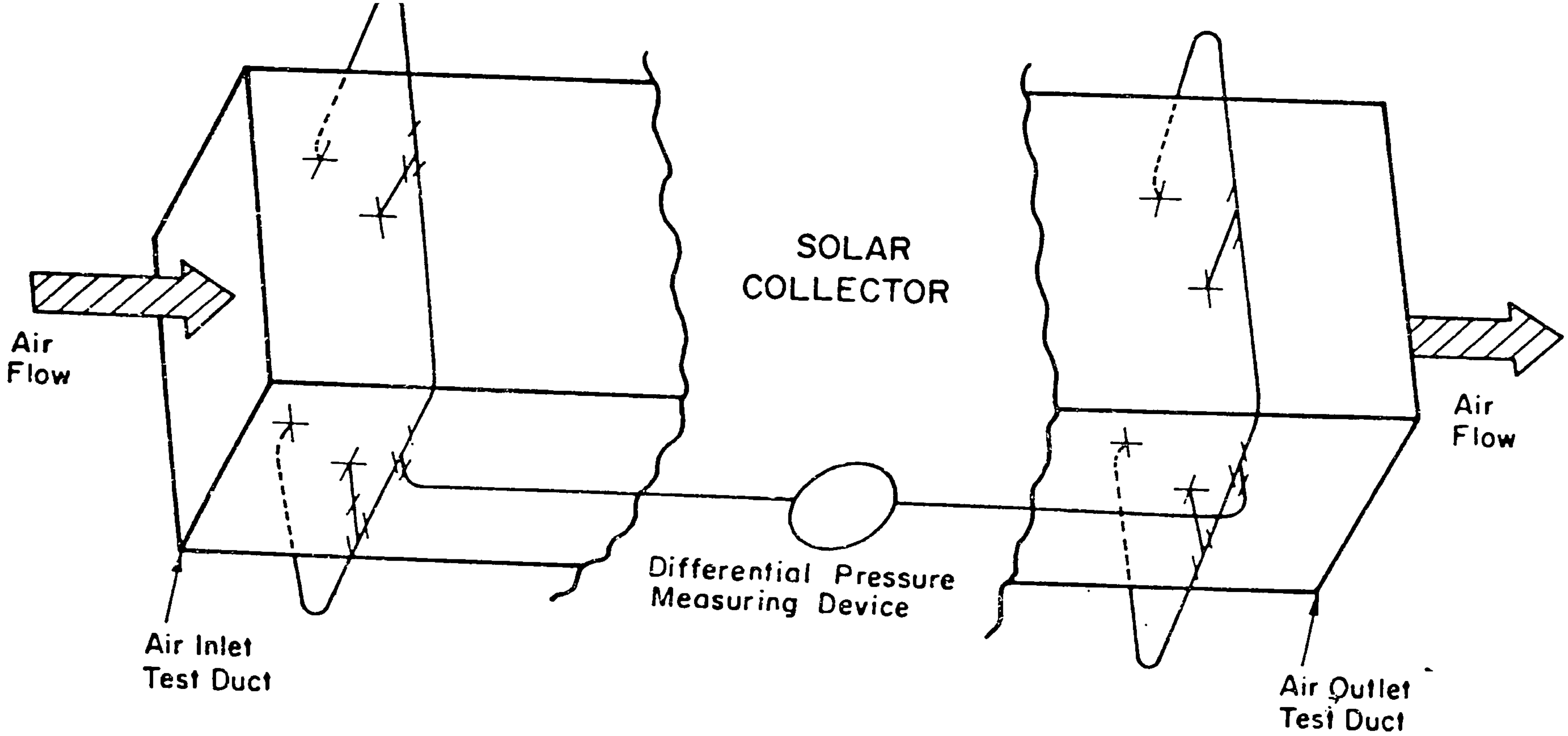

Fig. 6 Schematic Representation of the Measurement of Pressure Drop Across the Solar Collector when Air is the Transfer Fluid

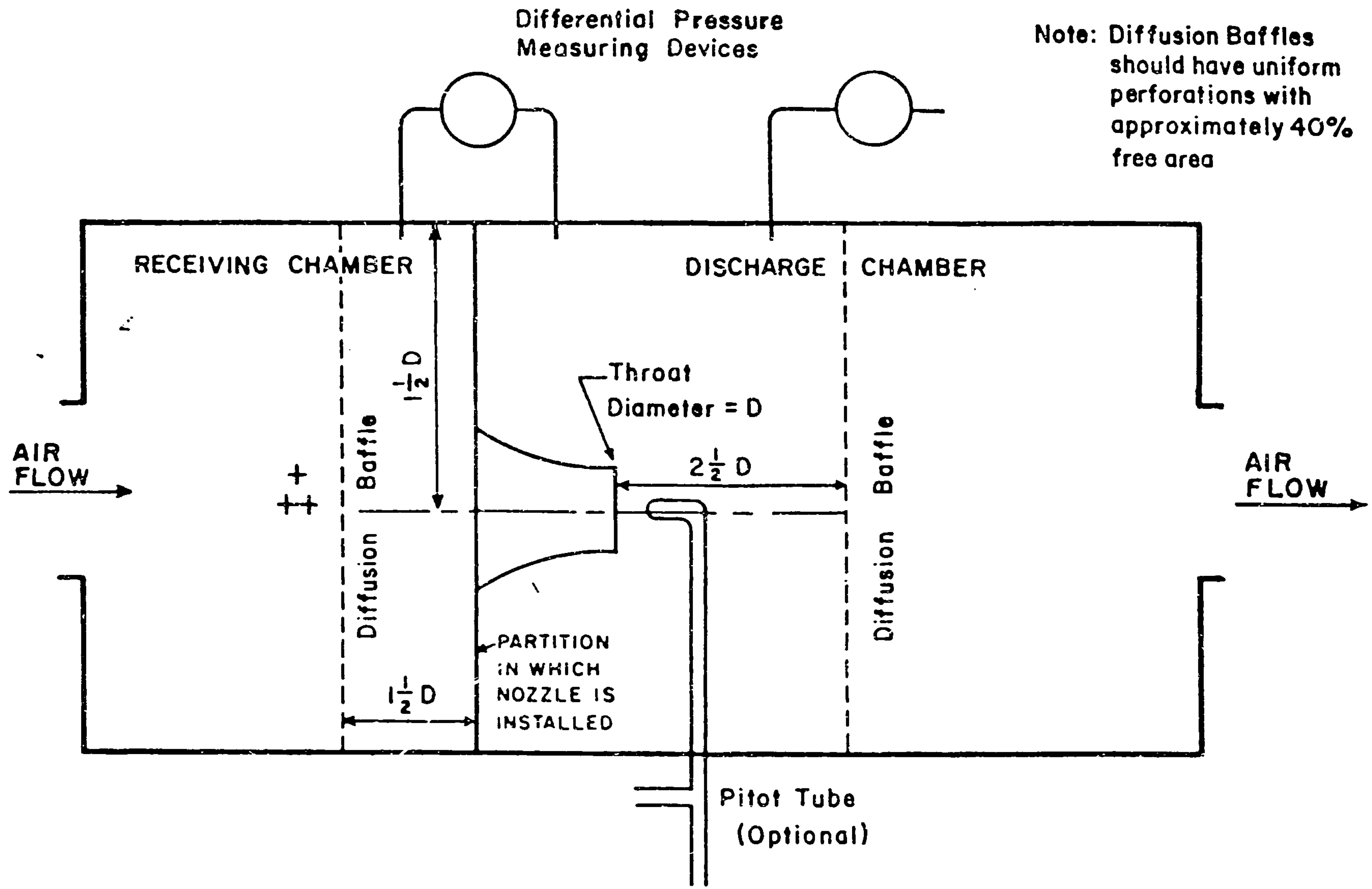

\+ CALIBRATED DRY BULB TEMPERATURE MEASURING DEVICE

++ CALIBRATED WET BULB TEMPERATURE MEASURING DEVICE

Fig. 7 Nozzle Apparatus for Measuring Air Flow Rate

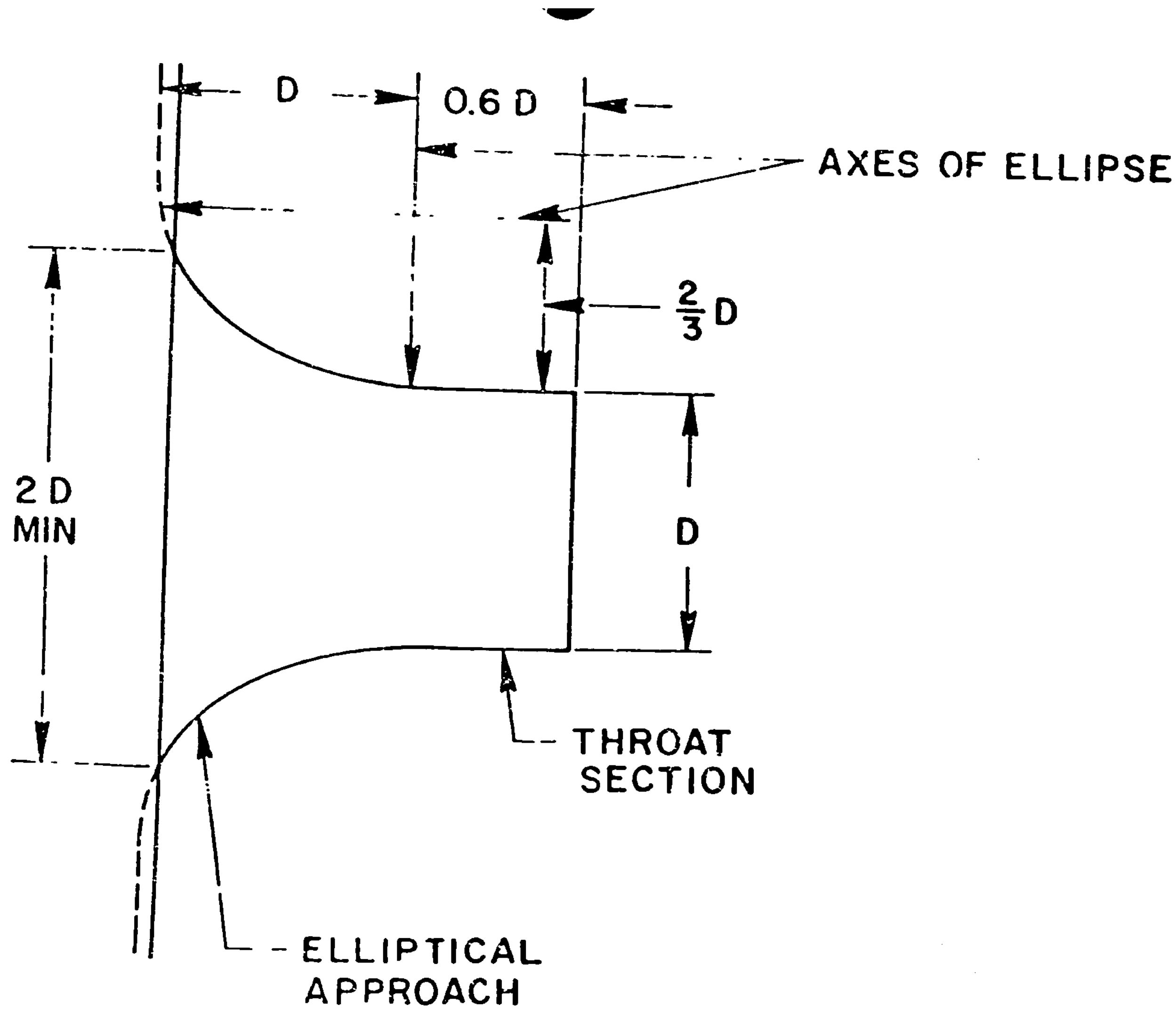

Fig. 8 Air Flow Measuring Nozzle

across the nozzle with a differential pressure measuring device. If the latter method is used, one end of the device shall be connected to a static pressure tap located flush with the inner wall of the discharge chamber, or preferably, several taps in each chamber should be manifolded to a single device.

Where the air flow rate is sufficiently small so that a nozzle constructed and installed in accordance with the requirements above would have a throat diameter of smaller than 0.025 m (1 in.), the above configuration should not be used and the air flow measuring apparatus shown in Fig. 4 should consist of a calibrated flow element where at least 10 pipe diameters of upstream and downstream pipe section have been included in the calibration.*

7.2.9 Air Leakage. Air leakage shall be minimized by taping and sealing all joints. Extreme caution is needed because small leakage rates can have significant effects on test results.

7.2.10 Air-Reconditioning Apparatus. The reconditioning apparatus shall control the dry bulb temperature of the transfer medium entering the solar collector to within ±1.0°C (±1.8F) of the desired test values at all times during the tests. Its heating and cooling capacity shall be selected so that the dry bulb temperature of the air entering the reconditioning apparatus may be raised or lowered the required amount to meet the applicable test conditions in Section. 8.

7.3 Indoor Testing With a Solar Simulator.

A solar simulator may be used in lieu of outdoor testing to determine the steady state thermal performance of the solar collector under controlled conditions of wind and ambient temperature. References 15, 16, 17 describe typical simulators used for testing collectors. Solar simulators employed in the testing procedure shall have the following characteristics.

7.3.1 Spectral Qualities. The simulator shall duplicate the spectrum of average North American irradiation as closely as possible. This average is best represented by an air-mass 2 solar spectrum [15]. The measured energy spectrum shall not deviate from the air-mass 2 spectrum more than as specified in the following table:

Band λ μm	Air Mass 2, Percent of Energy in Band	Maximum Deviation of Simulator
0.3-0.4	2.7	15%
0.4-0.7	44.4	9
0.7-1.0	28.6	3
1.0-∞	24.3	10

In addition, the calculated solar absorptance, α, of the spectrally selective surface described in Reference 18 irradiated by the simulator shall not differ more than 1 percent from the value measured under air-mass 2 sunlight.

There shall not be a significant change in the simulator's energy spectrum for variations in power output. The calculated solar absorptance of the above specified selective surface [18] irradiated by the simulator shall not change by more than 1% for a change in radiation flux from 0.45 to 0.75 of one Solar Constant.*

7.3.2 Uniformity. The departure from uniformity of the illumination of the solar simulator beam over the test plane (the plane of the collector aperture) shall be such that the high and low irradiation values of the illuminated plane shall not exceed ±10% of the average illumination.

7.3.3 Collimation. The collimation shall be such that 95% of the energy output of the simulator is within a subtended angle of less than 12 degrees. A collimation of greater than this is required for collectors with concentration ratios greater than 2/1.

7.3.4 Air Flow Across the Collector. A fan shall be provided to cause a substantially uniform air flow across the collector surface. The fan shall be capable of producing an air velocity of at least 3.5 m/sec (7.6 mph).

7.3.5 Simulator—Collector Configuration Factor. The collector configuration factor** between the solar simulator surface and the solar collector shall not exceed 0.05.

8. TEST PROCEDURES AND COMPUTATIONS

8.1 General

The thermal performance of the solar collector is determined in part by obtaining values of instantaneous efficiency for a combination of values of incident radiation, ambient temperature, and inlet fluid temperature. This requires experimentally measuring the rate of incident solar radiation onto the solar collector as well as the rate of energy addition to the transfer fluid as it passes through the collector, all under steady state or quasi-steady state conditions. In addition, tests are performed to determine the time response characteristics of the collector as well as how its steady state thermal efficiency varies with the incident angle between the direct beam and the collector.

8.2 Basic Performance Equations

8.2.1 Collector Thermal Efficiency. It has been shown and discussed by a number of investigators [21,

*For small flow elements, the discharge coefficients associated with such elements vary considerably from those associated with the larger elements. In addition, for small pipe or duct sizes, the ratio of pipe circumference to pipe area becomes large and the characteristics of the upstream and downstream pipe sections affect the behavior of the element itself.

*1 353 W/m² (429.2 Btu/hr·ft²) [20]

**Configuration factor, radiation exchange factor or radiation shape factor are defined in most heat transfer text books, for example, Reference 39.

22, 23, 24] that the performance of a flat-plate solar collector operating under steady state conditions can be successfully described by the following relationship:

$$\frac{q_u}{A_a} = I_t(\tau\alpha)_e - U_L(t_p - t_a) = \frac{\dot{m}}{A_a} c_p(t_{f,e} - t_{f,i}) \qquad (8.1)$$

A very similar equation can be used to describe the performance of concentrating collectors [24]. Equation (8.1) becomes modified as follows:

$$\frac{q_u}{A_a} = I_{DN}(\tau\alpha)_e \rho\Gamma - U_L \frac{A_r}{A_a}(t_r - t_a) = \frac{\dot{m}}{A_a} c_p(t_{f,e} - t_{f,i}) \qquad (8.2)$$

To assist in obtaining detailed information about the performance of flat-plate collectors and to preclude the necessity for determining the average temperature of the receiver surface, it has been convenient to introduce a parameter F_R where:

$$F_R = \frac{\text{actual useful energy collected by a flat-plate collector}}{\text{useful energy collected if the entire flat-plate collector surface were at the inlet fluid temperature}}$$

Introducing this factor into Equation (8.1) results in

$$\frac{q_u}{A_a} = F_R\left[I_t(\tau\alpha)_e - U_L(t_{f,i} - t_a)\right] = \frac{\dot{m}}{A_a} c_p(t_{f,e} - t_{f,i}) \qquad (8.3)$$

If the solar collector efficiency is defined as

$$\eta_g = \frac{\text{actual useful energy collected}}{\text{solar energy incident upon or intercepted by the collector}} = \frac{q_u/A_g}{I_t} \qquad (8.3a)$$

then the efficiency of the flat-plate collector is given by:

$$\eta_g = (A_a/A_g)F_R\left[(\tau\alpha)_e - U_L\frac{(t_{f,i} - t_a)}{I_t}\right] = \frac{\dot{m}c_p(t_{f,e} - t_{f,i})}{A_g I_t} \qquad (8.4)$$

Equation (8.4) indicates that if the efficiency η_g is plotted against $(t_{f,i} - t_a)/I_t$, a straight line will result where the slope is equal to $(A_a/A_g)F_R U_L$ and the y intercept is equal to $(A_a/A_g)F_R(\tau\alpha)_e$. In reality, U_L is not a constant but rather a function of the temperature of the collector and of the ambient weather conditions. In addition, the product $(\tau\alpha)_e$ varies with the incident angle between the solar beam and the collector.

The procedures outlined in this document have been developed in an attempt to control the test conditions so that a well defined efficiency curve can be obtained with a minimum of scatter.

Figure 9 shows typical test results taken from Reference 25 for a double-glazed flat-plate collector using air as the transfer fluid. The tests, which included two air flow rates, were conducted outdoors. The higher efficiences were obtained with an air flow rate of 0.015 $m^3/(s \cdot m^2)$ (3.0 cfm/ft^2) and the lower efficiencies were obtained with an air flow rate of 0.01 $m^3/(s \cdot m^2)$ (2 cfm/ft^2).

Figure 10 was taken from Reference 26 and is for a flat-plate collector tested with a solar simulator using water as the transfer fluid.

An example of an outdoor test for a water-heating flat-plate collector under quasi-steady state conditions is given in Fig. 11 [7].

Although a straight-line representation of the efficiency curve will suffice for many flat-plate solar collectors, some flat-plate collectors and most concentrating collectors require the use of a higher-order-fit, i.e., a second order polynominal, due to variation of U_L with receiver temperature.

8.2.2 Collector Time Constant. It is necessary to determine the time response of the solar collector in order to be able to evaluate the transient behavior of the collector, and to select the proper time intervals for the quasi-steady state or steady state efficiency tests.

Whenever transient conditions exist, the equalities defined by Equations (8.1), (8.2) and (8.3) do not govern the thermal performance of the collector since part of the solar energy absorbed is used for heating up the collector and its components.

The governing equation for the transient behavior of a solar collector is:

$$\frac{C_A}{A_a}\frac{dt_f}{dT} = F_R I_t(\tau\alpha)_e - F_R U_L(t_{f,i} - t_a) - \frac{\dot{m}c_p}{A_a}(t_{f,e} - t_{f,i}) \qquad (8.5)$$

If (a) the solar radiation I_t, or inlet fluid temperature $t_{f,i}$ or both I_t and $t_{f,i}$ are suddenly changed and held constant, and if (b) $(\tau\alpha)_e$, U_L, t_a, $\dot{m}$ and c_p can be considered constant for the transient period, and if (c) the rate of change of the transfer fluid exit temperature with time is related to the rate of change of transfer fluid average temperature with time by:

$$\frac{dt_f}{dT} = K\frac{dt_{f,e}}{dT} \qquad (8.6)$$

where from Reference 29,

$$K = \frac{\dot{m}c_p}{F'U_L A_a}\left[\frac{F'}{F_R} - 1\right] \qquad (8.7)$$

and where

$$F' = \frac{\text{actual useful energy collected by flat-plate collector}}{\text{useful energy collected if the entire flat-plate collector surface were at the average fluid temperature}}$$

then Equation (8.5) can be solved to give the exit temperature of the transfer fluid as a function of time:

$$\frac{F_R I_t(\tau\alpha)_e - F_R U_L(t_{f,i} - t_a) - (\dot{m}c_p/A_a)(t_{f,e,T} - t_{f,i})}{F_R I_t(\tau\alpha)_e - F_R U_L(t_{f,i} - t_a) - (\dot{m}c_p/A_a)(t_{f,e,initial} - t_{f,i})} = e^{-\dot{m}c_p T/KC_A} \qquad (8.8)$$

The quantity $KC_A/\dot{m}\,c_p$ is known as the time constant and is the time required for the quantity of the

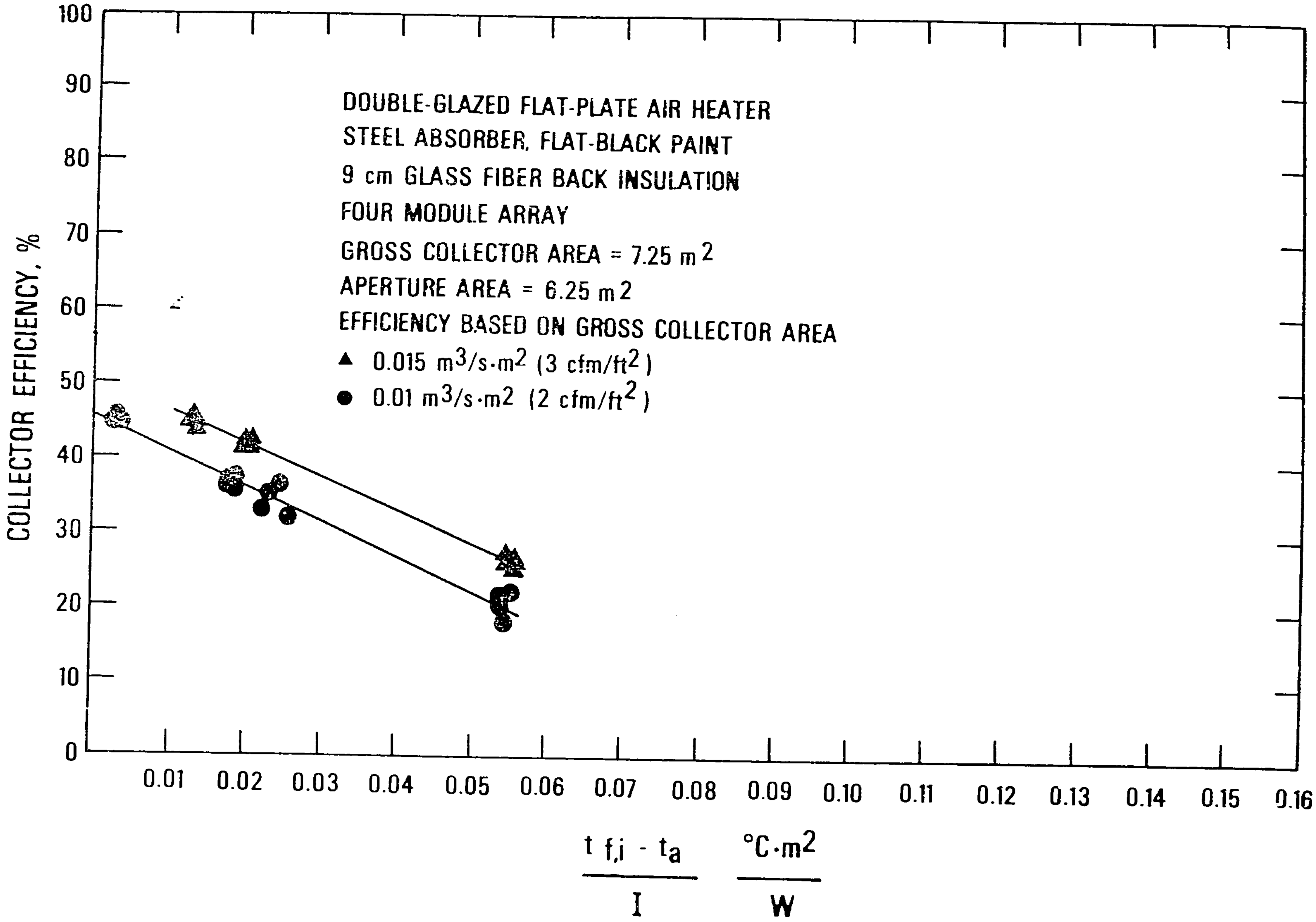

Fig. 9 Thermal Efficiency Curves for a Flat-Plate Collector Using Air as the Transfer Fluid at Two Different Flow Rates [25]

Tests conducted inside using a solar simulator
1.22 m by 1.22 m liquid-heating collector
insulation unspecified
aluminum absorber, black-nickel selective coating, α = 0.95

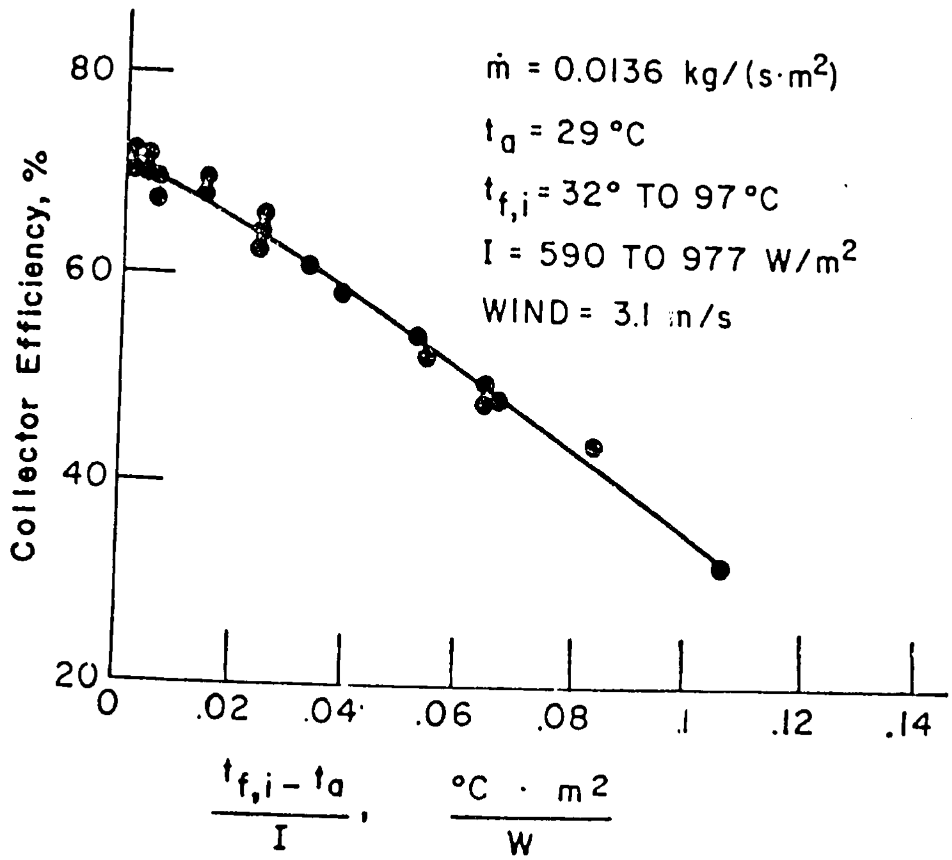

Fig. 10 Thermal Efficiency Curve for a Double-Glazed Flat-Plate Liquid-Heating Solar Collector with a Selective Coating on the Absorber[26]

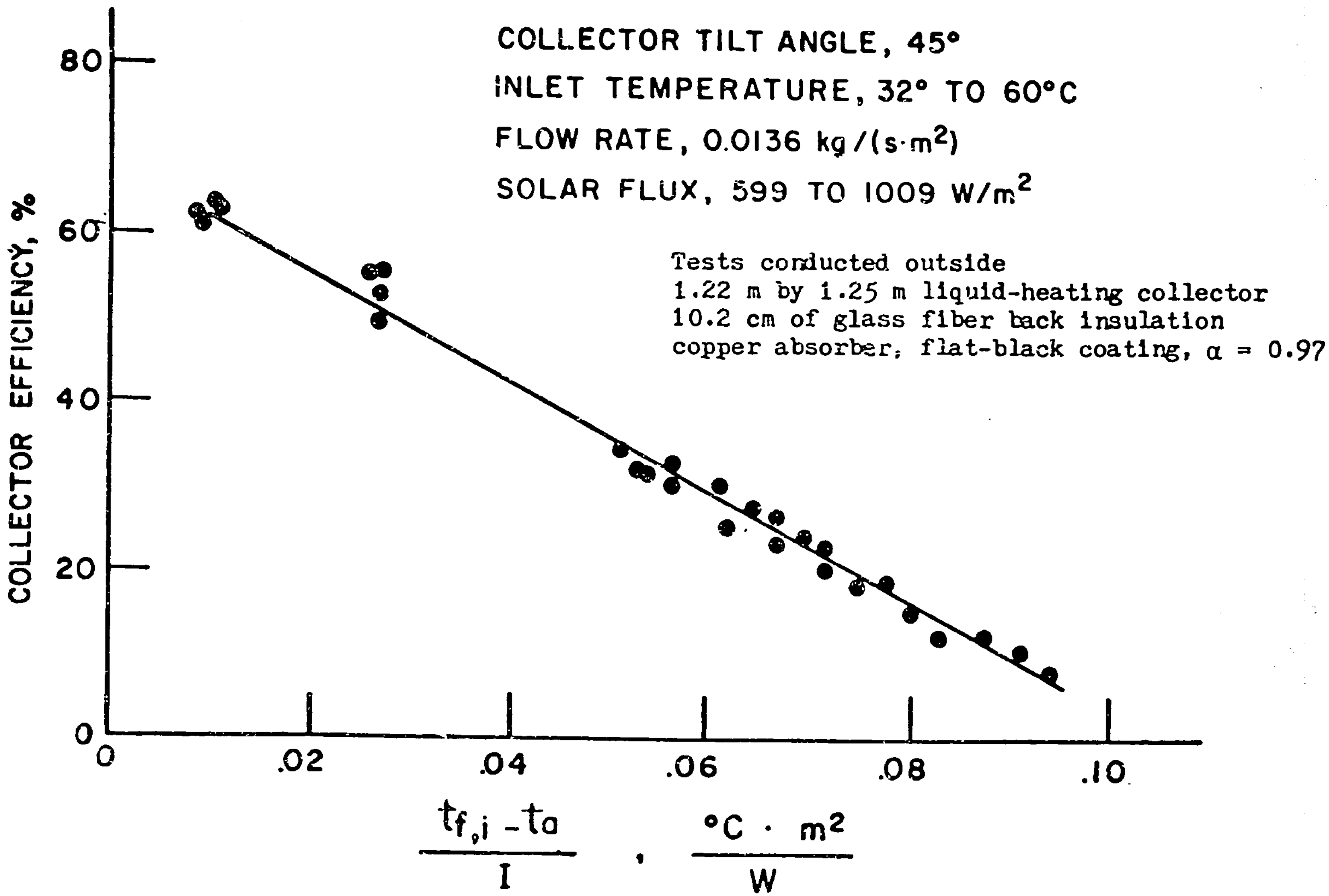

Thermal Efficiency Curve for a Double-Glazed Flat-Plate Liquid-Heating Solar Collector

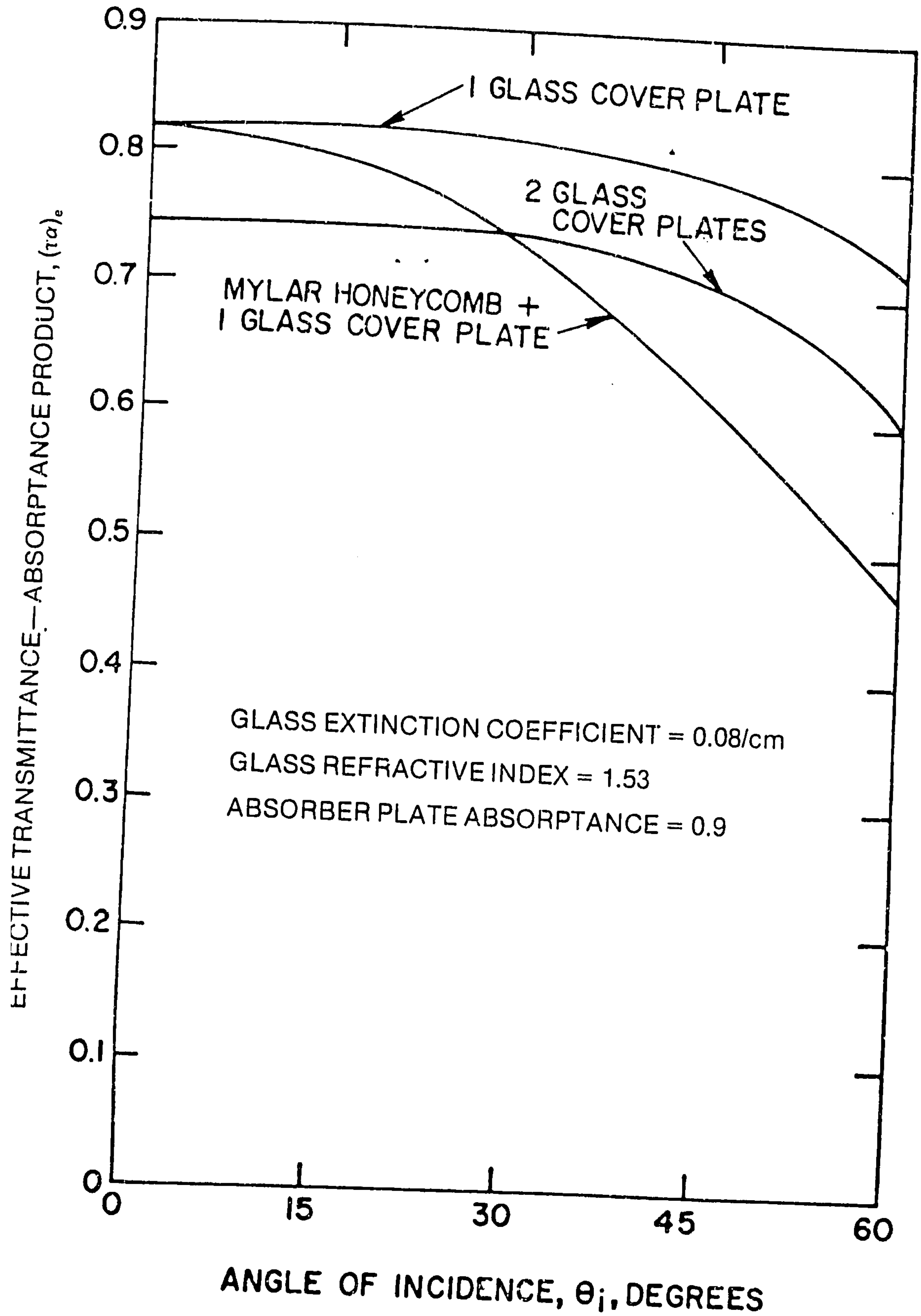

Fig. 12 Effective Transmittance-Absorptance Product for Three Flat-Plate Solar Collectors with Non-Selective Coatings on the Absorber [28]

left side of Equation (8.8) to change from 1.0 to 0.368, where 0.368=1/e.

8.2.3 Collector Incident Angle Modifier. The effective transmittance-absorptance factor $(\tau\alpha)_e$ can be replaced in the general equations (8.1), (8.2), (8.3) and (8.4) by the value at normal incidence, $(\tau\alpha)_{e,n}$, provided another factor called the incident angle modifier $K_{\alpha\tau}$ is introduced [27]. Equation (8.4) then becomes:

$$\eta_g = (A_a/A_g)\, F_R\left[K_{\alpha\tau}(\tau\alpha)_{e,n} - U_L \frac{(t_{f,i}-t_a)}{I_t}\right] = \frac{\dot{m}c_p}{A_g I_t}(t_{f,e}-t_{f,i}) \quad (8.9)$$

It can be shown that for a wide variety of solar collectors, $(\tau\alpha)_e$ should vary with incident angle according to the general expression:

$$(\tau\alpha)_e = a - \frac{b}{\cos\theta} \quad (8.10)$$

Examples of this type of variation are shown in Fig. 12 for three different flat-plate collectors [28]. Comparing Equations (8.9) and (8.10)

$$K_{\alpha\tau}(\tau\alpha)_{e,n} = a - \frac{b}{\cos\theta} \quad (8.11)$$

Solving the equation for $K_{\alpha\tau}$ and recognizing that $(\tau\alpha)_{e,n} = a-b$:

$$K_{\alpha\tau} = 1 - \frac{b}{a-b}\left(\frac{1}{\cos\theta}-1\right) \quad (8.12)$$

In terms of one constant, the incident angle modifier $K_{\alpha\tau}$ is:

$$K_{\alpha\tau} = 1 - b_0\left(\frac{1}{\cos\theta}-1\right) \quad (8.13)$$

Figure 13 shows the variation of $K_{\alpha\tau}$ with incident angle for the three solar collectors of Figure 12. Figure 14 shows plots for $K_{\alpha\tau}$ as a function of $((1/\cos\theta)-1)$, verifying the applicability of the general form of equation (8.13). Reference [29] shows that equation (8.13) has also been found valid for an evacuated tubular collector.

The significance of the incident angle modifier to the test procedures outlined herein is that the thermal efficiency values are determined for the collector at or near normal incidence conditions. Therefore, the y intercept of the efficiency curve is equal to $(A_a/A_g)\, F_R(\tau\alpha)_{e,n}$. A separate test is conducted to determine the value of $K_{\alpha\tau}$ so that the performance of the collector can be predicted under a wide range of conditions and/or time of day using Equation (8.9).

It is recognized that some collector designs may require tests at two different incident angles to account for non- symmetrical response to irradiation as solar azimuth and altitude vary throughout the day.

8.3 TESTING PROCEDURE

The first performance test to be conducted on the solar collector is the determination of its time constant. The method for conducting this test is explained in Section 8.3.1. After this is completed, a series of thermal efficiency tests is conducted as explained in Section 8.3.2. Finally, the value of the collector incident angle modifier is determined as a function of incident angle in accordance with Section 8.3.3. The incident angle modifier test is not required for those flat-plate collectors for which the angular response characteristics are known; included in this category are single- and multiple-covered flat-plate collectors without reflectors, honeycombs, convection baffles, selective surfaces with directional characteristics, etc.

8.3.1 Experimental Determination of the Collector Time Constant. The testing of the solar collector to determine its time constant can be done by one of two methods.

Method (1) The inlet temperature of the transfer fluid, $t_{f,i}$, is adjusted as closely as possible (preferably within ± 1°C(± 1.8 F)) to the ambient temperature while circulating the transfer fluid through the collector at the flow rate specified in Section 8.3.2 and maintaining steady state or quasi- steady state conditions with an incident solar flux of greater than 790 W/m² (250 Btu/(hr·ft²)). The incident solar energy is then abruptly reduced to zero by either shielding the collector from the sun or shutting off the solar simulator. The former may be accomplished most appropriately by turning the collector to the North (on a movable mount) and/or shading with a white, opaque cover. The cover should be suspended off the surface of the collector so that ambient air is allowed to pass over the collector as prior to the beginning of the transient test. The temperatures of the transfer fluid at the inlet, $t_{f,i}$, and outlet, $t_{f,e}$ are continuously monitored as a function of time until:

$$\frac{t_{f,e,\tau}-t_{f,i}}{t_{f,e,initial}-t_{f,i}} < 0.30$$

Method (2) The collector is shielded from the sun as specified above, or tested at night, or tested indoors without the use of a solar simulator. The inlet temperature of the transfer fluid is maintained at 30°C (54F) above the ambient temperature, while circulating the transfer fluid through the collector at the flow rate specified in Section 8.3.2, for a period of time sufficient to establish a constant outlet temperature, $t_{f,e}$. After equilibrium is reached, the inlet temperature, $t_{f,i}$, is abruptly reduced as near as possible to within ± 1°C (± 1.8F) of the ambient temperature. The temperature of the transfer fluid at the inlet, $t_{f,i}$ and outlet $t_{f,e}$, are continuously monitored as a function of time until:

$$\frac{t_{f,e,\tau}-t_{f,i}}{t_{f,e,initial}-t_{f,i}} < 0.30$$

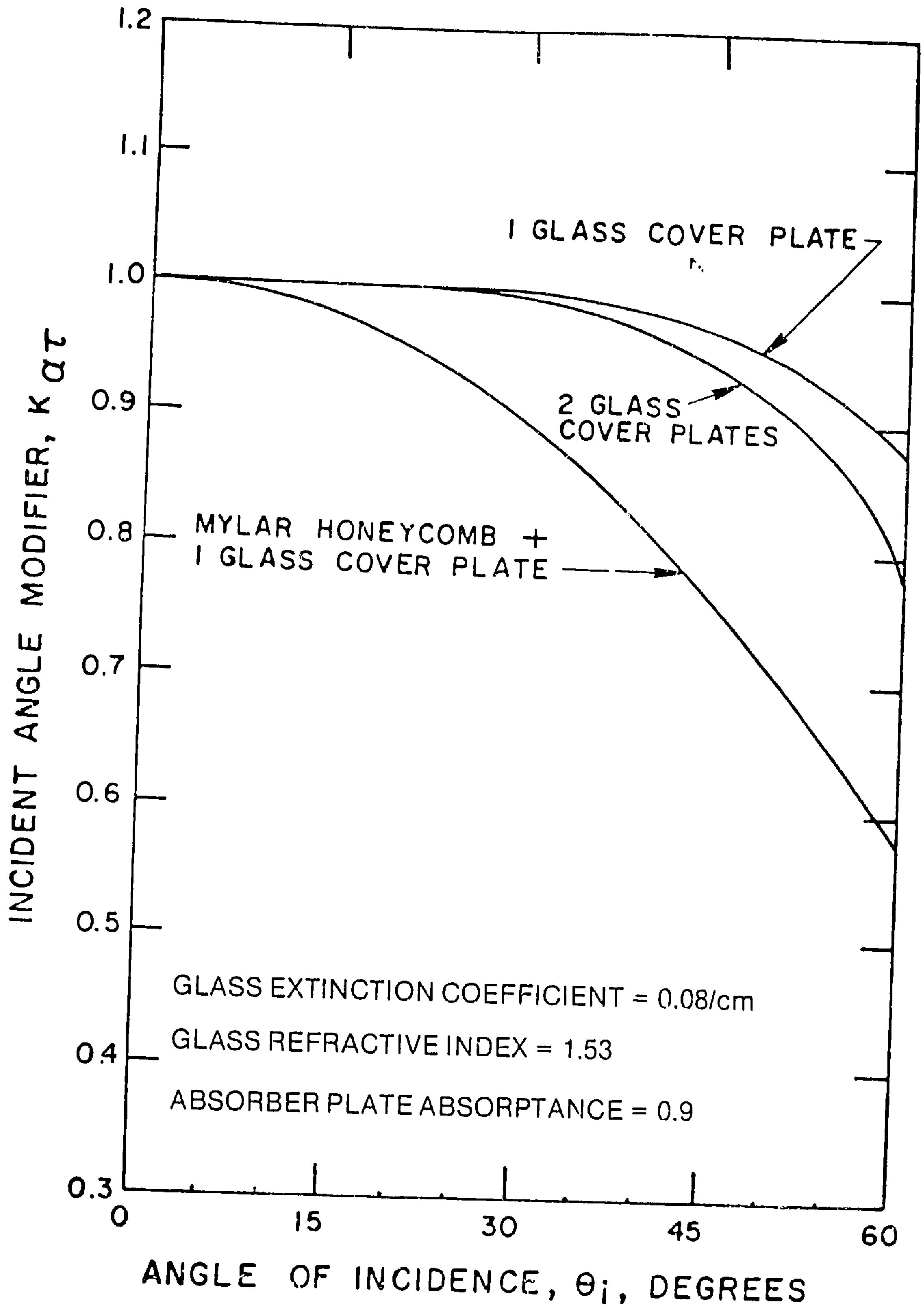

Fig. 13 Incident Angle Modifier for Three Flat-Plate Solar Collectors with Non-Selective Coatings on the Absorber

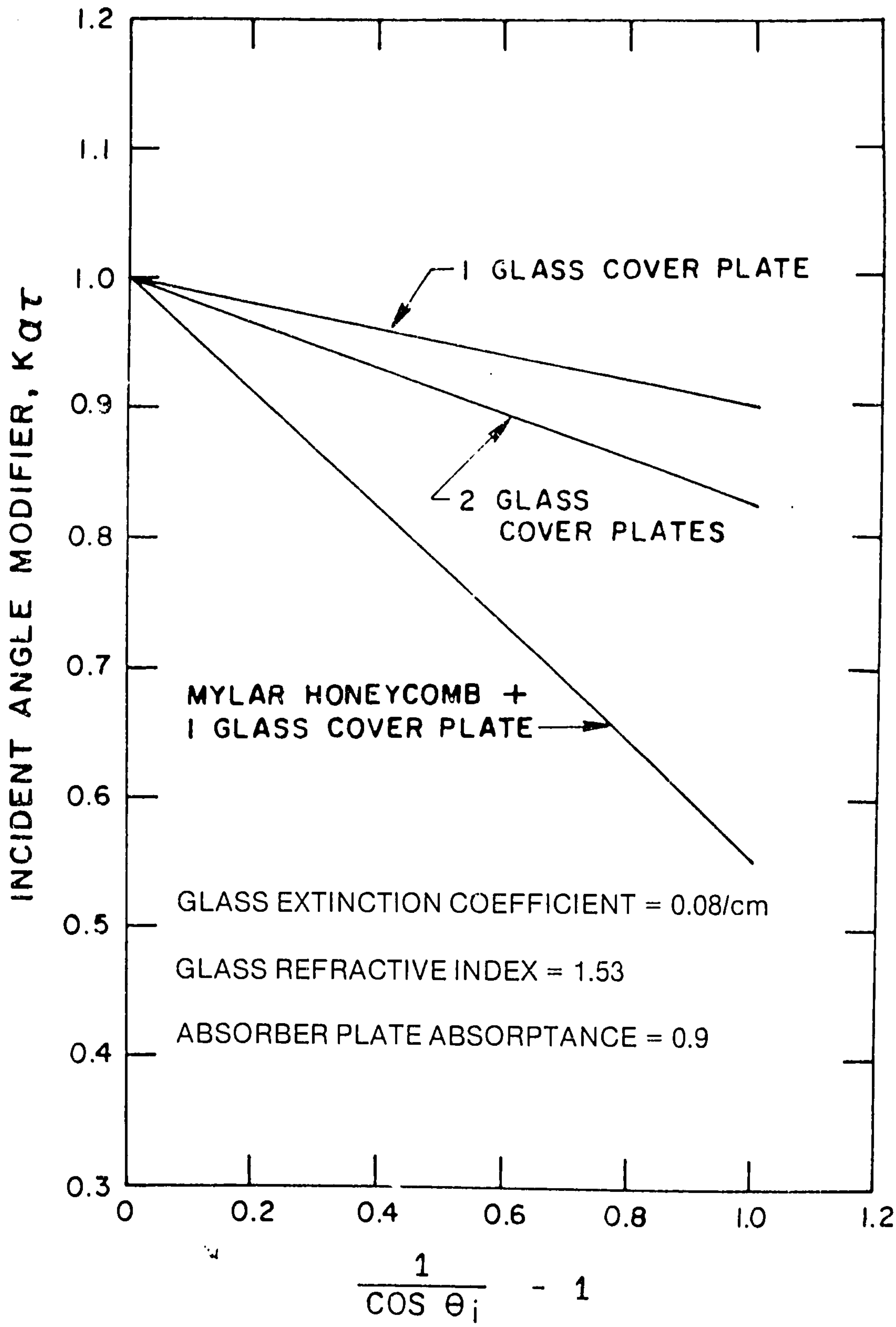

Fig. 14 Incident Angle Modifier for Three Flat-Plate Solar Collectors with Non-Selective Coatings on the Absorber

For either method the actual time constant is the time T required for the quantity $((t_{f,e,\tau} - t_{f,i})/(t_{f,e,initial} - t_{f,i}))$ to change from 1.0 to 0.368.

8.3.2 Experimental Determination of the Collector Thermal Efficiency. The testing of the solar collector to determine its thermal efficiency shall be conducted in such a way that a governing efficiency curve for near normal incidence is determined for the collector under test conditions described in Sections 5. and 8. At least four different values of inlet fluid temperature shall be used to obtain the values of $\Delta t/I_t$. An acceptable distribution of inlet temperatures for flat-plate collectors is to set the Δt at 10, 30, 50 and 70% of the stagnation temperature rise obtained at the given conditions of solar intensity and ambient air temperature.

At least four data points shall be taken for each value of $t_{f,i}$; two during the time period preceding *solar noon* and two in the period following *solar noon*, the specific periods being chosen so that the data points represent times symmetrical to solar noon. This latter requirement is made so that any transient effects that may be present will not bias the test results when they are used for design purposes. The requirement for obtaining data points equally divided between morning and afternoon is not mandatory when testing with an altazimuth mount. All test data shall be reported in addition to the fitted curve (see Section 9) so that any difference in efficiency due solely to the operating temperature level of the collector can be discerned in the test report. The curve shall be established by data points that represent efficiency values determined by integrating the data over a time period equal to the time constant, determined in accordance with Sections 8.3.1 and 8.4, or 5 minutes, whichever is larger. The integrated value of incident solar energy will be divided into the integrated value of energy obtained from the collector to obtain the efficiency value for that test period.

When an indoor solar simulator is employed and true steady-state conditions can be obtained, the time interval specified above is not applicable. In this case, data may be considered as steady state when the collector outlet temperature does not change (within the limits of measurement) in a five minute time period. Instantaneous data may then be used to determine instantaneous efficiency.

If a normal-incidence altazimuth mount is used for the tests outside, the time interval specified above may be reduced to five minutes or 1/2 the time constant of the collector, whichever is larger.

In conducting the tests outside, care should be taken to ensure that the incident solar radiation is steady for each time interval during which an efficiency value is calculated. Either electronic integrators or continuous pen strip chart recorders may be used to determine the integrated values of incident solar radiation and temperature rise across the collector. However, a strip chart recorder with a recommended chart speed of 30 cm/hr (12 in./hr) or greater must always be used to monitor the output of the pyranometer to ensure that the incident radiation has remained steady during the test period. Figures 15 and 16 show strip chart recordings of incident solar radiation on a horizontal surface. Whereas the conditions of Fig. 15 would be perfectly acceptable for obtaining efficiency values, those of Fig. 16 would not be.*

The surface of the collector cover plate (if present) as well as exposed envelopes of the pyranometer(s) and pyrheliometer (if used) should be wiped clean and dry prior to the tests. If local pollution or dust has formed a deposit on the transparent surfaces, the wiping should be carried out very gently, preferably after blowing off most of the loose material or after wetting it a little, in order to prevent scratching of the surface. This is particularly important for the solar radiation measuring instruments since such abrasive action can appreciably alter the original transmission properties of the enclosing envelope.

The pyranometer(s) shall be checked prior to testing to see if there is any accumulation of water vapor enclosed within the glass cover. The use of wet pyranometers (where moisture is visible) shall not be allowed.

In order to obtain sufficiently good steady state or quasi-steady state conditions for the solar collection process, the transfer fluid should be circulated through the collector at the appropriate inlet temperature level until the temperature has remained constant for 15 minutes prior to the period in which data will be taken to calculate the efficiency values.

When using an indoor simulator, the following starting procedure has been found satisfactory. The transfer fluid is circulated through the collector at the inlet temperature chosen for the test. After equilibrium is established for the chosen inlet temperature, the simulator is turned on and the desired radiant flux obtained by adjusting the lamp voltage. A check should be made to ensure that the flow rate of the transfer fluid does not vary by more than ±1% and that the incident radiation is steady as described above.

The flow rate of transfer fluid through the collector shall be standardized at one value for all data points. The recommended value of flow rate per unit area (transparent frontal or aperture) for tests are 0.02 kg/(s · m²) (14.7 lbm/(hr · ft²)) when a liquid is the transfer fluid and 0.01 m³/(s · m²) (2 cfm/ft²) of standard air when the transfer fluid is air. For air heaters, efficiency is much more a function of flow rate than with collectors using a liquid as the transfer fluid

*One or two "slips" of 10 s or less occurring during the test period such as at 12:18 in Fig. 15 are acceptable.

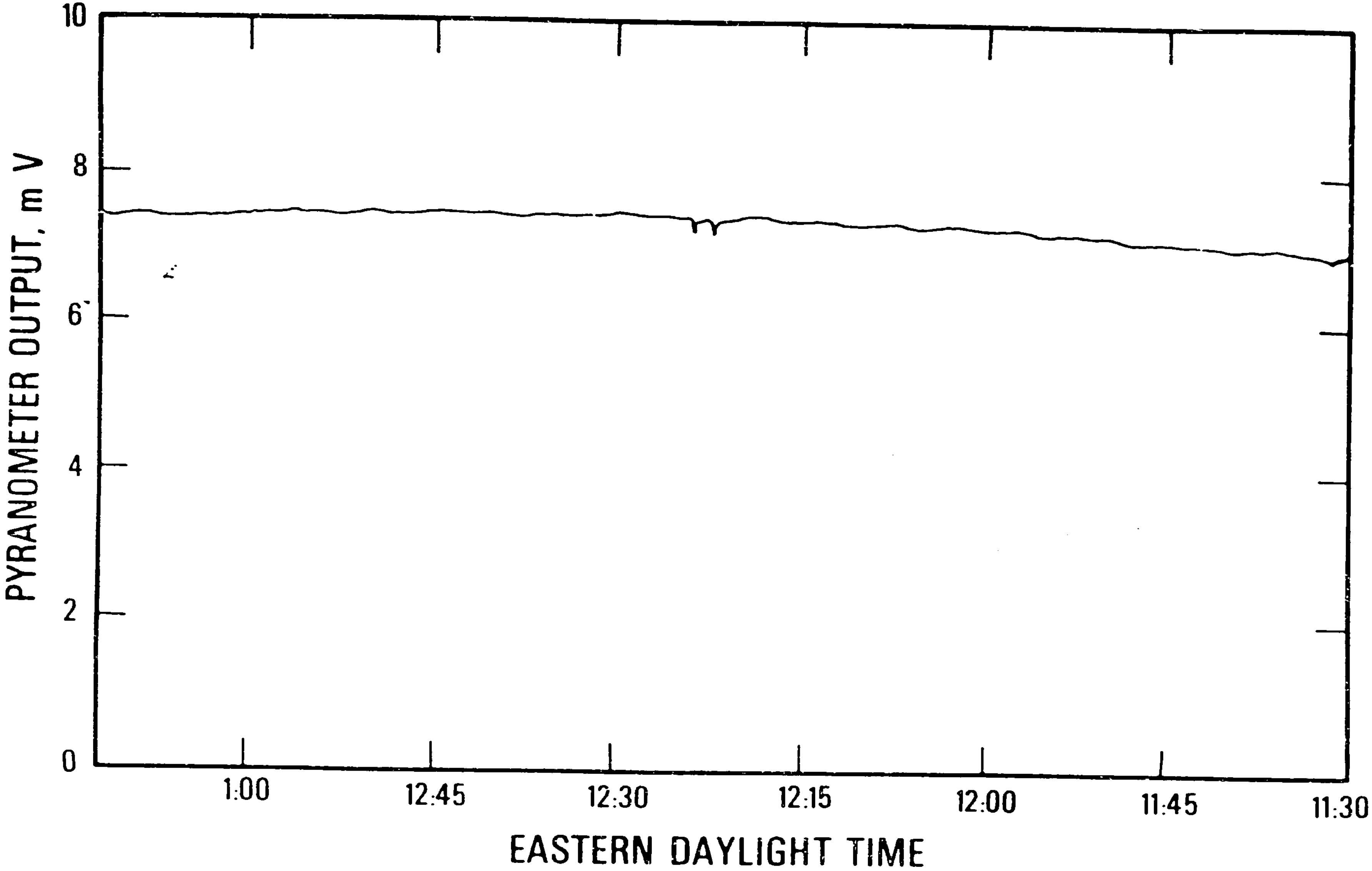

Fig. 15 Incident Solar Radiation on a Horizontal Surface in Gaithersburg, MD, March 13, 1974

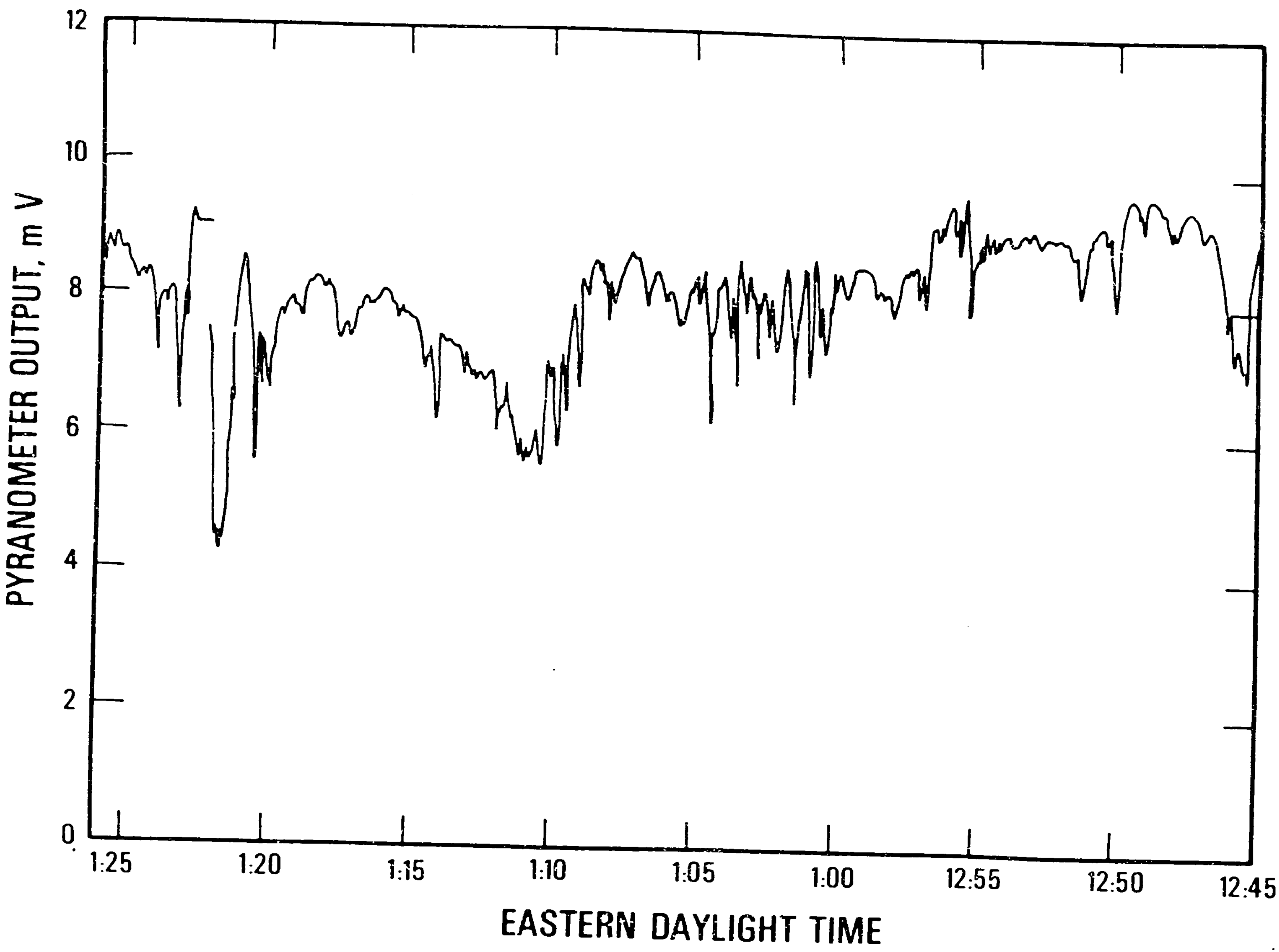

Fig. 16 Incident Solar Radiation on a Horizontal Surface in Gaithersburg, MD, March 11, 1974

and a second test sequence using 0.03 $m^3/(s \cdot m^2)$ (6 cfm/ft²) is recommended. It is recognized that in some cases the collector will have been designed for a flow rate much different than specified above. In such cases the design flow rate should be used.

In order to determine and report the fraction of the incident solar radiation which is diffuse for each efficiency value, the use of both a pyrheliometer and pyranometer is preferred (it is required for those collectors that do not accept diffuse radiation). In the absence of a normal incidence pyrheliometer, two pyranometers may be used, one of which uses a shading band [8], or only a single pyranometer may be used. When only a single pyranometer is used, its sensing element shall be shaded from the direct beam of sun just prior to and just following each testing period and the value of the incident diffuse radiation determined. This shall be accomplished by using a small disk attached to a slender rod held in a direct line between the pyranometer and the sun. The disk should be just large enough to shade the sensing element alone. As an example in Ref. 4, this is accomplished by a disk 100 mm in diameter and held at a distance of one meter from the sensing element of the pyranometer.

The steady wind velocity across the collector as measured per paragraph 5.1.7 and Section 6.8 shall be less than 4.5 m/s (10 mph).

8.3.3 Experimental Determination of Collector Incident Angle Modifier for Stationary Collectors. The testing of the solar collector to determine its incident angle modifier can be done by one of two methods.

Method (1) This method is applicable for testing indoors using a solar simulator, or outdoors using a movable test rack so that the orientation of the collector can be arbitrarily adjusted with respect to the direction of the incident solar radiation. Four separate efficiency values are determined in general accordance with the method described in Section 8.3.2. For each data point, the inlet temperature of the transfer fluid is controlled as closely as possible (preferably within ±1°C (±1.8F)) to the ambient air temperature. The collector is oriented so that the average incident angles between it and the direct solar radiation for the four test conditions are respectively, approximately 0, 30, 45 and 60 degrees. The foregoing values are appropriate for conventional flat-plate collectors. At least one angle should be greater than the acceptance angle, for concentrating collectors.

Method (2) This method is applicable for testing outside using a permanent test rack where the collector orientation cannot be arbitrarily adjusted with respect to the direction of the incident solar radiation (except for adjustments in tilt). Six separate efficiency values are determined in general accordance with the method described in Section 8.3.2. For each data point, the inlet temperature of the transfer fluid is controlled, if possible, to within ±1°C (± 1.8F) of the ambient air temperature. The efficiency values are determined in three pairs, where each pair includes a value of efficiency early in the day and a second value late in the day. The average incident angle between the collector and the solar beam for both data points is the same. The efficiency of the collector for the specific incident angle shall be considered equal to the average of the two values. As with Method (1), data should be collected for average incident angles of approximately 0, 30, 45 and 60 degrees.

8.4 Computation of Collector Time Constant

According to the definition of time constant given in Section 8.2.2, it is the time required for the left-hand side of equation (8.8) to equal 0.368. Regardless of which experimental method in Section 8.3.1 is used, the incident solar radiation is equal to zero and the inlet fluid temperature is held sufficiently close to the ambient air temperature so that $(t_{f,i} - t_a) \approx 0$. Therefore, by monitoring the entering and exit fluid temperatures as a function of time, the time constant is the time required for:

$$\frac{t_{f,e,T} - t_{f,i}}{t_{f,e,initial} - t_{f,i}} = 0.368 \tag{8.14}$$

If the inlet fluid temperature cannot be controlled to equal the ambient air temperature within ±1°C (±1.8F), an estimate of the $(A_a/A_g)F_R U_l$ product should be made for the collector for the conditions of the test and the time constant calculated as the time required for:

$$\frac{(A_a/A_g)F_R U_l (t_{f,i} - t_a) + \frac{\dot{m}c_p}{A_g}(t_{f,e,T} - t_{f,i})}{(A_a/A_g)F_R U_l (t_{f,i} - t_a) + \frac{\dot{m}c_p}{A_g}(t_{f,e,initial} - t_{f,i})} = 0.368 \tag{8.15}$$

8.5 Computation of Collector Thermal Efficiency

For the test interval for each efficiency data point, the efficiency value is calculated using the equation:

$$\eta_g = \frac{\dot{m}\, c_p \int_{\tau_1}^{\tau_2} (t_{f,e} - t_{f,i})\,d\tau}{A_g \int_{\tau_1}^{\tau_2} I\,d\tau} \tag{8.16}$$

The quantities $\dot{m}$ and c_p have been taken out of the integration in the numerator since they remain essentially constant during the test. Note that the collector area used for the calculation is not the absorbing surface area but rather the gross collector area. For those collectors that do not accept diffuse radiation, the computation should be done twice: once where I in the denominator of equation (8.16) is the total radiation, I_t, and once where it is only the direct component, I_D. For flat-plate collectors, I_t shall be used.

At least sixteen data points shall be obtained for the establishment of the efficiency curve and an equation for the curve shall be obtained using the standard technique of a least-squares fit.* In most cases, a linear or second order fit will suffice. The curve shall not be extrapolated beyond the limits of data.

8.6 Computation of Collector Incident Angle Modifier

Regardless of which experimental method in Section 8.3.3 is used, three different values of the thermal efficiency of the collector shall be determined corresponding to three different values of incident angle. Since the inlet fluid temperature is held sufficiently close to the ambient air temperature so that $(t_{f,i} - t_a) \approx 0$, the relationship between $K_{\alpha\tau}$ and the efficiency, according to equation (8.9), is:

$$K_{\alpha\tau} = \frac{\eta_g}{(A_a/A_g)F_R(\tau\alpha)_{e,n}} \qquad (8.17)$$

Since $(A_a/A_g)F_R(\tau\alpha)_{e,n}$ will have already been obtained as the Y-axis intercept of the efficiency curve determined in accordance with Sections 8.3.2 and 8.5, three different values of $K_{\alpha\tau}$ can be computed for the different incident angles using equation (8.17). The value of b_o may be determined using equation (8.13) and the standard technique of a least-squares fit to a first-order polynomial. Other methods of correlation may be used to describe an equation for the incident angle modifier.

If the inlet fluid temperature cannot be controlled to equal the ambient air temperature within ±1°C (±1.8F), an estimate of the $(A_a/A_g)F_RU_L$ product should be made for the collector for the conditions of the test and each value of $K_{\alpha\tau}$ computed as:

$$K_{\alpha\tau} = \frac{\eta_g + (A_a/A_g)F_RU_L(t_{f,i} - t_a)/I}{(A_a/A_g)F_R(\tau\alpha)_{e,n}} \qquad (8.18)$$

For those collectors which can accept diffuse radiation, I in equation (8.18) should be the total irradiation, I_t; for those collectors which cannot accept diffuse radiation, I_D should be used.

Alternately, each data point can be plotted on the same plot with the efficiency curve determined in accordance with Section 8.3.2 and 8.5 and a curve drawn through each point parallel to the efficiency curve and made to intersect the y axis. The values of the y intercept are the efficiency values that would have resulted had the inlet fluid temperature been controlled to equal the ambient air temperature. Therefore, these values can be used in conjunction with equation (8.17) to compute the different values of $K_{\alpha\tau}$.

8.7 Computation of Air Flow Rate

The air flow rate through the nozzle is calculated by the following equations:

$$Q_{mi} = 1.41\ C_nA_n(p_v v_n')^{0.5} \qquad (8.19)$$

$$v_n = 10.1 \times 10^4 v_n'/p_n(1 + W_n) \qquad (8.20)$$

The air flow rate of standard air is then:

$$Q_s = Q_{mi}/(1.2v'_n) \qquad (8.21)$$

8.8 Computation of Nozzle Reynolds Number

The Reynolds number is calculated as follows:

$$N_{Re} = f_t V_a D_n \qquad (8.22)$$

The temperature factor f_t is as follows for air:

Temperature °C	°F	Factor, f_t
−6.7	20	78275
+4.4	40	72075
+15.6	60	67425
+26.7	80	62775
+37.8	100	58125
+48.9	120	55025
+60.0	140	51925
+71.1	160	48825

8.9 Computation of Theoretical Power Requirements

In order to calculate the theoretical power required to move the transfer fluid through the solar collector, the following equation shall be used:

$$P_{th} = \dot{m} \cdot \Delta p/w \qquad (8.23)$$

9. DATA TO BE RECORDED AND TEST REPORT

9.1 Test Data

Table 1 lists the measurements which are to be made at the beginning of the testing day and during the individual tests to obtain an efficiency data point.

9.2 Test Report

Table 2 specifies the data and information that shall be reported in testing the solar collector.

10. REFERENCES

1. Morrison, C. A. and Farber, E. A., "Development and Use of Insolation Data for South Facing Surfaces in Northern Latitudes," *ASHRAE Trans.* 1974, Part II.

2. *ASHRAE Handbook of Fundamentals,* American Society of Heating, Refrigerating and Air-Conditioning Engineers, Inc., 345 East 47th Street, New York, N.Y. 10017, 1977.

3. Morrison, C. A. and Farber, E. A., "Clear-Day Design Values," Chapter IV, Applications of Solar Energy for Heating and Cooling of Buildings," ASHRAE GRP 170, ASHRAE, New York, 1977.

4. *Guide to Meteorological Instrumentation & Observing Practices,* Secretariat of the World Meteorological Organization, Geneva, Switzerland, 4th Edition, 1971.

5. *ASHRAE Handbook of Applications,* American Society of Heating, Refrigerating and Air-conditioning Engineers, Inc., 345 East 47th Street, New York, N.Y., 10017, 1978.

*One should consult any standard text discussing analysis of experimental data for a presentation of this technique (e.g., Refs. 10 and 11)

6. Latimer, J. R., "Radiation Measurement," *International Field Year for the Great Lakes, Technical Manual Series, No. 2,* The Secretariat, Canadian National Committee for the International Hydrological Decade, No. 8 Building, Carling Avenue, Ottawa, Canada, 1971.

7. Vernon, R. W., "Solar Collector Performance Evaluated Outdoors at NASA-Lewis Research Center," *NASA TM X-71689, Proceedings of the Workshop on Solar Collectors for Heating and Cooling of Buildings, New York, November 21-23, 1974,* Report No. NSF-RA-N-75-019, University of Maryland, May, 1975.

8. Coulson, K. L., "*Solar and Terrestrial Radiation, Methods and Measurements,*" p. 129, Academic Press, 1975, New York.

9. "Standard Measurements Guide: Section on Temperature Measurements," *ASHRAE Standard 41.1,* American Society of Heating, Refrigerating and Air- Conditioning Engineers, Inc., 345 East 47th Street, New York, N.Y. 10017, March 1974.

10. Benedict, Robert P., *Fundamentals of Temperature, Pressure and Flow Measurements,* Wiley Publishing Co., 1969.

11. Faison, T. K., Davis, J. C., and P. R. Achenbach, "Performance of Louvered Devices as Air Mixers" *NBS Building Science Series 27,* March, 1970. (Available from the Superintendent of Documents, U.S. Government Printing Office, Washington, D. C. 20401—order by SD Catalog No. C 13.29/2:27, $0.30.)

12. "Methods of Testing Unitary Air-Conditioning and Heat Pump Equipment," *ASHRAE Standard 37-69,* American Society of Heating, Refrigerating and Air-Conditioning Engineers, Inc., 345 East 47th Street, New York, N.Y. 10017, July 1969.

13. "Instruments for Climatological Observations, Circular B," United States Weather Bureau Service, 11th edition, January, 1962.

14. "Instruments and Apparatus, Part 2, Pressure Measurement," Supplement to the ASME Power Test Codes, American Society of Mechanical Engineers, 345 East 47th Street, New York, N.Y. 10017, July 1964.

15. Yass, K., and H. B. Curtis, "Low-Cost Air Mass 2 Solar Simulator," *NASA TM X-3059,* 1973.

16. Simon, F. F., and P. Harlamert, "Flat-Plate Collector Performance Evaluation, the Case for a Solar Simulator Approach," *NASA TM X-71427,* 1973.

17. Ramsey, J. W., Borzoni, J. T., and T. H. Holland, "Development of Flat-Plate Collectors for the Heating and Cooling of Buildings," *NASA CR-134804,* June, 1975.

18. Tabor, H., "Selective Surfaces for Solar Collectors," Chapter VI in "Applications of Solar Energy for Heating and Cooling of Buildings," ASHRAE GRP 170, ASHRAE, New York, 1977.

19. Sparrow, E. M. and Cess, R. D., *Radiation Heat Transfer,* Brooks/Cole Publishing Company, 1966.

20. Thekaekara, M. P., "Solar Electromagnetic Radiation," *NASA SP-8005,* revision of May, 1971.

21. Hottel, H. C., and B. B. Woertz, "The Performance of Flat-Plate Solar Heat Collectors," *ASME Transactions,* Vol. 64, p. 91, 1942.

22. Bliss, R. W., "The Derivation of Several 'Plate- Efficiency Factors' Useful in the Design of Flat-Plate Solar Heat Collectors," *Solar Energy,* Vol. 3, No. 4, p. 55, 1959.

23. Whillier, A., "Prediction of Performance of Solar Collectors," Chapter VIII of "Applications of Solar Energy for Heating and Cooling of Buildings," ASHRAE GRP 170, ASHRAE, New York, 1977.

24. Duffie, J. A., and W. A. Beckman, *Solar Energy Thermal Processes,* John Wiley and Sons, 1974.

25. Hill, J.E., Jenkins, J.P., and Jones, D.E., "Testing of Solar Collectors According to ASHRAE Standard 93-77," ASHRAE Transactions, Vol. 84, Part II, 1978.

26. Simon, F. F., "Status of the NASA-Lewis Flat-Plate Collector Tests with a Solar Simulator," *NASA TM X-71658, Proceedings of the Workshop on Solar Collectors for Heating and Cooling of Buildings, New York, November 21-23, 1974,* Report No. NSF-RA-N-75-019, University of Maryland, May, 1975.

27. Simon, F. F., and E. H. Buyco, "Outdoor Flat-Plate Collector Performance Prediction from Solar Simulator Test Data," *NASA TM X-71707,* presented at the 10th AIAA Thermal Physics Conference, Denver, Colorado, May 27-April, 1974.

28. "Solar Thermal Electric Power Systems—First Quarter Progress Report," Report No. NSF/RANN/SE/GI-37815/PR/74/1, Colorado State University, April, 1974.

29. Simon, F. F., "Flat-Plate Solar Collector Performance Evaluation with a Solar Simulator as a Basis for Collector Selection and Performance Prediction," *NASA TM X-71793,* 1975.

30. Holman, J. P., *Experimental Methods for Engineers,* McGraw-Hill, Second Edition, 1971.

31. Bevington, P. R., *Data Reduction and Error Analysis for the Physical Sciences,* McGraw-Hill, 1969.

BIBLIOGRAPHY

1. Chinnery, D. N. W., "Solar Water Heating in South Africa," Bulletin No. 44 (Report No. 248), National Building Research Institute, Council for Scientific and Industrial Research, Pretoria, South Africa, (1971).

2. Hill, J. E., Streed, E. R., Kelly, G. E., Geist, J. C. and Kusuda, T., "Development of Proposed Standards for Testing Solar Collectors and Thermal Storage Devices," NBS Technical Note 899, National Bureau of Standards, Washington, DC 20234, February, 1976.

3. Hill, J. E. and Streed, E. R., "Testing and Rating of Solar Collectors" Chapter X in "Applications of Solar Energy for Heating and Cooling of Buildings," ASHRAE GRP 170, ASHRAE, New York, 1977.

A SIMPLIFIED SOLAR SYSTEM DESIGN TECHNIQUE FOR TROPICAL REGIONS

N. Pacheco, Associate Professor
Department of Mathematical Sciences
U.S. Air Force Academy
Colorado Springs, Colorado

K. G. Soderstram, Associate Director
Center for Energy and Environment Research
University of Puerto Rico
Mayaguez, Puerto Rico

ABSTRACT

The countries in the Caribbean region, all of which are petroleum importers, receive high annual insolation, especially on their coastal zones. Therefore, solar energy is an attractive alternative energy source. Due to the lack of widespread computer availability and expertise in simulation techniques, the Caribbean region has a need for simplified solar system design methods. Most of the popular methods for simplified design, such as f-Chart and GFL, have been developed for space-heating applications in temperate and cold regions. In the Caribbean region, however, solar energy is applied for domestic and commercial water heating and for air heating for crop drying purposes.

In this study, conducted at the Center for Energy and Environment Research (CEER) in Puerto Rico, simplified design methods are developed specifically for domestic and commercial water heating and for air heating applications for crop-drying in tropical regions. Constants are established and verified by detailed simulation programs previously carried out by CEER researchers and by modified f-Chart comparison for three metropolitan locations in Puerto Rico (San Juan, Ponce, Mayaguez). Based on the solar data for each of these locations, three systems are modeled: a solar water-heating system, (1) with and (2) without a load heat exchanger, and (3) an air-based system. For the benefit of technology-transfer programs in the region, the entire algorithm to establish the constants has been programmed on a micro-computer. Nomographs, designated as PASO charts, were developed from this. Their use is equivalent to utilization of a single step tool for solar system design for tropical climates for the typical systems in these zones.

A. INTRODUCTION

The prediction of the amount of electric energy and/or fuel oil which can be offset by the solar system is of prime importance in a solar system design. This information is required in the initial planning stages of a domestic or an industrial development or when a retrofit of an existing facility to solar is being considered. This information is also useful to government planners for making long-term economic forecasts and energy plans. These forecasts are of particular importance to Puerto Rico and to the nations of the Caribbean because most of them import their entire energy supply in the form of petroleum. On the other hand, the Caribbean region receives abundant sunshine throughout the year, and solar energy is an attractive alternative energy source.

Although many studies have been done on questions of solar design, most of the work has been devoted to studies of space heating applications in cold climates. In Puerto Rico, however, there are no space heating requirements. The requirements that do exist which can be answered in the short term by solar energy are for hot water heating for domestic and industrial use, and for air heating for industrial and agricultural use, and for air heating for industrial and agricultural applications such as crop drying. In Puerto Rico and the Caribbean and in tropical regions other than on mainland USA, a need exists for simplified design methods which do not require large, expensive computers and accompanying expertise for analysis and design.

One of the first approaches to simplified design is the well-known method developed by Klein et al (1) that has become known as the f-Chart method.*

This original f-Chart method, however, was based on space heating models which are not appropriate to tropical regions. Modest and Soderstrom (3) later designed detailed simulation models for solar hot water systems in tropical climates. These detailed simulations showed that the f-Chart method, with some modifications, could be extended to these applications within certain ranges of design values. The f-Chart, though, tended to over-estimate the solar contribution for larger systems by as much as ten percent.

The reasons for these errors are two-fold. First, the space-heating problem has certain characteristics which are different from the water-heating problem, such as load profile. Secondly, the original f-Chart was inflexible in that certain critical parameters

*The f-Chart method will provide the percentage of the total monthly energy load which can be supplied by solar energy, known as the f-value, as a function of certain design parameters and weather data. This much-used method was based on a statistical correlation of a large number of runs of TRNSYS (2), a detailed computer simulation model.

such as desired water temperature and storage volume could not be varied from their nominal assigned values or extended outside of a short range of values. Nevertheless, this study showed that the f-Chart method could be used with precautions as a general guide to water heating designs in tropical climates.

An expanded version of the f-Chart method was later developed by Beckman et al (4). In this extension of the original f-Chart, a design method was provided for hot water heating only. Correction factors were provided which allowed for changes in certain design parameters such as storage mass, required water temperature, air flow rate in air-based collectors and heat exchanger efficiencies. This improved method, however, reintroduced some of the computational difficulty which the original method was attempting to reduce. Lameirc and Bendt (5) have estimated that a complete set of calculations for this method done on a hand calculator could take as long as four hours. Although the method is available for programmable hand calculators or computers, it is not of great use in the Caribbean which is below the latitude for which the software was developed. In addition, computer use is not widespread in this region.

Lameiro (5) provided a breakthrough in computational simplicity in solar design when he discovered a simple second order exponential fit to the f-Chart values. This method, known as the GFL method, allows calculations by hand of f-values in about five minutes with accuracies of under two percent when compared with the f-Chart. Unfortunately, the GFL method, which is site specific, was also based on spaceheating requirements and did not address tropical regions.

In this investigation, a method based on the simplicity of the second order exponential fit and correlated with the expanded version of f-Chart, with appropriate modifications, is developed for tropical regions. The resulting parameters are then used in the construction of simple nomographs, herein named PASO Charts. These PASO Charts provide a simple design tool for various systems and locations.

B. TECHNICAL DISCUSSION

The principles of solar engineering are well documented in recently published texts in this field. The books by Duffie and Beckman (6), Kreider and Kreith (7), and Lunde (8) among others, contain detailed engineering and mathematical analyses of the principal components of solar energy systems. In actual systems such components as the collectors, storage tanks, heat exchangers, and associated valves and tubing intereact with each other and with the environment in complex ways. The exact solution to the coupled integro-differential equations which describe such a system is not easily found. To make matters more difficult, the forcing functions are not deterministic, but rather are random processes which describe the insolation and other weather data. Although the investigation of these equations remains an interesting theoretical problem, the need of the designer is for sound approximations which can be used to design actual systems.

Due to the problems just mentioned, a commonly used approach to solar systems analysis is computer simulation. With this method, a specific design with all of its subcomponents, can be modeled in the computer. Actual insolation and weather data measured at fixed time intervals (usually hourly) is then fed to the computer. The computer simulation program will model the thermal and other physical interactions between the various components at discrete time intervals and arrive at approximate system operation profiles which can be used for extensive analysis and for the design of an optimal system.

The degree of approximation to an actual system can be quite high, depending on the amount of detail which is introduced. The TRNSYS simulation program developed at the University of Wisconsin-Madison by Klein et al (2) in 1973 is one of the best-known solar simulation programs. In addition to the large data processing capacities required for a detailed simulation program, a problem inherent in these types of programs is that any change in a design parameter requires a rerunning of the entire simulation. This is very costly and out of the question from a design viewpoint for all but the most expensive solar applications.

The f-Chart method was developed from many runs of TRNSYS in which design parameters were varied and statistical correlation equations were obtained. A detailed discussion of this method is found in Beckman (4). The following is a summary of the governing equations involved in this method.

1. Hot Water Systems

For hot-water systems, the f-Chart correlation equation is:

$$f = 1.029\ Y - 0.065\ X - 0.245\ Y^2 + 0.0018\ X^2 + 0.0215\ Y^3, \qquad (1)$$

where X and Y are dimensionless quantities given by

$$X = F_R' A\ U_L\ (11.6 + 1.18\ T_o + 3.86\ T_i - 2.32\ T_a)\ \Delta t/L \qquad (2)$$

and

$$Y = F_R' A\ S\ (\overline{\tau\alpha})/L, \qquad (3)$$

valid for $0 \leq Y \leq 3.0$ and $0 \leq X \leq 18.0$.

The parameters in these equations are defined as follows:

f = solar fraction (percent of monthly load which can be supplied by solar energy)

F_R = collector heat removal factor (dimensionless)

F_R' = collector - heat exchanger efficiency factor (dimensionless)

A = collector area (M^2)

U_L = collector overall energy loss coefficient ($W/M^2{}^\circ C$)

T_o = desired water temperature (°C)

T_i = water main temperature (°C)

$\bar{T}_a$ = monthly, average ambient temperature (°C)

Δ_t = one-month period, in seconds

$\overline{\tau\alpha}$ = Average value of the collector transmittance - absorbance product. This can be taken as .93 ($\tau\alpha$) for most flat plate collectors.

S = average total monthly insolation in the plane of the collector (GJ/M^2)

Correction factors are provided for storage capacity and load heat exchanger sizing as follows:

Storage correction: $(V_s/75)^{-.25}$, (4)

where V_s is the storage volume per unit area of collector {lit (H_2O)/M^2} and is valid for $37.5 < V_s < 300$. The storage correction factor multiplies the X variables.

Load heat exchanger correction:

$$0.39 + 0.65 \exp.(-139/\lambda), \quad (5)$$

where $\lambda = \varepsilon_L (C_{min}/Q_L)$

and ε_L = load heat exchanger effectiveness.

C_{min} = minimum fluid capacitance rate (mC_p) min in units of (W/°C) where m is the flow rate and C_p the specific heat of the liquid.

Q_L = heat load expressed in units consistent with C_{min} so as to make λ dimensionless {(W/°C) in this case}. The load heat exchanger correction factor multiplies the Y variable.

2. Air Systems

For air systems, the correlation equation is

$$f = 1.040\,Y - .065\,X - .159\,Y^2 + .00187\,X^2 - .0095\,Y^3, \quad (6)$$

with X now defined as

$$X = F_R' A U_L (100 - \bar{T}_a)\,\Delta t/L, \quad (7)$$

valid for

$$0 \le Y \le 3.0,\ 0 \le X \le 18.0.$$

Corrections are provided for pebble bed storage mass and collector air flow rate as follows:

Storage correction: $(.25/V_s)^{.3}$, (8)

where V_s is the storage volume per unit area of collector M^3/M^2 and is valid for

$$0.125 \le V_s \le 1.0.$$

Air flow rate correction:

$$(M/10.1)^{.28}, \quad (9)$$

where M is air flow rate per unit area of collector (lit/sec)/M^2 and is valid for $5 \le M \le 20$.

3. Modifications

Several modifications are required for tropical applications. First, for freezing conditions, a collector heat exchanger is used quite often. This is unnecessary for the tropics since freezing conditions never exist at any time of the year. Therefore, F_R' was set to one. Second, there is a difference between a closed-loop space heating system in which the major losses are through the walls of the building, and an open-loop water heating system in which the water is heated, used in a process, and discharged outside the building. Therefore, in system designs where a load heat exchanger is used, the value of C_{min}/Q_L is set to one and λ is therefore set equal to ε_L. This has the expected effect of lowering the f-value by as much as 10%. Third, as discussed in Modest and Soderstrom (3), the expected storage tank losses should be added to the load. In space heating applications where the storage tank is located inside the building, tank losses are considered to be not true losses, since they aid in heating the air. In tropical situations, however, the tank is usually located outside the structure so that

$$L = L_{load} + L_{Losses} \quad (10)$$

where

$$L_{losses} = (UA)_{tank} (\bar{T}_{tank} = \bar{T}_a)\,\Delta t \quad (11)$$

is a good approximation. This can be compensated for in the GFL method at the load calculation stage, as discussed later.

4. The GFL Method

This discussion follows Lameiro (5) with appropriate tropical modifications. The purpose of the GFL method is to find an exponential fit to the f-values for a given design. As the collector area is increased, the f-values will increase in an approximately proportional manner. However, as larger collector areas are used, the rate of growth of the f-values slows down. There are two reasons for this. First, large collector areas may collect excess energy during high insolation periods, causing "boil-off" effects in the tank. Secondly, regardless of the size of the collector area, there remains the probability of a cloudy period of sufficient length to make the solar system supply less than the required energy. The first reason is of more importance in tropical regions than is the second because insolation values are much less variable than in colder regions. Therefore, there is not as much of a dampening effect at high f-values. This is borne out in the exponential curve fits found for the locations in Puerto Rico.

The best fit found by Lameiro (5) was a second order exponential function:

$$f = 1-\exp(-RA - SA^2) \quad (12)$$

Typical errors in the use of this formula were ±2% for $0.0 \leq f \leq .9$ and ± 1.5% for $0.4 \leq f \leq .8$. R and $\bar{S}$ are mathematically derived constants found by forcing the exponential to pass through f = .5 and f = .75. Any two such f-values may be used, however, in this formulation the system design parameters are related to f through R and S. A change in a design parameter would cause a change in R and S. This formulation is not useful due to the large number of constants required to describe different systems at different locations. A more efficient formulation was found to be

$$f = 1 - \exp(-R\,Y - S\,Y^2) \quad (13)$$

where $Y = F_R\,(\tau\alpha)\,A/L$

In this formulation R and S are, to a high degree of approximation, functions of $U_L/\tau\alpha$ only. Furthermore, the variation of R and S with $U_L/\tau\alpha$ is very nearly quadratic.

The actual variables used in the GFL method, the same used in this investigation, are:

$$Y = \left[\frac{F_R\tau\alpha}{(F_R\tau\alpha)_o}\right]\left[\frac{L_o}{L}\right] A \quad (14)$$

$$R = A + BX + CX^2 \quad (15)$$

$$S = D + EX + FX^2 \quad (16)$$

where

$$X = (U_L/\tau\alpha) - 8 \quad (17)$$

L_o and $(F_R\tau\alpha)_o$ are reference values to which the user can default if he does not wish to consider values other than those used in this analysis. A through F are constants which are found by performing a multiple linear regression of R and S against values of X.

C. RESULTS

The aforementioned procedure, adapted to tropical climates, was used to establish the constants A through F in Equations 15 and 16 for three different system designs. These three designs are shown schematically in Appendix A. System 1 is a water heating system for non-potable water, suitable as a pre-heater for domestic and commercial loads such as floor-washing and clothes-washing. System 2 is similar to system 1 except that a heat exchanger is used. This system can thus provide potable water for domestic and commercial loads such as dish-washing and food processing. System 3 is an air-based system with pebble storage. Such a system can provide pre-heating of air which can be flown through drums for crop-drying and similar applications. For each of these designs, a set of constants was established for the following locations in Puerto Rico:

San Juan (North Coast)
Ponce (South Coast)
Mayaguez (West Coast)

In establishing these constants, a multiple linear regression technique was used. For liquid-based systems, the coefficient of multiple correlation was typically .99 which signifies a nearly perfect degree of fit. For air-based systems, this dropped to .77. This drop is due to the smaller ranges of U_L and $\tau\alpha$ values found in air collectors which allow for a larger variation in the regression coefficients. Because of the more consistent climate conditions in the tropics, the accuracies of this method against f-Chart were even higher than those reported by Lameiro for mainland United States cities. Typical accuracies were under 1% for f-values between 0.2 and 0.75, and 2% for f-values under 0.9. A correlation chart of the two method is found in Figure 1.

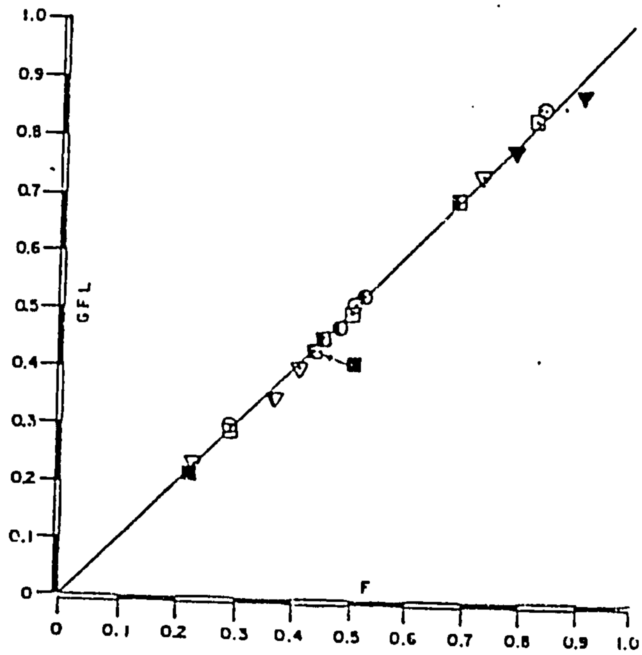

	LEGEND			
	LOCATION	SYSTEM 1	2	3
PUERTO RICO	MAYAGUEZ	⊙	◐	●
	PONCE	⊡	◧	■
	RIO PIEDRAS	▽	▽	▼

Fig. 1. Correlation of f-Chart and Modified GFL Methods for Systems 1, 2 and 3 for various Locations in Puerto Rico.

The constants A through F used in Equations 15 and 16, are listed in Appendix B. The differences in climatic regions in Puerto Rico are borne out in these constants with San Juan and Mayaguez appearing fairly similar and Ponce, in a much drier region, somewhat different.

The insolation data used to develop these constants was the data base maintained at CEER. This included four years of data for San Juan and Ponce, and six years of data for Mayaguez. The insolation data was transformed from a horizontal surface to a surface tilted at latitude, which was taken as 18° for Puerto Rico. The conversion method used was the well-known Liu-Jordan method in which the insolation is first broken up into beam and diffuse components. A discussion of this method is found in Liu (9). Modest and Soderstrom (3) discuss some sensitivity questions concerning this methodology in tropical regions.

Calculation of the Solar Fraction

The steps to be followed in using this analytical method are similar to those of the GFL method and are as follows:

1. From the collector efficiency curve, specify the collector parameters:

   $F_R\tau\alpha$ (dimensionless) from the intercept and

   F_RU_L (W/M² °C) from the slope.

2. Calculate the annual load required, L (GJ/yr). For liquid systems, include the expected tank losses given by Equation 11. For the designs used in this study, Equation 11 reduces to

$$L_{losses} = 1.58\ (UA)_{tank}\ (GJ/yr)$$

3. Select a collector area, A.

4. Calculate X and Y from

$$X = \frac{U_L}{\tau\alpha} - 8\ (W/M^2\,°C) \text{ and}$$

$$Y = \left[\frac{F_R\tau\alpha}{(F_R\tau\alpha)_o}\right]\left[\frac{1000}{L}\right] A\ (M^2),$$

   where $(F_R\tau\alpha)_o$ = 0.75 for liquid collectors. 0.50 for air collectors.

5. Calculate R and S from

$$R = A + BX + CX^2 \text{ and}$$

$$S = D + EX + FX^2.$$

6. Calculate the f-value from

$$f = 1 - \exp(-R\,Y - S\,Y^2).$$

To simplify this procedure even further a set of nomographs called PASO Charts have been developed as an aid in performing these calculations. They will be discussed later. In addition, numerical examples are included to demonstrate both the calculation method and the PASO Chart use.

D. AUTOMATED DATA PROCESSING

As has been mentioned earlier, the results of this method can be used for hand calculations. The establishment of the six constants of Equations 15 and 16, however, require the services of a computer. In order to enhance the technology transfer programs between CEER and Puerto Rico and the Caribbean region, the entire process for determination of these constants was automated and programmed on a microcomputer. The entire program run-time on an Apple II system with floppy disc drive is approximately 30 minutes per location and system design. This involves the running of five interconnected programs. However, once the actual data is entered interactively, the rest of the program flow is totally automated and involves no operator interaction. Therefore, someone not familiar with computers could easily run this entire method to establish the constants, assuming that the insolation data was available.

E. PASO CHARTS

Appendix C contains a series of nomographs, herein called PASO Charts, which allows the user a single-step solution, graphically, to obtain a good estimate of the f-value quickly. Each PASO Chart is site and system specific. The PASO Charts included in this report are for systems typically in use in tropical climates but they may be applied to any location in the world as long as the global insolation data is known.

Example Procedure for the Use of PASO Charts (See Figure 2)

Given: A solar hot water system as described by System 1 is located in Ponce, Puerto Rico. The total load of the system is 600 GJ/yr and the collector area is 200 M². Collector parameters are as follows:

$F_R\tau\alpha = 0.70$;

$F_RU_L = 4.0$ W/M² °C.

Procedure: The PASO Chart corresponding to System 1 is chosen and the solution worked directly on this nomograph by the following steps:

1. One may either calculate the ratio of the area/load or enter the two variables in the nomograph of lower left hand corner and read the corresponding value of area/load. Both the vertical (load) and horizontal (area)

scales may be multiplied by a factor of 10. Applying this factor, 600 GJ/yr enters at 60 and 200 m^2 enters at 20. At this intersection, follow up the corresponding diagonal line to the intersection of the (area/load) scale, which in this example corresponds to 0.33.

2. From this point, continue vertically upward until intersecting with the diagonal line corresponding to $F_R\tau\alpha = 0.70$ and then move horizontally to the right intersecting with the (AREA/LOAD) $F_R\tau\alpha$ scale at approximately a value of 0.23. Re-enter the nomograph at the right at that value and continue on a horizontal line.
3. Enter the lower nomograph at the two values corresponding to the collector parameters $F_R\tau\alpha = 0.70$; $F_RU_L = 4.0$. Follow the corresponding diagonal line at the intersection of these values until reaching the $\{(U_L/\tau\alpha)-8\}$ scale.

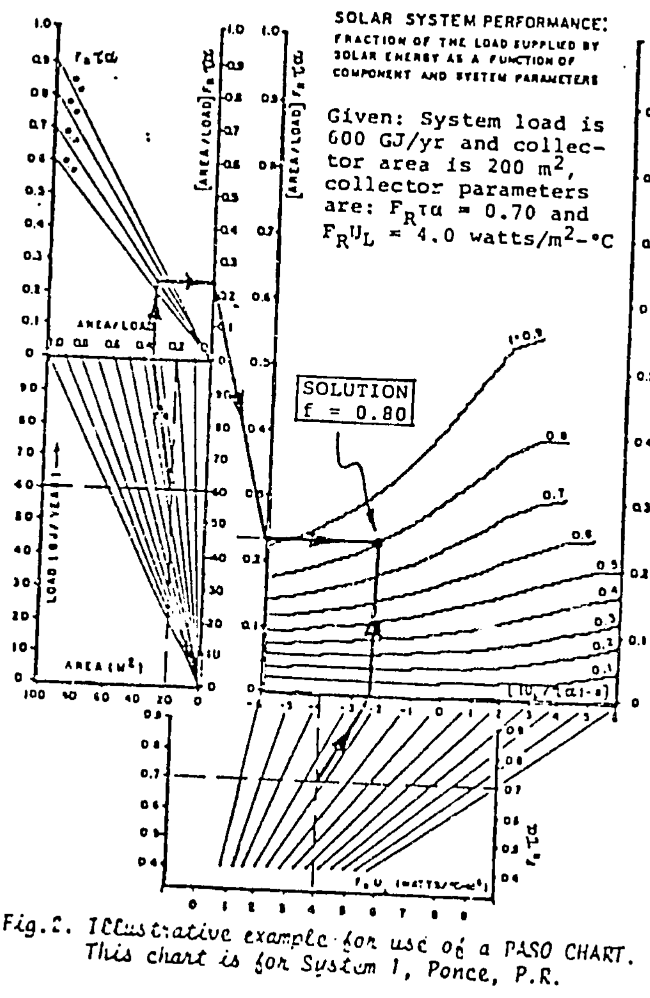

Fig. 2. Illustrative example for use of a PASO CHART. This chart is for System 1, Ponce, P.R.

4. Continue vertically until intersecting with the horizontal line described in the second part of step 2. At that intersection the value of f is interpolated as approximately .80.

To compare the results obtained by the previously described methods: f-Chart, modified GFL and PASO Chart, a series of combinations of systems, loads and collector parameters were run. Some examples of the results are tabulated in Table 1.

Location	System	A	L	A/L	F_RU_L	$F_R\tau\alpha$	$F_R\tau\alpha(A/L)$	$U_L/\tau\alpha-8$	f-Chart	Modified GFL	PASO Chart
	1	200	600	.33	4	.7	.23	-2.3	.803	.806	.80
	1	100	600	.17	6	.7	.12	.6	.440	.441	.44
P	2	200	600	.33	4	.7	.23	-2.3	.730	.736	.71
	2	100	600	.17	6	.7	.12	.6	.380	.381	.40
	3	200	600	.33	4	.5	.17	0	.800	.794	.80
	3	100	600	.17	6	.5	.09	4	.411	.410	.41
	1	300	1000	.30	4	.7	.21	-2.3	.631	.638	.63
	1	100	1000	.10	6	.7	.07	.6	.218	.214	.22
M	2	300	1000	.30	4	.7	.21	-2.3	.561	.567	.57
	2	100	1000	.10	6	.7	.07	.6	.181	.169	.18
	3	200	600	.33	4	.5	.17	0	.660	.664	.65
	3	100	600	.17	6	.5	.08	4	.320	.316	.31
	1	300	1000	.30	4	.6	.18	-1.3	.559	.564	.55
	1	100	1000	.10	5	.6	.06	2	.180	.169	.17
RP	2	500	1000	.50	4	.6	.30	-1.3	.677	.689	.68
	2	200	1000	.20	6	.6	.12	2	.273	.245	.25
	3	200	600	.33	4	.5	.17	0	.687	.650	.71
	3	100	600	.17	6	.5	.08	4	.337	.330	.31

Table 1. Comparison of Solar Fraction Values by Various Methods; P-Ponce, M-Mayaguez, RP-Rio Piedras.

F. CONCLUSIONS

The graphical methodology of PASO Charts developed in this project provides the designer a rapid method for both analysis and design. One can very easily compare the performance of the same solar system and components in various locations, given the PASO Chart for each location. It is expected that PASO Charts may be similarly developed for other systems and it is the intent of the authors to do so in the future.

ACKNOWLEDGEMENTS

The research for the preparation of this paper was performed at the Solar Energy Division of the Center for Energy and Environment Research (CEER), University of Puerto Rico, Mayaguez, Puerto Rico.

Dr. Nelson Pacheco-Santiago performed his research while he was on academic leave from the U.S. Air Force Academy, Colorado Springs, Colorado. He worked under the sponsorship of the Oak Ridge Associated Universities' Summer Faculty Research Program.

The authors would like to extend their appreciation to the scientific staff members of the Solar Division of CEER, especially to Dr. Angel M. López and Dr. Fernando E. Plá. Also, thanks are due to Miss Virginia L. Woodring, an Oak Ridge Associated Universities sponsored student, whose work in the summer of 1981 contributed to this project.

REFERENCES

1. Klein, S., Beckman, W., and Duffie, J. "A Design Procedure for Solar Heating Systems". Solar Energy. 18, 113-127, 1976.

2. TRNSYS, A transient simulation problem, Engineering Experiment Station Report No. 38. Solar Energy Laboratory, University of Wisconsin, Madison, Wisconsin.

3. Modest, M. and Soderstrom, K. "Thermal Design Criteria for Solar Hot Water Systems in Tropical Climates". Presented at the AZAA-ASME Thermodynamics and Heat Transfer Conference, Palo Alto, Calif., May 24-26, 1978.

4. Beckman, W., Klein, S., and Duffie, J. Solar Heating Design by the F-CHART Method. New York, John Wiley and Sons, 1977.

5. Lameiro, G., and Bendt, P. "The GFL Method for Sizing Solar Energy Space and Water Heating Systems". Report No. SERI-30, Solar Energy Research Institute, Golden, Colo.

6. Duffie, J. and Beckman, W. "Solar Energy Thermal Processes. New York, John Wiley and Sons, Inc., 1974.

7. Kreith, F. and Kreider, J. Principles of Solar Engineering. New York, McGraw-Hill Book Company, 1978.

8. Lunde, P. Solar Thermal Engineering, New York, John Wiley and Sons, 1980.

9. Liu, B. and Jordan, R. "The interrelationships and characteristic distribution of direct, diffuse, and total solar radiation". Solar Energy. 4, 1960.

APPENDIX A

Fig. A-1. Basic Solar Hot Water System

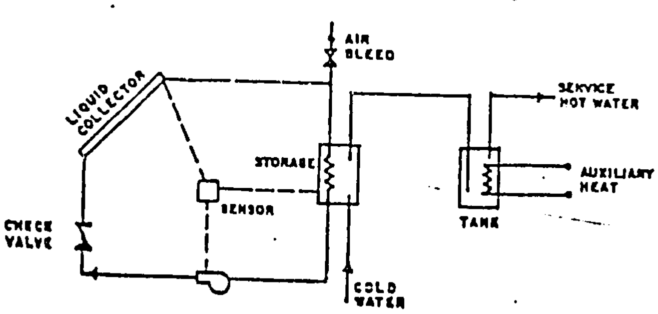

Fig. A-2. Basic Solar Hot Air System

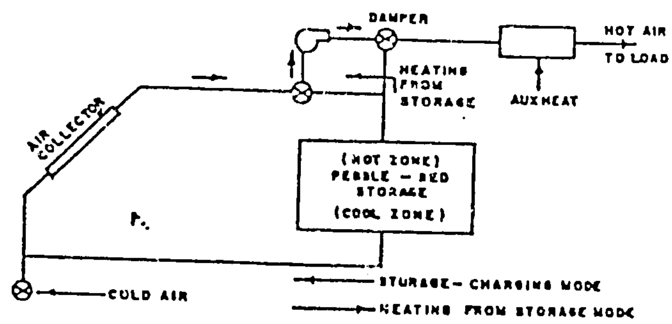

Table A-1. Reference values for system designs

	SYSTEM 1	DESIGN 2	3
DESIRED WATER TEMP (°C)	75	75	NA
WATER STORAGE CAPACITY (kg/m²)	75	75	NA
HEAT EXCHANGER EFFECTIVENESS	N/A	.75	N/A
AIR STORAGE CAPACITY (m³ PEBBLE/m²)	N/A	N/A	.25
AIR FLOWRATE THROUGH COLLECTOR (1/m²)	N/A	N/A	10.1
F_RU_L RANGE (w/m² °C)	3-9	3-9	3-6
$F_R\tau\alpha$ RANGE	.8-.9	.8-.9	.6-.75
REFERENCE $F_R\tau\alpha$	.70	.75	0.5
REFERENCE LOAD (GJ/yr)	1000	1000	1000

APPENDIX B

Table B-1. Modified GFL Constants for Puerto Rico

Location	Design #	A	B	C
Mayaguez Puerto Rico	1	2.74E-03	-3.01E-04	-3.21E-05
	2	2.14E-03	-3.59E-04	-3.05E-05
	3	2.03E-03	-2.10E-05	-1.80E-08
Ponce Puerto Rico	1	3.83E-03	-2.10E-04	-2.91E-05
	2	3.23E-03	-2.60E-04	-3.15E-05
	3	2.50E-03	-1.21E-05	-3.10E-06
Río Piedras Puerto Rico	1	2.96E-03	-1.84E-04	-3.19E-05
	2	2.37E-03	-3.38E-04	-3.21E-05
	3	2.12E-03	-2.78E-05	-2.45E-06

Location	Design #	D	E	F
Mayaguez Puerto Rico	1	2.22E-07	-5.92E-08	1.78E-07
	2	4.45E-07	2.40E-07	1.49E-07
	3	3.76E-06	-5.03E-07	1.93E-08
Ponce Puerto Rico	1	1.67E-07	-7.18E-07	2.24E-07
	2	1.99E-07	-7.41E-08	2.00E-07
	3	6.72E-06	-7.18E-u7	7.80E-09
Río Piedras Puerto Rico	1	1.67E-07	-1.74E-07	1.88E-07
	2	2.99E-07	1.42E-07	1.62E-07
	3	4.10E-06	-5.12E-07	2.93E-08

APPENDIX C

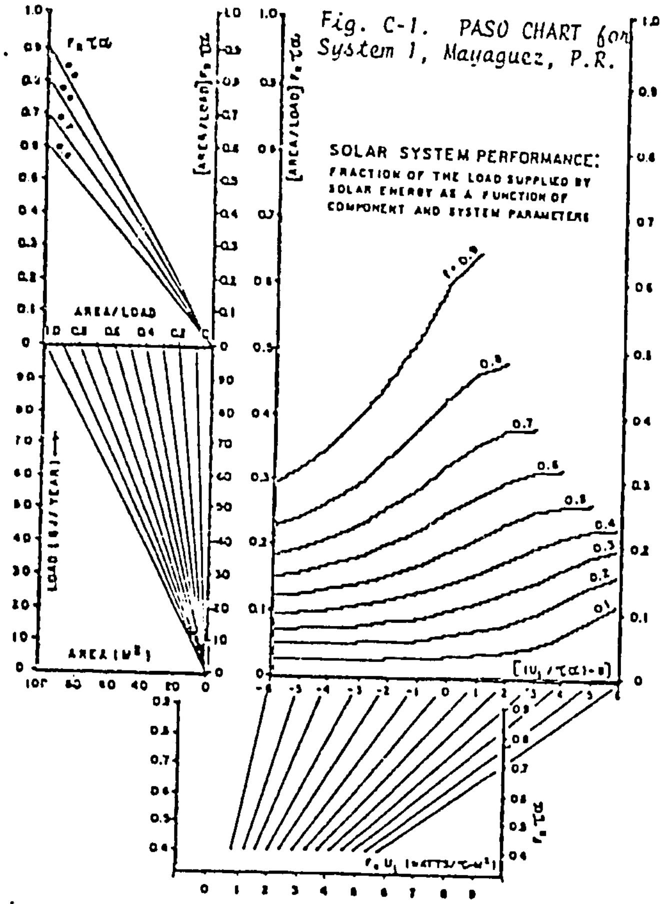

Fig. C-1. PASO CHART for System 1, Mayaguez, P.R.

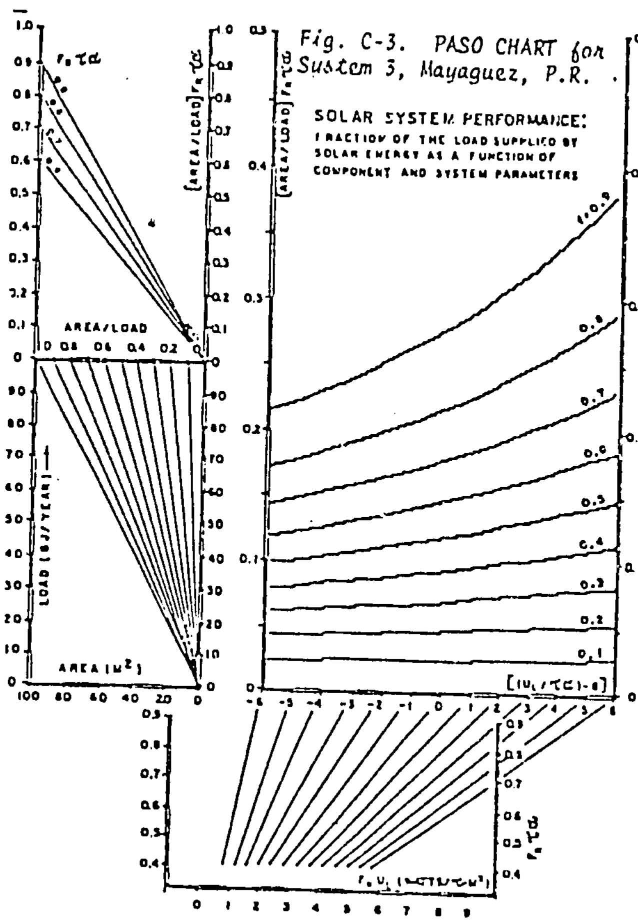

Fig. C-3. PASO CHART for System 3, Mayaguez, P.R.

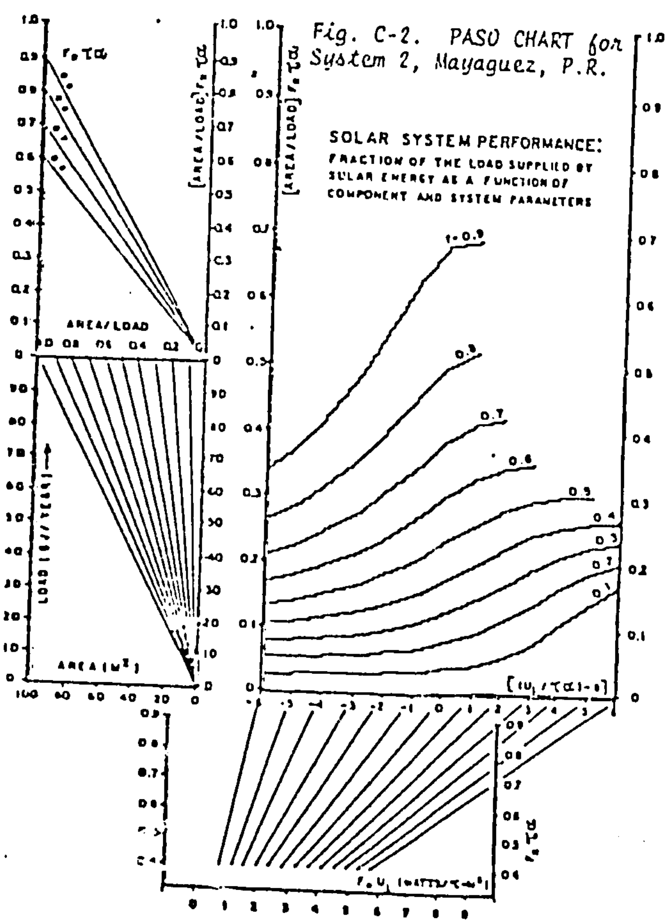

Fig. C-2. PASO CHART for System 2, Mayaguez, P.R.

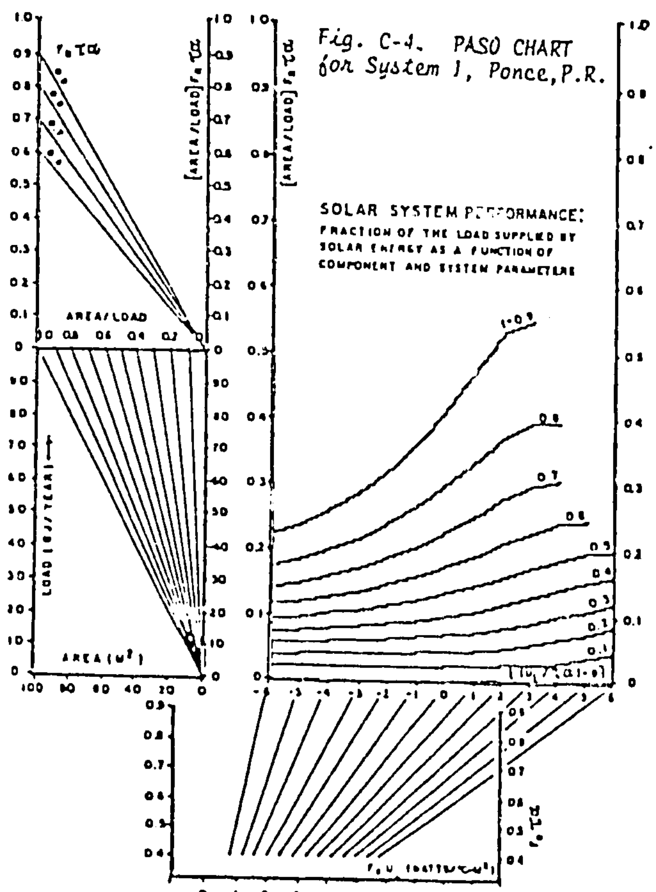

Fig. C-4. PASO CHART for System 1, Ponce, P.R.

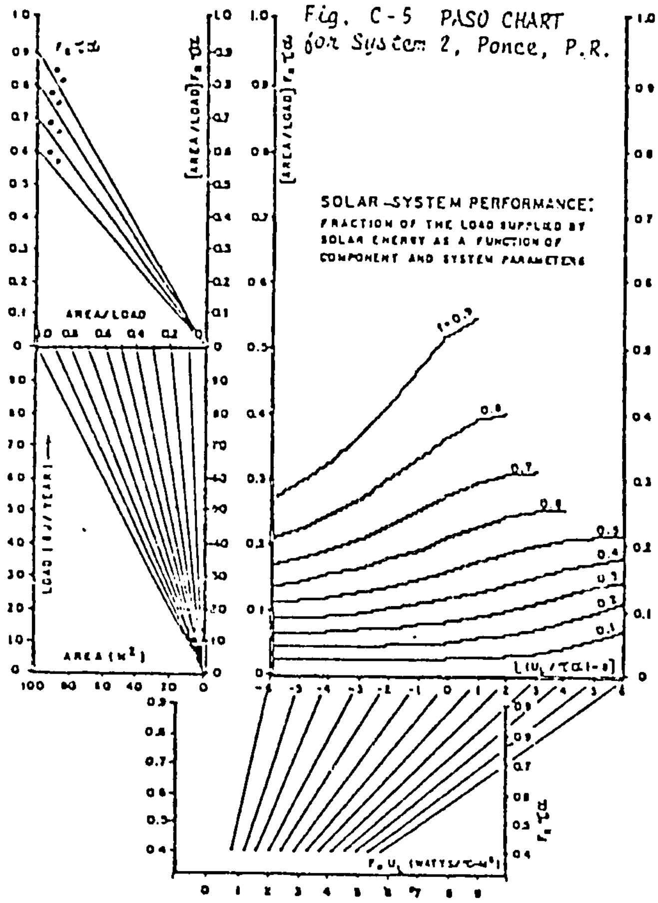

Fig. C-5 PASO CHART for System 2, Ponce, P.R.

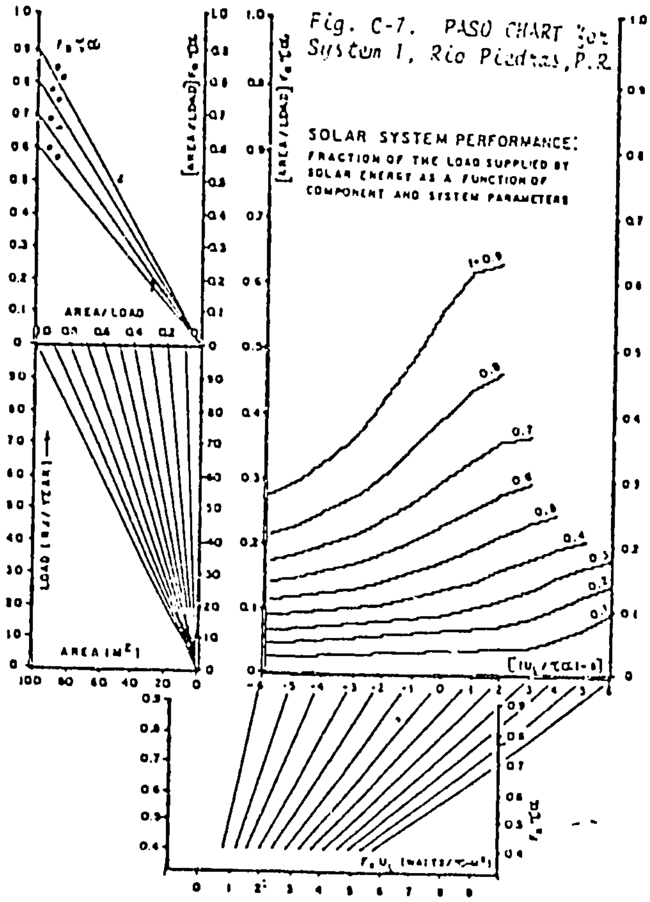

Fig. C-7. PASO CHART for System 1, Rio Piedras, P.R.

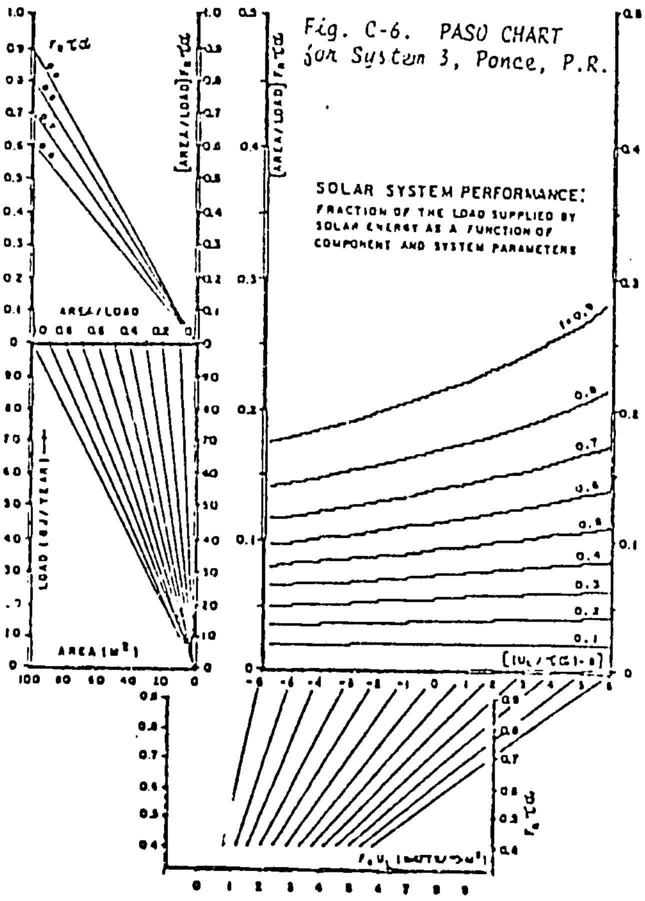

Fig. C-6. PASO CHART for System 3, Ponce, P.R.

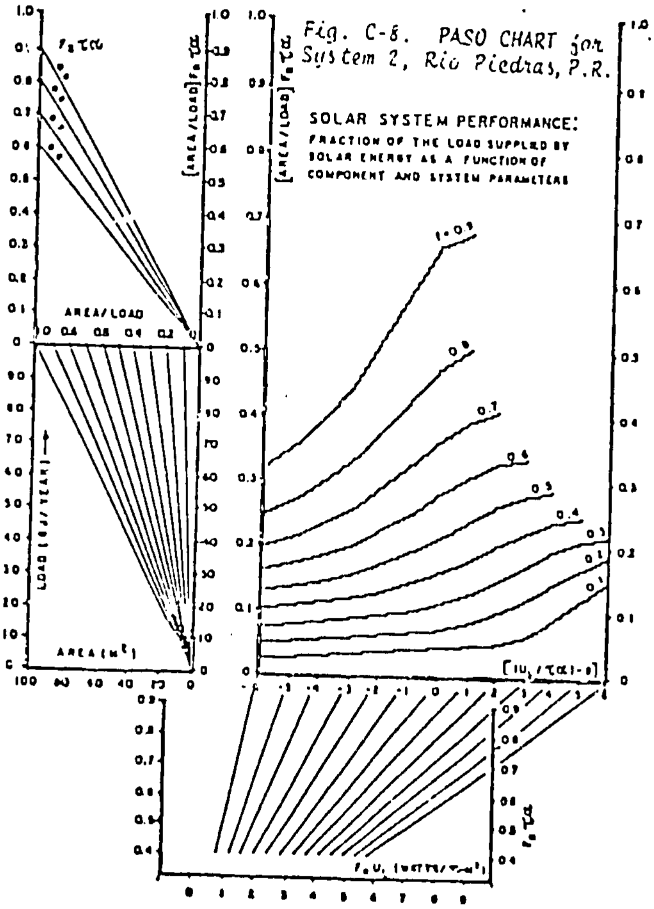

Fig. C-8. PASO CHART for System 2, Rio Piedras, P.R.

Thermal Performance of Flat Plate Solar Collectors By Generic Classification

By
James C. Huggins
David L. Block
Florida Solar Energy Center
300 State Road 401
Cape Canaveral, FL 32920

ABSTRACT

This paper presents thermal performance equations for glazed flat-plate solar collectors categorized by generic classification. The equations are derived from analyses of experimental test data collected for the past six years on tests of 270 solar collectors performed according to ASHRAE 93-77 procedures and leading to certification by the Florida Solar Energy Center (FSEC). Presented here are the straight line efficiency curves (intercept and slope values) for eight solar collector generic classifications based on the number of covers, the cover plate material, and the absorber plate coating used in their construction. The collector efficiency curves were developed from a computer search to establish a list by generic type and then from a statistical evaluation of each generic listing. Of the 270 test collectors, 170 were tested at FSEC and 100 were tested at other laboratories.

From the generic thermal performance equations presented, a solar designer is able to select a generic type of solar collector for a particular application and then to size and evaluate the performance of the selected system based on the developed generic thermal efficiency curve. This procedure allows the designer to make decisions on system performance and economics early in the design process and before selecting a specific collector manufacturer.

INTRODUCTION

The solar collector is the crucial component and critical design variable of a solar system -- it is the heart of the system. In designing solar systems, most designers first select a particular solar collector manufacturer and then structure the design around the selected manufacturer's collector. It would certainly be beneficial if, instead, the designer could base the solar system design upon the desired collector characteristics and then, when the design is complete, select the collector manufacturer on a competitive basis.

The purpose of this study was to provide discriminatory design criteria by determining the relationship between collector thermal performance and solar collector generic classifications. This relationship was established by analyzing ASHRAE 93-77 solar collector test results for 270 collectors in the solar collector certi[illegible]tion program at FSEC.

COLLECTOR THERMAL PERFORMANCE

The thermal performance of a solar collector is evaluated by establishing the collector's thermal efficiency curve. The thermal efficiency curve is obtained experimentally by performing tests on a collector according to the test procedures described by ASHRAE Standard 93-77, "Methods of Testing to Determine the Thermal Performance of Solar Collectors" (1).

In the ASHRAE procedures, a collector is tested under a prescribed set of conditions. Measurements are made of the flow rate, the temperature rise across the collector, and the incident radiation. The flow rate and the inlet water temperature are kept constant. The measured flow rate multiplied by the fluid specific heat and the measured temperature rise across the collector is the instantaneous energy collected by the collector. This quantity divided by the measured incident radiation is the instantaneous collector efficiency. Performing the test at several inlet water temperatures supplies additional data points.

The efficiency curve is derived from the data points by a least squares fit of the data points assuming either a first or second order efficiency curve. In this study, the first order efficiency curve based on the Hottel-Whittier-Bliss analytical model is used. This efficiency curve is described as follows:

$$\eta = F_R\ (\tau\alpha)_e - F_R U_L \frac{(T_i - T_{amb})}{I}$$

where

η = collector instantaneous thermal efficiency

F_R = collector heat removal factor

$(\tau\alpha)_e$ = effective transmittance-absorptance product

U_L = heat transfer loss coefficient [$W/(m^2 \cdot {}^\circ C)$ or $Btu/(hr \cdot ft^2 \cdot {}^\circ F)$]

$\frac{(T_i - T_{amb})}{I}$ = efficiency fluid variable consisting of inlet fluid temperature minus ambient air temperature divided by incident radiation.

The coefficients $F_R(\tau\alpha)_e$ and $F_R U_L$ (intercept and slope of efficiency curve, respectively) are functions of the collector's generic characteristics -- the materials, components and/or configuration used in the manufacture of the collector. Each collector manufacturer constructs each collector model with a unique combination of generic characteristics. The ASHRAE 93-77 tests thus produce, for each collector test, a combination of distinct coefficients $F_R(\tau\alpha)_e$ and $F_R U_L$ (intercept and slope).

The intercept and slope coefficients for flat plate collectors are, in general, a function of seven generic characteristics which are briefly described as follows:

1. Number of cover plates. The majority of collectors certified in the FSEC program have one cover plate. Double glazed, two-cover plates, are more commonly used in colder climates.
2. Cover plate material. The transparent cover plate materials commonly used are:
   Glass, the most widely used glazing material with high transmittance and long-term durability.

Glass is fragile and heavy. Because iron in glass reflects the sun's radiation, a low iron content in glass is desirable. The iron content of glass was not considered in this study.

Fiber reinforced plastic (FRP), the second most widely used material. FRP is not as optically efficient or as durable as glass but it is lightweight and less costly.

Thin film plastics with the trade names of Tedlar, Mylar, Teflon and Lexan. These have high transmittance qualities and are inexpensive. However, they do not retain heat very well and have a tendency to deteriorate under ultra-violet exposure.

3. Absorber Plate Coating. Common coatings are: Selective surface coatings such as black chrome, black nickel and copper oxide which have high absorptance and low emmitance properties. Selective coatings are more expensive than paint. The infrared emissivity of these surfaces is below 0.2.

   Moderately selective surface coatings, special paints which have moderately selective surface properties. The emissivity of these surfaces range from 0.2 to 0.7.

   Flat black paints, non-selective, high heat resistant paints that are inexpensive but which do not possess the emittance qualities of a selective surface. The emissivity of these surfaces range from 0.7 to 0.98.
4. Absorber material Type. Absorber materials are copper, aluminum and stainless steel. These materials may be used in combinations of tubes and fins, or integral tubes in plates.
5. Absorber configuration. The absorber may be configured with parallel pipes, series or serpentine pipes, a parallel and series combination, or plate flow.
6. Enclosure type. The frame holding the collector components may be either metallic or non-metallic.
7. Insulation materials. The insulation materials used to keep heat from escaping from the back and sides of the collector are fiberglass, foam, or a combination of both.

Presented in this paper are statistical mean and standard deviation values of the coefficients $F_R(\tau\alpha)_e$ and F_RU_L as a function of these collector characteristics within generic collector categories.

FSEC SOLAR COLLECTOR PROGRAM

The Florida Solar Energy Center (FSEC) has been setting standards for, testing, and certifying solar collectors since 1977 when the Florida Legislature passed a statute (Florida Statute 377.705) requiring these activities. In 1980 the certification program became mandatory for all collectors manufactured and/or sold in the state.

The present certification program uses ASHRAE 93-77 as the test method and follows the certification procedure developed by FSEC (2,3). This certification program is also equivalent to the procedures set by the Interstate Solar Coordination Council (ISCC). The current sequence of tests is as follows:

1. Receiving inspection.
2. Static pressure test.
3. Thirty-day exposure test.
4. Thermal shock/water spray tests.
5. Thermal shock/cold fill test.
6. Static pressure test.
7. Collector time constant determination test (ASHRAE 93-77)
8. Post exposure thermal performance test. (ASHRAE 93-77)
9. Incident angle modifier test. (ASHRAE 93-77)
10. Disassembly and final inspection.

The results of an FSEC certification are published in several forms. A complete test report is issued by the testing laboratory for each test that is conducted. For each FSEC certification, a Summary Information Sheet is published to give the consumer a brief description of the collector, the thermal performance equations, and a thermal performance rating.

From the inception of the certification program, FSEC has certified 520 flat-plate collectors representing 145 manufacturers. Of the 520 collectors, 120 are no longer being manufactured, thus, there are 400 current certifications. Of the 400 current certifications, 364 are for glazed collectors and 36 are for unglazed collectors.

RESULTS

This study addresses six years of test results on glazed collectors for which ASHRAE 93-77 test results are available. Presented in Table 1 are the number of collectors tested during each of the six years.

TABLE 1. Number of Collectors Tested Per Year

Year	Number of Glazed Collectors
1977	15
1978	52
1979	37
1980	68
1981	55
1982	43
Total	270

Of the 270 tested collectors, 170 were tested at FSEC and 100 were tested by other testing laboratories. The apparent discrepancy between the 520 and 270 numbers can be accounted for by the fact that some collectors are certified under more than one manufacturer's name and many collector models of differing surface areas are certified through a single collector test. The 270 total represents a listing of only the collectors on which an ASHRAE 93-77 test was performed. All evacuated tubular, unglazed, and triple-glazed collectors were excluded from the list.

In presenting these collectors and tests, the following general comments are made:

- The weather conditions under which the ASHRAE tests were performed were variable by location (Florida, Arizona, California, etc.). Tests were done during all months and days of the year. All weather conditions did prescribe to the limits of ASHRAE standards.
- The collector tests represent performance easurements made before exposure testing and after exposure testing. Prior to March 1981, collector performance was determined by tests conducted only before exposure testing. After March 1981, collector performance was determined by tests conducted after 30 day exposure. Both conditions are used herein.
- The collectors represent those of manufacturing companies both active and defunct, from small backyard operations to large corporations.

It is believed that FSEC, because it is both a state agency and a research and development organization, is unique in having test results for such a large number of collectors. These unique qualifications made this study possible.

The study began approximately one and one-half years ago when FSEC started a project to place all certified solar collector data on the FSEC computer. This project was then accomplished by analyzing the tested collectors by generic classifications. When a listing by generic type had been compiled, calculations were made to determine the mean and standard deviation of the collector efficiency curve (intercept and slope) and of the collector incident angle modifier.

Before considering the results of this study, a comment needs to be made concerning the accuracy of ASHRAE test procedures. The results presented here are based on the ASHRAE 93-77 test procedures. Consequently, errors in measurements built into the AHSRAE procedures will also appear in the results presented. The errors associated with ASHRAE test procedures have been thoroughly discussed by Streed and Waksman (4) and Lumsdaine (5). Streed and Waksman found an average error of approximately ±2.4% of the measured value in the intercept obtained by a number of test laboratories under a wide range of conditions. The variation in the slope of the performance equations was found to be ±8.4%. Reference is made to these publications for further discussion of measurement errors and the subsequent accuracy or inaccuracy of the test results.

The first analysis was to construct a listing of collectors according to the seven collector characteristics described in the Collector Thermal Performance section.

This produced a listing of 116 different collector characteristic combinations. The largest number of collectors in a separate list was 30, and the second largest number of collectors was 15. The analysis also produced 74 combinations with only one collector and 18 combinations with only two collectors. Because more than half the combinations had only a single collector, the results from using seven generic types were not statistically significant and were not used.

The seven generic types were then reduced t four -- the number of cover plates, the cover plat material, the absorber coating and the absorber type Table 2 presents a listing of the number of collector for each generic type as a result of this analysis.

TABLE 2. Number of Collectors per Generic Type for the Four Generic Classifications

Number of Collectors per Generic Type	Number of Generic Types	Total Collectors
1	37	37
2	9	18
3	5	15
4	3	12
5 or above	8	188
		270

The results of Table 2 show 46 generic types with only one or two collectors. However, it is important to observe that 188 of the 270 collectors (70 percent) are represented by eight generic types.

Presented in Table 3 is a list of the eight generic types in which there are five or more collectors. The first three columns specify the generic type, the fourth column shows the number of collectors in each category, and the final columns list the statistical values for intercept and slope. Under the intercept and slope columns, the values given are the mean, the standard deviation, and the maximum and minimum values. To show the scatter distribution of a particular generic type, the 26 collectors comprising the single cover, FRP, copper tube and fin, flat black paint classification were plotted and are presented in Figure 1. The dashed line represents the mean intercept and slope.

Table 3. Collector Intercept and Slope by Generic Type.

GLAZING & COVER MAT'L	ABSORBER MAT'L & TYPE	ABSORBER COATING	NUMBER OF COLLECTORS	INTERCEPT				SLOPE (Btu/hr °F ft²)			
				MEAN	STANDARD DEVIATION	MAX	MIN	MEAN	STANDARD DEVIATION	MAX	MIN
Single Glass	Copper Tubes and Fins	Flat Black Paint	47	67.2	5.0	75.6	56.2	-115	14	-72	-140
Single Glass	Copper Tubes and Fins	Moderately Selective	9	73.0	3.6	78.0	68.0	-112	11	-100	-130
Single Glass	Copper Tubes and Fins	Selective Surface	58	71.7	3.3	81.4	62.0	-83	11	-61	-124
Single Glass	Copper Tubes and Aluminum Fins	Flat Black Paint	22	69.1	6.0	84.6	58.8	-116	12	-96	-138
Single Glass	Copper Sheet Integral Tubes	Selective Surface	6	70.5	5.1	77.4	62.0	-89	17	-71	-120
Single FRP	Copper Tubes and Fins	Flat Black Paint	26	61.9	5.5	70.5	53.0	-117	15	-86	-147
Single FRP	Copper Tubes and Aluminum Fins	Flat Black Paint	11	57.1	6.2	65.5	48.1	-114	10	-102	-132
Double Glass	Copper Tubes and Fins	Flat Black Paint	9	59.7	6.7	66.1	44.4	-84	9	-69	-95

solar collector and to perform system sizing and analysis. With this information, system performance decisions can be made early in the design process, and the collector options can be evaluated before a specific manufacturer is selected.

Using the results of Table 5 the effects of different variables can be evaluated. Figure 3 shows a comparison of selective vs. moderately selective vs. flat black paint absorber surface for single glass cover plate collectors. As expected, the selective surface shows better performance. Figure 4 presents a comparison of glass vs. FRP cover plates and selective vs. non-selective surfaces. As expected, glass and selective surfaces perform better. Finally, Figure 5 shows a comparison of single vs double glazings for glass covered collectors. This result is also as expected.

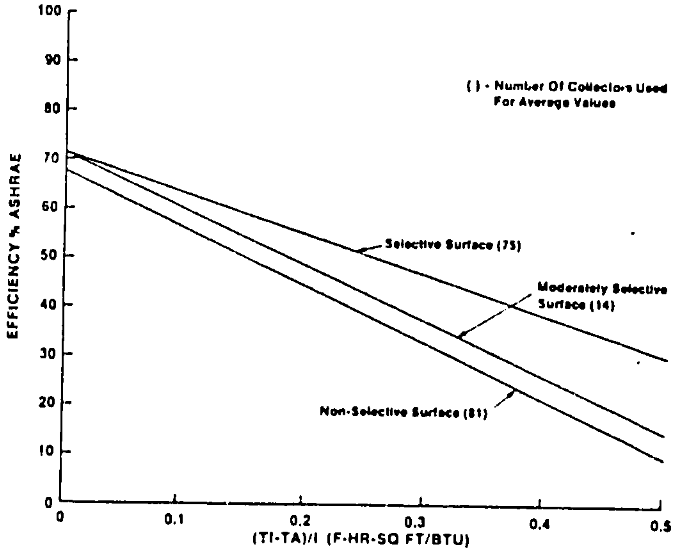

Figure 5. Comparison of Average Efficiency Curves for Absorber Coatings and Glass Cover Plates.

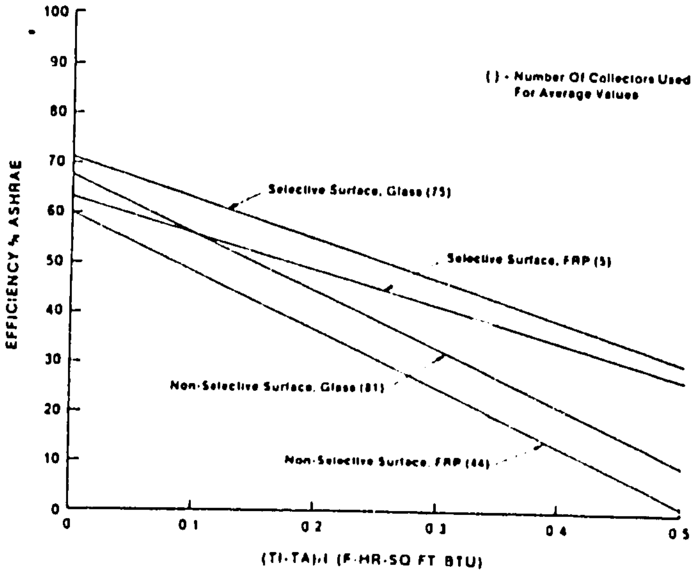

Figure 4. Comparison of Average Efficiency Curves for Selective vs Non-Selective Absorber Coatings and for Glass vs FRP Cover Plates

CONCLUDING REMARKS

Results have been presented which give thermal peformance equations for flat-plate solar collectors by generic classification. The final classification considers the number of cover plates (either single or double), cover plate material (either glass or fiber reinforced plastic), and absorber coating (selective, moderately selective or flat black paint). From these results, the mean, standard deviation, maximum and minimum values of the intercept and slope of the linear collector performance curve and of the incident angle modifier are determined for each generic classification.

The results are based entirely upon the performance analysis of 270 solar collectors tested according to ASHRAE 93-77 procedures and certified by the Florida Solar Energy Center. The results represent six years of FSEC collector testing activities.

Using the generic thermal performance equations, designers can size and evaluate the performance of a solar system by generic collector type. This procedure should lead to more efficient system design and more competitive procurement of collectors. Also, these performance characteristics may be useful in comparing collectors within the generic type or determining if a particular collector is better than average for that generic type.

Figures based on the derived results are also presented which compare selective vs. non-selective surfaces, glass vs. fiber reinforced plastic cover plates, and single vs. double glazing.

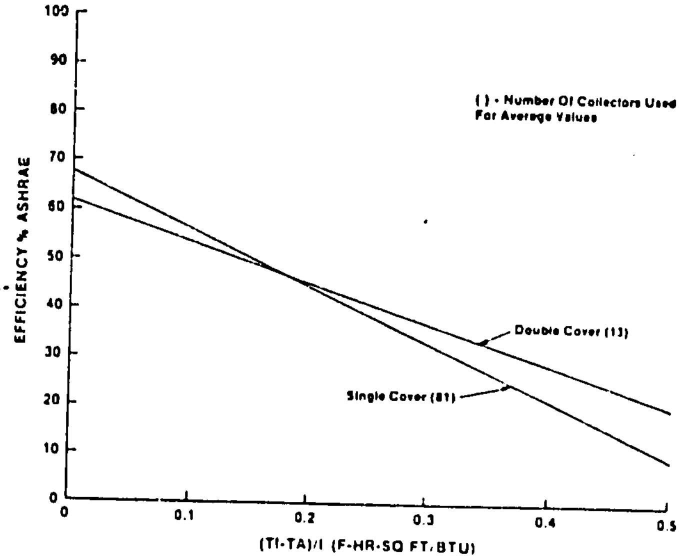

Figure 5. Comparison of Average Efficiency Curves for Single vs Double Glass Cover Plate Collectors with Flat Black Paint.

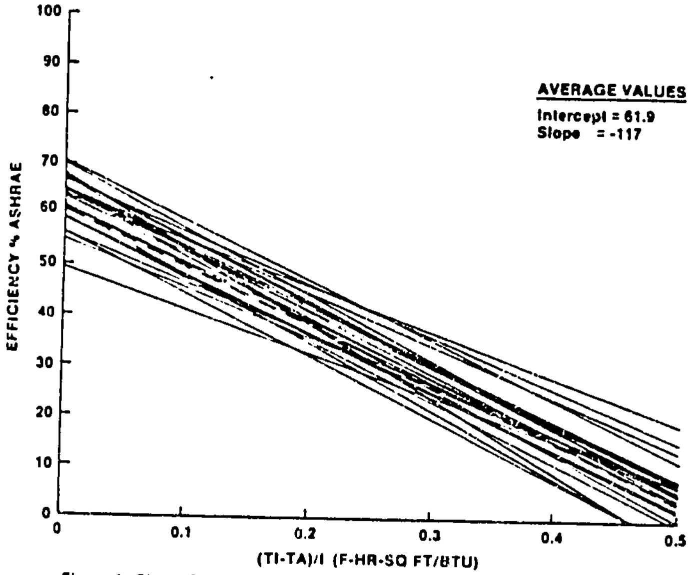

Figure 1. Plot of 26 Collector Efficiency Curves and the Average Efficiency Curve for the Generic Classification of FRP Cover, Flat Black Paint and Copper Tube and Fin Absorber.

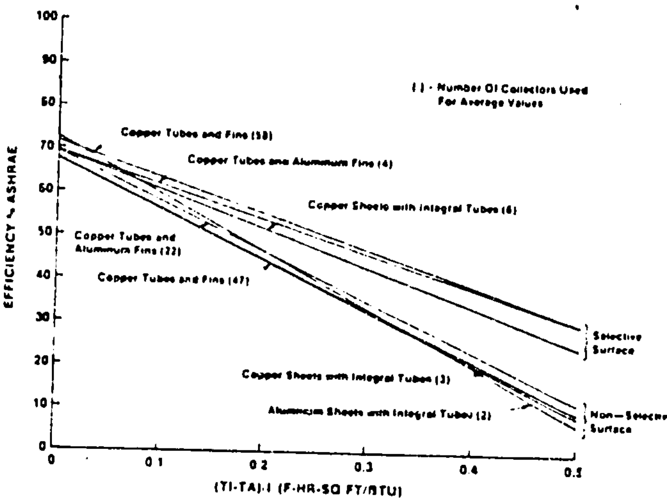

Figure 2. Comparison of Average Efficiency Curves for Absorber Type and for Selective and Non-Selective Surfaces and Glass Cover Plates.

Figure 2 presents a graphic comparison of the effects of different absorber types used in single-glazed, glass-covered collectors with selective and flat black paint surfaces. The comparison indicates that the absorber type is not a major factor in the generic classification. Thus, the absorber type was eliminated from the generic list which was then reduced to three characteristics -- the number of covers, the cover plate material and the absorber coating.

Table 4 presents the results of the analysis for these three generic types.

The three generic types represented by Table 4 are the minimum acceptable if the results are to be meaningful. Table 5 presents a listing of the results for the three generic types and for cases with five or more collectors per generic type. These results agreed well with those obtained by Kirkpatrick (6).

TABLE 4. Number of Collectors per Generic Type for the Three Generic Type Classifications

Number of Collectors per Generic Type	Number of Collectors	Total Number of Collectors
1	7	7
2	3	6
3	2	6
4	0	0
5	1	5
6 or above	6	246
		270

Note that the Kirkpatrick results are for 117 collectors tested as part of the DOE test program and do not separate the collectors by glazing materials as was done for this study: the Kirkpatrick results only consider the number of glazings and the absorber coating.

Table 5 presents the primary results of this study. These results allow a designer to select the thermal performance equation for a generic type of

Table 5. Collector Intercept, Slope Incident Angle Modifier by Generic Type.

GLAZING & COVER MAT'L	ABSORBER COATING	NUMBER OF COLLECTORS	INTERCEPT				SLOPE (Btu/hr °F ft²)				INCIDENT ANGLE MODIFIER			
			MEAN	STANDARD DEVIATION	MAX	MIN	MEAN	STANDARD DEVIATION	MAX	MIN	MEAN	STANDARD DEVIATION	MAX	MIN
Single Glass	Flat Black Paint	81	67.6	5.6	84.6	51.3	-116	13	-72	-140	-0.11	0.05	-0.02	-0.25
Single Glass	Moderately Selective	14	71.4	4.6	78.0	59.7	-112	14	-89	-141	-0.13	0.06	-0.05	-0.23
Single Glass	Selective	75	71.2	4.5	81.4	62.0	-82	13	-61	-124	-0.14	0.10	-0.04	-0.23
Single FRP	Flat Black Paint	44	60.0	6.2	70.5	48.1	-117	15	-86	-157	-0.12	0.07	-0.05	-0.20
Single FRP	Moderately Selective	6	59.6	6.6	66.4	51.6	-115	14	-100	-130	-0.12	0.01	-0.10	-0.14
Single FRP	Selective	5	63.2	1.7	64.9	61.4	-73	7	-66	-79	-0.14	0.01	-0.13	-0.15
Double Glass	Flat Black Paint	13	61.9	6.7	70.6	44.4	-84	9	-69	-95	-0.11	0.06	-0.05	-0.20

REFERENCES

1. "Methods for Testing to Determine the Thermal Performance of Solar Collectors, Standard 93-77," American Society of Heating, Refrigeration and Air Conditioning Engineers, Inc., 345 E. 47th St., New York, NY 10017.

2. "Test Methods and Minimum Standards for Solar Collectors," FSEC 77-5-R80, Cape Canaveral, FL 32920.

3. "Operation of the Collector Certification Program," FSEC 77-6-R80, Cape Canaveral, FL 32920.

4. Streed, Elmer and Waksman, David. "Uncertainty in Determining Thermal Performance of Liquid Heating Flat Plate Solar Collectors," National Bureau of Standards, Tech Note 1140, April 1981.

5. Lumsdaine, Edward. "On the Testing of Solar Collectors to Determine Thermal Performance," Proceedings of ISES Annual Conference, Denver, CO, June 1978.

6. Kirkpatrick, D.L. "Solar Collector Data Manual," Final report to the Solar Energy Research Institute, Golden, CO, July 1981.

Performance of a Plastic Suspended Screen Solar Air Heater

by

K. V. Chau, C. D. Baird, and L. O. Bagnall*

Abstract:

A 104 m^2 inflated plastic air heater with black plastic suspended screens as extra absorbing surfaces was tested and compared against an air heater without the screens. There was a definite improvement in collector performance with the addition of one or two suspended screens. The increase in efficiency more than offsets the cost of the screens.

1. Introduction

In agriculture, there are many applications requiring heated air at relatively low temperatures. Traditionally, the heat source for these applications are usually natural gas or LP gas, but recent concern regarding the availability of these non-renewable energy sources has promoted new interests in the use of solar energy for at least some of these applications.

Several investigations have evaluated the use of solar energy for crop drying (1,2,3). Collectors of different designs, with flat or corrugated plates, with or without a plastic glazing have been studied (4,5,6,7). It has also been shown that screens could serve as efficient absorbers (8).

The objective of this work is to develop a low-cost solar air heater capable of moderate air temperature rises that can be used f

*Assistant Professor, Associate Professor, Associate Professor, Department of Agricultural Engineering, University of Florida, Gainesville, Fl 32611.

crop drying and other applications requiring heated air. The collector under investigation is basically a plastic flat plate collector, with one of two black plastic screens suspended between the clear plastic glazing material and the black plastic absorber. The suspended plastic screens are woven mesh screens. Behind the black plastic, there is a layer of insulation board to reduce heat losses. The plastic mesh screen and the black plastic serve as the absorbing, heat transfer surface. The addition of the plastic mesh screen increases the heat transfer area and the convective heat transfer coefficient between the absorber and the air. Since the heat transfer is increased, the temperature of the absorber is reduced and heat losses to the surroundings are consequently less. Also, by operating at lower temperature, the useful life of the plastic absorber is extended. This type of plastic collector should be more efficient than the conventional plastic air heater, especially when relatively high temperature rises are needed. This collector is intended for use in solar grain drying; however, it can also be adapted for any use requiring heated air.

2. Experimental Facilities

The Collector

The experimental solar collector was 3.66 m wide by 29.26 m long (Fig. 1). It was constructed primarily from plastic materials and wood. The collector floor was made of urethane insulation boards, 32 mm thick, with aluminum foil on both sides. The insulation boards were supported by 3 mm x 10 mm boards spaced 1.20 m apart, and laid on the ground. The collector was covered with 0.15 mm clear polyethylene sheet. Between the black plastic and the clear plastic, there were either one to two black polypropylene screens (greenhouse shade cloth) depending on the tests. The sides of the collector were

25 mm x 203 mm boards with an aluminum locking device for mounting the clear plastic. The locking device was of the type commonly used in plastic greenhouses and consisted of a fixed base rail and an insert, that fitted inside the base rail to hold the plastic in place. At each end of the collector, there was a metal plenum to guide the air flow.

Originally, the collector was built so that it could be tilted to collect more energy, but the collector was later changed to lay flat on the ground all the time. It was felt that because of the low latitude (29°N) of Gainesville, Florida, no significant gain could be expected by tilting the collector, and there would be increased costs to make the collector sufficiently sturdy to withstand its own weight and the strong wind occasionally experienced in Florida.

Instrumentation

The air was delivered at the inlet end of the collector by a vaneaxial fan. A differential measuring flow element connected to an electronic differential pressure indicator was used to measure air flow rates through the collector.

Two grids of shielded thermocouples measured the inlet and outlet temperatures of the collector. The thermocouples at the inlet were placed after the fan so that the heat added by the fan did not enter in the calculation of the efficiency. Thermocouples were also placed at four stations along the length of the collector to measure the temperatures of the black plastic, the plastic screen, and the air stream. At each station, there were fo[illegible] thermocouples spaced across the width of the collector for each of the temperatures measured; i.e.; four thermocouples under the black plastic, four thermocouples woven into the plastic screen, and four shielded thermocouples in the air stream 3 inches above the collector floor.

Solar radiation was measured with a 72-junction thermopile pyranometer and also with a mechanical pyranograph for quick references. Ambient temperatures were recorded by a shielded thermocouple placed in a weather shelter.

The thermocouples and pyranometer outputs were recorded by a data acquisition system that scanned every five minutes and recorded the data on magnetic tape.

3. Results and Discussion

Collector performance and grain drying tests were conducted in June, September, October, November, December 1976, in late May and early June 1977, and in April and May 1978. The range of air flow rates tested was from 0.30 to 1.03 $m^3\ min^{-1}\ m^{-2}$ of collector surface. During this period, the collector was also used to dry corn and soy bean in two 100-bushel bins. During all tests, the collector was flat on the ground, with an East-West orientation. Collector tests were conducted only during bright and calm days to reduce the effect of wind.

Collector with One Suspended Screen, 47% Shading

The term 47% shading indicates that the screen has 47% opaque area and 53% open area. During the months of September, October, November, and December 1976, the collector with one suspended plastic screen (47% shading) was tested under various air flow rates and solar radiation intensities.

In the evaluation of the performance of solar collectors, the following simplified energy balance equation is usually used:

$$Q_c = aQ_s - U(\overline{T}_c - T_a) \quad (1)$$

where

Q_c = useful energy collected

a = product of the transmissity of the glazing and the absorptivity of the absorber plate

Q_s = available solar energy falling on the collector

U = overall heat loss coefficient

$\overline{T}_c$ = average fluid temperature in the collector

T_a = ambient temperature

The collector efficiency can be expressed as :

$$E = \frac{Q_c}{Q_s} = a - \frac{U(\overline{T}_c - \overline{T}_a)}{Q_s} \quad (2)$$

If the collector efficiency is plotted against the normalized temperature rise $\frac{\overline{T}_c - \overline{T}_a}{Q_s}$, one would get a straight line, the slope of which is equal to the overall heat loss coefficient U, and the y-intercept is a, the product of the glazing transmissivity and the absorber plate absorptivity.

Figure 2 shows a plot of the collector efficiency versus the normalized temperature rise. The equation for the straight line of best fit is:

$$E = 0.46 - 15.04 \frac{\overline{T}_c - \overline{T}_a}{Q_s} \quad (3)$$

with a correlation coefficient of 0.65 which is very low. The temperatures are in ^oC and the solar radiation Q_s is in W/m^2. There is quite a lot of scatter of the data points. Equation (2) assumes that the collector efficiency is not affected by the fluid flow rate. But it was found that with the suspended plastic screen collector, the efficiency is definitely affected by the air flow rate, probably due to the change in the heat transfer coefficient of the screen. To illustrate the dominant effect of the air flow rate, all the data used in Figure 2 were used to plot efficiency versus air flow rate as shown in Figure 3. There is much less scattering of the data points. Using the least squares method, an equation relating efficiency (E) and air flow rate (FR) was found to be:

$$E = -0.384(FR)^2 + 0.733(FR) \qquad (4)$$

with a correlation coefficient of 0.93. The air flow rate is expressed in cubic meters per minute per square meter of collector area.

Figure 3 shows that the efficiency definitely varies with air flow rates. As the air flow rate is increased, first, the operating temperature of the collector is decreased and heat losses are thus reduced; secondly, the convective heat transfer coefficient between the air and the plastic screen is increased, making the heat transfer more efficient. Because the back of the collector is insulated, most of the heat losses are radiative losses from the absorber and some convective losses through the clear plastic. Since radiative losses are related to the 4th power of the absolute temperature of the absorber, the reduction of the absorber temperature is very significant.

In order to include the effect of radiation on the collector efficiency, an empirical equation relating efficiency, air flow rate and radiation was determined:

$$E = -0.463(FR)^2 + 0.80(FR) - 3.5\ 10^{-5}(Q_s) \qquad (5)$$

where Q_s denotes the solar radiation in W/m^2. This equation shows that radiation has a very slight effect on efficiency. The collector is a little more efficient at low radiation rate because the operating temperature of the collector is lower and thus heat losses are lower.

Since the air temperature rise across the collector is of special importance for design purposes, the data were used to find the relationship between the temperature rise TR, the air flow rate FR and the radiation rate Q_s:

$$TR = -24.76(FR)^2 + 11.84(FR) + 0.0476(Q_s) \qquad (6)$$

As expected, it was also found that the collector efficiency decreases later in the year because the collector was not tilted. For the early part of December 1976, the average efficiency at 0.67 $m^3\ min^{-1}\ m^{-2}$ was 28.7% as compared to an average of 31.7% during the October, November period.

Figure 4 shows typical temperature profiles along the length of the collector. The air stream temperature in Figure 4 is the air temperature at a level 7.5 cm above the black plastic. It is not the mixed average air stream temperature but it does give an indication of the air temperature variation along the length of the collector. Attempts were made to relate this temperature with the mixed average air stream temperature by experimentally determining the vertical air temperature profile from the collector floor to the clear plastic but the results were too inconsistent to be meaningful. The black plastic and the plastic screen temperatures are usually fairly close to each other, with the black plastic temperature normally higher than the screen temperature around solar noon, but the screen temperature becomes higher than that of the black plastic later in the afternoon. At noon, a larger percentage of the incoming radiation is let through the screen openings onto the black plastic, and later in the afternoon when the sun is low, the screen obstructs more of the incoming radiation.

Comparison tests for Collectors With and Without the Suspended Screen

All the efficiencies reported here are all-day average efficiencies. Figure 5 shows the efficiencies of collectors with and without the suspended plastic screen. The data were from the tests performed in late May and June 1977.

A more meaningful comparison between the two types of collectors can be made by comparing their performance as a function of air temperature rise since the temperature rise is the principal parameter in the use of air heaters. Figure 6 shows the efficiency versus temperature rise curves at two radiation levels, 700 W/m^2 and 475 W/m^2. These curves are constructed from the curves in Figure 5.

Figure 6 shows that the difference in efficiency between the two types of collectors is even larger than is indicated in Figure 5. This is because the collector with the suspended plastic screen, being more efficient, operates at a higher air flow rate than the collector without the screen for any given temperature rise. The higher air flow rate in turn increases the efficiency even more as indicated by Figure 5.

From Figure 6, at a radiation rate of 700 W/m^2 and a temperature rise of 15°C, the collector efficiency is 41% with the suspended screen and 30% without the screen. The efficiency is thus increased by 37% by the introduction of the screen. In other words, without the plastic screen, the collector has to be 37% larger to collect the same amount of heat at these conditions.

Another advantage of the suspended plastic screen is that it helps reduce the temperature of the black plastic. For the same temperature rise, the peak temperature of the black plastic was 10°C to 15°C lower if the plastic screen was installed. The reduced temperature for the black plastic means that it should have a longer useful life.

Collectors With Two Suspended Plastic Screens

In 1978, the same collector used during the previous two years were fitted with 2 suspended plastic screens to evaluate the effect of an additional screen on the collector efficiency. The clear plastic was still 0.15 mm polyethylene; the screens were black polypropylene, spaced 50 mm apart.

a.) Two suspended plastic screens, each with 75% opening

Results are presented in Figure 7. The collector efficiency is very much affected by air flow rates as in previous years when only one screen was used. However, there is marked improvement in collector efficiency when two screens are used instead of one. For example, at an air flow rate of 0.75 m^3 min^{-1} m^{-2}, the efficiency increases from 34% to 42%, a 24 percent increase in efficiency when two suspended screens are used instead of one. The additional screen increases the heat collection and transfer area and increases air turbulence resulting in a higher heat transfer rate.

b.) Two suspended plastic screens, a 75% open over a 53% open screen

The only difference between this arrangement and the previous one is the amount of shading of the lower screen. Results are presented in Figure 8. Again, a two-screen arrangement gives a higher efficiency than a one-screen arrangement; however, by using a more dense lower screen (53% instead of 75% open) the collector efficiency does not appear to be affected. In fact, the two efficiency curves are almost identical as shown if Figure 8.

Collector Cost

The cost of the collector as described, excluding labour, instrumentation and fans is U.S. $10.80/$m^2$. The insulation boards account for 32% of the total material cost and the two metal plenums at both ends of the collector account for another 30%. The plenums were custom-made and were rather expensive compared to the rest of the collector. The plastic screen costs only U.S. $0.94/$m^2$ or about 9% of the total cost of materials; the clear and black plastic cost U.S. $0.22/$m^2$.

If insulation were not used and less expensive plenums were used, it would be possible to bring the cost down to around U.S. $5/$m^2$. Naturally, if insulation were not used, the temperature rise obtainable would be somewhat less and efficiency will decrease, but probably by less than 5 percentage points (if not operating under excessive temperature) since the ground provides some insulation and thermal storage. Such a collector was built (9) in 1978. The material cost (not including the fan) was U.S. 4.95/m^2 and the efficiency ranged from 30 to 45% for 15^{o}C to 25^{o}C temperature rise. All the costs listed above are 1978 prices. As of October 1979, these prices have increased by approximately 22%, mostly due to the increase in lumber prices.

4. Conclusion

A plastic solar air heater with one of two suspended plastic screens is more efficient than a collector without one. It is also capable of higher air temperature rises and remains quite efficient. For the same air temperature rise, the temperature of the black absorber is also lower when the plastic screen is installed, therefore extending the useful life of the black plastic.

The collector performance is very dependent on air flow rate During the Fall, the efficiency is 20% at an air flow rate of 0.33 m^3 min^{-1} m^{-2} and 35% at 0.90 m^3 min^{-1} m^{-2} for a collector with one suspended plastic screen. Solar radiation has only a very slight effect on efficiency; the collector is slightly more efficient at lower radiation rates.

A collector with two suspended plastic screens is even more efficient than a collector with only one suspended screen and definitely much more efficient than a collector without a screen. Since the plastic screen is fairly inexpensive (U.S. \$0.94/m^2), the increase in efficiency due to the screens is well worth the extra cost.

Acknowledgment

The authors wish to acknowledge that this project was funded by DOE through USDA/ARS.

REFERENCES

1. Kline, G. L. Solar collectors for low temperature grain drying. ASAE Paper No. 77-3007, 1977.

2. Chau, K. V.; Baird, C. D.; Bagnall, L. O. Drying of corn and soybeans with solar energy in the Southeast. ASAE Paper No. 78-3014, 1978.

3. Peterson, W. H.; Hellickson, M. A. Solar-electric drying of corn in South Dakota. Trans. ASAE, 1976, 19(2):349-353.

4. Kranzler, G. A.; Bern, C. J.; Kline, G. L. Grain drying with supplemental solar heat. ASAE Paper No. 75-3001, 1975.

5. Morrison, D. W.; Shove, C. G. Bar plate solar collector grain drying bin. ASAE Paper No. 75-3513, 1975.

6. Willians, E. E.; Okos, M. R.; Peart, R. H.; Badenhop, A. F. Solar grain drying and collector evaluation. ASAE Paper No. 76-3512. 1976.

7. Parker, B. F. Performance test of three solar air heaters. Trans. ASAE, 1978, 21(3):530-533,536.

8. Chau, K. V.; Henderson, S. M. Performance of a matrix solar collector for heating air. Trans. ASAE, 1977, 20(3):558-561.

9. Oppenheim, P. A low cost solar air heater for grain drying. M. S. Thesis, University of Florida, 1978.

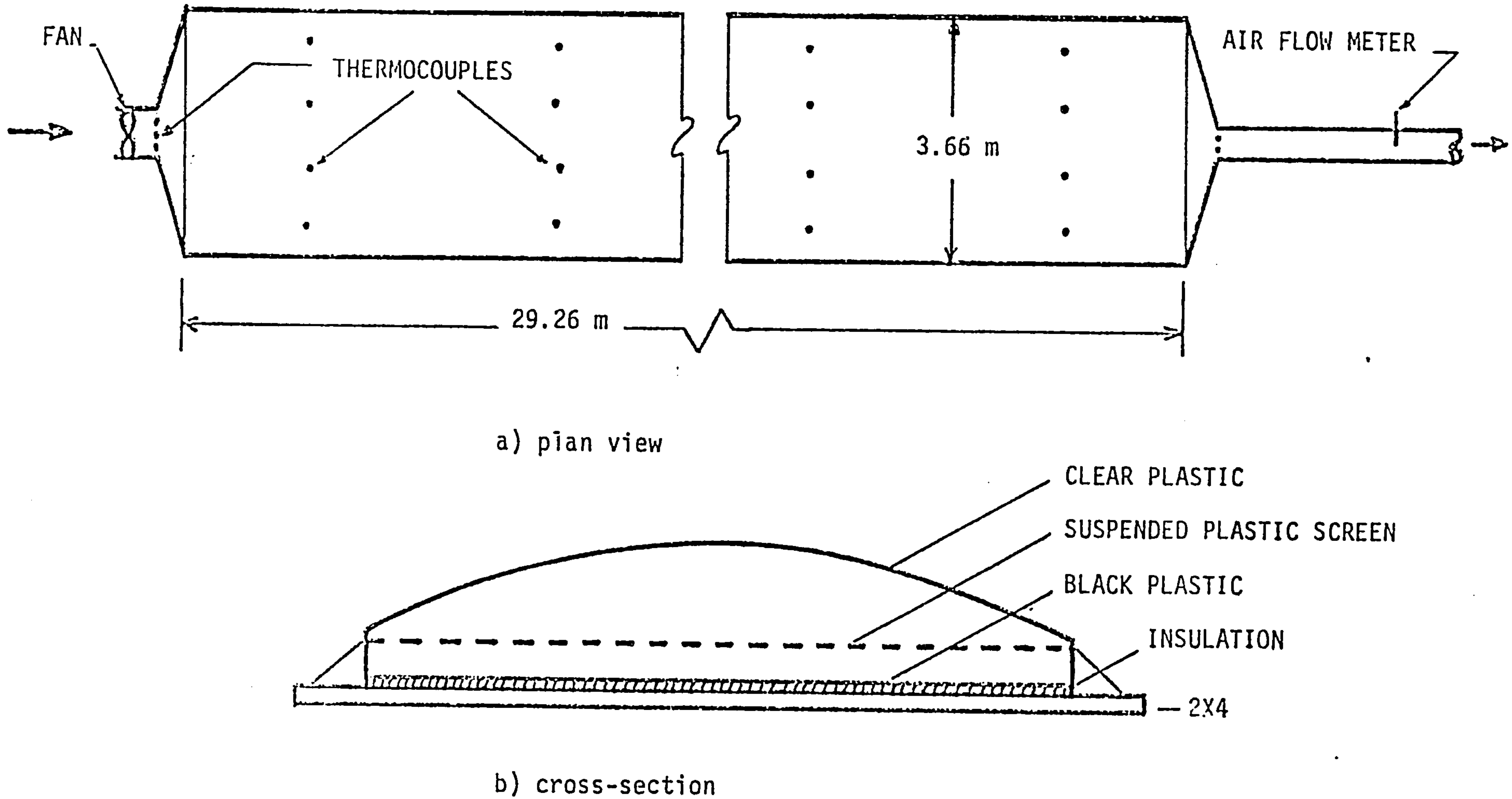

Schematic diagrams of the plastic air heater.

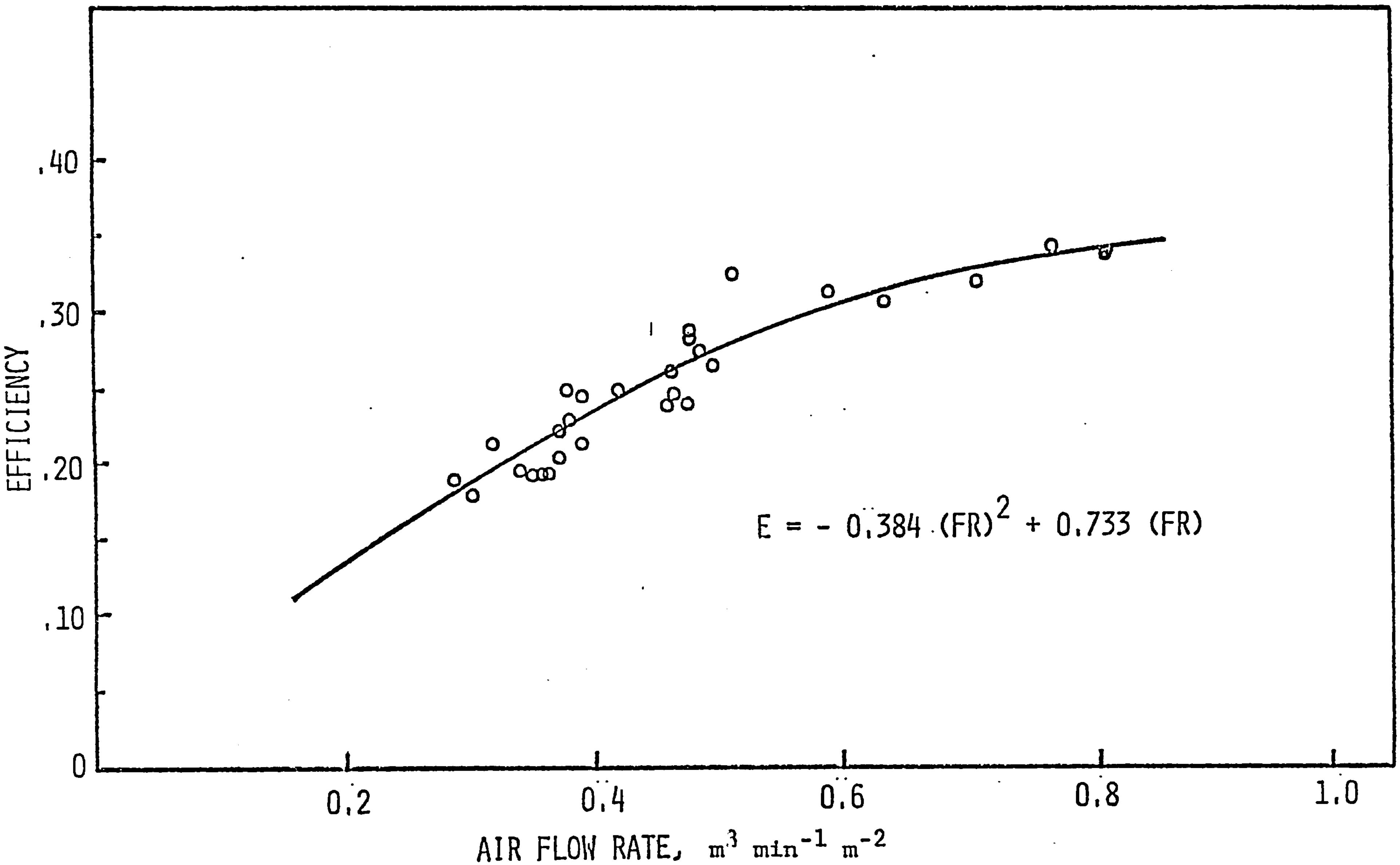

FIG. 1 Efficiency versus air flow rate.

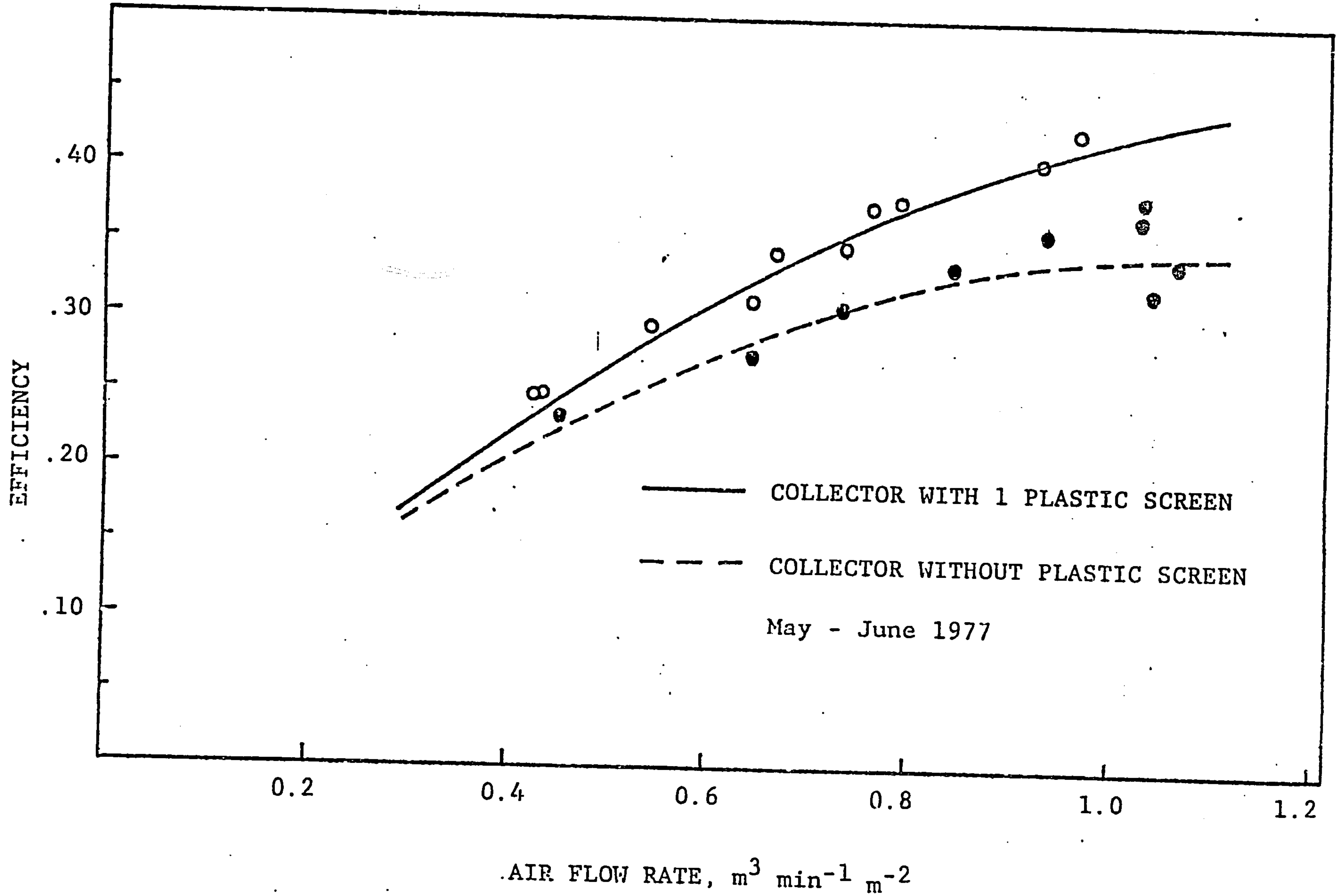

FIG. 2 Efficiency versus air flow rate.

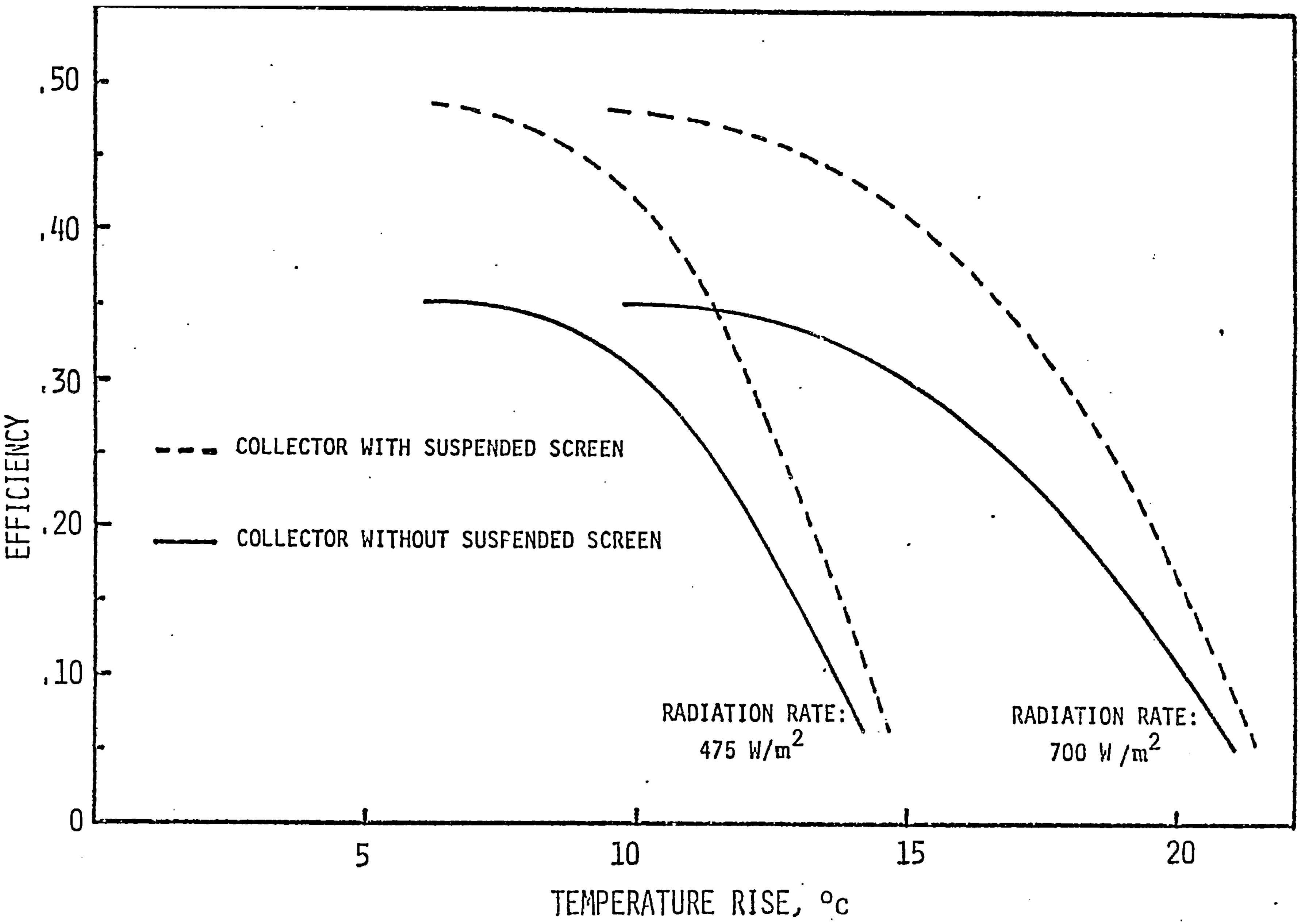
.50
.40
.30
.20
.10
0
EFFICIENCY
5
10
15
20
TEMPERATURE RISE, °c
COLLECTOR WITH SUSPENDED SCREEN
COLLECTOR WITHOUT SUSPENDED SCREEN
RADIATION RATE: 475 W/m2
RADIATION RATE: 700 W /m2

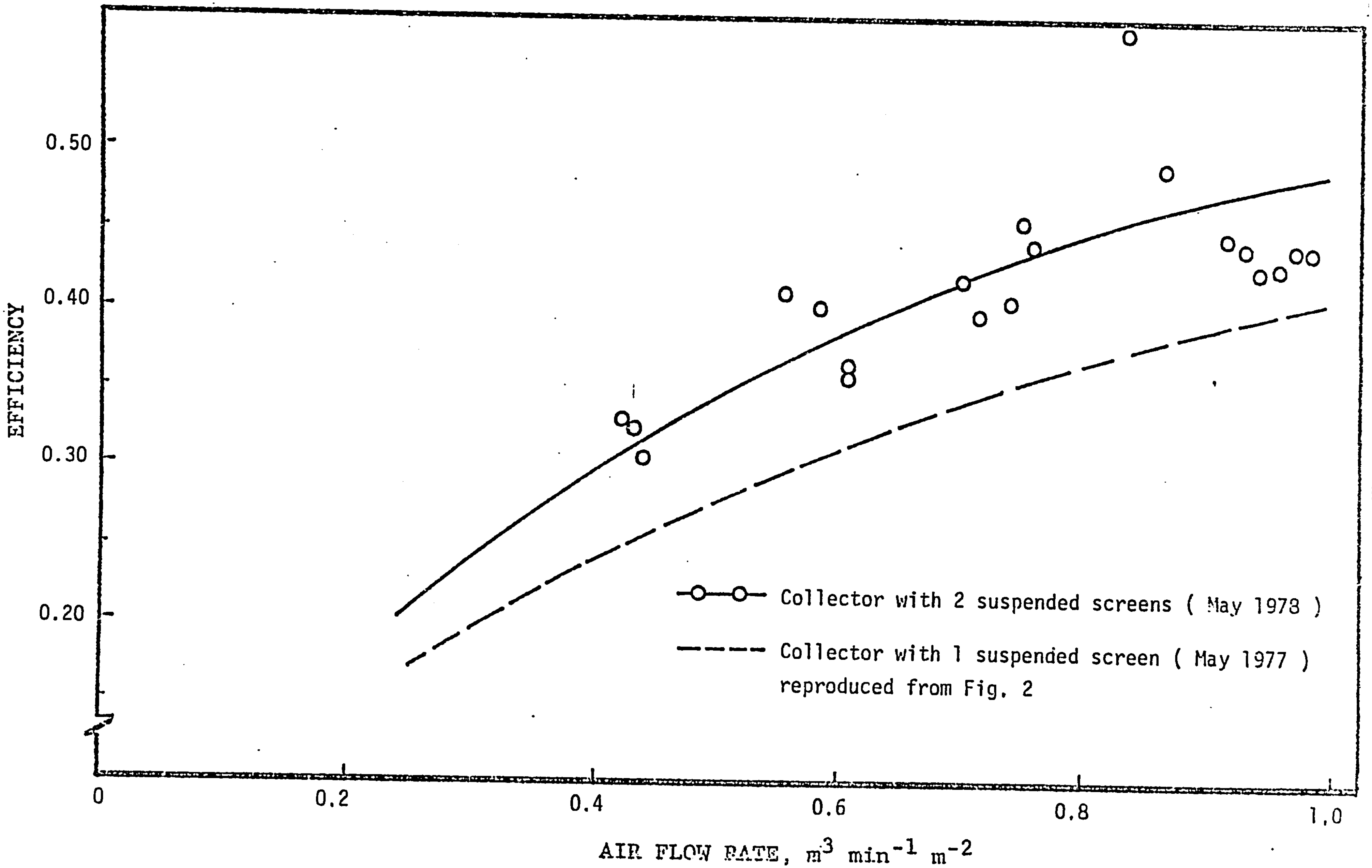

Figure 4. Comparison of collectors with 1 and 2 suspended screens.

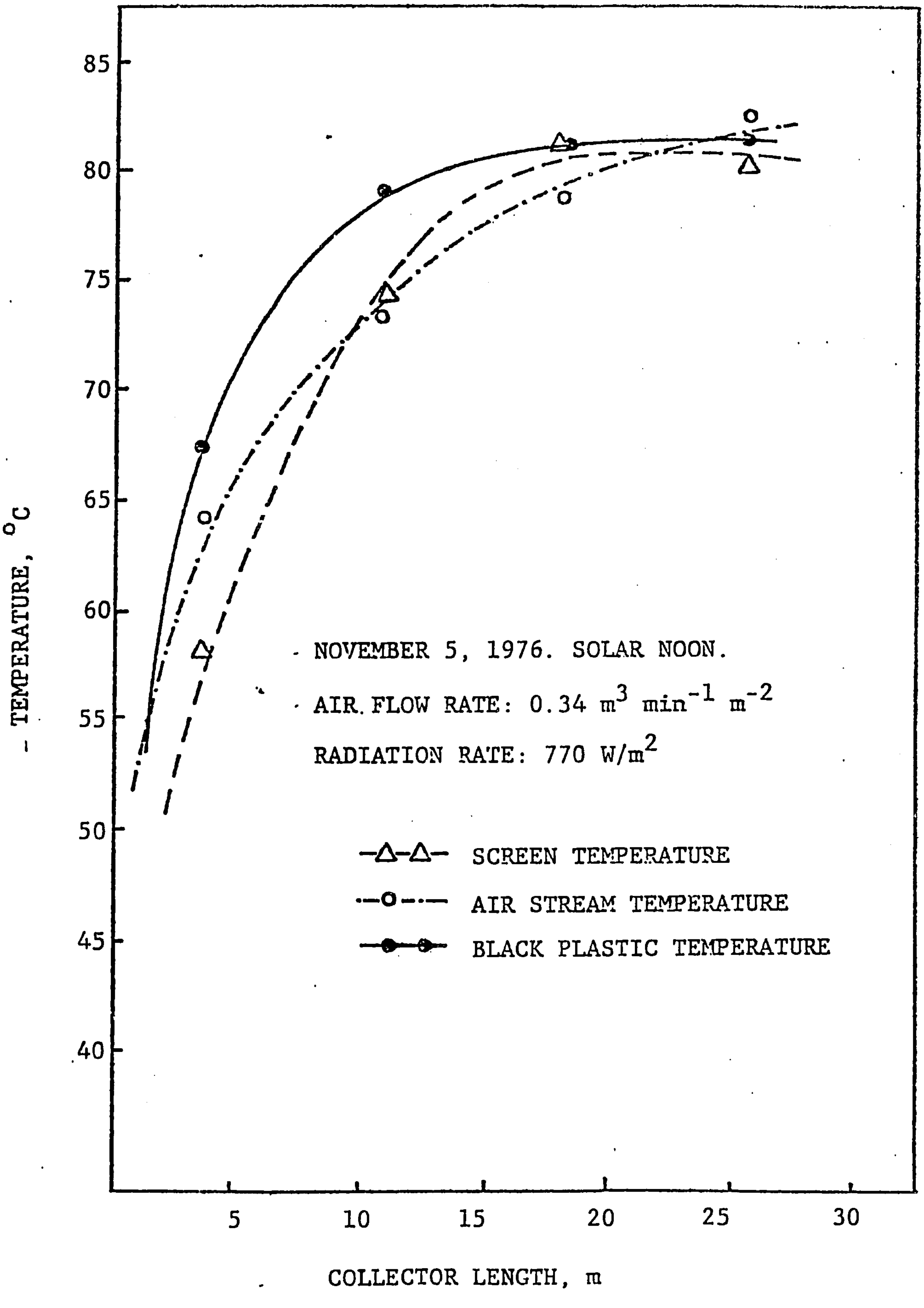

Temperature profiles in the collector

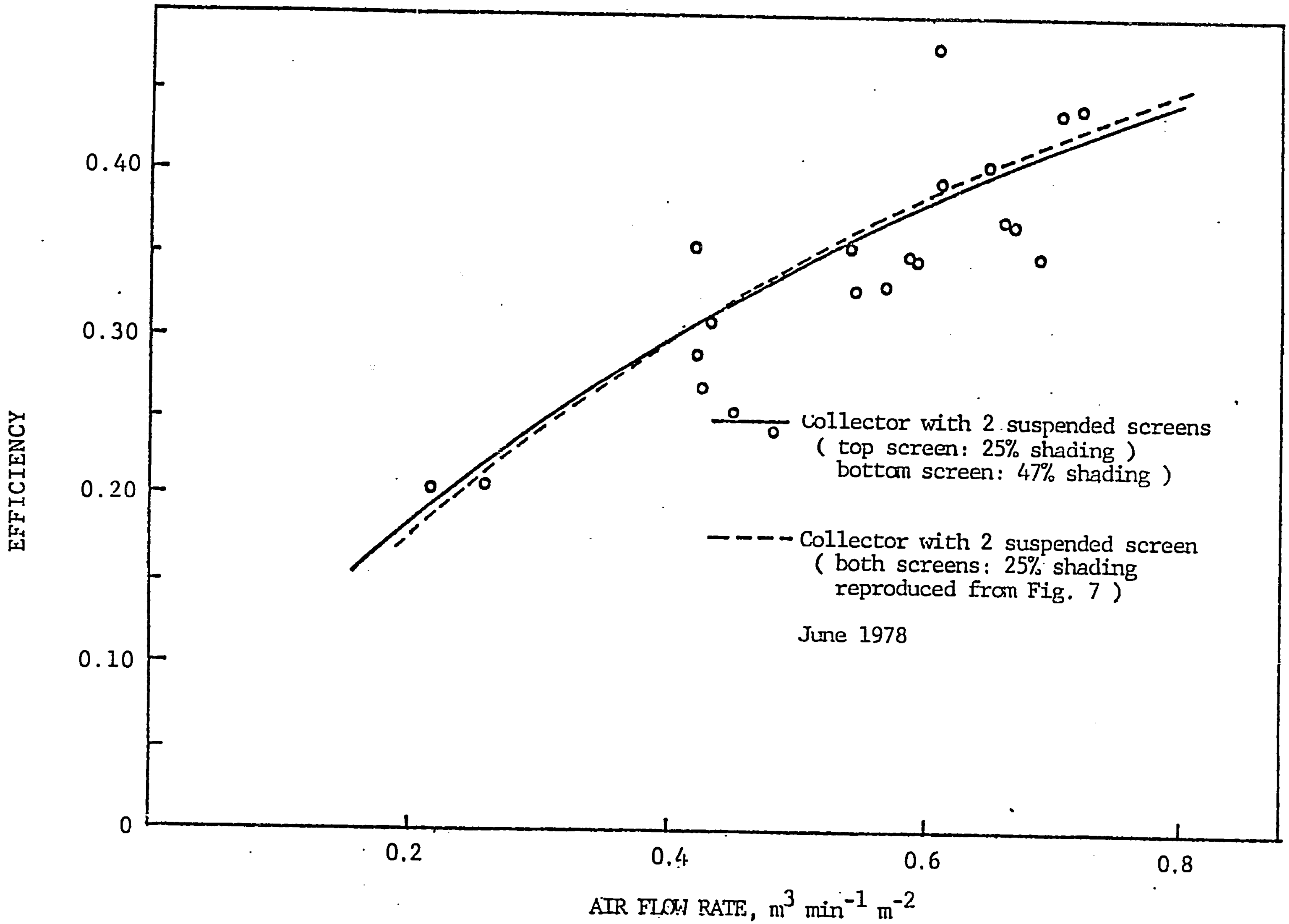

Collector efficiency versus air flow rate

From the Proceedings of the Florida Nutrition Conference.
Orlando, Florida. Jan 17, 1980

ENERGY REQUIREMENTS OF VARIOUS METHODS OF DRYING CORN

K. V. Chau
Department of Agricultural Engineering
University of Florida
Gainesville, Florida 32611

SUMMARY

Drying corn with heated air requires large amounts of energy. In fact, it accounts for about 3/4 of the direct energy used in corn production. Removing water from corn with heated air dryers requires anywhere from 3000 to 7000 kilojoules per kilogram of water. The variation is due to the type of dryers used, airflow rate, drying air temperature, ambient conditions and grain condition. Generally speaking, the high-temperature, high-speed dryers such as crossflow dryers are less energy efficient than dryers that use low temperature, low airflow rate and a deep grain bed such as a bin dryer. However, the latter type has some disadvantages including lower capacity, slow drying rate making the grain vulnerable to mold, and overdrying of the bottom layers. Combination drying, either dryeration or partial high temperature drying, will increase energy use efficiency. When ambient temperature and humidity are high, this method should be used with great caution. Solar drying is technically feasible but still not economically competitive at this time.

Drying grain is a very energy-intensive process. Energy is needed to evaporate moisture in the grain, to run the blowers and various conveyors. It has been estimated that the annual energy requirement for drying corn is 5.9 10^{10} MJ, equivalent to about 2.3 million m^3 (612 million gallons) of LP gas (3). Table 1 shows the approximate direct energy requirement per hectare of corn (6). It can be seen that drying makes up about 3/4 of the total direct energy input. However, artificial grain drying is a much needed operation. It allows the farmer to have more control over his farming operations and flexibility in the scheduling of equipment and labor during the harvest season. It will permit harvest at the optimum time to obtain maximum yield and minimum field losses. Figure 1 shows the allowable storage time for corn at various temperatures and moisture contents. The higher the moisture and temperature, the shorter the storage time. This is why it is so important to dry corn quickly after harvest in Florida where ambient temperatures are high in the summer.

Table 1

Approximate Energy Requirements for Corn Per Hectare.

Operation	Liters Gasoline
Moldboard plow	24.3
Disk (once over)	8.4
Harrow	3.7
Plant	8.4
Spray	1.4
Anhydrous ammonia application	15.0
Combine	16.8
Transport	3.7
Subtotal	81.7 (= 2,735 MJ)
Drying (13 percentage points of moisture removed - 6.3 tons/ha) . . .	305 ℓ (LP gas) = 7,789 MJ
TOTAL ENERGY REQUIRED	10,524 MJ

Effects of Corn Moisture Content at Harvest

The moisture content at harvest has definite effects on the total heat requirement for drying and also on the corn yield. Many farmers do not appreciate the magnitude and the source of harvest losses. Figure 2 shows that dry matter accumulation is at its maximum when the moisture content is approximately 26% (4). Harvesting before or after this point constitutes a maturity loss. On the other hand, leaving the corn in the field to dry exposes the grain to insect, bird and weather damages. In addition, machine losses (picker or combine) increase as the moisture content decreases due to increased grain shattering. To minimize all these losses, corn has to be harvested when its moisture content reaches approximately 26%. Harvesting early, at 30% instead of 26% moisture content, increases the heat requirement for drying by about 25%.

Energy Requirement vs. Drying Air Temperature

From a temperature standpoint, most farm drying falls into one of the following categories:

a) Natural air bin dryers. The drying potential comes from the ambient air and the fan heat. The fan heat adds approximately 1 - 1.5°C to the air temperature.

b) Low-temperature bin dryers. Typical drying air temperatures are in the 15 - 32°C range.

c) Medium-temperature bin dryers; 60-70°C air temperature range.

d) High-temperature dryers; 70°C and higher. They include bin, column, and concurrent flow dryers.

Natural air and low-temperature dryers are used only in areas where the ambient temperature and relative humidity are low. Practically all of the dryers used in the Southeast are high-temperature dryers.

Table 2 shows the estimated energy required to evaporate one kilogram of water from corn (9). It indicates that drying is more efficient

Table 2.

Approximate Energy Required in Kilojoules Per Kg of Water Evaporated For Grain Dried at Different Operating Temperatures.*

Operating Temperature	Moisture Content		
	27%	25%	20%
38-49°C	3132	3482	3712
71-82°C	4062	4062	4292
82-104°C	4062	4292	5103

* Based on ambient temperature of 16°C. (Walker)

at low temperatures than at high temperatures. However, it should be pointed out quickly that the fuel inefficiency at high temperatures as indicated by Table 2 is not due to the high temperature per se; it merely reflects the inefficiency of the different drying systems operating at different temperatures. The lower drying temperatures are associated with bin dryers which are very energy efficient, and the higher temperatures are associated with the high-speed column dryers which are less energy efficient. With high drying air temperatures, the grain bed has to be thin (except for concurrent dryers) to reduce overdrying of the grain layer that is first in contact with the drying air. As a result, the discharged air still has a lot of drying potential left that is wasted unless the dryer has an air recirculation or heat recovery feature.

For a given high-speed dryer, such as a crossflow dryer, decreasing the air temperature will actually decrease the energy efficiency as illustrated by Figure 3 (7). For a given airflow rate, the drying energy required decreases when the drying air temperature increases. Therefore, attempting to lower the operating temperature of a crossflow dryer to save energy will actually result in an increase in energy consumption. It should be noted that increasing the operating temperature will increase the moisture differential in the grain mass and may increase stress cracking.

Drying Efficiency vs. Drying Techniques

Table 3 shows the estimated performances of the various grain drying techniques (1). With presently available equipment, the efficiency of fuel utilization tends to decrease as the drying rate increases. Higher speed and higher temperature dryers are usually less efficient for the reasons already given in the last section. Comments on the various drying techniques are also included in Table 3. The next section will be devoted to the discussion of some of the techniques that are relatively new or not well-understood.

Combination Drying

Combination drying is a process that uses two or more drying techniques to remove moisture from the grain. The two most common combination drying systems are dryeration and partial high temperature drying.

Dryeration is a process in which the grain is removed from the dryer when its moisture content is about 2 percentage points higher than the desired moisture content. The hot grain is allowed to temper for several hours in a separate bin. Then it is cooled with an airflow rate of about 0.5 m^3/min-tonne. The final 2 percentage points of moisture are removed during this cooling period.

Partial high temperature drying is similar to dryeration except that the grain is removed from the high temperature dryer at a moisture content of about 20% and transferred to a bin dryer where the remaining moisture is removed. The advantage of combination drying lies in the fact that this process allows the high-speed, high-temperature dryer to operate only in the high moisture range where it is most efficient while leaving the drying at low moisture to a deep bin drying and cooling process. Dryeration can save about 20-25% and the partial heat drying can save up to 60% of the energy normally used in a crossflow dryer (2). The amount of energy saved depends on the ambient conditions and other factors.

Combination drying can result in better quality grain. The tempering and cooling phases allow the grain to be cooled slowly resulting in a decrease in stress cracks in the grain. In a conventional crossflow dryer, the grain is rapidly cooled during the last stage of the drying process. This rapid cooling can impose great thermal stresses in the kernels, causing them to crack.

Disadvantages of combination drying include the additional handling of the corn, a much closer monitoring of the grain temperature and moisture content, and the extra management of the slow drying phase. Under high ambient temperature and humidity conditions, special caution should be taken to make sure there is no molding of the top grain layer during the slow drying phase.

Concurrentflow Drying

In this process, the air and the grain move in the same direction. The hot air that enters the dryer is in contact with the wettest grain, and the air is rapidly cooled by the high rate of water evaporation from the grain. Drying temperatures of 150°C - 260°C can be used without causing excessive temperature in the grain. Air introduced at 150°C is quickly cooled to 83°C in travelling 5 - 7 cm into the corn at 25% wet basis (8). The temperature of the corn kernel is even much lower at this point because it has been exposed to the drying air for only a very short time, and the high rate of water evaporation helps keep it cool.

The concurrentflow dryer is more energy efficient than a crossflow dryer as shown in Table 4 (2). There is also a reduction in stress cracks and grain damage during subsequent handling because the grain temperature is relatively low during drying.

Solar Drying

During the past few years, there have been renewed interests in solar grain drying due to the dramatic rise of the cost of fossil fuels. At the present time, the general consensus is that solar corn drying is technically feasible but it is still not economically favorable. The solar drying system is used only during a short drying season each year, therefore prolonging its payback period, unless some other uses can be found for the solar collector during the rest of the year. Almost always, a conventional backup system is needed to allow for periods of inclement weather. This is particularly important in the Southeast where the corn has to be dried to a safe moisture for storage in just a few days to prevent spoilage.

A typical collector used for grain drying in Florida can be expected to collect about 5700 KJ/m^2-day. When comparing with LP gas at 13.2¢/liter (50¢/gallon), 5700 KJ is worth 3 cents. This means that if the solar drying system costs \$10/m^2, the payback period is 333 drying days, not counting the interest on the initial investment. 333 days may mean 5 - 15 seasons, depending on the amount of use each year. When interest on the initial investment and maintenance costs are taken into account, the payback period will be even longer unless the cost of fossil fuels will rise dramatically. One also has to keep in mind that when the price of fossil fuels goes up, so will the cost of the materials used to make the collector. The above figure gives an indication on how much one can afford to pay for a solar dryer. In order to compete successfully, the solar grain dryer has to be very inexpensive. The Department of Agricultural Engineering at the University of Florida is currently developing a low-cost plastic collector that performs well for grain drying. The material cost is only about \$4/m^2, but it is still not economically competitive. Collectors can be made to be more efficient in trapping solar energy, but their cost will increase.

Conditions of high ambient temperature and humidity in Florida promote rapid mold growth and accelerate grain spoilage. The high incidence of aflatoxin contamination is another special concern. Corn has to be dried to a safe moisture level in a very short time. This adds extra constraints to the success of solar grain drying since collectors have to be made larger and operate at higher temperature to have the short drying time desired. Larger collectors mean higher initial investment and operating at higher temperature means lower collector efficiency.

Problems in the Rating of Grain Dryers

It is very difficult for farmers and elevator operators to make the right choice when selecting dryers because dryer ratings are not based on standardized tests. It is very difficult to compare the energy efficiency of one dryer against another because so many factors affect the performance rating. These factors include initial and final moisture contents, grain temperature, physical properties of the grain, resistance to air flow through the grain, and ambient conditions. Keener (5) reported the following findings. Based on a 10-point moisture removal from 30% to 20%, a dryer would have a 7.7% higher drying rate than an equivalent one evaluated for 25 - 15% when using air at 72°C. Different types of corn and hybrid varieties having different physical characteristics affect the drying rate and drying efficiency by 15 - 20%. Air flow resistance by the grain can have widely varying effects on drying rate and drying efficiency. When the grain is clean, the airflow rate and the drying rate are generally higher for a given fan size. However, the drying efficiency can either increase or decrease depending on the systems.

Other Considerations

So far, discussions have been presented on the direct energy efficiencies of various types of dryers and drying techniques. There are other factors to be considered. The direct energy savings have to be weighed against the initial cost of the dryers. Dryer capacity is another factor. A drying technique that is energy efficient but requires extra equipment, handling and management may not actually be energy efficient from an overall energy standpoint. The extra equipment requires some prior energy investment; the extra management and labor have their energy costs also.

When selecting a dryer or a drying technique, one should be very mindful of the local ambient conditions. A system that works well and is very energy efficient at one location may not be efficient or even work at another location with different climatic conditions.

Table 3

Energy Efficiencies of Various Drying Techniques

	Drying Technique	Drying Efficiency* (ton/m^3 of LP gas)	Comments
1.	Batch or continuous flow w[illegible] cooling in dryer (82°C to 104°C).	43.8	High capacity, flexible, high kernel stress from fast drying and cooling, incomplete air saturation.
2.	Batch or continuous flow with dryeration+ (82°C to 104°C).	54.5	Increased capital investment, two handlings to storage, 50 to 60% increase in throughout, improved product quality.
3.	Bin drying without stirring device (5.5°C rise with 55% relative humidity humidistat control.	62.0	Overdrying in bottom layers, difficult to manage for optimum performance.
4.	Bin drying with stirring device (38°C to 60°C).	62.0	Mechanical reliability may be a problem, flexible in grain depth, fast batch procedures.
5.	Bin batch-drying cooling in bin (49°C to 60°C).	62.0	Modest price, medium capacity, additional manual labor for daily leveling and unloading.
6.	Electric bin drying (1°C to 4°C rise).	51.9	Slow drying rate, increased threat of mold, good grain quality, limits on grain moisture content.
7.	Combination system, 5% with batch or continuous-flow drying, 2% with dryeration, 3% with aeration.++	84.8	Same as technique 1 or 5, except final drying (without heat) and cooling done in another bin; increase in potential for mold during final drying.
8.	Drying with ambient air (1°C rise).	----	Slow drying, grain must be below 20% in moisture content, vulnerable to mold, weather conditions critical.
9.	Solar heat drying	----	Still in the developmental stage; use as a supplemental source of heat may become practical with new technology.

(Continued next page)

Table 3 Continued.

* Based on drying 10 points (25% to 15% wb), 4875 KJ per Kg of water for high-temperature dryer, and 3482 KJ per Kg of water for bin drying systems.

+ Dryeration response is a constant 2 points of drying, assuming a kernel temperature of 49 to 60°C.

++ Based on dryeration airflow of 1.1 m^3/ton min for 20 hr plus aeration airflow of 0.6 m^3/ton min for 30 days.

Adapted from Agricultural Engineering, May 1975.

Table 4.

Energy Consumption (MJ/tonne) for Several Systems for Drying Grain to 15% wb.

Drying From	Batch-in Bin	Cross-flow	Con-current	Dryera-tion	Partial Heat
30% wb	1091.7	1232.6	979.7	1091.7	955.3
28	909.8	1032.7	830.7	909.8	749.2
26	749.2	868.4	682.3	720.9	570.3
24	606.5	682.3	545.9	553.8	393.9
22	454.9	516.4	415.3	382.1	228.8
20	321.1	363.9	291.7	228.8	---

LITERATURE CITED

Anon. 1975. To conserve energy in agriculture. Ag. Eng., May 1975: 17-19.

Brooks, R. 1979. Concurrentflow and combination drying methods to reduce energy use and increase capacity. Paper presented at the 9th International Congress of Agricultural Engineering. Michigan State University, East Lansing, MI, July 8-13, 1979.

Harris, W. L. 1976. Solar energy applications in agriculture: potential research needs and adoption strategies. Md., Agr. Exp. Sta. Bul. A-184.

Johnson, W. H. and B. J. Lamp. 1966. Corn harvesting. AVI Publishing Co., Inc., Westport, Connecticut.

Keener, H. M. and T. L. Glenn. 1978. Measuring performance of grain drying systems. Paper No. 78-3521. ASAE, St. Joseph, MI.

Maddex, R. L. and F. W. Bakker-Arkema. 1978. Reducing energy requirements for harvesting, drying and storing grain. Ext. Bul. E-1168, Michigan State University.

Morey, R. V., H. A. Cloud, and W. E. Lueschen. 1976. Practices for the efficient utilization of energy for drying corn. Trans. of the ASAE. 19:151-154.

Thompson, T. L., G. H. Foster, and R. M. Peart. 1969. Comparison of concurrentflow, crossflow, and counterflow grain drying methods. USDA Marketing Research Report 841.

Walker, J. N. 1975. Energy usage in crop systems. Proceedings of conference-workshop on energy in agriculture. Atlanta, Georgia, October 1-3, 1975.

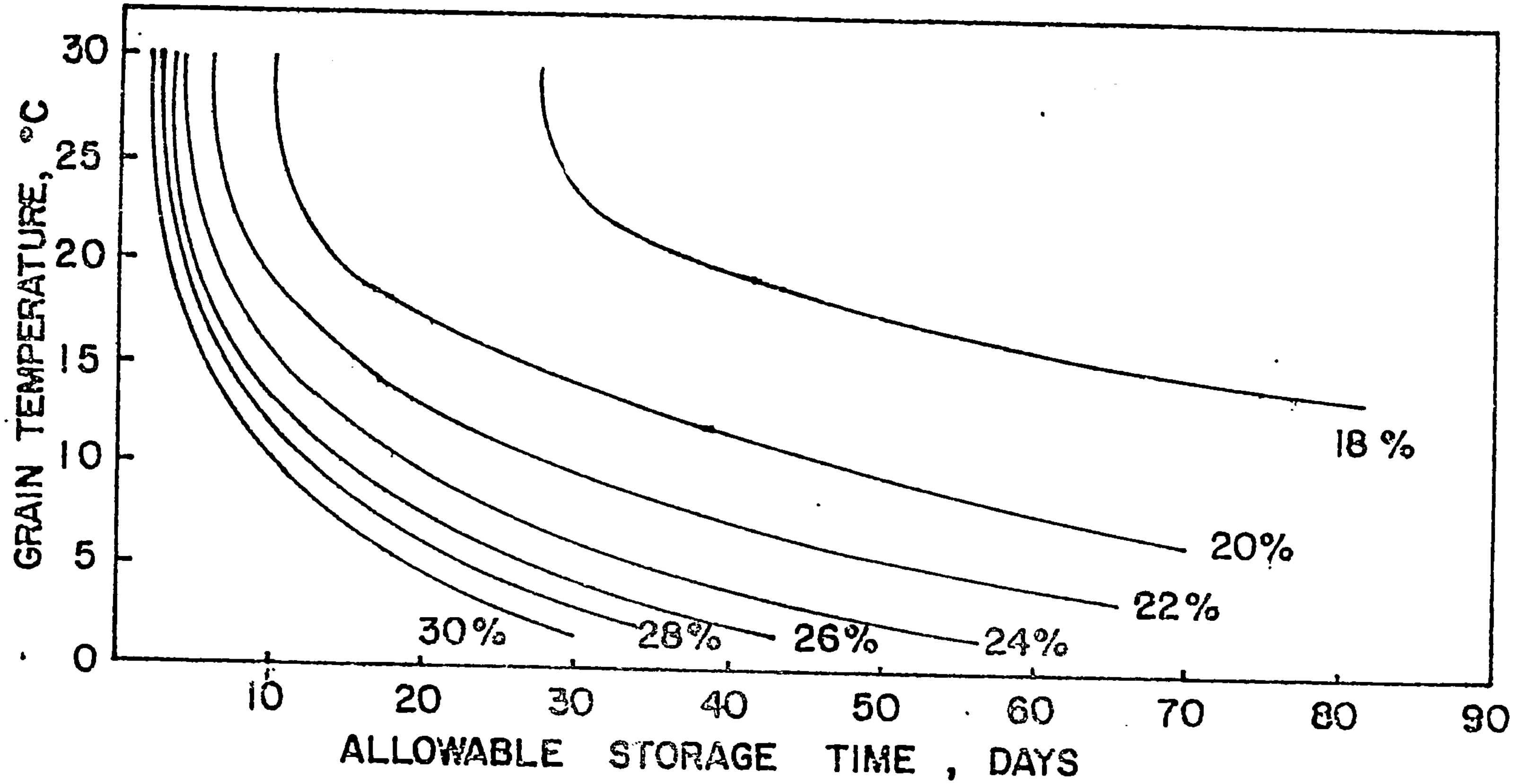

Fig. 1. Allowable storage time for shelled corn at various temperatures and moisture contents. Data from USDA Grain Storage Research Lab., Ames, Iowa.

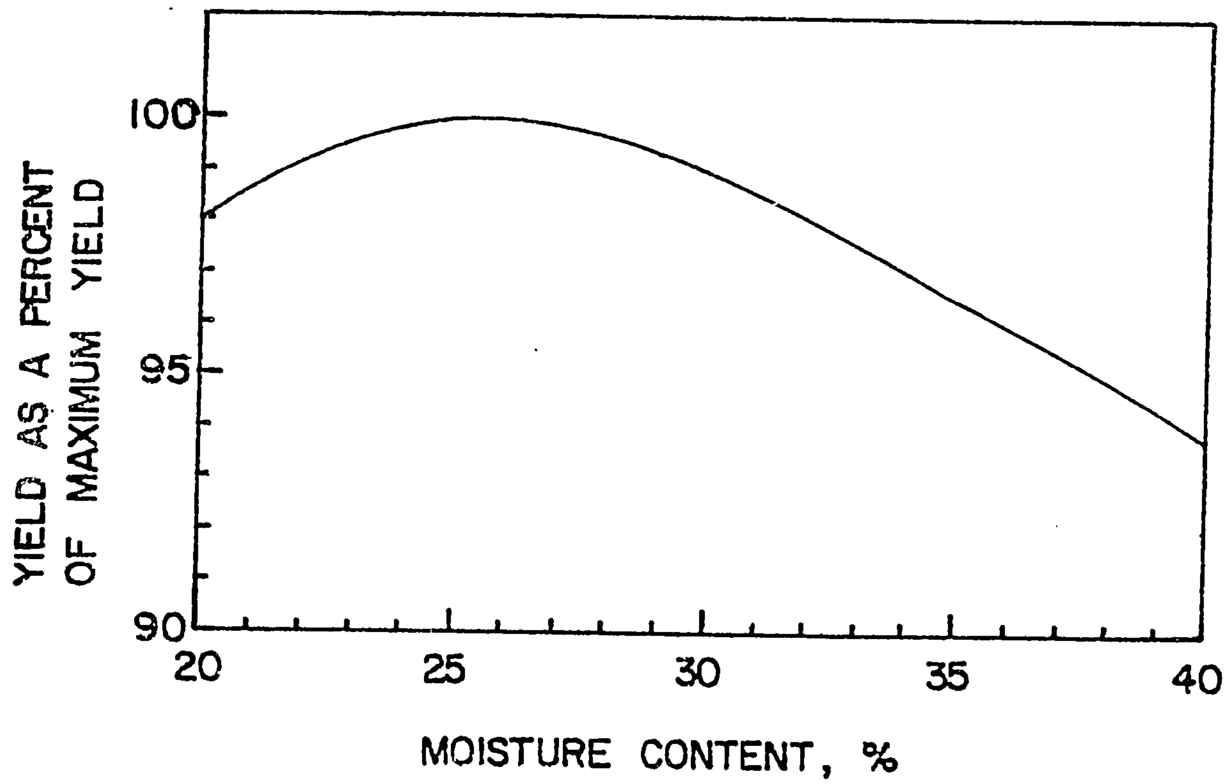

Fig. 2. Relationship between moisture content and yield (Johnson).

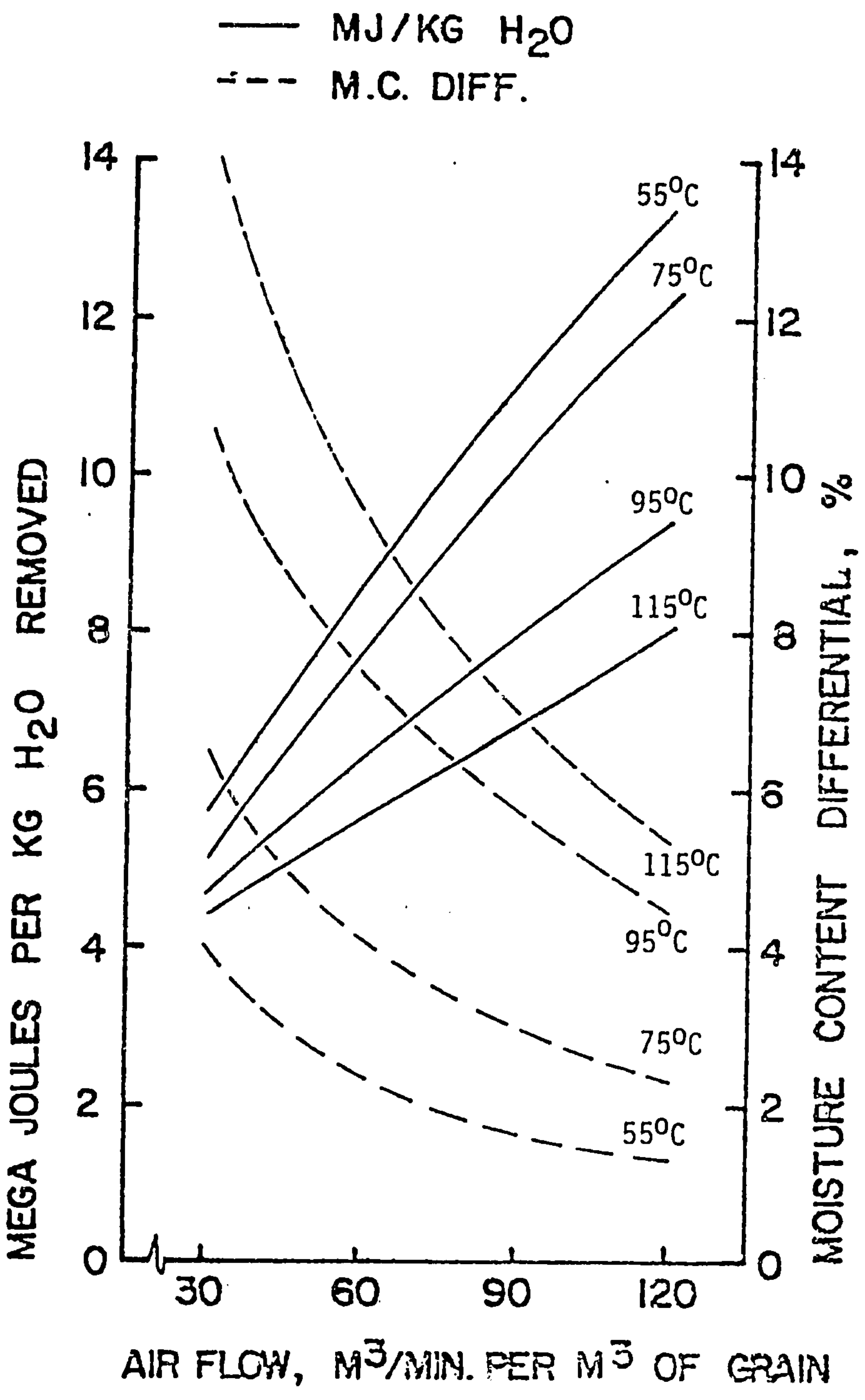

Fig. 3. Heat energy requirements and moisture content differentials for a continuous crossflow dryer (25-15% w.b., 30% cooling section, 10°C and 75% R.H. ambient conditions). (Morey)